PROCEEDINGS

OF

THE JAPAN-FRANCE SEMINAR

ON

SOLAR PHYSICS

EDITED BY

F. MORIYAMA AND J. C. HENOUX

PROCEEDINGS

OF

THE JAPAN-FRANCE SEMINAR

ON

SOLAR PHYSICS

EDITED BY

F. MORIYAMA AND J. C. HENOUX

PREFACE

The Japan-France Seminar on Solar Physics, jointly sponsored by Japan Society for the Promotion of Sciences and Centre National de la Recherche Scientifique, was held in Tokyo from 15 to 18 October 1980. The organizing committee responsible for the program consisted of Drs. J. C. Pecker, J. C. Henoux, M. Semel, W. Unno and F. Moriyama. About 50 scientists in both countries gathered to exchange recent information on the subject of the active sun, and to discuss conflict findings and divergent interpretations. Also attended by solar physicists from neighboring countries the meeting was successful, and more than 50 contributions (including 15 review articles) which are compiled in this proceedings were presented.

Holding the seminar and publication of the proceedings were possible only with the cooperation and help from many people. We are particularly grateful to Drs. J. C. Pecker, D. Jacquot and Boulon for their kind and active support. Thanks are also due to Dr. E. Ribes for her help in the organization of the meeting and the preparation for publication.

F. Moriyama
J. C. Henoux

List of Participants

J. C. Pecker, College de France
J. Rosch, Observatoire du Pic du Midi
J. L. Leroy, "
R. Muller, "
J. C. Henoux, Observatoire de Paris
P. Mein, "
J. Rayrole, "
M. J. Martres, "
Z. Mouradian, "
M. Semel, "
E. Ribes, "
A. Mangeney, "
J. Heyvaerts, "
N. Bel, "
J. P. Lafon, "
B. Leroy, "
R. Bonnet, Laboratoire de Physique Stellaire et Planetaire
H. S. Yun, Seoul National University
B. Chen, Purple Mountain Observatory
M. Wu, Yunnan Observatory
T. Li, Nanking Astronomical Instrument Factory

Z. Suemoto, Tokyo Astronomical Observatory, University of Tokyo
K. Nishi, "
Y. Uchida, "
E. Hiei, "
F. Moriyama, "
T. Hirayama, "
M. Makita, "
K. Tanaka, "
K. Nariai, "
K. Kai, "
T. Kosugi, "
T. Watanabe, "
W. Unno, Department of Astronomy, University of Tokyo
T. Takakura, "
Y. Osaki, "
H. Yoshimura, "
H. Kawakami, "
K. Kawabata, Department of Physics and Astrophysics, Nagoya University
H. Ogawa, "
I. Kawaguchi, Hida and Kwasan Observatories, Kyoto University
M. Kanno, "
Y. Nakai, "
H. Kurokawa, "
Y. Funakoshi, "
R. Kitai, Institute for Astrophysics, Kyoto University
T. Nishikawa, "
K. Shibata, "
Y. Suematsu, "
J. Kubota, Osaka Keizai University
O. Kaburaki, Astronomical Institute, Tohoku University
S. Shibata, "
M. Okazaki, Tsuruoka Technical College

CONTENTS

THE ACTIVE SUN AS A STAR .....

Jean-Claude Pecker
Collège de France

I have the great honour of being the first speaker from abroad. It gives me the pleasure of expressing to our japanese colleagues our deepest thanks for their warm hospitality this week and for the permanent stimulation which is given, to their french colleagues, by the various cooperative programs in the making, at the solar telescopes, or behind the computers, or again in the midst of the equations. In particular, I would like to express my gratitude to Professor Zenzaburo Suemoto, to whom solar physics owes so much, and I would like to recall that we met for the first time more than thirty years ago, at the Institut d'Astrophysique ... Solar Physics has indeed always been a very friendly science, all over the world. I would like also to express our deep thanks to Professor Moriyama, Head of the Solar Division of the Tokyo Observatory in Mitaka, and to Professor Unno, who contributed both so efficiently to build up the program of this meeting, and we know that it has not been always easy, especially to find suitable dates; and I must apologize to them for the many constraints that the french side has perhaps put on this meeting ... Finally I would like to thank all members of the Tokyo Observatory and of all other Japanese Institutions, who are present here, amongst whom we have many old-time friends and colleagues, and who are making so much now to make our stay scientifically efficient, and most pleasant on the purely human side. Japan is a great country, full of beauties, rich of its past, and of its future. We are very glad to be here ... Thank you very much indeed. Dom Aligato !

Japan is in particular the country of the morning sun, rising on the eastern horizon, above the Pacific ocean. May this symbol guide the spirit of our meetings ...

For a very long time indeed, it was not even conceived that one could ever compare the Sun, a large luminary rising in the morning, setting in the evening, and following a rather complicated network of apparent motions around the observer, and those stars, fixed with respect to each other, and defining a reference frame for the solar motion and not much else. A very early attempt to determine the size

of stars, from their "apparent diameter" (which was not yet identified with an artifact of the eye or of the instrument), and from their minimum distance, (assuming that it was necessary to explain they had not any observable annual parallax, as a consequence of the copernician description), gave diameters at least thousands of times bigger than that of the Sun ... This was a disappointment, which led Tycho Brahé to even doubt the copernician system ...

The first one to decide that stars may after all be other suns, was Giordano Bruno, and he was burned for that in 1600. Galileo discovered stars in the Milky Way, but he did not, explicitely at least, admit a parenty between these very weak bright points and the Sun ... Fontenelle, in his "Discours sur la Pluralité des Mondes", and the newtonian school, went along the line of Bruno; but the similarity between Sun and stars became obvious only at the time of the first true distance determinations (which enabled us to compare the absolute brightness of the Sun with that of the stars) made by Bessel in Germany, Henderson at the Cape, and Wilhelm von Struve in Russia. -in the late eighteen-forties; at the time of the first radius determination, by Vogel in 1888, of Algol, an eclipsing binary; and at the time of the first stellar line spectra, obtained by Huggins, at about the same time, in the years 1860 ...

To make a long story short, the stars were, undoubtedly, similar in nature, size, etc... to the already rather well-known Sun. The stars were suns ... That was indeed the main conclusion of the XIXth century.

The enormous flow of observations, which gave place to the bulk of stellar classification, and the theoretical studies of gaseous spheres in equilibrium conditions, gave both a great coherence to the description of the many families of the stellar world; the calibration in size, mass, temperature, of the various types or classes of stars had achieved in the XXth century, a state of completedness, which was, in spite of a few drawbacks on which I shall not comment today (see Pecker, 1973), rather remarkable.

Hence several authors started to ask one first question; if the Sun were, say, at a distance of 10 parsecs, what would be its classification as a star, what would be its "stellar" properties ? Many papers appear as typical of this attitude, which was a conscious attempt to calibrate better the stellar sequence by the use of the solar well-established properties. It was then decided that the Sun was a star of type G 2, of luminosity class V. Amongst these many papers, I would like to quote, as an epoch-making one, the chapter written by Bengt Strömgren, in 1952, in Kuiper's "The Sun", under the title "The Sun as a Star". There, the internal structure is

sketched, the extent of the convection zone estimated to 200000 km. But boundaries are hardly described by anything else but the value of the effective temperature, and the vanishing of density and pressure. An outline of solar evolution was also described, in a rather promising way. Tons of papers, after that paper, have been devoted to "the Sun as a star", even when this was not the exact title of the paper. In most of the cases, authors did present elaborated views on solar and stellar structure and evolution, and went as far as deducing, from the solar photospheric properties, some necessary properties of the stars and as searching for them. We could for example quote the systematic look at eclipsing binaries for limb darkening data; or the study, from the spectrum, continuous, and lines, of the physical stratification of the photospheric layers. But the recent improvements in photometric accuracy have opened a new field : we measure minute variations of the solar constant, due to the rotation (and disappearance behind limb) of spots; we measure variations on the solar disk of K_{23} emission and can detect stellar plages.

In another line of thought, the fact that the Sun is variable, at least over some parts of his surface, with time, has led to a solar-like nomenclature : one has been speaking of spotted stars, of flare stars, of active stars. But the claimed analogy could be highly misleading, as it was, indeed, quite superficial, and did not imply any physical resemblance ... How indeed could it otherwise be ? The fine structure of the Sun is non-observable on stars ! I think about the granulation, the active features, spots or prominences, or the flares; moreover, the time resolution of the instruments is not at all of the same order of magnitude; no stellar eclipse is sufficiently comparable to solar eclipses to let the observer guess the temperature rise in the chromosphere and corona; all of this was, more and less, induced from theoretical reasonning, inasmuch as one knew something, not always very much, about the mechanisms of the solar phenomena.

As solar physicists, with the blooming of space research, got more and more interested in chromospheric and coronal events, in the solar wind, in the magnetic features, -the stellar physicists did not realize at first how these new and rapidly growing fields of research could be of some interest to them. However, some astrophysicists -and you must pardon me if I quote now a paper by Thomas and myself (1976)- advocated strongly the fact that the Sun, irrespective of its spectral classification, more or less irrelevant because of its simplicity, the Sun as it is, with all its complexity, was indeed a sort of microcosm, a stellar laboratory; there all sorts of phenomena, that could be very large and intense in some stars, could be easy to study on a moderate scale, even very moderate, and allow a much better understanding of similar stellar phenomena, that appear often, in the stellar con-

text, as gigantic or even cataclysmic.

The study of solar-like GK m.s.-stars is now indeed filling the gap, and allows us to feel more confident, or perhaps to reject what initially was only an analogy.

Putting the active Sun as the center of our analogic study, means, essentially, that we feel that we are concerned with an effort for a better angular resolution, now conceivable for stars, with an effort for a better time resolution also, allowing to detect very rapidly variable phenomena, and, evidently, with an effort for a better spectral coverage, allowing now to reach chromospheric and coronal layers through X and UV spectra.

Clearly, in the coming days, we shall cover only a few questions, dealing with what we can realistically study, being what we are, having the instruments we have, and limited by our budgets; we shall concentrate mostly on active features of short and long duration, and on their understanding. But we must keep in mind that several aspects, about which we shall not speak, of the "solar activity", may be later discovered in stars, or even are already known in them, and that their knowledge may perhaps, in some occasions, illuminate what we are able to study in the solar features; and the reverse is still more true.

And, at this point, we should probably remember, as a guide line, a comment made, I believe, by Cecilia Payne-Gaposhkin, who said, after looking at the first UV spectrum of the Sun, obtained by Tousey and others : "Well, well .. But this is a typical Wolf-Rayet star !..".

Indeed, to me, the "active Sun" is the ensemble of solar features which are variable with time, -at any scale of time, -and which rarely affect the whole of the solar surface; it is also, accordingly, the ensemble of solar features which occupy a definite part of this surface, large, as the supergranular cells, or small, as the spots, the flares, or even the granules ... Everything which departs from a gaseous sphere, spherically symmetric, in equilibrium, and stationary, i.e. from the traditional model of an ordinary star, is indeed what we are concerned with.

In introducing our debate, I shall be obliged, I feel, to bypass its scope, which had to be kept realistic ... I shall try to give a few examples of solar phenomena which have their analog in the field of stellar studies, or vice-versa. I hope you will pardon me if this quick coverage is neither exhaustive, nor very deep, and if my few examples are covered rather superficially. As I told the study of solar-like stars, now feasible, may alter somewhat the quality of some of the possible

analogies.

I shall follow more or less the natural trend of progress in our understanding, starting from phenomena which are very general, such as the chromospheres and coronae, the phenomena which are not closely linked to magnetic fields, such as pulsations, winds; .. and finally, the magnetic phenomena, spots or flares, in their optical manifestations; ending by considerations on stellar magnetism and stellar cyclic activity.

1. The solar and stellar chromospheric and coronal features

The solar spectrum is much more sensitive in the XUV, and in the radiowaves, to the active phenomena, as the latter influence strongly the chromospheric and coronal radiation, which in their turn, mark definitely the XUV and radio spectra, whenever the visible spectrum is hardly affected, except in the cores of some emission lines.

From spectra alone, the extension towards the short wave-lengths and the fine resolution of the spectra obtained using scanners or photon counters, gave already much more than the classical picture of equilibrium photospheres.

The non-LTE effects, even in photospheres, were obvious from studies pursued along the main sequence. Let us only recall the work by Mihalas, where he showed beyond doubt that the behaviour of the magnesium lines could not be explained with a single value of the abundance, but only by taking into account a proper non-LTE treatment, whenever it was thought necessary, before his important papers, to admit that the magnesium abundance was varying along the main sequence, from a value of $4 10^{-5}$ in the solar case, to a value of 10^{-3}-10^{-4} in the case of OB stars.

The existence of chromospheres was first inferred from the feeling of their necessity : the early theories of the chromospheric heating led to consider that a chromosphere should appear in stars were an hydrogen and/or helium ionisation convective zone was present near the surface. Hence people expected chromospheric features to appear in the spectrum of many stars of type later than A but not earlier. Truly enough, some emission features were known, but mostly in rather exceptional cases. But, the space-gathered spectra have later shown, indeed, that the heating of a chromosphere is quite a general phenomenon and a variable one which concerns the whole of the spectral sequence : and this shows at least that one should come back with a new eye on the theory of solar chromospheric heating; it shows also that if hints can be obtained from solar studies, none of the solar studies are final, -and the benefit is mutual.

Quite typical of a stellar chromospheric phenomenon, and, moreover, of a law

which can relate chromospheric properties to overall stellar properties is the well-known Wilson-Bappu (WP) effect. I have not, I presume, to recall the essential features of the relation which seems to associate, in a one variable dependance, the absolute magnitude Mv to Wo, the full width at half maximum of emission cores of ionized calcium H and K lines. It may be interesting however to note that this effect was indeed discovered more than fifty years ago by the solar physicists, Deslandres and Burson, working in Meudon.

Similar effects, i.e. one-variable correlations, have been found in the cores of other intense lines, -such as Lyα , or MgII doublet. Wings of H and K obey also relations of the same type.

It is remarkable to note that the WB effect concerns a very large range of magnitudes (more than ten magnitudes). The role of other parameters have been looked for : the metallicity indices seem not to influence the line width;neither is it correlated with the importance of the emission, which possibly measures the depth of the chromosphere, whenever its width measures the non-thermal velocity fields.

There is no need of much thinking to say that the study of the cores of these lines, in the solar spectrum, may enable us to understand better their formation, in active regions notably, and hence to infer some interesting interpretation of the stellar chromospheric data. We shall speak certainly of our solar results in the following days.

One normal approach to the problem is theoretical; one has to build up a good theory of the formation of H and K lines, vary the parameters, play with the models, the abundances, the velocity fields, the geometry, etc... The other one is statistical. If one judges the respective advantages of both methods from their results, it is clear that the first one has not been as satisfactory as one might have thought; since the earlier researches by Miyamoto, in the late forties, much progress of course has been accomplished, but not enough, in the sense that one does not yet describe properly the velocity fields in the chromospheric layers. So why not to try also the statistical approach, from the stellar view point, in order to understand better what parameters do in fact influence more the K and H profiles ? The recent study of 60 G stars I earlier mentionned goes into that direction.

The study of chromospheric features in the spectrum of faculae, in this respect, can be considered both ways. Either we could start from model techniques, to have realistic hints about the differences between quiet Sun physical parameters,

and facular physical parameters, explaining, by the differences in these parameters, the differences between facular and quiet-sun H and K lines, and compare them also with the stellar cases, in order to select those which are really significant, and to build a better facular model. Strange behaviours (as shown by Dumont et al, 1980) indicate a strange boundary behaviour of turbulence, -a phenomenon not likely to affect the spectrum of the star as a whole, hence significant physically, but not observable on stars ...

Time sequence were obtained of stellar chromospheric features. They concern of course first the visible spectrum, and in it the center cores of some emission lines. The case of Be stars is quite typical in this respect. A star like 50 Cygni displays variable Balmer lines, showing at the scale of minutes or hours, or at much larger scale, marked changes in the chromospheric structures. (Doazan et al.). It is remarkable to note that several stars appear as Be some times, as normal B at other phases; a 3-phase description can be done (Be, B shell, B norm.).

Many such observations are now piling, once the attention has been drawn upon them. Let us quote the increase by a factor 3 of OI 8446 in V 1016 Cyg between 1979 and 1980, the appearance of He II 10123 in HM Sge with a great intensity; an increase of a factor 2 of OI 8446 in MWC 349 A during the same period, -most of the other emission lines being unchanged during the same period ...

Emission features from high excitation, high ionization lines, are chromospheric indicators; they are in general, as on the solar surface, highly variable.

The existence of coronae proceeded from the same type of information. Lines of various ions, of an high degree of ionization, have been observed in the stellar spectra. And more recently, the Einstein discoveries -I mean the Einstein satellite- have shown that many stars were indeed surrounded by hot coronas, whatever their type, whatever their character of either double close binaries or detached stars ...

The Einstein satellite has been so sensitive as to bring the proof of existence of coronae, in ordinary stars, with X-ray luminosity ranging from 10^{26} to 10^{34} ergs per second. Young O, B, A stars, as well as late K and M stars, have coronae producing X-ray fluxes of 1000 to 1 million stronger than expected.

The dispersion of the diagramm, build for main sequence, F_X/F_V as a function of spectral type shows that the heating mechanisms depends upon (at least) a new parameter, to add to the classical T_{eff} -g Hertzprung-Russell theoretical coordina-

tes.

The X ray-Sun is well known. The case of the binary Alpha Centauri is also typical : the K star has a bright corona; the G star has a weak one, -contrary to some theoretical expectations inspired by solar theories. We should note it is not a close binary; hence X-ray emission is not associated, as in many other well-known cases, to the stellar duplicity.

One should also mention, as important in this respect, the discovery of strong X-ray stellar bursts, perhaps similar to radio solar bursts. These objects have seemingly a very high absolute X-ray luminosity, of 10^{37} (or more) ergs per second, and the flashes increase that luminosity by a factor of 10 to 1000.

Along the same line, P-Cygni-like profiles, indicative, in general, of rather noticeable mass loss, have a variable behaviour, proving indeed the modulation of the stellar wind by the fluctuations of coronal activity. Variations in X-rays of some stars led to similar conclusions, as shown for instance by Matsuoka and his associates at the Uchinoura station, using Makucho X-ray satellite.

They, for example (Inue et al.), find the emission line of O VII, at 0.57 keV (or 22 Å) in agreement with a temperature of the order of a million degrees K, in the X-ray spectrum of some large region, possibly interstellar -but is not there the heating mechanism similar to those of coronae ? X-ray flares are of course indicative of some coronal transients. We shall come back on them.

From that kind of studies, we can deduce that the stellar radio spectrum should also be indicative of coronae, and through coronae, of coronal activity, of stellar activity. Too little at this time is known on stellar radio spectrum, at least to my very limited knowledge, to enable me to comment on the radiastronomical side of the question. However, it is clear that radio data would be tremendously valuable; they would allow to distinguish between the different parts of the corona, because of the different behaviour of the Rayleigh-Jeans law in the radio waves, and of the Planck's law in the XUV.

One general conclusion we can draw, at first, from the bulk of these studies, of which I have only quoted some examples, is that chromospheres and coronae are a general phenomenon; and, as such, it is impossible to link their existence with that of the hydrogen-helium convection zones.Hence some other mechanism has to be found, in order to explain the heating of these outer layers, even in the case of Sun.

Recent studies by N. Mein have proved, beyond doubt, I think, the purely mecha-

nical wave dissipation to be totally inadequate. May be the magnetic waves or hydromagnetic waves dissipation may play an important role. Hence, for the sake of solar-stellar physics, we have got to ask one question : what are the parameters, -outside T_{eff}, g and the chemical composition, -which really command the source, inside the star, of the heating mechanism ?

Asking such a question is imperative; and one single additional parameter may not be sufficient, as seen from the distribution of X-ray flux in the HR diagramm.

2. The pulsating sun and pulsating stars

For years, pulsating stars, cepheids for example, have been known. But nothing was even suspected on the solar oscillations.

Nowadays, we know much about them; and the theory of vibrational instabilities and wave propagation has bloomed indeed, bringing much to both solar and stellar studies.

On the solar side, the first detection of oscillations was that of Leighton, Noyes and Simon, 1960, and very soon after, by a different technique, that of Evans and Michard. At that time, the evidence was pointing out to oscillations of five-minute period or so. They were clearly affecting the photosphere, in a more or less coherent way. The amplitude of the velocity modulation is of the order of 0.5 km sec^{-1} (r.m.s). In the photosphere they propagate at a velocity of 6 km s^{-1}.

Further studies (such as by Fossat and Grec) of the 5-minutes oscillations have shown them to be of a rather complex nature. They are standing acoustic waves, trapped near the solar surface in a 10000 km deep layer. The fundamental mode did not carry as much energy as the highest harmonics, found to have rather high n values, -being understood that one can distinguish radial modes, -denoted by n- and surface modes, -denoted by l, and m, -the analogs of the atomic quantum numbers.

Measurements during large periods of time, and of a sufficiently large part of the solar surface, helped to discover in the traditional time frequency-space frequency diagramm, -the ω-k. diagramm- a fine structure, or even a sort of hyperfine structure.

What is the nature of these waves ?

One should at this stage recall the study made of the restoring forces. In the ω-k diagramm, the regions of the diagramm differ mostly by the kind of restoring

force which acts the more efficiently. They can be compressibility (giving place to pressure waves), or the gravity (gravity waves). The first is acting in a compressible medium, even in absence of gravity; the other acts in a hydrostatically stable medium, even in the absence of compressibility of the medium (for example, the Archimedes forces).

Without entering here into the well-known details of the theory, one can clearly show that the 5-minutes oscillations are identified as sound standing waves formed in a cavity between the top of convective zone and the bottom of the chromosphere, not far from the temperature minimum. They have a damping time of about 600 periods, or 1 day 1/2. We shall of course refer the reader to more extensive papers on the question such as those by Leibacher and Stein, by Ando and Osaki etc...

Another type of pressure mode oscillations, of about 3 minutes period, is associated with the trapping in the chromosphere; they have been observed with OSO 8, in an extensive way, by French and American groups and correspond to a cavity above the chromosphere.

Another type of waves, note easy to interpret completely, and associated with oscillations of the Sun as a whole, have been recently found by several groups of observers, firstly by Severny, Kotov and their associates, with a period of 2 h 40 mn. These oscillations, detected from radial velocity measurements, are visible also in solar diameter measurements made by Hill and associates. They seem to be low order gravity modes which penetrate entirely the convective zone, and are observable. Their existence, questioned for some time, is now established beyond doubt by the very observers who expressed the doubts the more seriously, Fossat and Grec, in Nice. They observed from the exact location of South Pole, during several no-stop sequences including one of 120 hours in a row, and, being so located, ruled out definitely any interpretation by a modulation due to terrestrial influence (2 h 40 mn being exactly 1/9 of a day). Moreover, the phase (assuming a period of exactly 2 h 40 mn) has been changing during the few years of observations, and the observers now agree with the value of 2 h 40 mn 1 s $\pm$ 0.1 s. for these oscillations; the amplitude is very small, of only 4 m s^{-1}. They correspond to a low radial $\underline{n}$-order. Why is this isolated frequency alone, without harmonics ? A coupling with the high precision clock which solar rotation is, has been advocated.

Oscillations being observed on the whole solar disk, one is tempted to think about pulsating stars, just in the same way as about the pulsating Sun. The theory has been elaborated, due to the extent of solar studies, so much, that predictions

could possibly be done in a near future in stellar cases. Observations of cepheids have mostly revealed radial pulsation internal gravity modes, of low order numbers. Not only the fundamental mode, but its harmonics, have often been observed. A good example is that of the β Cephei stars, another one that of γ Scuti variables. It is difficult to give here a complete survey and many other examples should be given.

We can quote also a recent example of non-radial modes observed by Myron Smith in the case of 53 Per. This star, of type O 4.5 V, displayed, in 1976-77, retrograde oscillations of periods 4.5 and 9.0 hours, in 1978 oscillations of 14.1 and 22.9 hrs in the prograde sense, through studies of line Si III 4552. Other stars (10 Lac, 22 Ori, ι Her, -of types OB-IV, V) seem to have a comparable behaviour.

Direct diameter oscillations are still out of the possibilities of stellar observers; but the possibilities of speckle interferometry and arrays of telescopes are still quite open, and might progress considerably. On the other hand, solar physics could progress from the study of cepheids and other variables. We should remember that the oscillations theory, has made much benefit out of the good early studies of the propagation of waves in oscillating cepheids.

3. Solar and stellar winds

The existence of the solar wind, between the Sun and the Earth, and beyond the Earth, is a rather well-known phenomenon. We know it through cometary tails studies, and through many spacecraft measurements at distances to the sun varying form less than 0.5 UA to several UA. Its basic properties are its variability and the fact that its characteristics can be explained by assuming large sectors of definite magnetic polarity from the solar photosphere throughout the solar environment.

Stellar winds, on the other side, are detected only through spectral characteristics, essentially through P Cygni profiles.

It is however possible (for example in the Rosette nebula or in the Trifid) to see cometary -like features, undoubtedly due to some kind of expansion or wind; but they teach us rather little on the properties of the wind.

The wind is essentially defined at a given time, and at a given point on the star by its flux of mass and by its velocity; altogether, the average velocity and the integrated loss are parameters which might be helpful to know. Clearly enough, there is not much correlation between these two parameters and the classical two parameters on the HR theoretical diagramm. Only can be found a very vague indication

that mass loss is more important for stars of high luminosity, cold or hot. Clearly, winds are associated with a rather slow decrease of density outwards (up to a decrease in r^{-2}), and this may be the origin of rather dense or thick chromospheres and coronae.

The winds are essentially variable, as can be easily and frequently observed in the UV or visible spectra of many O-B stars.

A difficult point is brought up by the question of gas accretion by hot OB stars. It can be shown that the collapse time of a pre main-sequence massive star is longer than the duration of its stay on the main sequence; in other terms, the protostellar cloud is still infalling, whenever the star is already formed and even evolved; and we do often observe winds ... How can these facts be compatible ? We should remember that rotation of the OB stars is rapid; hence the accretion may be polar, whenever the wind may be more or less equatorial ... It would be of a great interest to look at this question around the Sun : the existence of the solar wind does not necessarily exclude a certain amount of accretion, perhaps polar, in spite of the (small) rotational velocity of the Sun.

4. The solar and stellar surface spottedness

Variations in the spectrum, i.e. indicators of cinematical and physical variations in the outer layers, this is one aspect of the stellar activity, allowing to detect pulsations and winds ...

Another one is the spottedness of the active regions. For a long time, since the earlier works of Armin Deutsch, I believe, one thought that the irregular distribution of physical properties on the surface of stars could explain periodical changes, with the period of the rotation. This was the more often advocated cause for the variability of some Ap stars, and this idea was much developped for example in Moscow, by Khokhlova and her co-authors. However, should we compare that kind of description with solar spots ? Not really ... According Khokhlova, the difference between "metallic" regions and normal parts of the stellar surface is purely one in chemical composition, which makes of it, if true, a phenomenon quite different from the solar spots, -colder than the normal Sun but of about the same chemical composition.

It is difficult, in one respect, to compare the Sun to many very particular spotted stars; I mean to mention those stars of which one side is bright and hot, due to tidal effects, or illumination effects, linked with the existence of a close

bright companion. Many stars are members of double systems, and deeply influenced by this situation. The Sun is definitely not, -even if one assumes Jupiter to be a very small stellar-like object.

Do we have some hope to detect spottedness, at a scale larger than on the Sun, but of the same nature ? Drift-velocity curves, of some low excitation and low ionisation lines could indeed be looked at, to determine the rotation period. Periodical variation in the continuous flux should be associated with them. To my knowledge, not much has been done in this respect. It is obvious that if spots are similar to solar sunspots, they are not detectable as yet although the time may be very close to enable us to detect solar-like spots ... Even during maximum, the total solar flux is diminished by a small factor (of the order of 10^{-4} to 10^{-3}), not yet detectable on a star. On the other hand, very large spots would basically affect the whole stellar structure and modify magnetic fields, rotational behaviour and the like. The spot behaviour and the spot physical properties might then have nothing to do with that of the solar spots ...

The best hope to study stellar spottedness is the speckle interferometry which already allows us to observe directly the limb-darkening of some very large stars, such as Betelgeuse or Mira Ceti. Multimirrors systems, such as the MMT 10 meters-complex, or the arrays of distant mirrors now under construction by Labeyrie at the Cerga may be a promising technique. Wait and see ! The resolving power is now of the order of 1/100 th of an arc second; it can certainly be largely improved, only by the existing projects, such as the ones in the Cerga, in ESO, or in Arizona.

5. The solar flares and the flare stars

One of the most beautiful and conspicuous phenomenon that can be seen in an active solar region is of course the flare. Observable in X rays and in the radio-wavelengths, as a rapid function of time, and with rapidly changing spatial configuration in a complicated magnetic area of the solar surface active, they display a variety of properties of which we shall certainly talk much in the coming days. Their main characteristic is the output of energy in the form of radiation (emission lines, and enhanced continua), taken almost certainly from the reservoir of magnetic energy distributed all over the Sun and which can dissipate in a few decades, being rebuilt out from the rotational convective energy of the Sun.

On the other side, we know many types of flare stars. Not to speak about the very special cases of novae, or supernovae, we can mention the cold M stars, of type UV Ceti, and the T Tauri stars as typical of flaring stars. We should a priori

eliminate those stars of which the flaring is due to the dissipation of some obscuring matter such as are probably the stars of the type FU Orionis, for example, which drastically change their spectral type, from before to after the flaring.

But can the T Tauri and the UV Ceti benefit of our studies of flares, or can they conversely help us to better understand solar flares ?

Some cases may be quoted, of recent studies. In the case of YZ C Mi, Whitehouse has been proving the simultaneity of flaring in X-rays, radiowaves, and visible emission lines. In the case of BY Draconis, the flares seem superimposed on top of a cyclic variation of an amplitude of some tenths of magnitude, the flaring occuring near maximum periods of maximum light, suggesting a phenomenon similar to the solar cycle, but with a small cyclic period, and a large spottedness.

What can we say about SS433 ? To keep the eyes open is the only rule for the (solar) physicists. Some mechanism could be there at work that could be moderate on the solar surface; one is temptated to associate SS433 phenomena with bursts of type III, which moves through the solar corona with velocity of one third the velocity of light ...

The continuous survey of X-ray sources, together with optical studies of their visible counterpart is a very promising way of study of these flares, as shown at the Uchinoura launching station optical telescope by Matsuoka and his co-authors. An interesting case is that of the radio-source Sgr A, -the center of the Galaxy, which after all may be stellar-like, and which is certainly flaring in the X-ray.

As many phenomena are linked with optical solar flares, many must be associated also with the flaring of the flare stars. One has looked, unsuccessfully I believe, in the radio wavelengths, for possible flares of T Tauri, UV Ceti and other similar stars. I shall certainly be interested, during the course of this conference, to hear form our radio-colleagues what they do expect to observe in this respect in the coming years.

6. The solar and stellar magnetism

More difficult is still be study of stellar magnetism and its variation. There are methods which allow to determine the magnetic r.m.s. field, from magnetic intensification, i.e. from curve of growth analysis putting in evidence the differential behaviour of lines with high and low Landé factor. In the Sun (M. Fitremann, private communication) a stochastic r.m.s. field of 100 to 200 gauss seems to be present;

more studies are underway; in the stars, similar effects could be easily detected.

But the strong fields that are observed in the center of the umbra of a sunspot are seemingly out of reach, for the time being; a much better angular resolving power could only enable to get to it. The speckle techniques might do it, or the multimirrors, and arrays equipments. But this is not for tomorrow, -perhaps the day after tomorrow !

In stellar cases, the use of polarization is hardly a way to determine magnetic fields; the only possible way is to use the Zeeman splitting, in the spectrum of the whole stellar disk. Since 1948 one knows the general magnetic field of 78 Vir of the order of 500 Gauss. Many peculiar A stars have fields ranging from 100 to 30000 G, or so. Rayrole has shown for 53 Cam, that a 3800 G field exists. Unno, and Kato have been making use of other determinations. In many cases the field is variable. Often variations in the spectrum, or in the brightness, do confirm somewhat the comparison between spotted regions and non-spotted regions of the solar surface. It seems that the field strength and the luminosity are correlated sometimes (53 Cam) but often also anticorrelated ! On the Sun, it seems that there is some kind of compensation. Spots are cold, but faculae are hot with respect to the so-called quiet sun; as a whole, it is not obvious that the spotted solar surface at maximum activity surface is on the average darker than the solar surface at minimum solar activity.

Variations of the solar constant throughout the solar cycle have been seeked for, and only guessed; variation in the IR, anticorrelated apparently with the total brightness, indicate a change in the average structure, -but the spotted surface is so small than the solar effects can be considered as linked more to the facular behaviour. In the case of heavily spotted stars, it could very well be the reverse; and more studies, especially in the IR, could lead to interresting results.

Theories of stellar magnetism link it, as in the solar case, with the dynamo effect of the rotation combined with the existence of convective cells. To say nothing about the case of binary magnetic models, one should perhaps pay some attention to the oblique rotators theory, which incidently, allows to eliminate the consequences of Cowling well-known theorem (according which a completely closed and symmetrical poloïdal field would not be stable). The period of magnetism in oblique rotators is that of the rotation itself, and has nothing to do with the cycle. We should remember here that Trellis has shown from 150 years of heliographic data, in a way which has convinced only very few persons (but I am amongst the few) that the Sun was a very weak oblique rotator, the inclination of the axis being of the

order of 0.5 degrees; the magnetic axis precesses around the rotation solar axis with a period of about 7 cycles.

It may be interesting to note that magnetic fields exist in some cepheids; the effect of magnetic field on the structure and pulsational properties of cepheids may be sufficient to explain the discrepancy between masses of cepheids, when estimated either by the pulsational or by the evolutionary theories. Magnetic pressure has to come in the equations and to possibly make the trick.

7. The solar and stellar cycles of activity

One may identify active feature time changing phenomena, magnetisms or winds, on any given star. But another problem is the existence (or not) of a cycle of activity, undoubtedly to be linked with the internal structure of the star, taking into account the necessary coupling between : rotation; differential rotation (of course); convective motions at large scale, able to transport kinetic momentum; and the overall structure of the magnetic fields. It is even difficult to ask the question in a clear way ! When one sees a time-variation at any given scale, of any given feature, -can one say that it is an isolated phenomena, individual so to say (some large flare, localized, or some important explosive event) ? Or is it only the statistical result of events occuring individually, at much shorter time-scales, and statistically resulting in a quasi-periodic variation of the overall activity ? I do notwant to say much more at this stage !

Possible ways of detecting a cyclic activity could be seeked for in stellar studies, essentially through some of the studies we have mentionned earlier. Measurements of the overall magnetic field, behaviour of oscillations along the cycle (a study to be done also in the case of the Sun), behaviour of P Cygni profiles with time, evolutions of stellar winds, of chromospheric and coronal indicators, of flare occurrence... It means indeed a very large program of studies, but a very fascinating one, of which very little has been done so far, except precisely in the case of solar-like cycles by Wilson and associates.

Could we think over the detection of more than the 22 years cycle ? Grand cycles, like the Gleissberg 80 years or the Yoshimura 55 years, could they be detected ? Or even the Link 400 years-cycle ? They could be studied only for stars of which the normal magnetic activity cycle could be much shorter than that of the Sun. The case of BY Draconis might give a candidate for further studies ... But I feel we should be very patient and careful in that sort of blind studies, which are possibly not blind alleys !

Concluding remarks

It appears clearly that, in most of the fine structure active solar phenomena, especially those of which we shall speak in the coming days, it is not much, in a reasonable amount of time, that we can hope to observe in the stars. The vague behaviour of magnetic stars exists in the stellar world. But not much in term on physical understanding can be expected from their studies, except possibly the behaviour of a few phenomena with T_{eff} or with gravity ... So the Sun is still the only way to reach that kind of phenomena which certainly do affect deeply the stellar structure, without being yet observable in them in good enough conditions. We have two ways of approach in front of us. For faculae, active regions, flares in them, -the Sun may give hints towards the physics; the important parameters may emerge, and orient us to the study of those stars the more likely to display them. On the other side, the systematic study of what we can observe in stars, similar to solar phenomena, may orient the study towards a systematic statistical determination of the influence of T_{eff}, of g, etc ..., hence reorienting again the theory in one direction or another.

The Sun is an active star. All stars are active. Hence the study of solar activity is a prototype study for study of stars; just as the quiet Sun has been a prototype for the stationary description of stars, -now well advanced, but valid of course as an average solution description of any star, not more. On the other side, the study of active -like phenomena in stars may orient the theory of the mechanisms of solar activity. Clearly the theoreticians have to keep two eyes open, -and in two different directions ! It may be somewhat uncomfortable, but it may be very fruitful ...

BIBLIOGRAPHY

IAU Symp. n°56, 1973, "Chromospheric Fine Structure", R.G. Athay ed., Reidel,Dordrecht

IAU Symp. n°57, 1973, "Coronal disturbances", G.Newkirk ed., Reidel, Dordrecht.

Proceedings of the 1st European Solar Meeting, 1975, C.Chiuderi, M.Landini, A.Righini ed., in "Osservazioni e Memorie dell Osservatorio astrofisico di Arcetri".

Deuxième Assemblée Européenne de Physique Solaire, et coll. international du C.N.R.S., 1978, J.Rösch ed, "Pleins feux sur la physique solaire", CNRS, Paris.

Fifth European Regional Astronomy meeting "Variability in Stars and Galaxies", Liège 1980, under prep.

Proceedings of the S.O.T. Symp; NASA, GSFC, 24-25 janv. 1980.

Ayres,T.R. 1979, Ap.J., 228, 509.

Billings,D. 1966, A guide to solar corona, Acad.Press, N.Y.

Bray,R.J., Loughhead,R.E. 1964, Sunspots, Chapman & Hall, London.

Conti,P.S., Leep,E.M. 1979, Ap.J., 228, 224.

Doazan,V., Stalio,R., Thomas,R.N. Stellar individuality, observations and implications, IAU Coll n°59, Trieste 1980, under prep.

Evans,J.W., Michard,R., 1962, Ap.J., 136, 493.

Evans,J.W., Michard,R., Servajean,R., 1965, in de Jager: The solar spectrum, Reidel, Dordrecht, p.116.

Fontenelle,B., 1686, Entretiens sur la pluralité des mondes.

Fossat,E., Grec,G., 1980, in Fifth European Regional meeting on "variability in stars and galaxies", Liège.(under prep.).

Gilman,P.A. 1974, A.Rev.Astr.Astrophys., 12, 47.

Henry,R.C., Mihalas,D., 1964, Ap.J., 140, 873.

Inoue,H., et al., 1979, Ap.J.Lett., 227, L 85.

Kotov,V.A., Severny,A.B., 1980, in Fifth European Regional meeting on variability in stars and galaxies", Liège (under prep.).

Kuiper,G.P., 1953, The Sun, Chicago Univ. Press.

Leibacher,J., Stein,R.F., 1974, A.Rev.Astr.Astrophys., 12, 407.

Leibacher,J., Stein,R.F., 1981 in "The Sun as a star", NASA-CNRS monographs, under preparation.

Leighton,R.B., Noyes,R.W., Simon,G.W., 1960, Ap.J., 135, 474.

Leighton,R.B., 1963, A.Rev.Astr.Astrophys., 1, 19.

Matsuoka,M., avril 1979, Rapp. de l'Institut de Recherche Spatiale de l'Université de Tokyo.

Mihalas,D., 1972, Ap.J., 177, 115
1973, Sky and Telescope, 46, 79
1973, Ap.J., 179, 209.

Myron A. Smith, 1980, Ap.J.Supp., vol.42, 2, 261.

Pecker,J.-C., 1973, in Problems of calibration of absolute magnitudes and temperature of stars, IAU symp.n°54, B.Hauck and B.E.Westerlund ed., p.173-221, Reidel, Dordrecht.

Pecker,J.-C., 1965, in de Jager, the Solar spectrum, Reidel, Dordrecht, p.29.

Pecker,J.-C., Thomas,R.N., 1976, Space Sci.Rev., 19, 217.

Tandberg-Hanssen,E., 1967, Solar activity, Blaisdell publ., Waltham, Mass.,U.S.A.

Trellis,M., 1963, C.R. Acad. Sc. Paris, 256, 2300.

White,R.O., 1977, the Solar Output and its variation, Colorado Univ. Press, Boulder.

Yoshimura,H., 1979, Ap.J., 227, 1047.

Zirin,H., 1966, The Solar Atmosphere, Blaisdell publ., Waltham, Mass., USA.

THE SOLAR CYCLE - ITS INTERPRETATION IN TERMS OF A DYNAMO THEORY

Hirokazu Yoshimura
Department of Astronomy, University of Tokyo

First of all, I must explicitly state that this is not a review talk in usual sense. I concentrate on the progresses that I have followed myself over these 10 years. Some of you may feel the theory and the interpretation somewhat exotic and unfamiliar. As a matter of fact, however, the theory I will present here is a natural consequence of world-wide advancement of understanding of the solar cycle.

1. Observation

The phenomena of the solar cycle comprise every aspect of the solar activity and its related phenomena which show a definite cyclic behavior with 11 years period. Since the solar activity is a magnetic activity, the solar cycle represents an oscillating state of the magnetic fields in the interior of the Sun. The cycle period is doubled to 22 years when we take into account polarity of the fields. We shall consider here briefly the following questions:

(i) why are the magnetic fields created in the Sun?
(ii) why are the fields in an oscillating state?
(iii) how are they related to individual phenomena of the solar activity?
(iv) how does the solar cycle vary over longer time scales and why?
(v) what do the phenomena imply for studies of solar-like late type stars as well as stars of general categories?

Let me first remind you what the solar cycle is, and what characteristics of the phenomena we will consider to be basic for our understanding the phenomena. First, we know the time series of the sunspot relative number. This historical compilation of data is basic to our knowledge of the Sun and other cosmical objects in general. It tells us that the Sun, and a star in general, can be in a magnetically oscillating state. It tells us that the oscillating state can undergo various kinds of long-term modulations like the 80- or 55-year grand cycles or the series of Maunder Minima. Historical compilation of naked eye sunspots, as well as ^{14}C data

deposited in organic material on the Earth, as we will discuss later, suggest that the Sun is undergoing modulations of much longer time scales, like hundreds and thousands years. For its simplicity and easiness to obtain, the sunspot relative number should remain as an important index to register the long-term behavior of the Sun. Other indices so far devised, are either insensitive to the oscillating nature of the Sun or contaminated by other rather independent factors.

Secondly, we know the time evolution of surface distribution of sunspots and other solar active phenomena. We know the Maunder Butterfly Diagram of sunspots and the Diagram of Prominences by L. and M. d'Azambuja and by Ananthakrishnan. These diagrams show evolutionary structure of latitudinal distribution of the phenomena. When combined with its intensity and polarity and displayed by contour plots, the diagrams represent the following basic characteristics of the solar cycle:

(i) Schwabe-Wolf's law of the existence of the periodic oscillation of the sunspot occurrence,
(ii) Carrington-Spörer's law of the equatorial drift of the sunspot zones,
(iii) Hale-Nicholson's polarity rules of alternations in magnetic-field polarity of bipolar sunspot groups for the northern and southern hemispheres and for consecutive cycles,
(iv) the poleward migration of polar prominences,
(v) the slight indication that the sunspot zones also migrate towards the poles,
(vi) the cyclic variation of the number of higher latitude faculae and the phase shift between it and the lower latitude sunspot number variation.

In relation to the phenomena at the poles, we have

(vii) Babcock's law of polarity reversals of the solar polar fields.

Thirdly, we know the solar-cycle-associated changes of the corona and the related phenomena in the interplanetary space and the heliosphere. We know

(viii) the round shape of the corona at a maximum phase and its typical dipole-like shape with long streamers at the equator at a minimum phase of the solar cycle,
(ix) the equatorial migration of the low latitude coronal activity and the poleward migration of the high latitude activity as seen in 5303 Å lines,
(x) the Forbush's negative correlation between the solar cycle and the galac-

tic cosmic rays,

(xi) the negative correlation between the solar cycle and the high speed solar wind.

Fourthly, we come to know quite recently that

(xii) the rotational flows of the Sun also undergo solar-cycle-associated torsional oscillations.

According to Howard and LaBonte, the amplitude of the oscillations is on the order of 3m/sec. The wave pattern of the oscillations is symmetric about the equator and consists of four alternating zones of fast and slow rotation in a hemisphere. The whole pattern propagates from the poles to the equator with time scale of about 22 years. The latitude of maximum activity corresponds to the poleward boundary of a fast zone in low latitude zones.

These are the characteristics which have been known before the theory was developed. All of these are characteristics associated with one 22-year solar cycle. We will discuss later other characteristics associated with the long-term behavior of the solar cycle.

2. Theory

We now turn our attention to the theoretical aspect of the problem. In the development of understanding of the phenomena, we see a typical interplay of theory and observation. Theory is guided by hypotheses and their deduced consequences. Sometimes we see jumps of logic guided by intuition. These hypothesis and intuition will be verified later by observation. In fact, the theory of the solar cycle not only has given explanation and interpretation of the already known phenomena but also has predicted unnoticed characteristics of the phenomena which were later confirmed by analysing the observed data. The theory and the observation are progressing now side by side. Sometimes observation precedes theory and sometimes theory precedes observation.

We start from the governing equations; the well known equation of motions, the equation of continuity, the equation of energy transfer, and the MHD induction equation and the equation of magnetic flux conservation. If we can solve this set of equations for any general situations, any phenomena in astrophysics, where continuum approximation is valid, will be reproduced. However, this is impossible, at least at present, especially because the phenomena as we see in nature contain a multitude

of hierarchy of scales and so great variety of components. In such circumstances, we filter out the equations and simplify them using various kinds of approximations so that the equations are suitable for representing a phenomenon or a set of phenomena in mind, which are generally conceived by observing the nature. We do not ask whether the observation is correct or precise. Just a concept is enough at this stage.

2.1) The Concept of the Global Convection

In 1960's, a concept has emerged from the magnetograph observation of global distribution of magnetic fields at Mt. Wilson and from the statistics of sunspot proper motions of Greenwich Photoheliographic Results, that there seem to be giant scale flows in the Sun. Howard, Bumba, and Smith at Mt. Wilson thought it was convection, like the supergranulation, which was just discovered at those times. Ward, who analysed the sunspot proper motions, thought it was a kind of Rossby waves just like the general circulation in the Earth's atmosphere. The two kinds of flows correspond to the two of the three possible modes of motions in a rotating fluid sphere. The other is the sound wave modes with much shorter time scales. The difference between the former two is that vertical motions are important for the convective or gravity modes while horizontal motions dominate in the Rossby modes. Hence vertical heating is efficient to drive the convective modes while horizontal heating can easily excite the Rossby modes. Since no appreciable latitudinal temperature difference between the poles and the equator has been observed, the hypothesis of the Rossby waves in the Sun has eventually been dropped out. The effects of rotation on these two are also greatly different. So, we consider the convective modes hereafter and call it the global convection.

2.2) Linear Studies of the Nonzonal Velocity and Magnetic Fields

The first step is to study its linear structure and solve the linear set of equations for the velocity as well as magnetic fields. We study especially the effects of rotation on the field pattern. Even at this stage, it is known that the following important characteristics of solar activity can be understood if the global convection really exists in the solar convection zone:

(i) the existence of Unipolar Magnetic Regions (UMR's) and ghost UMR's and their rigid-body like rotation,
(ii) the existence of active longitudes and complexes of activity and their rigid-body like rotation,
(iii) the faster (slower) rotation of sunspots (magnetic features) than the averaged rotation of the solar mass in low (high) latitudes,
(iv) the preponderance of preceding spots of bipolar sunspot groups to the

following spots,

(v) the tilt of bipolar axes of the sunspot groups,

(vi) the forward inclination of normal axes of sunspots inferred from the east-west asymmetry of the appearance and total area of sunspots,

(vii) the association of the characteristics of an active region with the presence of an older active region in its vicinity and with the relative disposition of the two active regions; that is, according to Martres a sunspot group formed in the preceding sides of an older AR evolves to the type βf, the following spot showing a greater eastward motion than in the case of an isolated group, while a sunspot group in the following side of an older AR evolves to the type βp which is associated with a greater westward motion of the leading spot.

2.3) Formulation of the Equations governing the Zonal Fields

Second step is to study the second-order nonlinear effects of the flows. To study the effects, we perform another scaling. That is, we separate the fields into zonal fields $\langle Q \rangle$ and nonzonal fields Q'. The differential rotation and the general magnetic fields of the solar cycle are the zonal fields averaged over longitude. Nonzonal fields are fields that are associated with the global convection. We construct equations governing the zonal fields which contain the nonlinear effects of the nonzonal fields. Second-order correlation of the nonzonal velocity fields themselves shows that the global convection can transport angular momentum latitudinally and accelerate the equator preferentially. This problem depends on the modes of the convection which are achieved in the Sun and no final solution is obtained yet. Second-order correlation of the velocity and magnetic fields, which appears in the equation governing the zonal magnetic fields and which is deduced from the induction equation, gives rise to the growth of the magnetic field from an infinitesimal level of the field. In other words, the global convection can have the dynamo action. The governing equations thus obtained are as follows:

$$\frac{\partial \langle \underset{\sim}{H} \rangle}{\partial t} = \underset{\sim}{\nabla} \times (\langle \underset{\sim}{V} \rangle \times \langle \underset{\sim}{H} \rangle) + \underset{\sim}{\nabla} \times \langle (\underset{\sim}{V}' \times \underset{\sim}{H}') \rangle - \eta \underset{\sim}{\nabla} \times \underset{\sim}{\nabla} \times \langle \underset{\sim}{H} \rangle \quad , \tag{Eq.1}$$

$$\underset{\sim}{\nabla} \cdot \underset{\sim}{H} = 0 \quad , \tag{Eq.2}$$

which can be reduced to

$$\frac{\partial \Psi}{\partial t} = R\,\Phi + \left(\frac{(1-\mu^2)}{r^2}\frac{\partial^2}{\partial \mu^2} + \frac{\partial^2}{\partial r^2}\right)\Psi \quad , \tag{Eq.3}$$

$$\frac{\partial \Phi}{\partial t} = G\,\Psi + \left(\frac{(1-\mu^2)}{r^2}\frac{\partial^2}{\partial \mu^2} + \frac{\partial^2}{\partial r^2}\right)\Phi \quad , \tag{Eq.4}$$

where

$$\Psi = A\, r \cos\theta \ , \quad \Phi = B\, r \cos\theta \ , \tag{Eq.5}$$

$$\langle H_\phi \rangle = B \ , \ \langle H_\theta \rangle = \frac{1}{r}\frac{\partial}{\partial r} r A \ , \ \langle H_r \rangle = -\frac{1}{r\cos\theta}\frac{\partial}{\partial\theta}\cos\theta\, A \ , \tag{Eq.6}$$

and

$$G = (1 - \mu^2)\left(\frac{\partial\Omega}{\partial\mu}\frac{\partial}{\partial r} - \frac{\partial\Omega}{\partial r}\frac{\partial}{\partial\mu}\right) \ , \tag{Eq.7}$$

$$V_\phi = \Omega\, r \cos\theta \ , \tag{Eq.8}$$

and R is the regeneration factor. We normalize G and R by N_G and N_R, called the dynamo numbers representing the strength of the generation and regeneration processes. These equations are characterized by Ω and R.

Here we adopt a jump of logic and generalize the results obtained by the linear solutions using various approximations. We deform the profile of R topologically. If R is to be deduced from a certain type of flows, those flows can only be achieved in compressible stratified systems with proper effects of small scale turbulence.

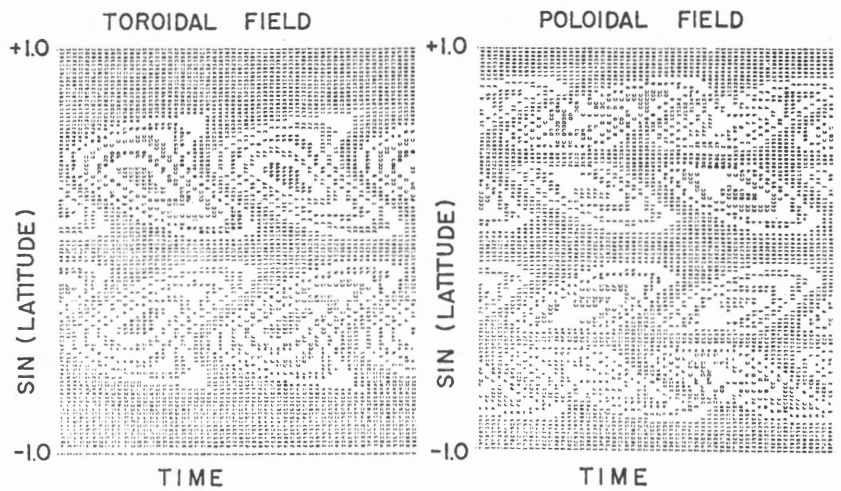

Fig. 1. The solar-cycle-simulating surface patterns of the solutions of the dynamo equation. The toroidal field pattern corresponds to the Butterfly diagram of sunspots. The poloidal field pattern corresponds to the Butterfly diagram of the surface poloidal general fields of Fig. 2.

In other words, a particular profile of R contains such various kinds of dynamics.

2.4) Linear Dynamo Problem and Characteristics of One Solar Cycle

Next step is to solve this set of equations, called the dynamo equations, for a given set of Ω and R. We solve them by a numerical method by computers. An example is shown in Figure 1. The equations up to this point are linear with respect to the general magnetic fields $\langle \underset{\sim}{H} \rangle$. Solutions of such equations become oscillatory waves which we call the dynamo waves. The characteristics of the dynamo waves as simulated by the equations can reproduce and explain the observed characteristics of the solar cycle described above. Growth of the solar magnetic fields and their oscillatory nature are thus attributed to the growth and oscillation of the dynamo waves driven by the differential rotation and the global convection. An interesting and basic property of the dynamo waves is that the waves propagate along isorotation surface of the differential rotation Ω. Since different set of Ω and R gives different set of surface pattern, we can infer the structure of Ω and R that are achieved in the Sun by choosing such set of Ω and R that give rise to the patterns which are similar to the observed ones.

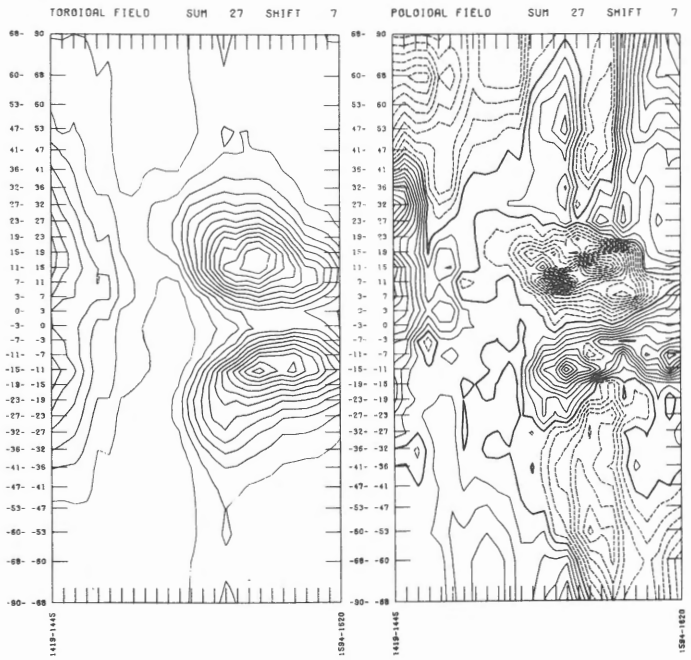

Fig. 2. The Butterfly Diagrams of the poloidal general magnetic fields (right) and of the toroidal general magnetic fields (left) deduced from the data observed at the surface.

At this stage, I myself encountered with a difficulty. The observed characteristics at those times could not determine how strongly the latitudinal gradient dominated the differential rotation. If the radial gradient exists, even slightly, the dynamo waves migrate towards the equator as the sunspot zones do. I needed an independent information to determine the degree of importance of the latitudinal gradient. The evolutionary surface pattern of the poloidal field, or of the radial component of the fields, could discern the cases with and without strong latitudinal shear. Especially the behavior of the fields at high latitudes was the key factor. So I analysed the data of the synoptic magnetic data, observed and accumulated at Mt. Wilson, and obtained the Butterfly Diagram of the poloidal fields as displayed in Figure 2. This diagram clearly shows that the latitudinal shear is important for the formation of the polar branches of the poloidal fields. At the same time, this diagram combines the various observations concerning the solar cycle phenomena at the polar region as listed above. This diagram gives a physical basis to the understanding of the prominence diagram of d'Azambujas and Ananthakrishnan. Although the latter does not have information concerning the polarity of the magnetic field, it does show that there certainly exist the polar magnetic branches migrating towards the poles.

Then I calculated the coronal magnetic fields associated with the solar cycle poloidal fields at the surface, obtained by theory as well as by observation. This study gave me interesting results. First, the coronal feild lines at maximum phases consist of many loops all over the globe so that the corona would look like a round ball as observed at maximum phases (see Fig. 3). The fields lines at minimum phases look like a dipole just like the real corona at minimum phases. At the same time, I noticed that the closed field lines at maximum phases and the open field lines at minimum phases can give us a unified interpretation of the solar cycle modulations of the galactic cosmic rays and the solar winds if the calculated coronal fields extend and fill out the entire heliosphere. Both cosmic rays and the solar wind are braked by the closed field lines at maximum phases but can stream in and out freely through open field lines at minimum phases. This gives us a sound basis of using ^{14}C data as deposited in the organic material on the Earth as a long-term indicator of the solar activity. At minimum phases, strong galactic cosmic rays produce many ^{14}C's in the Earth's atmosphere, while at maximum phases, the production is weakened. In fact, as Eddy analysed, the ^{14}C data revealed that the Sun underwent long-term modulations with time scales of hundreds and thousands years.

To discuss about the torsional oscillations with the same context of the linear

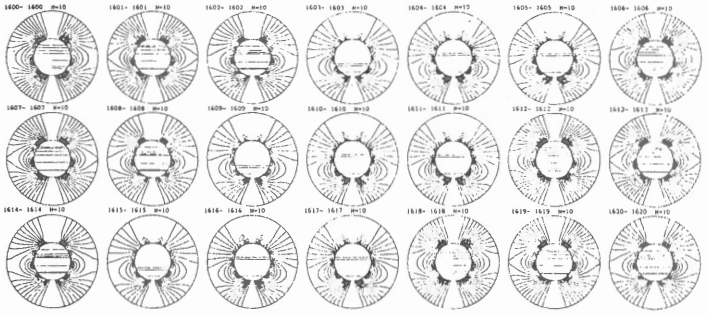

Fig. 3a. The dipole-like magnetic field lines of the corona at the minimum phase calculated from the surface fields of Fig. 2.

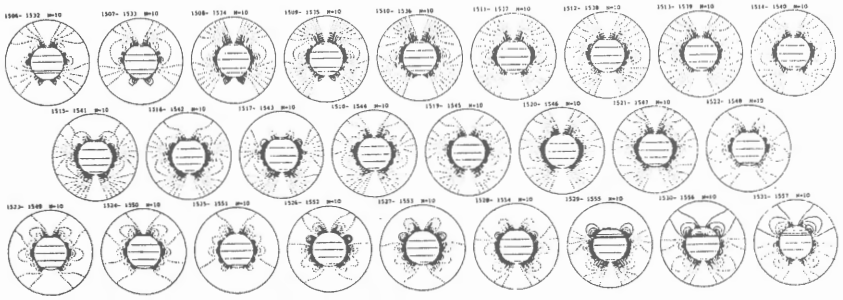

Fig. 3b. The round-shaped magnetic field lines of the corona with many loops during the maximum phase.

cases of the dynamo waves which are responsible for the characteristics of one cycle, I calculated the Lorentz force associated with the dynamo wave magnetic fields. The force consists of a nonoscillating part and an oscillating part, which I call the solar cycle Lorentz force waves. Only the nonoscillating part remains in the deep part of the convection zone. The oscillating part, which becomes conspicuous near the surface, has almost exactly the same pattern as that of the torsional oscillations (see Figs. 4 and 5). Rough estimate of excitation of the oscillations by the Lorentz force waves shows that the oscillations can in fact be driven by the force waves.

In this way, the characteristics of the solar cycle associated with one cycle can be understood in terms of the dynamo waves in the linear domain. The waves consists of a few mainly toroidal flux tubes that are successively created in the convection zone and are brought to the surface through formation of many active regions (see Fig. 5).

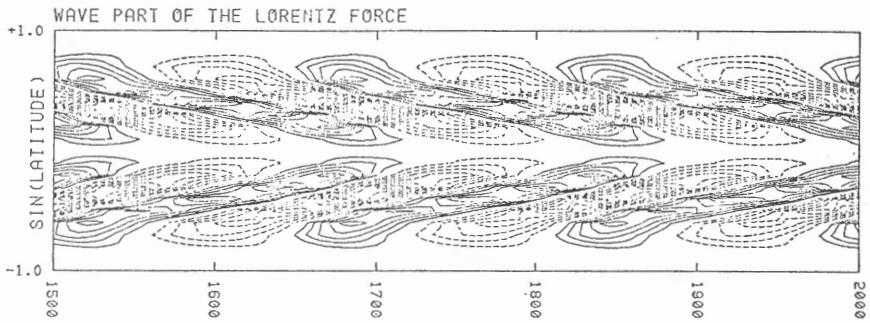

Fig. 4. The surface wave pattern of the Lorentz force of the dynamo waves of the solar cycle, simulating the pattern of the torsional oscillation. Ordinate is sin (latitude) and abscissa is time.

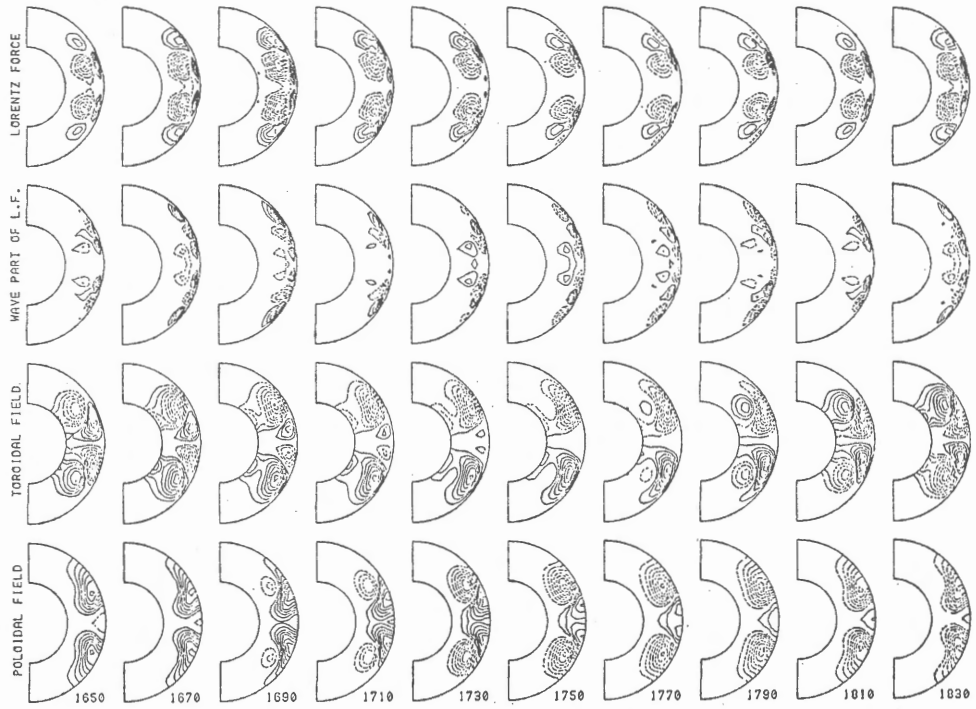

Fig. 5. Internal structures of the toroidal and poloidal general fields of the solar cycle, the longitudinal component of their Lorentz force, and its wave component. Numbers are time steps of the numerical integration of the dynamo equation.

2.4) Nonlinear Dynamo Problem

Next step is to study the long term modulations of the solar cycle. This is a nonlinear problem. There are two possible nonlinear mechanisms. One is through

eruption of the magnetic fields which depends on the strength of the fields. But this possibility was eventually ruled out because of its inefficiency and because of the existence of the Maunder Minima. For, in the Maunder Minimum, there were few active regions, so that the nonlinear effects should have been small and the dynamo should have operated strongly, which leads to a self-contradiction, provided the dynamo kept operating at those times. Another possibility is that the dynamo strength depends on the magnetic fields. In order to estimate the effects, however, we need to solve the full system of equations with the Lorentz force of the zonal as well as nonzonal magnetic fields. Before doing this, I did some numerical experiments, assuming an experimental formula for the dependence of the dynamo number N_G and N_R as follows

$$N_{G,R} = N^0_{G,R} \exp\left(- \sum_{i=1}^{N} a_{Ni} \left| \Phi\,(t - t_{di}) \right|^{N_{fi}}_{MAX}\right) ,$$

The formula represents the suppressive feedback action of the field on the flows and eventually on the dynamo processes. Since it takes time for the magnetic fields to influence the flows, I assumed a time delay in the feedback. Some interesting results of this study are the following:

(i) A long-term modulation with 80-year or 55-year period naturally results in the solar cycle oscillations with the basic period of 11 years when the feedback is represented by a single delay time parameter. The theory predicted a hysteretic relation between periods and amplitudes.

(ii) Higher-order modulations with time scales of hundreds and thousands year periods can be superposed on the modulated oscillation when the feedback is represented by multiple delay time parameters. Especially, the Maunder-Minimum-like eras with few surface activity but with oscillating internal fields can be reproduced.

(iii) With no time delay, the solutions becomes either stationary oscillations or stationary steady states. This opens a way to study in parallel the solar-like stars with oscillating fields, as O. C. Wilson observed, and the stars with steady fields like the Earth and possibly early-type magnetic stars with convective cores.

(iv) With time delay, the steady field solutions display occasional polarity reversals as observed for the case of the geomagnetic reversals.

(v) The theoretical prediction of the hysteretic relation between the periods and the amplitudes led to the discovery of the 55-year grand cycle in the observed solar cycle. (see Figs. 6 and 7). This is a new basic property of the solar cycle which any model of the solar cycle must take into

account.

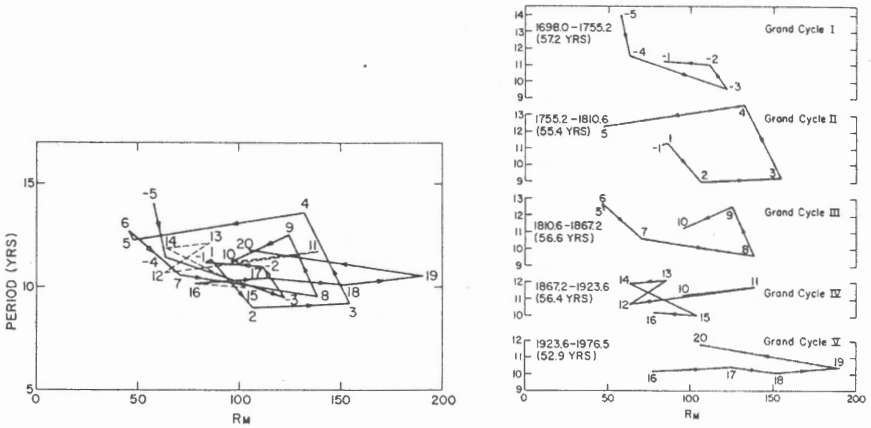

Fig. 6. Period-amplitude relation of the observed sunspot relative number curve. This shows that the solar cycle oscillation has a hysteresis and that the oscillation is undergoing the 55-year grand-cycle modulation.

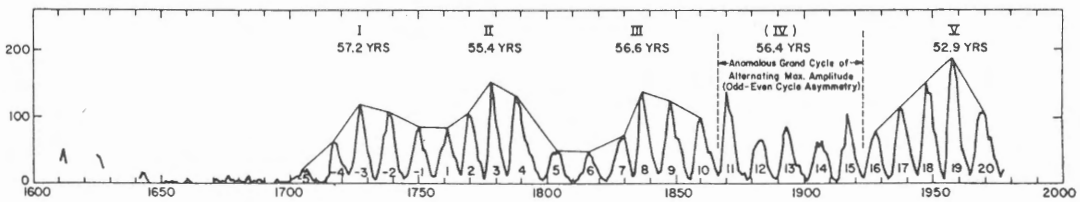

Fig. 7. The sunspot relative number curve divided into five 55-year grand cycles, each consisting of five 11-year cycles. Cycle 21 is the start of grand cycle VI.

In summary, we have a dynamo model to answer the five questions listed in the beginning of this talk. The magnetic fields of the Sun are created by the dynamo action of the differential rotation and the global convection. The oscillatory nature of the fields is a natural state of such dynamo processes. The global and local magnetic processes, associated with the dynamo mechanisms, which are operated by the differential rotation and the global convection, naturally cause the individual phenomena of the solar activity. The steady field-like geomagnetic field is a special state achieved by delicate nonlinear balance between the dynamo and the diffusion processes. This delicate balance is destroyed often and the field reverses its polarity in the oscillatory modes. The long-term modulations of the solar cycle with multiple-periods are also inherent and universal characteristics of the non-linear dynamo. With different Ω and R (i.e. with different convective structure

and different dynamical processes), magnetic fields of other stars may also be studied within the same context. However, the theory as well as observation are still incomplete. Both are progressing now side by side.

References

Interested readers are referred to the general references cited in the following papers on which the present talk is based:

Publ. Astron. Soc. Japan 23, 57-73(1971), 26, 9-51(1974)

Solar Phys. 18, 417-433(1971), 22, 20-33(1972), 33, 131-143(1973), 47, 581-600(1976), 50, 3-23(1976), 52, 41-52(1977), 54, 229-258(1977)

IAU Symp. 71, 19-35(1976), 71, 137-143(1976), 71, 409-413(1976)

Ap. J. Suppl. No. 294, 29, 467-494(1975)

Ap. J. 178, 863-886(1972), 201, 740-748(1975), 220, 692-771(1978), 221, 1088-1099 (1978), 226, 706-719(1978), 227, 1047-1058(1979), 235, 625-649(1980), submitted (1980).

THEORETICAL PREDICTION OF EIGENFREQUENCIES OF THE SOLAR FIVE MINUTE OSCILLATION

G. Berthomieu[1], A.J. Cooper[1,2], D.O. Gough[1,2], Y. Osaki[1,3], J. Provost[1], and A. Rocca[1]

[1]Observatoire de Nice, France

[2]Institute of Astronomy, University of Cambridge, UK

[3]Department of Astronomy, University of Tokyo, Japan

Abstract

Problems of calculating theoretical eigenfrequencies of the solar five minute oscillation are discussed. First, the numerical accuracy of calculations and uncertainty in physics, which might influence theoretical eigenfrequencies, were examined. It was found that the precision of our numerical calculations was good enough to compare meaningfully theory with observations. Then, the dependence of theoretical eigenfrequencies of five minute oscillation modes on the envelope structure of the sun was investigated. It was found that the p mode frequencies are quite strongly correlated with the depth of the convection zone. Comparison of theory with observation suggests that the solar convection zone is about 200,000 km deep.

1. Introduction

Recent observations by Deubner (1975, 1977) and by Rhodes, Ulrich, and Simon (1977) together with parallel theoretical development by Ando and Osaki (1975), and by Ulrich and Rhodes (1977) have now established beyond doubt that the solar five minute oscillation is identified as the global eigenmodes of the sun. This discovery has opened a new field of research called "solar seismology" in which observed oscillations may be used to probe the solar envelope structure (Gough 1977, Ulrich and Rhodes 1977). To achieve this objective, one must study the sensitivity of the computed eigenfrequencies to variations in both the basic solar model and the assumptions of the normal mode theory. In this work, we examine this problem, and results of theoretical eigenfrequencies are then compared with the most recent observations by Deubner, Ulrich, and Rhodes (1979) in the diagnostic (k,ω)-diagram.

2. The Equilibrium Models

The equilibrium models were constructed by combining the Harvard Smithsonian

Reference Atmosphere (HSRA) with envelope models calculated by using Vitense's mixing length theory for convection. The mixing length of convection, ℓ, was taken to be proportional to the local pressure scale height, H_p, and its ratio $\alpha=\ell/H_p$ was varied to obtain several equilibrium models with different depths of the convection zone. We have constructed models by integrating inwards from a point in the chromosphere to a depth of about 5×10^5 km.

One of equilibrium models was chosen as a standard because it was thought to match a model of the interior of the sun. It was used for various accuracy tests of eigenfrequencies. Its model parameters were: the hydrogen abundance X=0.745, the heavy element abundance Z=0.02, the mixing length ratio $\alpha=\ell/H_p=1.75$, and the depth of the convection zone $=1.95\times10^5$ km.

3. Method of Computations

Eigenfrequencies of oscillations were calculated mostly by solving the equations of linear adiabatic nonradial oscillations. The boundary conditions used were that the vertical displacement vanished at the base of the envelope and that the Lagrangian pressure perturbation vanished at the upper surface. The governing differential equations were integrated by second-order accuracy centred finite differences using the programme described by Baker et al. (1971), in much the same was as had been done by Ando and Osaki (1975, 1977). Subsequent improvements to the eigenfrequencies were made by substituting into variational integrals, which were evaluated to fourth-order accuracy.

4. Accuracy of Normal Model Analysis

Test were made for numerical accuracy by varying the number of mesh intervals N and using Richardson extrapolation to estimate the limiting eigenfrequencies as $N\to\infty$. It was found that eigenfrequencies calculated with 200 mesh intervals differed in most cases less than 0.1 % from those with $N\to\infty$. Comparison was also made between eigenfrequencies calculated by directly solving difference equations and those calculated from variational integrals. Their difference was again found to be small.

Having examined numerical accuracy, we have investigated sensitivity of eigenfrequencies upon several physical assumptions used. We computed nonadiabatic eigenfrequencies by treating radiative transfer in the Eddington approximation, and compared them with adiabatic frequencies. Eigenfrequencies of normal modes were also computed subject to various other upper boundary conditions: vanishing of Eulerian pressure perturbation and of vertical displacement, and matching to a running wave in an isothermal corona. The results depended upon the modes selected, but in all cases the deviations from the reference f and p mode adiabatic eigenfrequencies were less than the uncertainties in the corresponding observations.

5. Sensitivity of Eigenfrequencies on the Equilibrium Models

This analysis was performed by computing the changes in the eigenfrequencies of modes of degree (of spherical harmonics) ℓ=200 and 600 resulting from variations in the parameters determining the equilibrium model. Composition, the atmospheric T-τ relation, the mixing length were varied separately. Also, models were computed using a nonlocal theory.

Broadly speaking, the eigenfrequencies were most strongly influenced by the mixing length, which determines the adiabat deep in the convection zone and hence controls the depth of that zone. A model having larger α and hence deeper convection zone generally yields a lower frequency for a given p-mode, and its eigenfrequencies tend to fit better with observed ridges of five-minute oscillation in the (k,ω)-diagram. Eigenfrequencies calculated for the standard model with $\alpha=\ell/H_p=1.75$ and the convection zone depth of 195,000 km fit fairly well with observations, but they are still slightly higher than observations indicated. The results of calculations are illustrated in figure 1 for one of equilibrium models (with $\alpha=\ell/H_p=2.5$) that reproduced observations tolerably. This model had a convection zone 230,000 km deep. Figure 1 shows the frequencies of its lowest order eigenmodes, regarded as continuous functions of the horizontal wavenumber, superposed on the power spectrum of Deubner et al. (1979).

Changes in the atmospheric structure had very little effect on the f and p mode eigenfrequencies, except for the chromospheric modes. Thus we conclude that provided the eigenvalue analysis is a good representation of the five minute oscillations, the observations imply that the depth of the solar convection zone is at least about 2×10^5 km.

References

Ando, H. and Osaki, Y. 1975, Publ. Astron. Soc. Japan, 27, 581.

Ando, H. and Osaki, Y. 1977, Publ. Astron. Soc. Japan, 29, 221.

Baker, N.H., Moore, D.W., and Spiegel, E.A. 1971, Quart. J. Mech. Appl. Math., 24, 391.

Deubner, F.-L. 1975, Astron. Astrophys., 44, 371.

Deubner, F.-L. 1977, The Energy Balance and Hydrodynamics of the Solar Chromosphere and Corona, ed. R.-M. Bonner and Ph. Delache (G. de Bussac, Clermont-Ferrand), p.45.

Deubner, F.-L., Ulrich, R.K., and Rhodes, Jr., E.J. 1979, Astron. Astrophys., 72, 177.

Gough, D.O. 1977, The Energy Balance and Hydrodynamics of the Solar Chromosphere and Corona, ed. R.-M. Bonner and Ph. Delache (G. de Bussac, Clermont-Ferrand), p.3.

Rhodes, Jr., E.J., Ulrich, R.K., and Simon, G.W. 1977, Astrophys. J., 218, 901.

Ulrich, R.K. and Rhodes, Jr., E.J. 1977, Astrophys. J., 218, 521.

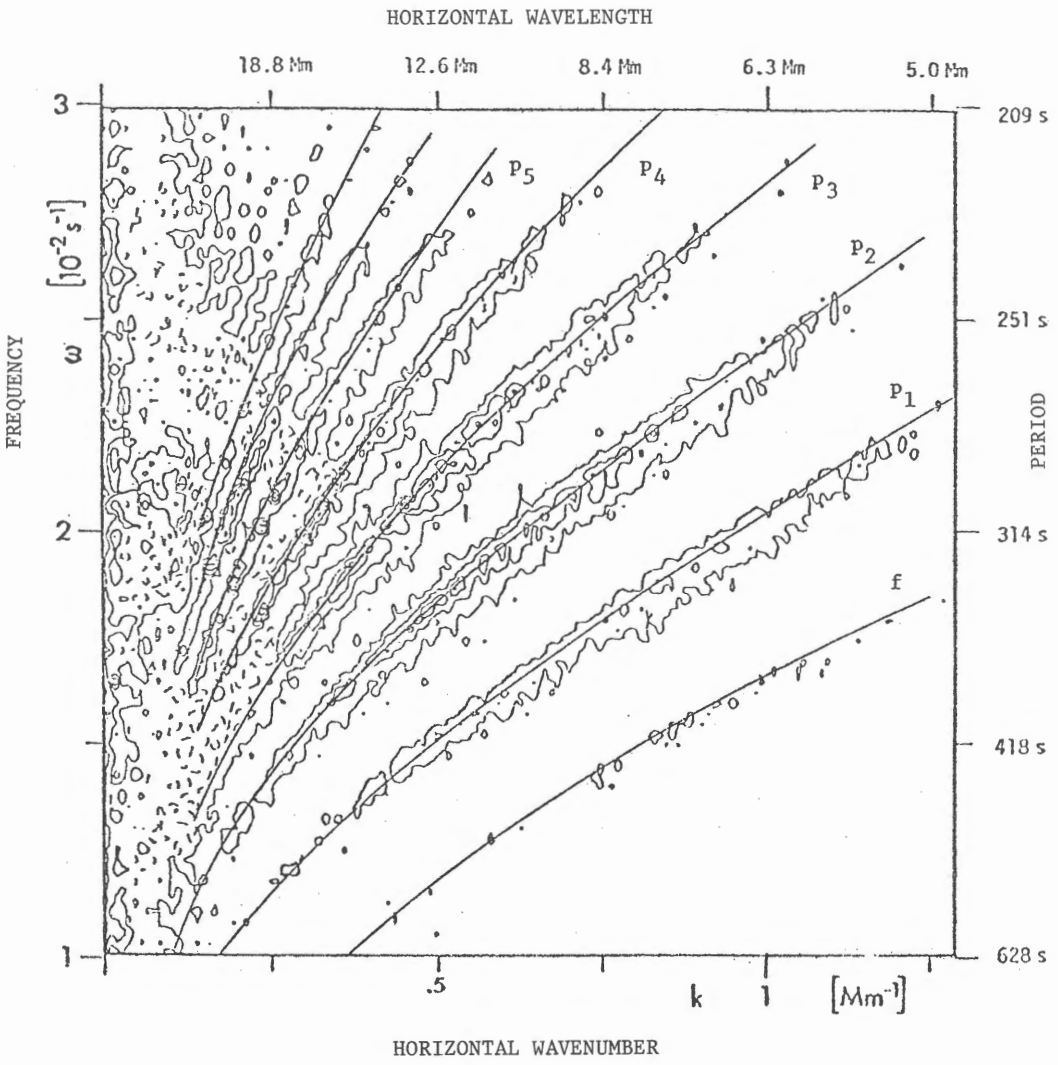

Figure 1. Eigenfrequencies of a model envelope, regarded as a continuous function of the horizontal wavenumber k, superposed on the power spectrum obtained by Deubner et al. (1979).

SOLAR PHENOMENA AS MHD MANIFESTATIONS

Wasaburo Unno
Department of Astronomy, University of Tokyo,
Bunkyo-ku, Tokyo 113

Abstract

Nonstatic characteristics are emphasized for plasma in magnetic tubes in different parts of the solar envelope. The subjects discussed here are the role of the magnetic buoyancy on statistical properties of the magnetic field in the convection zone, a photospheric dynamo driven by a horizontal vortex motion, and the siphon action in the MHD flow forming a dark filament.

1. Introduction and Summary

In a recent IAU symposium held in Kyoto, Nariai (1980) conjectured that stellar magnetic configurations could not be in static equilibrium in general. In fact, various spatial and temporal scales associated with mechanical and thermal processes are different with and without magnetic field, and gaseous motions usually occur in realistic situations in which the magnetic field is embedded over many scale heights in nonmagnetic medium. A sunspot is often considered as an example of a quasi-static magnetic structure. However, the Evershed flow in penumbre and an inflow in umbra in the chromospheric level are observed. A large extension above the photosphere seems to prohibit a hydrostatic equilibrium of a spot field. As Semel (1980) has shown in the present seminar, a hydrostatic configuration is not the low velocity limit of a steady flow configuration because of the constraint of the continuity of matter for the steady flow. Therefore, the hydrostatic assumption is not generally justified for the interpretation of quiescent solar phenomena. Three different topics will be discussed in what follows.

The first problem concerns with the formation of magnetic ropes under the influence of magnetic buoyancy. Parker (1975) argued that the magnetic buoyancy could set an extremely serious limit on the solar dynamo. Although it was over-estimated in his study (cf. Unno and Ribes 1976, Schüssler 1977), the magnetic buoyancy can still give a limit on the field strength. At least, it can be efficient for forming a rising flux rope distinguishable from fluctuations. The dimensional analysis will be given to describe roughly the state of magnetic flux

ropes in the convection zone.

The second problem is on the photospheric dynamo. An empirical law found by Martres, Soru-Escaut, and Rayrole (1973) describing the relation between the time variation of the field strength and the sense of rotation of the horizontal vortex motion depending on magnetic polarity is found to be fullfilled in a number of examples in the solar collaboration observations between Meudon and Mitaka (Martres et al. 1980). This law is here claimed to be the manifestation of the magneto-activity of the photosphere where the fluid motion can reform the magnetic field in significant degree. The third problem concerns with a dark filament. A steady flow model by Ribes and Unno (1980) aimed at the fitting to the observation by Mein (1977). Drastic transitions between the chromospheric state or a dark filament and a very high-speed low density flow of a coronal cavity are regarded as a characteristic feature of the chromosphere-corona region in a siphon composed of magnetic tubes.

Three problems discussed here are different aspects of solar magnetic field in different levels in the solar envelope. A lot of solar phenomena are still left to be unexplained magneto-hydrodynamically, and a lot of theories have to be worked out in order to obtain a complete understanding of the solar magnetic field.

2. Magnetic Ropes in the Convection Zone

The characteristic time scale of the solar cycle, ω_{sc}^{-1} (=2π/period) is determined by the association of the α- and ω-mechanisms (see, Yoshimura in the present seminar), and is about 3.6 years. The maximum possible field strength B_M was predicted by Galloway et al. (1978); $B_M \sim (\nu/\nu_m)^{1/2} B_{eq}$, where ν and ν_m denote the kinematic and magnetic viscosities, and B_{eq} is the equipartition field, $B_{eq}^2 = 4\pi\rho v_c^2$. For turbulent convection, we may take $\nu \sim \nu_m$. Then, the Alfvén velocity v_A corresponding to B_M turns out to be the convective velocity v_c. Remembering that the terminal speed of a buoyant magnetic tube is estimated to be v_A by Parker (1975), we see that the time scale of lifting is about 0.1 year from the depth 10^{10} cm where $v_c \sim 3 \cdot 10^3$ cm. This means that the dynamo wave propagates before B_M is reached by means of convection and that the magnetic buoyancy sets an upper limit to the magnetic field strength in the convection zone.

Let us now suppose that this upper limit of the field strength is realized during the solar cycle. The terminal speed of rise of a flux rope w is $\sim v_A^2/v_c$, if the turbulent viscosity is taken into account (Unno and Ribes 1976). The time of rise for depth D is then given by

$$\tau_b \sim D v_c / v_A^2 \quad . \tag{1}$$

On the other hand, the diffusion time τ_d in turbulent convection is given by

$$\tau_d \sim D^2 / (v_c \ell / 10) \ , \tag{2}$$

where ℓ denotes the mixing length and the numerical factor of 10 takes account of the efficiency of turbulent diffusivities (cf. Nakano et al. 1979). We assume that

$$\tau_b \sim \omega_{sc}^{-1} \sim \tau_d \ , \tag{3}$$

where the second approximate equality is necessary for the solar cycle to be completed. Then, we obtain

$$D \sim (10^{-1} \omega_{sc}^{-1} v_c \ell)^{1/2} \quad \text{and} \quad v_A \sim 10^{-1/2} (\ell / D)^{1/2} v_c \ . \tag{4}$$

If typical values are taken at a depth of 10^{10} cm in the convection zone so that $v_c \sim 3 \cdot 10^3$ cm s^{-1}, $\ell \sim 6 \cdot 10^9$ cm, $\rho \sim 5 \cdot 10^{-2}$ g cm^{-3}, then we obtain

$$D \sim 1.4 \times 10^{10} \text{ cm} \quad \text{and} \quad B \sim 500 \text{ G} \ . \tag{5}$$

The approximate agreement of D with the assumed depth 10^{10} cm means that the magnetic buoyancy could be marginally important for the solar cycle.

The conservation of the magnetic energy should also be considered. The decrease of B by rising motion is estimated to be $w|B|/D$. The increase of $|B|$ results from poloidal field stretched by the differential rotation $\Delta\Omega$. Then we have

$$|B_p| \sim |B| w / (D\Delta\Omega) \sim |B| / (\tau_b \Delta\Omega) \sim 20 \text{ G} \ .$$

Fluctuations must be inherent in the turbulent convection. Then, the increased buoyancy associated with fluctuations of larger field intensity will give rise to the formation of the flux tube. There is also the excess buoyancy due to the thermal inhomogeneity resulting from the differences in the superadiabatic temperature gradient and in the turbulent thermal conductivity in a magnetic tube (Unno and Ribes 1976). The latter thermal effect may be effective for the breaking up of a flux rope into the thickness of the order of a scale height, e.g., $6 \cdot 10^4$ km. The total magnetic flux of an active region would then be $\sim 10^{23}$ M_x. The enhancement of the magnetic intensity of a flux rope can be made in upper convection zone where the Alfvén velocity is fairly large and the hydraulic concentration becomes effective (Parker 1976).

3. Photospheric Dynamo

In the photosphere, ion motions are governed by collision with neutral atoms

that are the main constituent of the medium. Electrons, on the other hand, are more tightly bound to the magnetic field. These properties are essential to the photospheric dynamo (Sen and White 1972). Note, however, that the MHD processes in the photosphere are not independent of the situation in the convection zone as emphasized by Heyvaerts (1974) and Kaburaki (1975, 1979).

The polarity-helicity rule of a magnetic vortex (Martres et al. 1973) seems to be a typical representation of the photospheric MHD behavior. The magnetic field changes in time as if an electric current opposite in direction to the vortex motion is increased in the periphery of the magnetic region. Figure 1 shows the electric field E and the current j_r that are considered as common between the photosphere and the convection zone. The interpretation of the law is described elsewhere (Unno, Tanaka, and Semel 1980). The essential point is that electrons move with $v_{\theta,c}$ which is the rotating velocity of a deeper layer in the convection zone, while ions move with v_θ of the photospheric medium.

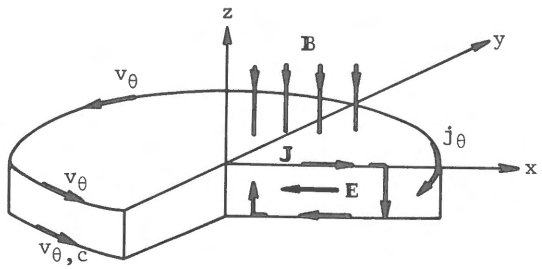

Fig. 1

The empirical law will then be explained by an increase of $(v_{\theta,c}-v_\theta)$ with time. The vortex motion may be brought by a large scale turbulent motion. Then, there will be the difference in time scale of the angular momentum transport between the photosphere and deeper layers. At a phase of large v_θ, the magnetic field is twisted and the torque exerted on the photospheric medium will decrease v_θ more rapidly than $v_{\theta,c}$ statistically.

4. Continuous Flow Forming a Dark Filament

Many MHD phenomena are observed in the chromosphere-corona regions. Flows are present in sunspots, faculae, spicules, moustaches, prominences, coronal arches, etc. Unresolved magnetic structures are discussed by Ribes (1980) and by Semel (1980) in the present seminar. Here, we regard a dark filament as a representative MHD event showing a drastic change in the thermal condition of plasma. Recently, Ribes and Unno (1980) constructed an analytical model of a dark filament and attempted to reproduce Mein's (1977) observational results by the parameter fitting. The model exhibits the physical characteristics similar to the Kippenhahn-Schlüter (1957) model within the filament, except that the matter is continuously replenished. The matter must be suspended by the magnetic field, if the free-fall of several $10^2\,\mathrm{km\,s^{-1}}$ should be avoided. The matter supply is due to a sudden condensation of an extremely rare-

fied high-speed plasma in the surrounding coronal cavity within a helmet structure. Also, the evaporation of filament matter into the coronal cavity should occur as the reverse process. Such discontinuous transition is controlled by the thermodynamics of the transition layer, and this is a characteristic feature of MHD in the chromosphere-corona region (cf. Leroy in the present seminar).

The model fitting to Mein's (1977) observation shows that the speed of flow should change from 0.2 km s^{-1} at the chromospheric foot point of a magnetic arch to 450 km s^{-1} into the coronal cavity, although uncertainties are involved. Also, the pressure at the foot-point is required to be ten times as high as the normal chromospheric pressure. The problem turns out to be the formation of a coronal cavity composed of a very high-speed low-density plasma. Low lying magnetic configuration (multiple component) may be particularly important, since it would provide high pressure and a geometry necessary for accelerating a Bernoulli flow along a magnetic tube.

References

Galloway, D. J., Proctor, M. R. E., and Weiss, N. O. 1978, J. Fluid Mech., 87, part 2, 243.

Heyvaerts, J. 1974, Solar Phys., 38, 419.

Kaburaki, O. 1975, Publ. Astron. Soc. Japan, 27, 45.

Kaburaki, O. 1979, Science Rep. Tohoku Univ., Ser. 1, 61, 232.

Leroy, J. L. 1980, present seminar.

Martres, M. J., Soru-Escaut, I., and Rayrole, J. 1973, Solar Phys., 32, 365.

Martres, M. J., Rayrole, J., Semel, M., Soru-Escaut, I., Makita, M., Moriyama, F., Tanaka, K., and Unno, W. 1980, in preparation.

Mein, P. 1977, Solar Phys., 54, 45.

Nakano, T., Fukushima, T., Unno, W., and Kondo, M. 1979, Publ. Astron. Soc. Japan, 31, 713.

Nariai, K. 1980, read at the IAU Symp. 1980 , Kyoto.

Parker, E. N. 1975, Astrophys. J., 198, 205.

Parker, E. N. 1976, Astrophys. J., 204, 259.

Ribes, E. 1980, present seminar.

Ribes, E., and Unno, W. 1980, Astron. Astrophys., in press.

Schüssler, M. 1977, Astron. Astrophys., 50, 439.

Semel, M. 1980, present seminar.

Sen, H. K., and White, M. L. 1972, Solar Phys., 23, 146.

Unno, W., and Ribes, E. 1976, Astrophys. J., 208, 222.

Unno, W., Tanaka, K., and Semel, M. 1980, submitted to Publ. Astron. Soc. Japan.

Yoshimura, H. 1980, present seminar.

SOME EVIDENCE FOR DOMINANTLY HORIZONTAL VELOCITIES IN THE PHOTOSPHERE

Jean Rayrole
Observatoire de Paris-Meudon

The magnetic field of active regions is one of the most studied parameters in present day Solar Physics.

Less studied but as important is the study of the velocity field.

During the next years a lot of research will be directed toward the understanding of solar flares and their relation to the magnetic and velocity fields. It is necessary to well know the main properties of the two vectorial fields before studying the instabilities regions.

We are not able to observe all the physical parameters necessary to solve the problems. By necessity, we have to simplify the MHD equations, keeping only the most important terms.

For instance, the continuity equation, in the case of structures by far larger than the density scale height of the photosphere indicates that the mass flow must be dominantly horizontal. Such a result can be directly shown from observations.

What do the observations give ?

Let us consider the coordinate axis defined in Figure 1. The longitudinal component of the velocity vector V is given by :

$$VL = V[\sin\psi \cos\phi \sin\theta + \cos\Psi \cos\Theta]$$

or $$VL = VH\cos\phi \sin\Theta + VZ \cos\theta$$

For $V \neq 0$, the longitudinal component will be equal to zero if :

$$\cos \phi = 1/\tan\psi \tan\theta$$

On the VL = 0 line the ψ angle cannot take any values ($\pi/2 - \theta \leq \psi \leq \pi/2+\theta$)

We are able to recognize the VL = 0 line (when $V \neq 0$) anywhere on VL maps all over the sun surface but the observed structures depend of the θ and ψ values :

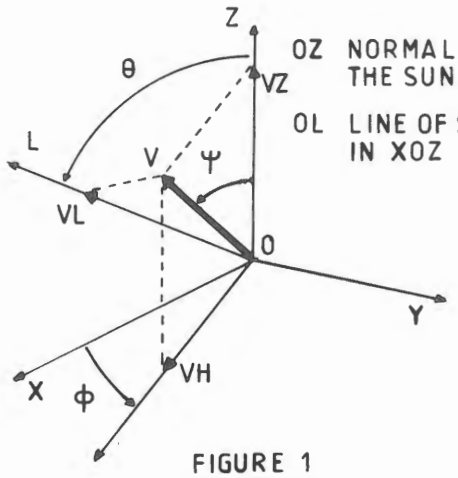

FIGURE 1

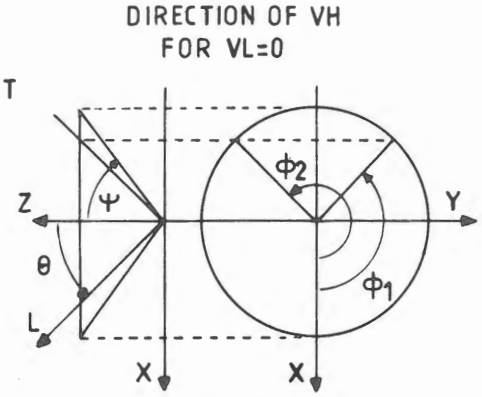

FIGURE 2

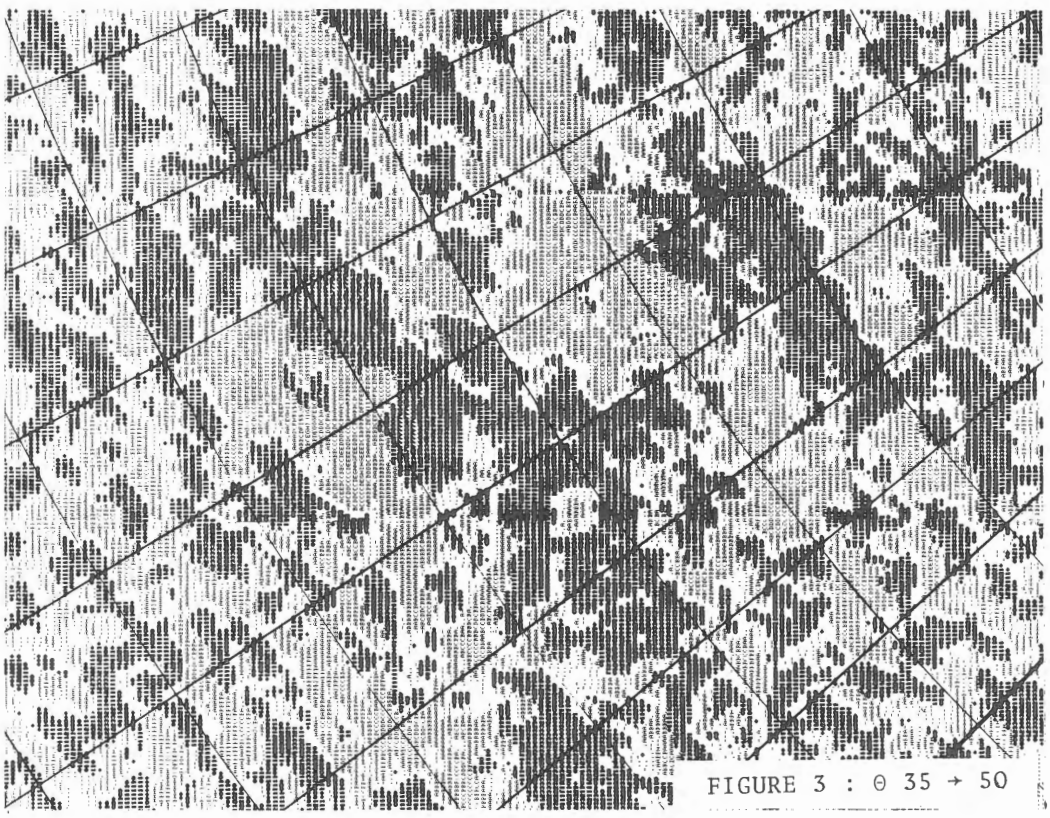

FIGURE 3 : Θ 35 → 50

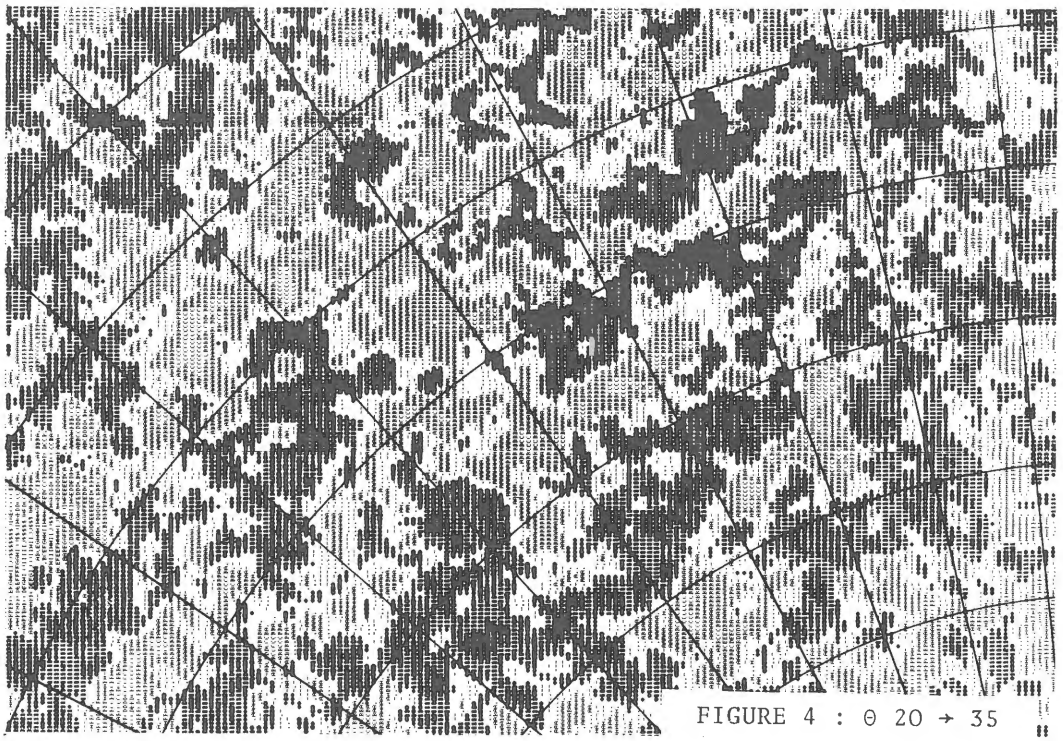

FIGURE 4 : θ 20 → 35

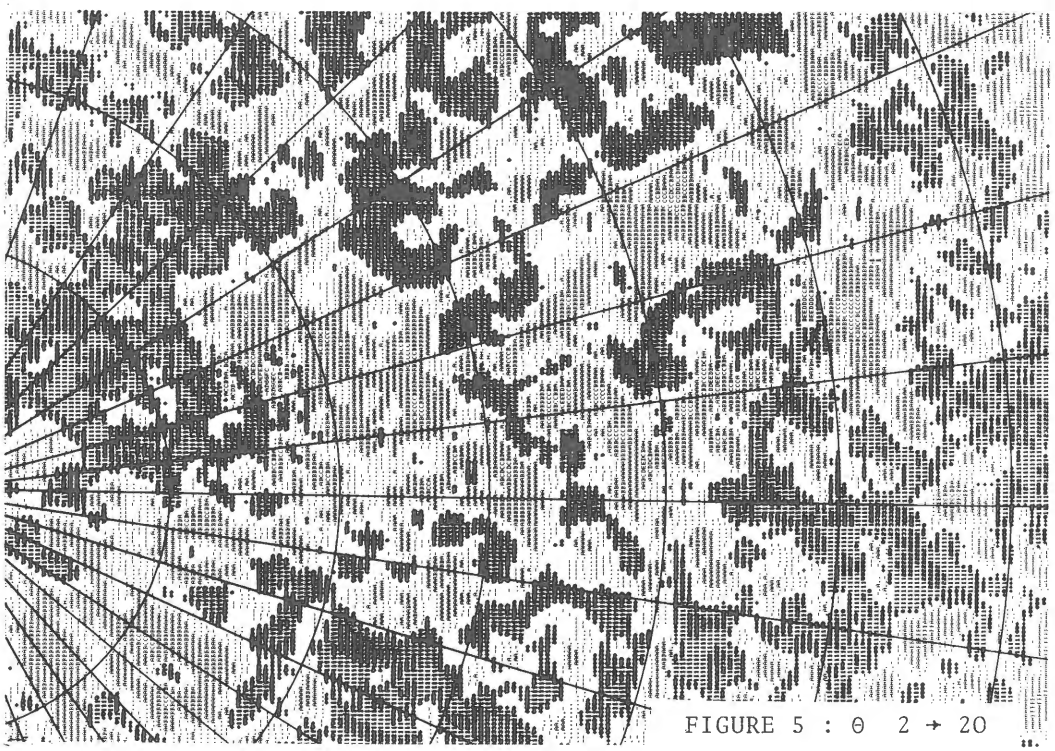

FIGURE 5 : θ 2 → 20

High θ values ($\theta > 35°$) : Most of the VL = 0 lines are perpendicular to the disk centre direction and some of them are directed toward it. Figure 3.

Mean θ values ($15° < \theta < 35°$) : Many VL = 0 lines are directed toward the disk center Figure 4.

Small θ values $\theta < 15°$: A new king of structures appears - "horse shoe structures". Figure 5.

The peculiar VL = 0 line directions and the center to limb effect on the visible structures show us that the mass flow in active regions is built up with "Vortex" or "Star type" horizontal motions with a weak vertical component.

How does such motions appear ?

The appearance of longitudinal structures ("Vortex" and "Star" motion) depends both of the θ and ψ values (Figure 2). If $\theta < \pi/2 - \psi$, then the observed structures do not show any inversion line VL = 0. For $\theta \sim \pi/2 - \psi$ we have the already defined "horse shoe" structures and for $\theta > \pi/2 - \psi$ two VL = 0 appear the angle between them increasing with θ.

Figure 6 shows that for a constant θ value (10°) the same results occur with Ψ variations. Figure 7 shows the observed structures for the four elementary "Vortex" and "Star" motions. (clockwise, counter clockwise, convergent or divergent flow). The absence of observed "horse shoe structure" anywhere on VL maps for high θ value (Fig. 3 and 8) proves that the mass flow in active region is dominantly horizontal.

Conclusion : The observations show a large scale organized horizontal mass flow which is of the greatest interest because it governs the evolution of active regions superimposed with it, small scale vertical motions, such as downward flow in magnetic tubes and local oscillations are also visible but it's not the object of this paper.

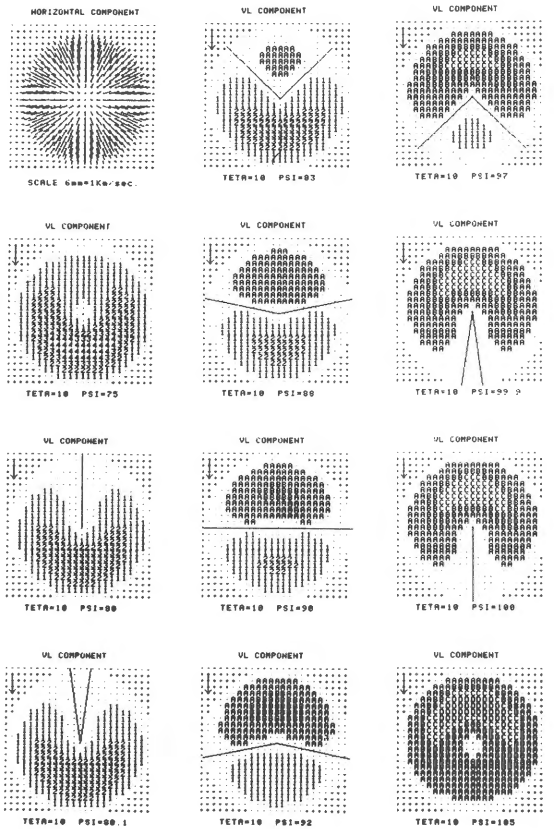

FIGURE 6

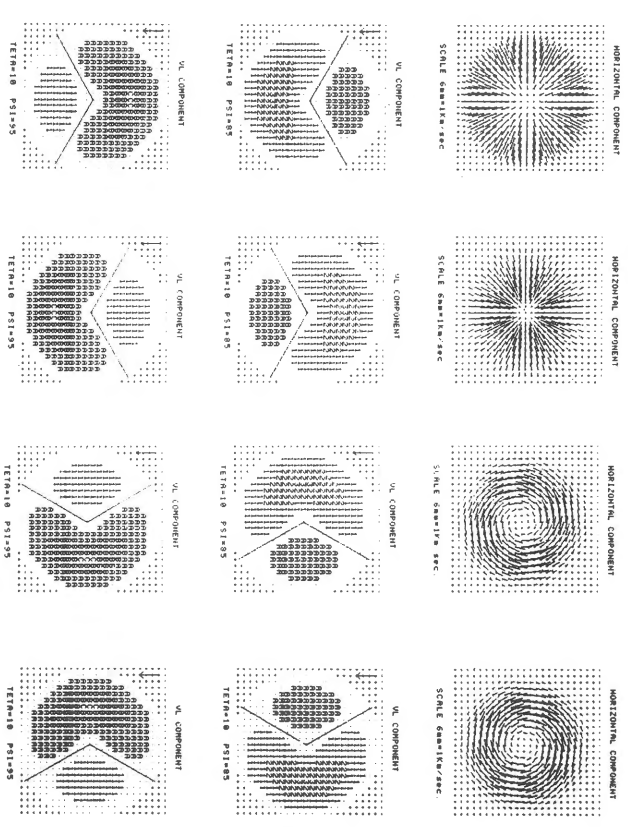

FIGURE 7

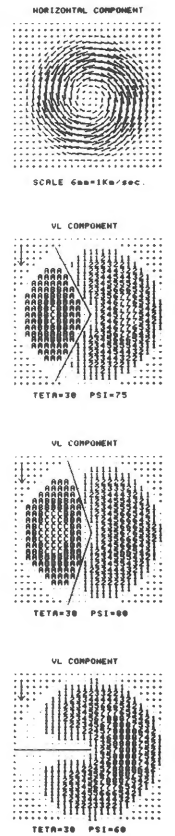

FIGURE 8

THE MAGNETIC FIELDS IN THE STELLAR PHOTOSPHERES

Kyoji Nariai
Tokyo Astronomical Observatory, the University of Tokyo

The theory of stellar atmosphere is, we may say in a sense, an applied solar physics. This is a great advantage for the part of stellar astronomers because, once solar physicists have a good theory on a solar phenomenon, stellar astronomers can apply it to stars with various values of gravity and effective temperature. However, it does not mean that this method always works well. Sometimes the theory turns out false after it is applied to stars as in the case of coronal heating by sonic waves. And sometimes a good theory for the solar phenomenon does not exist because solar physicists are content with semi-empirical models. In such a case, stellar astronomers are at a loss what to do or how to think because they have neither enough observational material to build a semi-empirical model nor a guiding principle for a theoretical study. A good example is the study of the region with strong magnetic field near the surface, i.e. sun-spots. Several theoretical attempts have been made of course, but they were unsuccessful. They do not provide any explanations concerning the fundamental characteristics of the sunspots such as, why the boundaries of the umbras and penumbras are sharp, why the spots are dark, what causes the Evershed flow, etc.

Many Ap stars are known to have strong magnetic field, the strongest average surface field observed being 34 kilo-gauss (Babcock 1958, 1960). These strong surface fields are believed to be related to some gigantic stellar spots. But, lacking the physical understanding of sun-spots, stellar astronomers cannot predict the behavior of these stellar spots. Therefore, their analysis is sometimes very primitive, and sometimes their research go further and further without checking the reliability of the first analysis on which their works are based. Let us see two important examples.

The gravity and the effective temperatures of Ap stars are comparable to those of late B-type main sequence stars. For the latter stars, $\log P$ is 3.1 at the reversing layer (Allen 1974). If we put the value equal to $\log (H^2 / 8\pi)$, we have approximately H=200 gauss. Therefore, at the surface of magnetic stars, the energy density of magnetic field is larger than the energy density of plasma by several orders of magnitude. It is clear that the atmospheric structure of magnetic stars is not determined without knowing the configuration of magnetic field. Yet, people analyse the spectrum of Ap stars with static plane-parallel models probably because they have sophisticated computer program for computing such models, and also because you solar physicists did not give them a recipe for making theoretical model of the region with strong magnetic field, the sun-spot.

Since Babcock (1958), it has been customary to use an equivalent dipole in order to represent the displacements of Zeeman lines in the two spectra corresponding to two circular polarization. Naturally, it should be considered as a convenient method of representing the average field strength in a simplified manner, and by no means, it should not be taken for granted that the stellar field is really dipole. However, many works have been done with the assumption of dipole field, and sometimes, with more sophisticated "de-centered dipole" or "quadrupole." In this example again, the dipole field or other force-free field was used because it was manageable. In other words, mathematical simplicity was more important than proper representation of physics of the system in their works. Of course, we do not have any guiding principle for the theoretical determination of the configuration of magnetic fields near the photosphere yet. But are we allowed to abandon the physics for that reason? I believe that the first thing we should do for the understanding of stellar spots is to know what physical processes are going on there. Then, we are able to describe the system. If we prefer mathematical or methodical simplicity, then we may have results in numerical form, but we are far from the true understanding of stellar spots.

As one of the trials to attack the problem, I showed in the IAU Symposium No. 93 which was held in July this year at Kyoto (Nariai 1980) that a static solution does not exist for the complex system of plasma, magnetic field, and radiation in the gravitational field.

Today I wish to talk about the behavior of a quasi-stationary magnetic tube filled with plasma moving along the tube. I assume that the atmosphere outside the tube is in quasi-static equilibrium. It is clear that plasma is closer to isentropic in the magnetic tube than in the ambient atmosphere because of the flow in the tube. Then, the stable position of a tube element for which the gravity and the buoyency cancel depends on the entropy gradient in the ambient atmosphere. We do not take the Lorentz force into account for the sake of simplicity. In a radiative atmosphere where $ds/dh>0$, a tube element is in stable equilibrium when it is horizontal. In a super-adiabatic environment ($ds/dh<0$), plasma in a magnetic tube is unstable against up and down motion. With regard to the slope, vertical position gives the stable state. In adiabatic zone ($ds/dh=0$), it is neutral against any change in its slope or height. These conclusions hold without regard to the direction of the flow. For a tube element in the

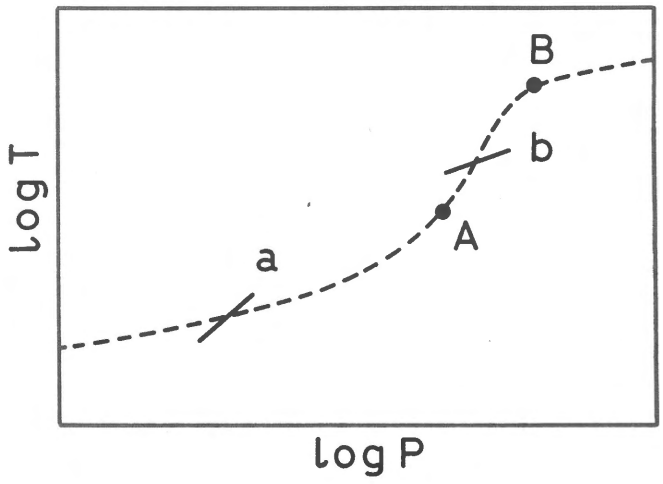

A schematic $\log P$ - $\log T$ diagram. A solar type atmosphere without magnetic field (dotted line) is divided into three parts, i.e. radiative zone (left of A), super-adiabatic zone (A to B), and adiabatic zone (right of B). Bold lines a and b correspond to adiabatic vertical tube elements in the radiative- and the super-adiabatic regions, respectively. Scale for $\log T$ is twice the scale for $\log P$.

existing structure which does not conform with our results, we may think either that the treatment of the tube and the ambient atmosphere is not good, or that the radiative process is rapid (or the motion of plasma is slow).

As the integration of ds/dx over the distance along the tube gives the inequalities between the entropy inside and outside of the tube, we can use our results not only to the tube and the ambient atmosphere, but also to a larger structure like sun-spots with appropriate corresponding assumptions. We may say that the penumbra or the region of Evershed flow is horizontal because the normal atmosphere at the same height is in radiative equilibrium, and that the wall of the umbra where it is supposed the Evershed flow comes from is vertical because the normal atmosphere at the same height is super-adiabatic. May we also conclude that the stellar photospheric magnetic field is almost horizontal as in the sun-spot penumbra because the atmosphere of B-type stars is radiative.

The direction of the flow determines its thermal character. If the ambient atmosphere is radiative, upward flow (or outward flow in the penumbra) is endothermic and the downward (or inward) flow is exothermic. The situation is opposite in a super-adiabatic region. This may be considered as a modification of adiabatic cooling by Russel (1921) applied to the flow in a magnetic tube. Departure from the ambient atmosphere depends on the heating time scale and the velocity of the plasma. It is easy to understand that the outward flow is below the inward flow for the penumbral region because originally the inward flow has higher entropy than the outward flow.

References

Allen, C. W. 1973, Astrophysical Quantities, 3rd ed. Athlone Press, p214.
Babcock, H. W. 1958, Astrophys. J. Suppl., 3, 141.
Babcock, H. W. 1960, Astrophys. J., 132, 521.
Nariai, K. 1980, Proc. I.A.U. Symp. No.93, Fundamental Problems in the Theory of Stellar Evolution, ed. D. Sugimoto et. al.
Russel, H. N. 1921, Astrophys. J., 54, 293.

NUMERICAL SIMULATIONS OF ACTIVE PHENOMENA IN THE SOLAR ATMOSPHERE

Kazunari Shibata
Department of Astronomy, Faculty of Science, University of Kyoto,
Kyoto 606, Japan

1. Introduction

The recent development of electronic computers have enabled us to solve nonlinear, nonsteady hydrodynamic or magnetohydrodynamic equations numerically. However, at present there does not exist such an almighty numerical scheme for solving these partial differential equations, as the Runge-Kutta scheme for the ordinary differential equations. Therefore in applicating numerical (magneto-) hydrodynamics to solar active phenomena, one is faced with many problems, e.g. selection of scheme, numerical instability, boundary condition and etc. Within a framework of the finite difference scheme, we first give a brief summary of these problems appearing in numerical (magneto-) hydrodynamics (Section 2). In spite of the immaturity of numerical (magneto-) hydrodynamics, applications to solar active phenomena have been done increasingly during the recent ten years and have developed solar physics. We next review the recent development of numerical solar (magneto-) hydrodynamics, especially applications to shock waves and jet phenomena (Section 3). Finally the limitations and the possibilities of numerical solar (magneto-) hydrodynamics in future are briefly discussed (Section 4).

2. Numerical (Magneto-) Hydrodynamics

2.1. Definition

We will define 'Numerical (Magneto-) Hydrodynamics' as the numerical simulation of (magneto-) hydrodynamical phenomena which is represented by the equations of conservations of mass, momentum, energy and magnetic flux, including the approximations of the incompressibility, the specified temperature and the nonmagnetic hydrodynamics.

2.2. Numerical Scheme

The schemes used in Numerical (Magneto-) Hydrodynamics are classified by their various characters, i.e. whether the grid is referred to space (Euler) or

mass (Lagrange); whether the space derivative is the past (explicit) of the present (implicit), that is, in the explicit case $\frac{\partial u}{\partial t} = \frac{\partial u}{\partial x} \rightarrow u_i^{n+1} - u_i^n = (u_{i+1}^n - u_{i-1}^n)/(2\Delta x/\Delta t)$, while in the implicit case $u_i^{n+1} - u_i^n = (u_{i+1}^{n+1} - u_{i-1}^{n+1})/(2\Delta x/\Delta t)$; what method is used to solve the original partial differential equations numerically, e.g. the finite difference method, the characteristic method and the finite element method. The most frequently used method is the finite difference method (FDM). This method is based on the direct approximations of the original partial differential equations to the difference equations, i.e. the finite difference approximations (Richtmyer and Morton, 1967). The characteristic method (CM) is also frequently used. In this method, the characteristic differential equations derived from the original partial differential equations are solved numerically (Hoskin, 1964; Richardson, 1964; Sauerwein, 1966). The finite element method (FEM) has not yet been used in solar physics (and probably in astrophysics) except for one case (Sakurai, 1976). This method is based on a variational teqnique known as Ritz's method (Strang and Fix, 1973). Although there are some methods other than these (e.g. Beam Scheme; see also Leibacher and Stein, 1975), almost all the methods used in solar physics can be classified into these three (see Table I).

The finite difference methods are also classified into many different schemes, i.e. the Lax-Wendroff (LW) scheme (Richtmyer and Morton, 1967), modified Lax-Wendroff (MLW) scheme (Rubin and Burstein, 1967), leapfrog scheme (see Roche, 1972), Flux Corrected Transport (FCT) scheme (Boris and Book, 1973; Book, Boris and Hain, 1975; Boris and Book, 1976) and etc. These schemes belong to the explicit and Eulerian ones in the finite difference methods.

2.3. Problems in Numerical Simulations

First of all, it must be emphasized that there is no almighty scheme, while there are many numerical schemes as shown in Section 2.2. Therefore we are faced with the problem of the selection of the scheme. The usual selection rule is as follows; (1) accuracy, (2) stability, (3) small computational time and (4) easiness of programing. The finite difference method satisfies this selection rule to a certain extent and has been used frequently. Therefore in later part of this section we will discuss about the problems appearing in the finite difference methods

The most serious problem in the finite difference methods is that of the numerical instability. For eample, in the Lax-Wendroff type scheme which is most frequently used, the numerical oscillations appears around the shock and the contact discontinuity. In some circumstances the amplitudes of these oscillations grow without limit, that is, the instability occurs. In the case of the shock

wave these oscillations can be removed by an introduction of the artificial viscosity (Richtmyer and Morton, 1967), but the oscillations around the contact discontinuity cannot be removed. FCT scheme significantly improved these behavors around the shock and the contact discontinuity (Boris and Book, 1973; Weber, 1978). As for the more detailed comparison of many FDM schemes, the reader is reffered to the review paper by Sod (1978).

The numerical instability is also produced by the reflection of the wave at the open boundary. Even if the instability does not occur, the reflection wave may affect the inner region of the numerical simulation. Therefore the boundary condition is very important (even for the characteristic method and the finite element method).

Mathematically a part of this problem is reduced to the mixed initial and boundary value problem. That is, the boundary condition must be compatible with the inner region. In the case of the one dimensional hyperbolic partial differential equations (e.g. compressible, inviscid and adiabatic MHD equations), this problem can be solved by the characteristic relations (Courant and Hilbert, 1962). Chu and Sereny (1974) applied these relations to the finite difference method. Nakagawa and Steinolfson (1976) introduced these relations to astrophysics and called them the compatibility relations. In the case of the two or three dimensional hyperbolic partial differential equations, however, the mixed problem has not yet been resolved mathematically (Nogi, 1979), although the characteristic relations can be formally constructed (e.g. Jeffrey and Taniuti, 1964; Richardson, 1964; Sauerwein, 1966; Shibata, 1979). The difficulty in multi-dimensional problem is originated from the fact that the chracteristic curve becomes the characteristic surface. From the same reason and the complexity of the formal characteristic relations, the multi-dimensional characteristic method (Richardson, 1964; Sauerwein, 1966) is not frequently used.

It should be noted that even the compatibility relations in one dimension cannot cmpletely remove the reflection of the wave at the open boundary. Hedstrom (1979) investigated a nonreflecting boundary condition for one dimensional hyperbolic equations. Rudy and Strikwerda (1980) also studied it for Navier-Stokes equations (see also Sundstrom, 1975; Orlansky, 1976; Gustafsson and Kreiss, 1979).

3. Applications to Solar Active Phenomena

In spite of the immaturity of Numerical (Magneto-) Hydrodynamics as shown

in the previous section, many simulations have been performed about solar active phenomena during the recent ten years. These simulations can be classified into following categories;

(1) sunspot and related phenomena---interaction between magnetic field and convection (2MHD) etc.
(2) acoustic waves and shocks in the photosphere and the chromosphere (1HD)
(3) jet phenomena---spicules and surges
(4) flare---thermal evolution (1HD) etc.
(5) coronal disturbances---MHD waves in the corona (2MHD) etc.
(6) others

(Some contents of them are summarized in Table I. Note that Table I does not include the numerical simulations of the dynamical phenomena associated with the solar wind because too many simulations have been performed in this field.) Since there is no space to review the whole contents of these simulations, we will confine ourselves to categories (2) and (3) in the following subsections.

3.1. Acoustic Waves and Shocks in the Photosphere and the Chromosphere

Although the title of this subsection does not seem to be related to active phenomena, the waves and the shocks are fundamentally important for understanding of the physics of active phenomena (see Section 3.2). Therefore we will present a simple review of the simulations in this category.

The first numerical simulation in this category was performed by Stein and Schwartz (1972). They computed the one dimensional vertical propagation of the single acoustic pulse including effects of radiation and ionization approximately, and compared the results with weak shock theory. Figure 1 shows a typical example of the acoustic wave propagation in the photosphere and the chromosphere, which is reproduced from the paper of Stein and Schwartz (1972). This figure includes almost all the fundamental physics of one dimensional propagation of acoustic waves and shocks in a stratified atmosphere. First, one sees in this figure that there is the formation of the shock wave from the finite amplitude acoustic wave. This is the well-known nonlinear effect. Second, the growth of the amplitude of the acoustic waves and shocks is found from this figure. This is also the well-known property of acoustic wave propagation in a gravitationally stratified isothermal atmosphere. (Note that in the solar photosphere and the chromosphere the temperature can be assumed to be constant within an error of factor two.) Third, the most interesting result in Figure 1 is the matter ejection by the passage of the shock wave in the upper chromosphere. Since the code used by Stein and Schwartz is the Lagrangian code, one will see in this figure that the matter

Table I Numerical Solar (Magneto-) Hydrodynamics

author (year)	dimension[1] HD or MHD	geometry[2]	energy[3] eq.	scheme[4]	level[5]	fundamental physics; application
[sunspot and related phenomena]						
Altschuler et al. (1968a,b)	2MHD(I)	r-z	T=const	?	ph	motion of ring current; Evershed motion, surge
Meyer et al. (1974)	2MHD(B)	x-y	cond.	Eu.Ex.	conv	interaction between magnetic field and convection, decay of sunspot, formation of intense fluxtube, running pennumbral waves
Peckover, Weiss (1978)	2MHD(B)	x-y	T=given	Eu.Ex.	conv	
Galloway (1978) Galloway, Moore (1979)	2MHD(B)	r-z	cond.	Eu.Ex.	conv	
Schüßler (1979a)	2MHD	x-y	T=const	FCT	conv	rising motion of horizontal flux tube due to magnetic buoyancy
Schüßler (1979b)	2MHD	x-y	T=given	FCT	conv	nonlinear dynamo
Cloutman (1979)	2HD	x-y	cond.	Eu.Im.	conv	convection; granulation
Shibata (1980)	1HD	along closed field (S≠const)	T=given	MLW	ph-ch	downflow in a rising flux tube; birth of sunspot
[acoustic waves and shocks in the photosphere and the chromosphere]						
Stein, Schwartz (1972, 1973)	1HD	r	rad.	Lag.Ex.	ph-ch	shock; heating of chromosphere
Kneer, Nakagawa (1976)	1HD	x	rad.	Eu.Im.	ph-ch	shock; radiative hydrodynamics; heating of chromosphere
Ulmschneider et al. (1977) Kalkofen, Ulmschneider (1977) Ulmschneider, Kalkofen (1977) Hammer, Ulmschneider (1978) Ulmschneider et al. (1978)	1HD	x	rad.	CM	ph-ch	radiative damping of acoustic waves, shock; heating of chromosphere
Gouttebroze, Leibacher (1980)	1HD	?	?	?	ph-ch	waves, oscillations; formation of Mg II K and Ca II K lines

Table I (continued)

author (year)	dimension HD or MHD	geometry	energy eq.	scheme	level	fundamental physics; application
[jet phenomena]						
Bessey, Kuperus (1970)	1HD	x	heating source fixed to mass	Lag.Ex.	ph-ch	shock, thermally driven gas motion
Steinolfson et al. (1979)	1HD	r	ad.	MLW	ch-co	mass ejection by the pressure gradient force; surge
Suematsu et al. (1980) } Shibata et al. (1980) }	1HD	x	ad.	MLW	ph-co	mass ejection by the shock wave and the pressure gradient force; spicule, surge
[flare]						
Hirayama, Endler (1975)	1HD	x	cond.	?	ch-co	conduction front, flare
Kostyuk, Pikelner (1975)	1HD	x	cond.	Lag.Im.	ch-co	conduction front, downward directed shock, heating by high energy electrons; flare
Kostyuk (1976)	1HD	along closed field (S=const)	cond.	Lag.Im.	ch-co	
Craig, McClymont (1976)	1HD	x	cond.rad.	Lag.Im.	co(pr)	conduction front, shock; heated flare filament
Henoux, Nakagawa (1978)	1HD	x	rad.	Lag.Im.	ph-ch	chromospheric response by irradiation of soft x-ray; flare
Antiochos, Krall (1979)	1HD	along closed field (S≠const)	cond.rad.	Lag.Im.	tr-co	conduction front, evapolation of chromospheric matter; flare
Nagai (1979)	1HD	along closed field (S=const)	cond.rad.	Eu.Im.	ph-co	conduction front, evapolation, downward directed shock; flare
Krall et al. (1980)	1HD	along closed field (S≠const)	cond.rad.	Lag.Im.	tr-co	conduction front, evapolation; long decay X-ray event
Smith, Auer (1980)	1HD			FCT		

Table I (continued)

author (year)	dimension HD or MHD	geometry	energy eq.	scheme	level	fundamental physics; application
[flare (continued)]						
Nakagawa et al. (1976)	2MHD	x-y	ad.	MLW	co	coronal response by emerging flux; infall impact theory of flare
Sokolov et al. (1977) Sokolov, Kosovichev (1978)	1MHD	x	joule heating	?	ph ch	instability due to local joule overheating; flare
Zeitsev et al. (1978)	1MHD	x		?	co	turbulent shock wave across magnetic field; moving cloud
[coronal disturbances]						
Nakagawa et al. (1975)	1HD	r	ad.	MLW	co	acoustic shock, coronal response by mass ejection; coronal transients
Wu et al. (1975)	1HD	r	friction	MLW	co	
Steinolfson, Nakagawa (1976,1977)	1HD	r	ad.	MLW	co	
Smith et al. (1977)	2MHD	x-y	ad.	MLW	co	MHD wave (fast mode), coronal response by flare or mass ejection; coronal transients
Nakagawa et al. (1978) Wu et al. (1978)	2MHD	r-ϕ(eq)	ad.	MLW	co	
Steinolfson et al. (1978) Dryer et al. (1979)	2MHD	r-θ(mer)	ad.	MLW	co	
[others]						
Browne, Bessey (1973)	1HD	x	rad.cond.	LW	ch-co	dynamical model of corona
Hildner (1974)	2MHD	x-y	rad.	LW	co	thermal instability; prominence formation
Kopp, Pneuman (1976)	1HD	along open & closed field (S$\neq$const)	T=const	CM	co	flow in moving magnetic flux tube; formation of loop prominence (post flare loop)

Table I (continued)

author (year)	dimension HD or MHD	geometry	energy eq.	scheme	level	fundamental physics; application
[others]						
Sakurai (1976)	3MHD		ad.	FEM	co(pr)	screw-mode instability of magnetic flux tube; eruptive prominence
Weber (1979)	2MHD	x-y	ad.	FCT	co	vertical neutral sheet; coronal streamer
Antiochos (1980)	1HD	along closed field (S≠const)	cond.rad.	Lag.Im.	co	thermal instability; formation of loop prominence (post flare loop)

1; e.g. 2MHD=2dimensional MHD, I=incompressible fluid, B=Boussinesq fluid

2; r-z=cylindrical geometry, x-y=cartesian, r=spherical, x=cartesian, S=cross section, eq=equatorial plane, mer=meridional plane

3; cond.=thermal conduction, rad.=radiation loss, ad.=adiabatic

4; Eu.=Eulerian, Lag.=Lagrangian, Ex.=Explicit, Im.=Implicit
FCT=Flux Corrected Transport Scheme, LW=Lax Wendroff scheme, MLW=Modified Lax Wendroff scheme, CM=Characteristic Method, FEM=Finite Element Method

5; ph=photosphere, ch=chromosphere, co=corona, tr=transition region, conv=covection zone, pr=prominence

which is initially located at the height of about 2000 km is ejected by the shock wave up to the height of more than 5000 km. This matter ejection is fundamentally the same as the spicule model of Suematsu, Shibata, Nishikawa and Kitai (1980). Finally, there is another interesting thing in this figure, i.e. a standing wave wake left behind the propagating acoustic wave (Lamb, 1932), which oscillates at the acoustic cut off frequency ($1/\tau_a$ = $c/(4\pi H) \approx 1/200\ s^{-1}$, where c is the sound velocity and H is the scale height). This is due to the dispersive effect of a gravitationally stratified atmosphere (i.e. the dispersion relation for an infinitesimal amplitude wave is that $\omega^2 = k^2c^2 + \omega_a^2$, where $\omega_a = \frac{2\pi}{\tau_a}$). This standing wave wake also becomes the shock wave at greater heights because of the nonlinear effect, and this recurrent shock waves produce the recurrent matter ejections. These results are also shown in the spicule model of Suematsu et al. (1980).

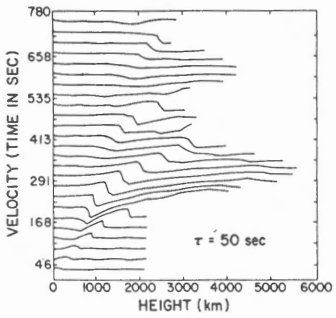

Fig. 1. Typical example of the acoustic wave propagation in the solar atmosphere, reproduced from Stein and Schwartz (1972).

After the computations of Stein and Schwartz (1972, 1973), many simulations have been performed in relation to the acoustic wave propagation in the solar atmosphere, improving the numerical scheme and the treatment of the radiation process (Kneer and Nakagawa, 1976; Ulmschneider et al., 1977; Kalkofen and Ulmschneider, 1977; Ulmschneider and Kalkofen, 1977; Hammer and Ulmschneider, 1978; Ulmschneider et al., 1978). However, the fundamental physics of the acoustic wave (and shock) propagation in the chromosphere is not significantly altered by these improvements because the radiative relaxation time is very large ($\gtrsim$ 100 sec) in this region (e.g. Giovanelli, 1978).

3.2. Jet Phenomena (Spicules and Surges)

Until quite recently, there was no time dependent jet model which agrees well with observations, although some simulations have been performed in order to account for surges (Altschuler et al., 1968) and spicules (Bessey and Kuperus, 1970).

Recently, however, the numerical simulations of the jet phenomena significantly developed. Steinolfson et al. (1979) presented the time dependent surge models for the first time, by performing one dimensional hydrodynamic simulations on the

assumption of adiabtic motion (Figure 2). In their models surges are constructed by the pressure gradient force which is the consequence of a sudden increase in pressure at the top of the chromosphere. On the other hand, Suematsu et al. (1980) presented the nonsteady spicule model for the first time, by using the similar method and assumptions to those of Steinolfson et al. (1979). In Suematsu et al.'s model, as described in Section 3.1, the jets are produced by the shock wave which is originated from a sudden appearance of the bright point in the photosphere or the low chromosphere. Therefore formation mechanism of the jet in the spicule model of Suematsu et al. (1980) is essentially different from that in the surge model of Steinolfson et al. (1979). Shibata et al. (1980) paid attention to this difference and computed various jet models whose roots

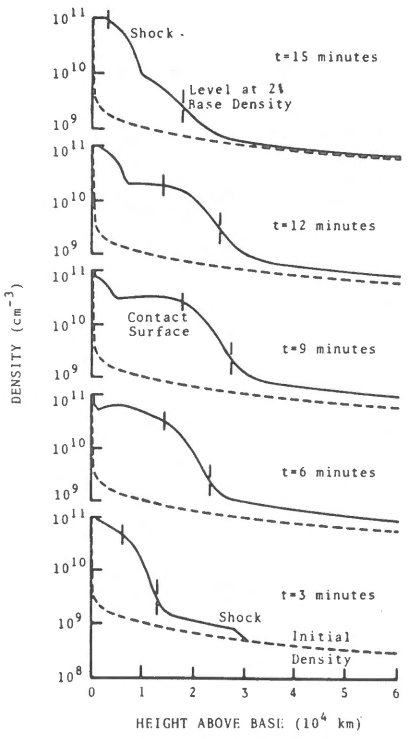

Fig. 2. Surge model of Steinolfson et al. (1979)

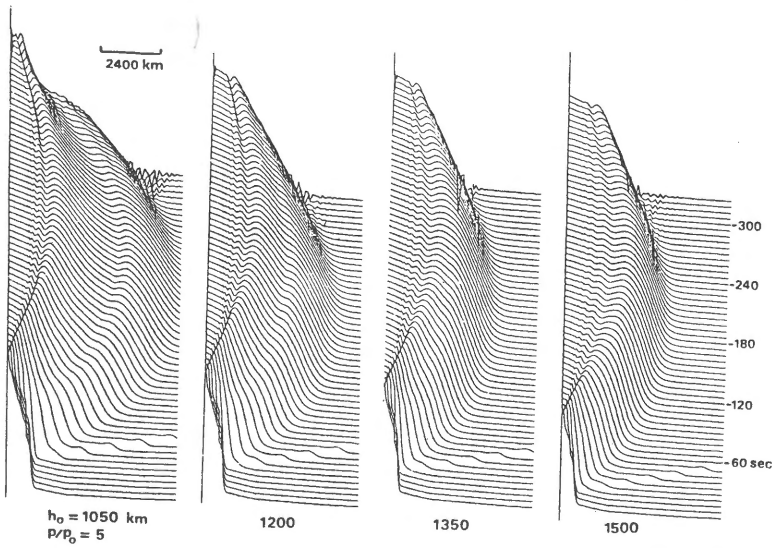

Fig. 3. Various jet models whose roots are located at various heights (h_0) in the chromosphere. The figures show the density.

(bright points or explosions) are located at various heights in the chromosphere, by performing one dimensional hydrodynamic simulations. The results are summarized as follows. The jets can be generally classified into two types. If the sudden pressure enhancements (bright points or explosions) occur below the middle chromosphere, the jets are constructed by the shock wave. Otherwise the jets are constructed by the pressure gradient force.

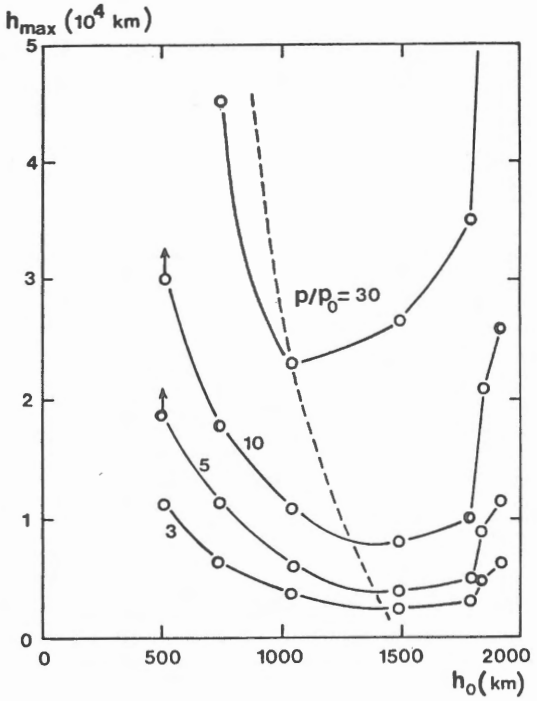

Fig. 4. Maximum heights of various jet models. The dashed curve denotes the critical heights (h_c) which separates two types of jet.

Figure 3 shows the example of the simulation results of Shibata et al. (1980). The h_0 is the height of the base of the model atmosphere, which is measured from $\tau_{5000} = 1$. The p/p_0 is the strength of the pressure increase at h_0. From this figure we see that there are two contact surfaces in the case of h_0 = 1050 km. The lower contact surface is ejected by the pressure gradient force, and the upper one is ejected by the shock wave. Since the upper contact surface corresponds to the top of the jet, it can be said that the jets in this type are produced by the shock wave. On the other hand, in the case of h_0 = 1500 km there can be seen only one contact surface, which is ejected by the pressure gradient force. The critical height (h_c), which separates two types, is about 1400 km for p/p_0 = 5. Figure 4 shows the maximum height of the jet as a function of h_0 for p/p_0 = 3, 5, 10 and 30. It should be noted that the local minimum (dashed line) corresponds to the critical height, i.e. in the right hand side of the dashed line the jets are produced by the pressure gradient force, and in the left hand side the jets are produced by the shock wave. The behavior of h_{max} curve can be qualitatively understood as follows. For $h_0 > h_c$, the jet materials are accelerated by the pressure gradient force per unit mass ($\frac{dv}{dt} = -\frac{1}{\rho}\frac{\partial p}{\partial z} - g$) near the base. Since the density (ρ) decreases with h_0, $\frac{dv}{dt}$ increases with h_0. Hence h_{max} increases with h_0. For $h_0 < h_c$, the jet matters

are accelerated by the shock wave. The strength of the shock wave decreases with h_0 for fixed p/p_0, because the growth of the shock wave decreases with decreasing the region of the shock propagation in the chromosphere (i.e. $h_{tr} - h_0$ decreases with h_0, where h_{tr} is the height of transition region). The h_{max} decreases with decreasing the shock strength. Thus h_{max} decreases with increasing h_0. It must be emphasized that the critical height ranges from 1000 km to 1500 km for $3 \leq p/p_0 \leq 30$. Hence, it is concluded that if the bright point (or explosion) occurs below 1000 km (middle chromosphere) the jets are constructed by the shock wave. This means that small surges associated with Ellerman bombs (Bruzek, 1974) are produced by the shock wave, because Ellerman bombs take place in the low chromosphere (Roy and Leparskas, 1973).

Finally we will mention that these two types of jet can be understood by the simple hydrodynamical principle. Figure 5 (a) and (b) represents the schematic

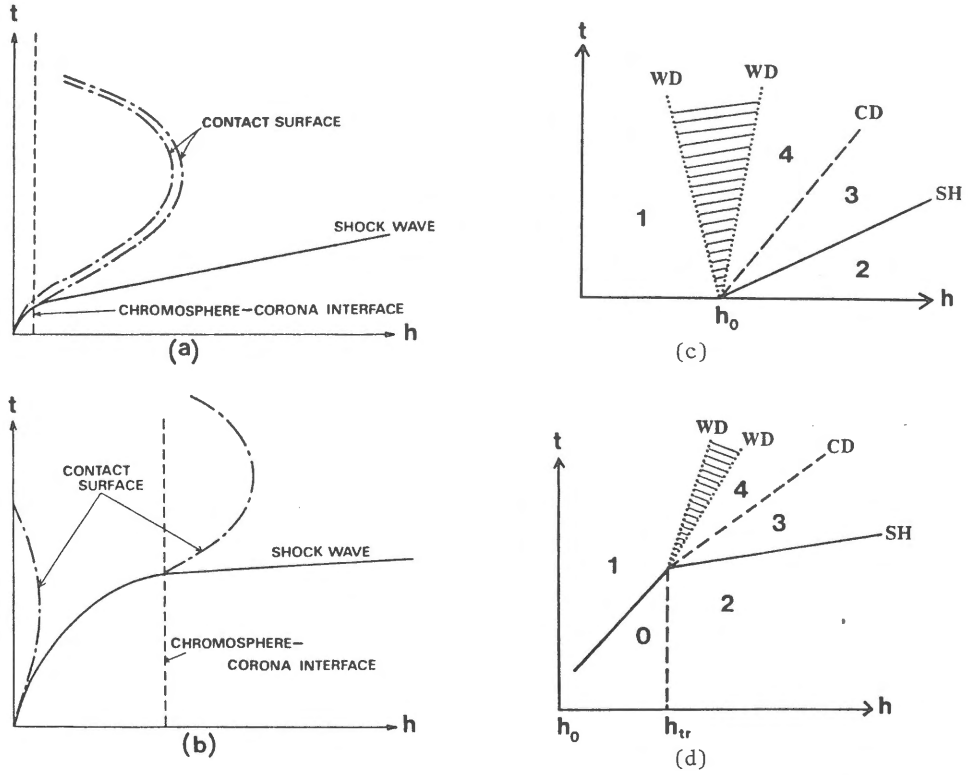

Fig. 5. Schematic diagram of the propagation of the contact surface and the shock wave for both types ((a) and (b)) and the idealized model of the initial discontinuity for both types ((c) and (d)).

diagram of the propagation of the contact surface and the shock wave for both types. An essential hydrodynamical structure of the jet in Figure 5 (a) is the same as that of the shock tube (Figure 5 (c)) if the gravity is neglected. On the other hand in the case of Figure 5 (b) the shock wave which has propagated through the chromosphere plays an important role for the formation of jet, and the final ejection of matter is determined from the collision of the shock wave with the chromosphere-corona interface (a kind of contact surface) as has been already pointed out by Osterbrock in 1961 (see Figure 5 (d)). Although the simulations are highly nonlinear and complex, the initial velocity of the shock propagation and the jet (contact surface) can be quantitatively explained by the idealized model of initial discontinuity in Figure 5 (c) and (d) (Shibata et al., 1980).

4. Prospects for Numerical Solar (Magneto-) Hydrodynamics

We will comment on the future possibility of numerical solar MHD from the view point of the computer's capacity. For example, let us consider whether or not 3MHD simulations or surges with similar method to that of Shibata et al. (1980) are possible. Since 1HD simulations (for the case of 200 grid points and 4000-8000 time steps) required 1-2 min by using Facom M200 at the Data Processing Center of Kyoto University, which is probably one of the most rapid cmputers in the world, 3MHD simulations ($200 \times 200 \times 200 \times$ factor) require more than 4×10^4 min ($\gtrsim 67$ hr). It is apparent that 3MHD simulations of surges are impossible at present and even in the near future. (These 3MHD simulations are also inhibited by the storage capacity of the computer.) However 2MHD simulations ($\gtrsim$ 200 min) are not impossible. (The intrinsic difficulty in the numerical solar MHD comes from the smallness of the scale height H in the photosphere and the chromosphere, e.g. $H \approx 150$ km at the level of T = 5000 K. As numerical computations require that Δz (grid size) $\lesssim H/10$ because of accuracy and stability, the vertical grid number becomes very large.)

References

Altschuler, M. D., Nakagawa, Y. and Lilliequist, C. G.: 1968a, Solar Phys. 3, 466.

Altschuler, M. D., Lilliequist, C. G. and Nakagawa, Y.: 1968b, Solar Phys. 5, 366.

Antiochos, S. K.: 1980, Astrophys. J. 236, 270.

Antiochos, S. K. and Krall, K. R.: 1979, Astrophys. J. 229, 788.

Bessey, R. J. and Kuperus, M.: 1970, Solar Phys. 12, 216.

Book, D. J., Boris, J. P. and Hain, K.: 1975, J. Comp. Phys. 18, 248.

Boris, J. P. and Book, D. L.: 1973, J. Comp. Phys. 11, 38.

Boris, J. P. and Book, D. L.: 1976, J. Comp. Phys. 20, 397.

Browne, S. L. and Bessey, R. J.: 1973, Solar Phys. 31, 351.

Bruzek, A.: 1972, Solar Phys. 26, 94.

Bruzek, A.: 1974, in Newkirk, G. Jr. (ed.), 'Cronal Disturbances', IAU Symp. 57, 323.

Chu, C. K. and Sereny, A.: 1974, J. Comp. Phys. 15, 476.

Cloutman, L. D.: 1979, Astrophys. J. 227, 614.

Courant, R. and Hilbert, D.: 1962, 'Method of Mathematical Physics', vol. 2, Interscience, New York and London.

Craig, I. J. D. and McClymont, A. N.: 1976, Solar Phys. 50, 133.

Dryer, M., Wu, S. T., Steinolfson, R. S. and Wilson, R. M.: 1979, Astrophys. J. 227, 1059.

Galloway, D. J.: 1978, Monthly Notices Roy. Astron. Soc. 184, 49P.

Galloway, D. J. and Moore, D. R.: 1979, Geophys. Astrophys. Fluid Dynamics 12, 73.

Gouttebroze, P. and Leibacher, J. W.: 1980, Astrophys. J. 238, 1134.

Gustafsson, B. and Kreiss, H. O.: 1979, J. Comp. Phys. 30, 331.

Hammer, R. and Ulmschneider, P.: 1978, Astron. Astrophys. 65, 273.

Hedstrom, G. W.: 1979, J. Comp. Phys. 30, 222.

Henoux, J. C. and Nakagawa, Y.: 1978, Astron. Astrophys. 66, 385.

Hildner, E.: 1974, Solar Phys. 35, 123.

Hirayama, T. and Endler, F.: 1975, Bull. Am. Astron. Soc. 7, 352.

Hoskin, N. E.: 1964, in Alder, B., Fernbach, S. and Rotenberg, M. (eds.), 'Methods in Computational Physics', vol. 3, Academic Press, New York and London, p. 265.

Jeffrey, A. and Taniuti, T.: 1964, 'Nonlinear Wave Propagation', Academic Press, New York.

Kalkofen, W. and Ulmschneider, P.: 1977, Astron. Astrophys. 57, 193.

Kneer, F. and Nakagawa, Y.: 1976, Astron. Astrophys. 47, 65.

Kopp, P. A. and Pneuman, G. W.: 1976, Solar Phys. 50, 85.

Kostyuk, N. D.: 1976, Soviet Astron. AJ19, 458.

Kostyuk, N. D. and Pikelner, S. B.: 1975, Soviet Astron. AJ18, 590.

Krall, K. R., Smith, J. B. Jr. and McGuire, J. P.: 1980, Solar Phys. 66, 371.

Lamb, H.: 1932, 'Hydrodynamics', 6th ed., Dover Publications, New York.

Leibacher, J. and Stein, F.: 1975, in Carel, R. and Steinberg, M. (eds.), 'Physique des Mouvements dans les Atmospheres Stellaires', Colloques Internationaux du Centre National de la Recherche Sci., No. 250, Paris.

Meyer, F., Schmidt, H. U., Weiss, N. O. and Wilson, P. R.: 1974, Monthly Notices Roy. Astron. Soc. 169, 35.

Nagai, F.: 1979, Ph. D. Thesis, Univesity of Tokyo, Japan.

Nakagawa, Y. and Steinolfson, R. S.: 1976, Astrophys. J. 207, 296.

Nakagawa, Y., Steinolfson, R. S. and Wu, S. T.: 1976, Solar Phys. 47, 193.

Nakagawa, Y., Wu, S. T. and Tandberg-Hanssen, E.: 1975, Solar Phys. 41, 387.

Nakagawa, Y., Wu, S. T. and Han, S. M.: 1978, Astrophys. J. 219, 314.
Nogi, T.: 1979, Private Communication.
Orlansky, I.: 1976, J. Comp. Phys. 21, 251.
Osterbrock, D. E.: 1961, Astrophys. J. 134, 347.
Peckover, R. S. and Weiss, N. O.: 1978, Monthly Notices Roy. Astron. Soc. 182, 189.
Richardson, D. J.: 1964, in Alder, B., Fernbach, S. and Rotenberg, M. (eds.), 'Methods in Computational Physics', vol. 3., Academic Press, New York and London, p. 295.
Richtmyer, R. D. and Morton, K. M.: 1967, 'Difference Methods for Initial Value Problems', 2nd ed., Interscience publishers, New York.
Roche, P. J.: 1972, 'Computational Fluid Dynamics', Hermosa Publishers, Albuquerque, New Mexico.
Rubin, E. L. and Burstein, S. Z.: 1967, J. Comp. Phys. 2, 178.
Rudy, D. H. and Strikwerda, J. C.: 1980, J. Comp. Phys. 36, 55.
Sakurai, T.: 1976, Publ. Astron. Soc. Japan 28, 177.
Sauerwein, H.: 1966, J. Fluid Mech. 25, 17.
Schüßler, M.: 1979a, Astron. Astrophys. 71, 79.
Schüßler, M.: 1979b, Astron. Astrophys. 72, 348.
Shibata, K.: 1979, Master Thesis, University of Kyoto, Japan (in Japanese).
Shibata, K.: 1980, Solar Phys. 66, 61.
Shibata, K., Nishikawa, T., Kitai, R. and Suematsu, Y.: 1980, submitted to Solar Phys.
Smith, D. F. and Auer, L. H.: 1980, Astrophys. J. 238, 1126.
Smithm Jr. J. B., Speich, D. M., Wilson, R. M., Tandberg-Hanssen, E. and Wu, S. T.: 1977, Solar Phys. 52, 379.
Sod, G. A.: 1978, J. Comp. Phys. 27, 1.
Sokolov, V. S. and Kosovichev, A. G.: 1978, Solar Phys. 57, 73.
Sokolov, V. S., Katsnelson, S. S., Kosovichev, A. G. and Slavin, V. S.: 1977, Solar Phys. 51, 293.
Stein, R. F. and Schwartz, R. A.: 1972, Astrophys. J. 177, 807.
Stein, R. F. and Schwartz, R. A.: 1973, Astrophys. J. 186, 1083.
Steinolfson, R. S. and Nakagawa, Y.: 1976, Astrophys. J. 207, 300.
Steinolfson, R. S. and Nakagawa, Y.: 1977, Astrophys. J. 215, 345.
Steinolfson, R. S., Schmahl, E. J. and Wu, S. T.: 1979, Solar Phys. 63, 187.
Steinolfson, R. S., Wu, S. T., Dryer, M. and Tandberg-Hanssen, E.: 1978, Astrophys. J. 225, 259.
Strang, G. and Fix, G. L.: 1973, 'An Analysis of the Finite Element Method', Prentice-Hall, Englewood Cliffs, New Jersey.
Suematsu, Y., Shibata, K., Nishikawa, T. and Kitai, R.: 1980, submitted to

Solar Phys.

Sundstrom, A.: 1975, J. Comp. Phys. 17, 450.

Ulmschneider, P. and Kalkofen, W.: 1977, Astron. Astrophys. 57, 199.

Ulmschneider, P., Kalkofen, W., Nowak, T. and Bohn, U.: 1977, Astron. Astrophys. 54, 61.

Ulmschneider, P., Schmitz, F., Kalkofen, W. and Bohn, H. U.: 1978, Astron. Astrophys. 70, 487.

Weber, W. J.: 1978, Ph. D. Thesis, Utrecht University, The Netherlands.

Weber, W, J.: 1979, Solar Phys. 61, 345.

Wu, S. T., Dryer, M., Nakagawa, Y. and Han, S. M.: 1978, Astrophys. J. 219, 324.

Wu, S. T., Dryer, M., McIntosh, P. S. and Reichmann, E.: 1975, Solar Phys. 44, 117.

Zeitsev, V. V., Parfenov, O. G. and Stepanov, A. V.: 1978, Solar Phys. 60, 279.

NUMERICAL HYDRODYNAMIC SIMULATIONS OF SPICULES

Yoshinori Suematsu
Department of Astronomy, Faculty of Science, University of Kyoto

1. Introduction

Solar spicules have intimate relations to the bright points in the network. (Stenflo, 1976). We suppose that the bright points at the footpoints of the spicule correspond to the bright elements of the photospheric network or faculae. According to Mehltretter (1974), the facular points appear and disappear within only 2-3 min. Therefore we investigate how the sudden heating at the photospheric level in a magnetic flux tube generates the spicule.

2. Method of Numerical Simulations

The idea and method of our simulations are similar to Steinolfson et al.'s (1979) who recently performed one dimensional hydrodynamic simulations of surges. We consider an initially static atmosphere in a vertically oriented magnetic tube. The static atmosphere has the temperature distribution given by HSRA model (Gingerich et al.,1971) and A model of Gabriel (1976). The pressure is enhanced abruptly by the heating at a base height (denoted by h_0) of this model atmosphere and the pressure enhancement (denoted by p/p_0) is kept for 5 min. The succeeding behavior of the atmosphere is pursued by solving hydrodynamic equations numerically by using the Modified Lax-Wendroff method with a artificial viscosity. The adiabatic motion and the constant cross section of the tube are assumed. From some empirical facular models we estimate h_0 in the range of 100-550 km and p/p_0 in the range of 1.1-2.2. The origin of the height is at the level of $\tau_{5000} = 1$ in HSRA model.

3. Results

The results of the simulations with parameters treated here are not qualitatively different each other. In Figure 1(a)-(b) we present the result which is gained when h_0 = 360 km and p/p_0 = 1.5. As seen in Figure 1(a), the pressure enhancement at the base generates a shock wave which gets strong as it passes upward through the chromosphere. Then the shock collides with the chromosphere-corona interface. As the result, the interface begins to move upward with average rising velocity of 30 km s^{-1} and reaches the maximum height of about 7000 km. The upward motion of the interface can be easily understood if one regard it

as a kind of contact discontinuity. Hence we can regard the cool and dense (see Figure 1(b)) chromospheric matter behind the moving interface as the solar spicule The spicule in our model shows nearly ballistic motion and recurrent behavior. The latter property is due to the shock generated by wake through a non-linear effect. The parameters $(h_0, p/p_0) = (0, 1.1), (180, 1.2), (540, 1.7)$ can yield the spicule whose height is 6000 km, while (180, 1.5) and (540, 3) yield

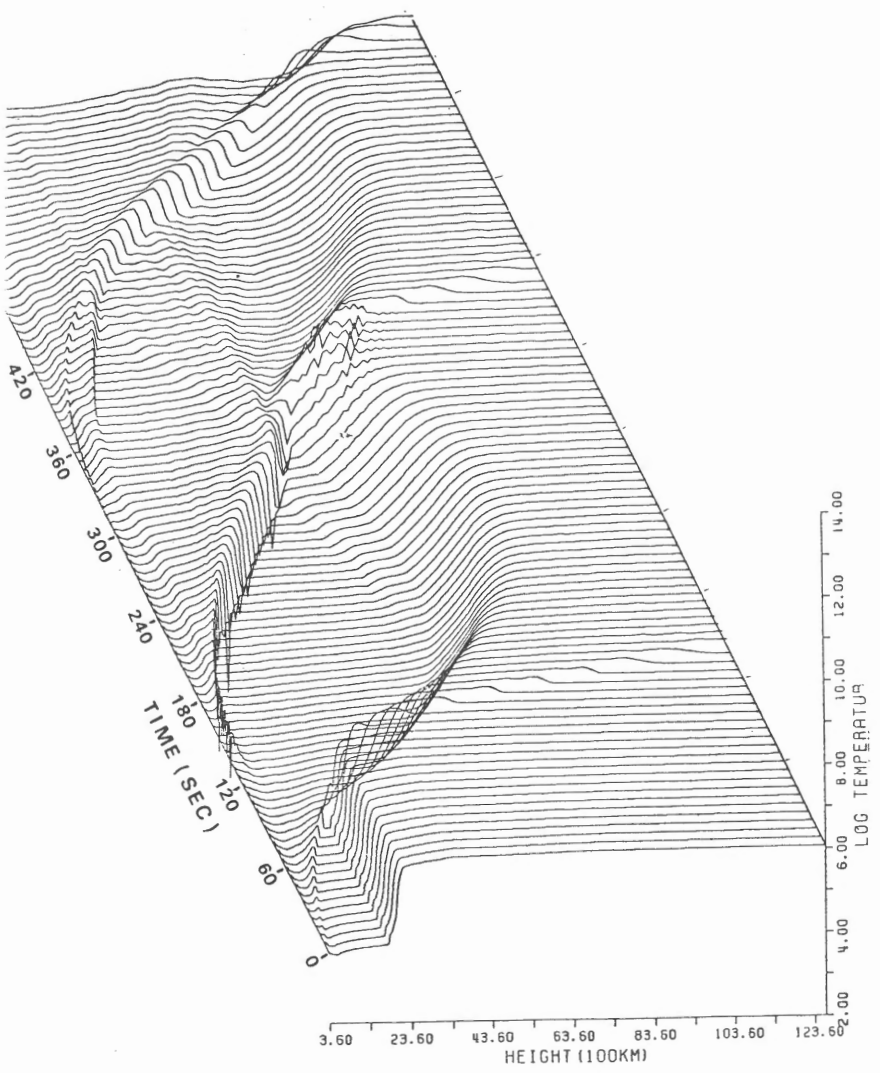

Fig. 1 (a)

the spicule with the height of 12000 km. These parameters do not conflict seriously with empirical facular models if the adiabatic pressure change corresponding to the maximum temperature excess of the facula is assumed.

Fig. 1 (b)

Fig 1(a) The time variation of the temperature distribution in the case of h_0 = 360 km and p/p_0 = 1.5. Each curve represent the profile of the temperature at every 6 sec. (b) The time variation of the density distribution.

References

Gabriel, A. H. : 1976, Phil. Trans. Roy.Soc. London, A281, 339.

Gingerich, O., Noyes, R. W., Kalkofen, W., and Cuny, Y. : 1971,
Solar Phys. 18, 347.
Mehltretter, J. P. : 1974, Solar Phys. 38, 43.
Steinolfson, R. S., Schmahl, E. J., and Wu, S. T. : 1979,
Solar Phys. 63, 187.
Stenflo, J. O. : 1976, in V. Bumba and J. Kleczek(eds.), 'Basic Mechanisms
of Solar Activity', IAU Symp. 71, 69.

OBSERVATIONAL PROOF OF THE INEFFICIENCY OF THE CORONAL HEATING BY ACOUSTIC WAVES

P. Mein, N. Mein, B. Schmieder
Observatoire de Paris Meudon

We know that pressure waves do exist in the solar photosphere and chromosphere. Since 1962, (Leighton et al. ; Evans, Michard) oscillations have been detected in dopplershifts and intensity fluctuations of line profiles. The period range is around 5 mn in the photosphere and 3 mn in the chromosphere. The location in the (k, ω) diagnostic diagram corresponds to pressure waves, progressive for the highest frequencies, evanescent for the lowest ones. More recently, works by Ando, Osaki, Ulrich, Wolff, Deubner and many others, have shown that the precise location was directly connected with the structure of the underlaying convection zone. Finally, several mechanisms can account for the generation of acoustic waves in this region, for example Lighthill mechanism or overtability due to κ-mechanism. In short, we know that acoustic waves exist and we know also the reason why.

The temperature increase from the low chromosphere to the corona is well-known since a much longer time. How can we explain that the temperature goes up from 4 500 to 10^6K within 2 000 Km ? Radiation processes, such as the Cayrel effect, are unable to account for a so steep gradient. Another heating mechanism is required. If acoustic waves are travelling through the atmosphere, the amplitude of waves are expected to increase with height, because of the density decrease due to the gravity. If this amplitude reaches the sound velocity, shock waves can occur and dissipate into thermal heating. Generation and dissipation of shock waves have been investigated as soon as 1948 (Schwarzchild, Schatzman, Osterbrok, Ulmschneider,...).

Our purpose in this little review is to check by observations whether the amount of acoustic energy flux in the high chromosphere is sufficient (or nor sufficient) to account for the heating of corona.

We must first recall briefly what kind of diagnosis can be used with the line observations. Assuming that we analyse observations at the center of the disk, we can classify the inhomogeneities according to their size (waves according to their

wavelength) with respect to the horizontal and radial (vertical) coordinates. Any wavelength smaller than a certain value (related to the line under study) cannot be "resolved" in the radial direction in terms of dopplershifts or intensity fluctuations (micro-disturbances). Any wavelength smaller than the cut-off corresponding to the spatial resolution of the instrument cannot be either resolved. "Unresolved" disturbances affect only line broadenings or asymmetries. It is obvious that unresolved waves are very difficult to analyse, because phase observations become impossible. Fortunately, two remarks can be done about this problem :

a) horizontal cut-off due to instrument is not so severe as it could be. Works by Keil and Canfield (78), Mattig (80), Hollweger et al. (78) show that macro-disturbances can be almost completely resolved by high resolution observations.

b) radial cut-off due to line formation can be introduced in modulation transfer functions (see below weighting functions), so that very short wavelengths can also be taken into account in flux calculations.

Roughly speaking, two kinds of analysis can be used in order to deduce wave energy flux from observations.

The fist method could be called a simulation method. The starting point consists in a mean model atmosphere and a given boundary condition : excitations which are in extreme cases pure oscillations or single pulses. By using hydrodynamics and radiative transfer equations (coupled or not), line profiles are computed as functions of time. The results are compared directly to peculiar events observed in time sequences of high resolution spectra. Since mechanical flux is easy to evaluate in the simulation process, any agreement could be, in principle, converted into flux observations. Such a method should be very powerful because non linear cases can be investigated, and unresolved as well as resolved waves can be taken into account. However, it is restricted necessarily to a few sets of amplitudes and phases for simulated waves (because of limited computer time). So far, many simulations have been performed (Cram 1974, Gouttebroze and Leibacher 1980) but they were limited to profile comparisons and did not lead to real flux determinations.

The second method consists in a linear and statistical analysis of observations, assuming that the amplitude of waves is small enough and that velocities and temperature (or pressure) fluctuations can be inferred from dopplershifts and line profile fluctuations by linear relationships. For example, weighting functions for velocities W_v are used to connect line dopplerhifts d and radial velocities v as functions of

the altitude z :

$$d = \int W_v (z)\ v (z)\ dz \qquad (1)$$

where the integral is extended to the whole visible atmosphere. Weighting functions for temperature W_T connect intensity fluctuations in the line with the temperature in a similar way :

$$\frac{\Delta I}{I} = \int W_T (z)\ \frac{\Delta T(z)}{\overline{T}\ (z)}\ dz \qquad (2)$$

Weighting functions can be computed with a mean model atmosphere for any given line (and any location in the line profile, defined by the wavelength distance $\Delta\lambda$ between the profile center and the point under study). Typical weighting functions are shown in fig. 1 for the K line of Ca II (Provost et al. 1979, Mein et al. 1980). It can be seen that they are sharper for velocities than for temperatures, because of coupling between atom-levels in the latter case. Fourier transforms of weighting functions lead to definitions of "formation altitudes" and "modulation transfer functions" (MTF) for velocity and temperature waves. Sharpest weighting functions correspond to highest MTF (fig. 2). As a consequence, high frequency waves (short

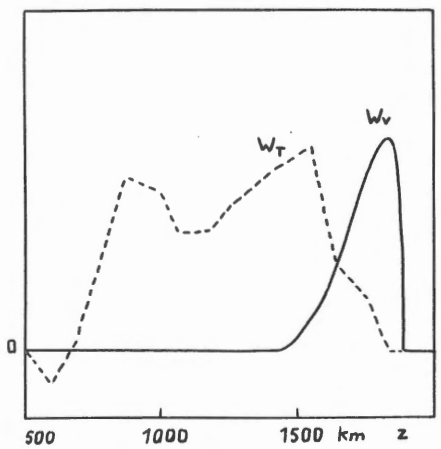

1 - Weighting functions for 3934 CaII in case of velocities (—) and temperature fluctuations (---).

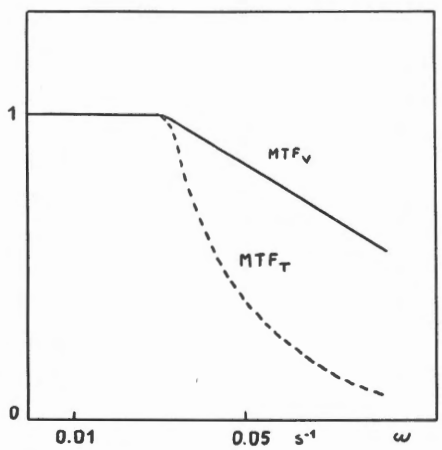

2 - Modulation transfer functions for 3934 CaII in case of velocities (—) and temperature fluctuations (---).

wavelength) will be more weakened by radiation transfer (low MTF) in the case of temperature analysis than in the case of velocity analysis.

Observations consist generally in time sequences of spectra. Statistical analysis combined with the use of weighting functions provides cross-correlation functions and cross-spectra for temperatures and velocities at various heights in the atmosphere (if various lines are involved). Following Eckart (1960) we can write the mechanical flux as

$$F = \langle V_z \, \Delta P^* \rangle \qquad (3)$$

in complex notation. For a given frequency ω, this can be written in different ways :

$$F_\omega = \frac{1}{2} P(z) \frac{\gamma}{\gamma-1} \left|\frac{\Delta T}{T}\right| \times |V| \cos\theta \qquad (4)$$

$$F_\omega = \frac{1}{2} \rho(z) \, |V|^2 \, Vg = \frac{1}{2}\rho(z) \, |V|^2 \frac{V_S^2}{V_\varphi} \qquad (5)$$

where $P(z)$ = mean pressure at altitude z, $\rho(z)$ = mean density, $|\Delta T/T|$ and $|V|$ = wave amplitudes in temperature and velocity, θ = phase shift between T and V, Vg = group velocity, V_S = sound velocity, V_φ = phase velocity. Propagation is assumed to be adiabatic.

Using formulae (4) or (5) implies that phase-shifts can be observed in order to determine θ or V_φ. If it is not the case, Vg can be replaced by V_S in (5) on the condition that the equality becomes an inequality :

$$F_\omega < \frac{1}{2} \rho(z) \, |V|^2 \, V_S \qquad (6)$$

Let us list briefly, now, some flux determinations performed in the last few years. A first class of works refers to acoustic flux taking only into account the range of 5 mn-oscillations. They use formulae (4) or (5). For each one, we note the relevant altitude (above continuous optical depth = 1), the reference and the flux value :

$\sim$ 130 Km	Canfield, Musman 1973	10^7 erg $cm^{-2}s^{-1}$
450	Zhugzhda 1973	10^6
490	Canfield, Musman 1973	8×10^5
520	Liu 1974	$2 \times 10^7 - 2 \times 10^6$
1000	Athay, White 1978	10^4

In order to cover all the frequency range and to take into account unresolved motions, some authors have given up phase determinations and used formula (6). Velocity amplitudes are deduced from estimates of MTF at high frequencies, or more simply from line widths or microturbulent velocities used in VAL model. The results are always upper limits of the real flux, because of the use of sound velocity instead of group velocity :

∿ 350 Km	Deubner 1976	7.7×10^8 erg $cm^{-2}s^{-1}$
560	" "	1.2×10^8
		10^9
1000	Athay, White 1978	10^7
1500	Boland 1975	10^5
2000	Athay, White 1978	6.7×10^4

A last class of works comes back to phase-determination (formulae 4 or 5) but uses integrals over a wide range of frequencies, up to periods as short as 80 or 60 s :

∿ 100 Km	Schmieder 1977	10^7 ergs $cm^{-2}s^{-1}$
450	Lites, Chipman 1978	2×10^6
700	Schmieder 1977	$< 10^3$
945	Lites, Chipman 1978	6×10^4
1275	Schmieder, Mein N. 1980	2×10^3 (formula 4)
1550	Mein N., Schmieder 1980	4×10^3 (formula 5)

The flux is very likely decreasing with height. The apparent inversion between the two latter values is probably due to the fact that propagation is not adiabatic, which leads to underestimates with formula (4).

Figure 3 shows the spectrum of acoustic flux corresponding to the highest altitude of this table. It can be seen that, in spite of corrections due to low MTF at high frequencies, the calculated flux does not seem to increase at short periods. This seems to indicates that the integrals cover a frequency range wide enough to reach a reasonable value of the total flux.

As a conclusion, we can say that all the results listed above are in qualitative agreement (let us remind that second list corresponds to upper limits). They show a very steep decrease of acoustic flux in the chromosphere (fig. 4). In fact, this decrease seems almost too strong to compensate the chromospheric radiative loss. But the most striking point is that the available flux at the top of the chromosphere

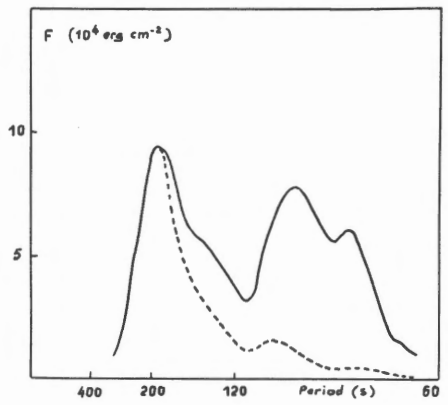

3 - Spectrum of the acoustic flux in the chromosphere derived from observations in CaII lines : with correction (—) and without correction (---) by modulation transfer functions.

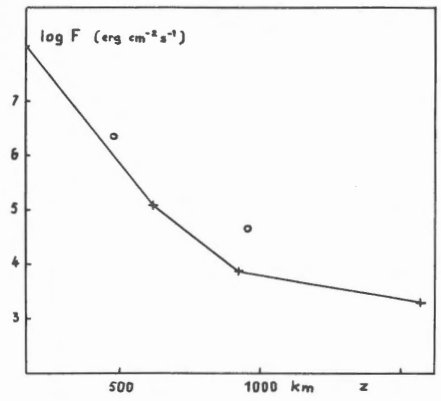

4 - Acoustic flux versus height in the solar chromosphere ; the period range is 120 - 400 s. Results are from Mein and Schmieder (+), Lites and Chipman (o).

is much smaller than the required value for heating of transition zone and corona. Indeed, this value is generally assumed to be about 3×10^5 erg $cm^{-2} s^{-1}$. The reason is not the weakness of velocity amplitude, but the very small value of the group velocity. Reflections on the transition zone are probably very efficient, and most of chromospheric acoustic waves are stationnary. The strong inhomogeneity of thin transition zone may perhaps account for that, more especially as local studies show variations of reflection powers across the disk (Mein N., 1978).

Other mechanisms should be found in order to heat the solar corona. Magnetic field is probably involved. Anyway, we must keep in mind - in particular for stellar approaches - that replacing the group velocity by the sound velocity in formula (5) for acoustic waves, can lead to overestimate the flux by one or two orders of magnitude.

REFERENCES :

Ando, H., Osaki, Y. : 1975, Publ. Astron. Soc. Japan, 27, 581.

Athay, R.G., White, O.R. : 1978, Astrophys. J., 226, 1135.

Boland, B.C., Dryer, E.P., Firth, J.G., Gabriel, A.H., Jones, B.B., Jordan, C., Mc Whirter, R.W.P., Monk, P., Turner, R.F. : 1975, MNRAS, 171, 697.

Canfield, R.C., Musman, S. : 1973, Astrophys. J., 184, L131.

Cram, L.E. : 1976, Astron. Astrophys., 50, 263.

Deubner, F.L. : 1975, Astron. Astrophys., 44, 371.

Deubner, F.L. : 1976, Astron. Astrophys., 51, 189.

Eckart, C. : 1960, Hydrodynamics of Oceans and Atmospheres, Pergamon Press.

Evans, F., Michard, R. : 1962, Astrophys. J., 135, 812.

Gouttebroze, P., Leibacher, J.W. : 1980, Astrophys. J., 238, 1134.

Hollweger, H., Gehlsen, M., Ruland, F. : 1978, Astron. and Astrophys., 70, 537.

Keil, S.L., Canfield, R.C. : 1978, Astron. Astrophys., 70, 169.

Leighton, R.B., Noyes, R.W., Simon, G.W. : 1962, Astrophys. J., 135, 474.

Lites, B.W., Chipman, E.G. : 1979, Astrophys. J., 231, 570.

Liu, S.Y. : 1974, Astrophys. J., 189, 359.

Mattig, W. : 1980, Astron. Astrophys., 83, 132.

Mein, N. : 1978, Solar physics, 59, 3.

Mein, N., Mein, P. : 1980, Astron. Astrophys., 84, 96.

Mein, N., Schmieder, B. : 1980, Astron. Astrophys. in press.

Osterbrock, D. : 1961, Astrophys. J., 134, 347.

Provost, J., Mein, N. : 1979, Solar Phys., 64, 43.

Schatzman, E. : 1949, Ann. Astrophys., 12, 203.

Schmieder, B. : 1977, Thesis, University of Paris VII.

Schmieder, B., Mein, N. : 1980, Astron. Astrophys., 84, 99.

Schwarzchild, M. : 1948, Astrophys. J., 107, 1.

Ulmschneider, P. : 1970, Astron. Astrophys., 4, 144.

Ulmschneider, P. : 1976, Solar Phys., 49, 249.

Ulrich, R.K. : 1970, Astrophys. J., 162, 993.

Wolff, C.L. : 1972, Astrophys. J., 177, L87.

Zhugzhda, Yu. D. : 1973, Astron. Letters, 13, 173.

ELECTRO MAGNETIC HEATING OF CORONAE

by
J. Heyvaerts
E. Schatzman

Abstract

Current ideas concerning coronal heating by alternating or direct electric current dissipation are briefly reviewed. It is stressed that Alfven wave heating is not excluded by observations. The promizing aspect of Joule heating by DC current in loops are emphasized, as well as the difficulties still met by such theories.

I) Summary of facts and numbers relevant to the problem

A successful theory of coronal heating should explain : energy, mass and momentum balance of the solar corona as a whole, as well as of specific structures (loops, holes, etc...).

a) Fluxes

Energy budget involves at least the most conspicuous losses, which are radiation, and solar wind enthalpy flux. Figures for these are compiled in the following table.

Region	Loss	Amount (ergs $s^{-1}cm^{-2}$)	Reference
Photosphere	Opt.Rad	$6.41\ 10^{10}$	Bray Loughhead (Table 7.2) Allen
Chromosphere	Opt.Rad UV lines	2-6 $5\bullet3\ 10^{6}$ $6\bullet2$	Bray Loughhead Vernazza et al (1980) Ulmschneider (1979)
Transition	UV	$6\ 10^{5}$	Athay-White (1979)
Corona	Opt+UV	$1.5\ 10^{4}$-$3\ 10^{5}$	Osterbrock & Athay (1966)
All	X(40-80Å)	$4.8\ 10^{3}$	Mewe (1978)
"Quiet"	X(2-60Å)	$8\ 10^{4}$	Vaiana Rosner (1978)
"Active"	X(")	$9.7\ 10^{4} \wr 10^{5}$	Vaiana Rosner (1976)
Holes	X(2-60) Solar Wind	$8\ 10^{3}$ $7\ 10^{5} \wr 10^{6}$	Vaiana Rosner (1978) Zirker (1980)

Note that coronal holes do not need smaller energy input.

The corona however is strongly structured, and consists of loops of various sizes, density, and physical properties. These loops and structures have widely different energy needs (Vaiana et al. 1976). A comparison of the energy fluxes necessary for each structure stresses again the fact that some of these fluxes differ by a factor as large as 50 from the mean. In the case of active regions it is as large as the flux needed to sustain chromospheric losses.

b) Detailed loop structure and consequences.

Detailed geometrical features of loops have been analysed by Foukal (1975, 1976, 1978), and have shown the following very important properties of cool core coronal loops.

(1) Aspect ratio (radius/length) $\gtrsim 10^{-1}$, (2) a lower pressure cooler core is imbedded in a hot mantle, (3) most loops last much longer than free fall time and cooling time (they are stationnary), (4) the cool material in the loop center does not suffer a siphon flow from one leg to the other but falls downwards along both legs at a velocity approaching free fall. This special fact implyes that the loop's magnetic field is permeable at least at the top for the matter. In other words matter is not frozen in. It slips through the field. This fact implies the existence of a dissipative process at some portion of the loop length at least.

II) Is mechanical heating by Alfven waves excluded from observation?

Athay and White (1979) have claimed to exclude the mechanical heating theory by putting an upper limit on energy flux from turbulent velocity observed in various chromospheric and transition region EUV line. They state :

$$F_{Mech} \lesssim \rho \xi^2 c_s = \bar{F} \qquad (1)$$

and exclude the possibility of higher limits due to Alfven transport on the apparently sound basis that, as you consider an average flux, you should use the average Alfven velocity, i.e. a 1 or 2 Gauss field, and this does not give a higher limit because $\langle v_A \rangle \gtrsim c_s$. Their upper limit derived from observations is compared to the losses upwards from the corresponding level. It is found to be too small by a factor ten at 2000km.

We believe that their conclusion may be disputed on diverse grounds but we want to stress what we believe is a fundamental difficulty in such estimations. The point is that the mechanical flux may escape observation if it is transported at Alfven speed in concentrated channels, because the more concentrated the field is, the faster corresponding Alfven velocity. We believe that Athay and White made a mistake in evaluating :

$$\langle F \rangle = \frac{1}{S} \iint_S \rho \, dx \, dy \, \xi^2(x,y) \, v_A(x,y) \qquad (2)$$

They neglected correlations between ξ^2 and v_A . They state implicitely

$$\langle F \rangle = \rho \langle \xi^2 \rangle \langle v_A \rangle \qquad (3)$$

whereas the correct evaluation is

$$\langle F \rangle = \rho \langle \xi^2 v_A \rangle \qquad (4)$$

The question is then, if we figure out a composite chromosphere permeated by more intense flux tubes, how much larger should ξ be in the tubes ? A bit of algebra gives the answer $\xi_{Tube} \sim 2.57 \, \xi_{Average}$, but the clumpiness can be arbitrary!!

III) Clues from stellar observations

Giacconi (1980) reports Einstein observations of stellar coronae, and Mewe (1979) reports those of HEAO1. Results of these observation seem to strongly conflict with mechanical heating theories. Recent developments on the observational side, seem to indicate that rotation may be the major parameter which after all determines coronal emission. These aspects are reviewed in RM Bonnet's book (1980).

IV) Alfven waves as a source of heating. Structuring neglected

According to Osterbrock (1961) Alfven waves do not contribute to coronal emission because :

1) They are much less effectively emitted than fast waves.
2) They damp in photosphere-low chromosphere.
3) They are reflected at the transition zone.

All these objections are known to fail. They were due to the fact that Osterbrock pictured out a weak diffuse magnetic field. Let us consider these in turn.

a) Wave emission

Sound wave emission, by a turbulent fluid is calculated by finding the non linear source term to pressure fluctuations which result from otherwise mainly incompressible motions. Because of the isotropy assumption, this source is quadripolar in nature and the result is :

$$\text{Power emitted} = \text{Vol}/4\pi \; \rho_0 v^2/(\ell/v) \; v^5/c_s^5 \qquad (5)$$

If gravity is taken into account (Unno, 1964), we also have dipole and monopole sources. Ulmschneider and Bohn (1980) report similar results for a non negligible field. Their result can be expressed as follows for n-pole emission (monopole, n=0)

$$(\text{Power emitted})_{n\text{-pole}} = \text{Vol} \, \frac{\text{En.density}}{\text{Correl.Time}} \left(\frac{\text{Corr.length}}{\text{Wavelength}} \right)^{2n+1} \text{ergs s}^{-1} \qquad (6)$$

The wavelength is that which corresponds to the correlation time. It can easily be checked that Alfven wave emission is favoured in low β conditions.

b) Wave Damping

Linear wave damping proceeds on a scale length :

$$\lambda_{\text{Damp ion}} = v_A^2/\omega^2 \; (\eta + \nu)^{-1} \qquad \lambda_{\text{Damp neutral}} = v_A/\omega^2 \; \frac{1+\alpha}{\tau_{\text{coll i-n}}} \qquad (7)$$

Uchida and Kaburaki (1974) have shown the damping to be very weak if B>10 Gauss.

c) Wave reflection and refraction

If we use geometrical optics as a guide, one deduces that slow and Alfven modes are channelled by B ($c_A \gg c_S$) but that pure sound or fast modes, obey Snell's law :

$$\sin i / c_S = C^t \qquad \text{or} \qquad \sin i / c_A = C^t \qquad (8)$$

They refract towards lower velocity regions, and such small fractions as $3\ 10^{-3}$ of an isotropic incident flux may reach the corona. The importance of this effect has been stressed by Schatzman (1970), who also discussed the possibility that this dramatic filtering be reduced by non plane layered inhomogeneities and coupling to field channelled modes.

Wave reflection has been discussed by Kaburaki & Uchida, and more recently by Wentzel, Hollweg, B. Leroy (cf. Leroy this meeting).

A recent work by E. Zweibel answers the objection that a fast isotropic MHD mode cannot produce loop type structures. He shows that under the combined effect of thermal instability and refraction, a faint mode heated structure spontaneously develops field aligned fibers.

d) Wave-wave interaction

A full theory of MHD wave heating should describe all the cascades that a wave spectrum suffers being transferred. As a result of these the rate of heating should be predictible. Such strong turbulence theory of heating has not yet appeared for the corona. Dobrowolny et al (1980) however give interesting results for the solar wind turbulence.

The idea of mode coupling has been examined in the weak turbulence approximation (Uchida, Kaburaki, 1974) counterstreaming Alfven waves produce sound waves which dissipate. The process would not work in coronal holes, and is weakly efficient in strong fields (Wentzel, 1976).

V) Role of magnetic structuring

Magnetic structures perturb wave propagation and introduce new modes. The simplest problem is one in which the field structure has one dimension (magnetic wall).

a) Surface waves

It can easily be shown that this structure supports surface waves, i.e. oscillations localized near the interface. No surface wave is absolutely incompressible, but in the limit $k_\parallel \gg k_\perp$ in the surface, this approximation is quite good, and we have a phase velocity intermediate between Alfven waves :

$$\omega^2/k^2 = c_{A1}^2 \, \rho_1/(\rho_1+\rho_2) + c_{A2}^2 \, \rho_2/(\rho_1+\rho_2) \qquad (9)$$

More complicated dispersion relations, valid in tubes, or when the uncompressibi-

lity fails are given by many authors (see for example Roberts and Webb).

None of them has up to now described the generation of surface waves in as much detail as sound emission has been described.

b) Perfect MHD damping of surface waves

The boundary between two regions is not discontinuous. The problem is then to find vibrations in and around a finite current sheet. The wave equation for this problem can be written, and the modes found (Barston, 1964). It is found that they form a continuum between $\Omega(\mp\infty)$ where $\Omega(x)$ is defined by :

$$\Omega(x) = k_{\parallel} v_A(x) \tag{10}$$

Each mode of frequency ω is singular at its resonant point x_ω where :

$$\Omega(x_\omega) = \omega \tag{11}$$

The surface proper mode has disappeared apparently, but it surfaces again if we produce regular packets of Barston's singular modes. It is found that these wave packets, may well start as a typical "surface mode", but that this mode is damped, and leaves assymptotically a secularly vanishing oscillation.

$$\xi(x,t) = t^{-1} \exp(i\Omega(x)t) \tag{12}$$

This decay is easily understood ; it represents a vibration of the structure in which each shell $x = ct$ oscillates at its own Alfven frequency $\Omega(x)$.
There is then a decay of the oscillations by phase mixing. It has been shown by solving the initial value problem that in the case of finite thickness current sheets, the surface mode appears as an exponentically damped transitory contribution. Sedlacek (1971).

In reality at a high degree of phase mixing, the dissipation by viscosity for example, will be effective, and the damping will be physical, and not only virtual. We may speak of this process as dissipation-less damping, just as we speak of collisionless damping. Dissipation-less damping has been observed in laboratory θ-pinch (Grossman et al, 1972). At a high rate of shearing, the scale of velocity perturbations becomes comparable to the ions gyroradius. Finite Larmor corrections need be considered. In a homogeneous plasma finite Larmor radius corrections to short perpendicular wavelength waves provide the possibility for the Alfven wave to propagate sideways because the dispersion relation becomes :

$$\omega^2 = k_{\parallel}^2 v_A^2 \left(1 + k_{\perp}^2 \rho_i^2 \left(\frac{3}{4} + \frac{T_i}{T_e}\right)\right) \tag{13}$$

In the inhomogeneous structure problem, this give us finite Barston modes (modified) because the resonantly excited oscillations do not stay where they are excited but propagate sideways. Hasegawa & Chen (1976) have discussed this.

c) Jonson (1978) has pushed this idea up to the construction of an explicit model of loop heating. The most salient feature of dissipation-less damping is that the energy is fed to a small region at the boundary, near the resonance layer. The width of that region is even smaller than the radial wavelength given by Hasegawa's theory if $\omega_{surf\ wave} < \gamma_{ii}$. The problem of these sort of theories is to explain how the heat is spread inside the loop. As I understand it Jonson figures out the system as similar to a hot vertical plate in air. A convective boundary layer would develop at its contact, and convect an enthalpy and mass flux upwards. In the loop case there is an extra problem to feature out what the mass and energy become at the top of the loop. Jonson argues that a Rayleigh Taylor instability there diffuses matter in the loop core where it cools by radiation and falls, closing the mass circuit.

VI) Joule heating of the corona

a) Joule heating is a viable theory from global budget point of view

The energy to be released in Joule heating or more generally by inter-

rupting or altering coronal currents is the magnetic free energy :

$$W_M = \int B_1^2/2\mu_0 \; d^3\underset{\sim}{r} \qquad (14)$$

B_1, the field due to local currents is mainly perpendicular to the current carrying loop, and smaller than a certain fraction of the longitudinal field, otherwise the whole loop turns kink instable ; we find ;

$$W_M \sim 2.5\ 10^{28}\ B_3^2 R_9^4 \ell_{10}^{-1} \quad ergs \qquad (15)$$

The build up time for this energy is :

$$\tau_{feed} \sim 2\pi R_{phot}/v_{Phot} = 6300\ R_{phB}\ v_{km/s}^{-1} \quad s \qquad (16)$$

Hence :

$$\dot{W}_M = 4\ 10^{24}\ v_{km\,s^{-1}}\ R_{PhB}^{-1}\ B_3^2 R^4 \ell_{10}^{-1} \quad ergs\ s^{-1} \qquad (17)$$

The photospheric field may not have a pressure larger than photospheric pressure, hence $B_3 \leq 1.6$. Taking this as a representative value, we find that $\dot{W}_M$ so calculated is large to meet the requirements of X ray luminosity of all known coronal structures. Nevertheless, the idea is not without difficulty.

b) Joule heating is impossible by normal resistivity processes

To convince onself of that, calculate $<j>$ from $B\theta$ and use σ from Spitzer's theory and 10^6°K. You find that the current has to be clumped to ridiculous sizes, to increase J^2/σ at the right value. Micro turbulence would occur much before.

c) Dissipation under microturbulent conditions does not work

If microturbulence is to be ever triggered, currents have to be collapsed to a fairly small sheet. Actually, the current density threshold is for ion acoustic or ion cyclotron waves:

$$J^* = 10\ n_e v_{Ti} \sim 16\ n_9\ T_6^{1/2} \quad Amp\ m^{-2} \qquad (18)$$

The total current $(2B_z/\mu_0 \ell)$ at this density has a clumpiness factor very small. It would occupy a strip of width :

$$\delta^* = 500\ R_8\ \ell_{10}\ n_9^{-1}\ T_6^{-1/2}\ B_3^{-1} \quad cm \qquad (19)$$

Once this regions is reached, the evolution is one of marginal stability (Heyvaerts, Kuperus, 1978).

The crucial problem is just to explain the current concentration, why the energy should be fed in the microturbulent sheet, and how the current concentration is maintained.

On all these three crucial points the microturbulence theory of Rosner et al (1978) fails badly in our opinion because :

1) The dissipation interests only a small part of the current structure.

2) The build up of such localized current is incredible. It would imply velocity gradients of 1km/s on 5m in the photosphere.

3) Such small current sheets spontaneously broaden their current profile by tearing modes on very small time scales.

BIBLIOGRAPHIE

Allen, G.W., 1968, Astrophysical quantities U. of London. Athlone Press.

Athay, G., 1966, A.P.J. 146, 223

Athay, G., White, S., 1979, A.P.J. 226, 1135

Barston, 1964, Ann. Phys. NY 29, 282

Bonnet, R.M., 1980, Proceedings of lectures of NATO Summer School held at Bonas (France)

Bohn, H.U., 1980, to be published (see Ulmschneider, 1980, in R.M. Bonnet, 1980)

Bray, R.J., Loughhead, R.E., 1974, The Solar Chromosphere. Chapman & Hall
Dolbrowolny, M., Mangeney, A., Veltri, P.L., 1980, Astron. Astrophys. 83, 26
Foukal, P., 1975, Solar Physics, 43, 327
Foukal, P., 1976, A.P.J., 210, 575
Foukal, P., 1978, A.P.J., 223, 1046
Giacconi, R., 1980, Scientific American (February, 1980)
Grossmann, W., Kaufman, M., Neuhauser, J., 1973, Nuclear Fusion 13, 462
Hasegawa, A., Chen, L., 1976, Physics of fluids, 19, 1926
Heyvaerts, J., Kuperus, M., 1978, Astron. Astrophys. 64, 219
Hollweg, J.V., 1972, Cosmic electrodynamics 2, 423
Ionson, J., 1978, A.P.J., 226, 650
Kaburaki, O., Uchida, Y., 1971, Pub. Ast. Soc. Japan, 23, 405
Mac Whirter RWP, 1978, Communication at Solar Winds in Astrophysics May 1978, Florence
Mac Whirter RWP, Thonemann, P.C., Wilson, R., 1977, Astron. Astrophys. 61, 859
Mewe, R., 1979, Space Science Reviews, 24, 101
Osterbrock, D., 1961, A.P.J., 134, 347
Roberts, B., Webb, A., 1979, Solar Physics, 64, 77
Rosner, R., Golub, L., Coppi, B., Vaiana, G., 1978, A.P.J. 222, 317
Schatzman, E., 1970, Cosmic Gas Dynamics I, p. 62, Uberoi ed. John Wiley
Sedlacek, 1971, J. Plasma Physics 5, 239
Uchida, Y., Kaburaki, O., 1974, Solar Physics, 35, 451
Ulmachneider, P., 1979, Space Science Reviews, 24, 71
Unno, W., 1964, I.A.U. Hamburg, 1964, p. 555
Vaiana, G., Rosner, R., 1978, Annual Review of Astr. Astrophys. 393
Vaiana, G., Krieger, A., Thimothy, Zombeck, 1976, Astrophys. Sp. Science, 39, 75
Vernazza, J.E., Avrett, E.H., Loeser, R., 1980, A.P.J., In press
Wentzel, D., 1976, Solar Physics, 50, 343
Wentzel, D., 1978, Solar Physics, 58, 307
Zirker, R., 1980, Lecture at NATO School see R.M. Bonnet (1980)
Zweibel, E., 1980, Solar Physics 66, 305

Magnetic Fields and Currents in the Corona

by

Yutaka Uchida
Tokyo Astronomical Observatory
University of Tokyo, Mitaka, Tokyo

Abstract

Methods for obtaining information about coronal magnetic fields are reviewed. Estimates using radio data are first discussed with some critical comments, and then, recently-recognized method of evaluating the coronal magnetic fields by using the three-dimensional pattern of X-ray loops together with the photospheric magnetic field is discussed. Current distribution in the corona can also be derived from the magnetic field thus obtained. Some discussion on the significance of the derivation of the current in the corona in relation to the flare theory is given.

1. Introduction

The direct measurement of the magnetic field in the corona by Zeeman effect is difficult due to the smallness of the effect combined with the large Doppler widths of the lines, because the magnetic field in the corona is usually weak and the temperature in the corona is high. We therefore have to recourse to other sources of information at present.

Some information is obtained through radio observations which are often the sole source of information on the magnetic field in the middle to high corona. Another more recently-recognized source of information is the X-ray or EUV observations of the shape of the loops of which the corona is found to be consisted (Vaiana et al 1973, Sheeley et al 1974, Svestka et al 1977). If we reasonably assume that the loops are the frozen-in inhomogeneity of the plasma along the field lines, we can tell with high trustability what the configuration and the strength of the magnetic field in the corona are, by knowing the three-dimensional

shape of the loops together with the field strength at one point along each loop, eg , at the photospheric footpoint (Sakurai and Uchida 1976, 1977).

In the following, a brief look at the estimates from radio observations is given in section 2, then the latter method utilizing the coronal loop pattern will be reviewed in section 3, and the discussion is given in section 4.

2. Estimates of the Coronal Magnetic Field from Radio Data

Various methods of obtaining information on the coronal magnetic field from radio observations have been proposed. These include the information from microwave spectra, from the propagation velocity and the band-splitting of type II burst sources, from the polarization of the second harmonics of type III burst, from Razin effect in moving type IV bursts, and so on. Takakura (1971), and more recently, Dulk and McLean (1978) summarized the estimates from radio data as in Figure 1.

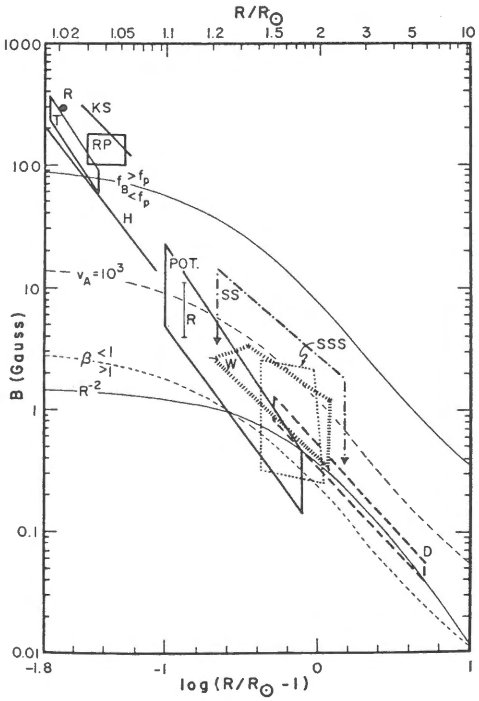

Fig.1. Magnetic field estimates from radio data (Dulk and McLean). T, RP, and KS are from microwave data, SSS, and W from type II burst data, SS from type III burst data, and D from moving type IV burst data, respectively. See original paper for details.

Dulk and McLean deduced an expression

$$B = 0.5\left(\frac{R}{R_0} - 1\right)^{-1.5} \quad G \qquad (1)$$

by best fitting the data regions derived by these various methods. The field strength (as given by expression (1)) duely deviates upward on R - B plane from the extrapolated value from in-situ measured field strength in the solar wind (Behannon 1976),

$$B = 3 \times 10^{-5}\left(\frac{R}{2.16 R_0}\right)^{-2} \quad G \qquad (2)$$

corresponding to the effects of the presence of the higher pole components of the fields in the neighborhood of the sun. Expression (1) is, of course, a very crude expression because it is based on information sources very inhomogeneous in quality, referring characteristically different points in the corona, and also relying upon information of other quantities like the density distribution which we have to infer from the data obtained from observations of other points and other instances. For example, information of the magnetic field from microwave spectra is coupled with the energy spectrum of the high energy particles emitting it which is not known, and that from the propagation of type II bursts is coupled with the model of the density distribution along their paths of propagation. The deduction of the field strength from the band spitting of type II bursts requires the information of shock strength in addition to that of density. Razin effect gives us the information of the magnetic field again only when information about the density is given. For example, Dulk and McLean assumed the density distribution of 2 x or 8 x Newkirk's model coronal density, but this, of course, does not represent the density in active region corona. Further, the motion of the source may well sample out both closed and open part of the magneteic field along the path. These arguments envisage the problems with such expression as expression(1), especially for highly structured low corona. Namely,some of the information comes from active regions and others from non-active regions (or from closed field regions and from open field regions), and so on, but all mixed together to give an averaged expression (1). This suggests that the information derived from radio data, at least at the present stage, should be taken merely as a rough measure of the magnetic field strength in the corona. In the outer part of the corona where there is no other way of measuring the magnetic field, however, expression (1) may serve as the only existing measure of the magnetic field and is useful.

3. Geometrical Method for Calculating the Coronal Magnetic Field from the Shape of the Coronal Loops

In the inner part of the corona ($R \lesssim 1.5 R_\odot$), X-ray and EUV observations from Skylab have revealed that the corona is consisted of highly inhomogeneous structures, mainly of loop shape. It was noticed that this allows a rather solid way of estimating the magnetic field in the corona (Sakurai and Uchida 1977). Namely, if we know the three-dimensional shape of the loops which are safely assumed to be the frozen-in inhomogeneities of the plasma along the field pattern, we can calculate the detailed distribution of the magnetic field in the corona by specifying the field intensity at, eg , the photospheric footpoints.

Complete determination of the three-dimensional pattern of the loops from observations with a suitable time separation should in principle reveal the field configuration in the corona , and further, the configuration of the electric current in the corona. The determination of the location and the configuration of the coronal electric current in the vicinity of the flare site and the change of it before and after the flare are extremely important in relation to the investigation of the mechanism of the flare. We give some comments about this direct method of determination in section 4.

More practicable alternative is to use models and determine parameter values in them by comparing the projection of the calculated pattern of the field with the observed loop shape. This approach followed the method initiated by Schmidt (1964) to calculate the potential field in planar geometry, and has been extended later by several authors to global potential field, and further, to non-potential fields.

3.1. Model Fitting by Potential Field

Schmidt's problem was to calculate the extention of the magnetic field into the corona by knowing the distribution of the field on the bottom boundary, the photosphere. Assuming a potential field, he obtained the solution by using Green function method in which the photospheric field distribution is replaced by the distribution of unit monopoles,

$$\phi(\mathbf{r}) = \int G(\mathbf{r}, \mathbf{r}')\, B_n(\mathbf{r}')\, d\mathbf{r}' \tag{3}$$

$$G(\mathbf{r}, \mathbf{r}') = \frac{1}{2\pi |\mathbf{r} - \mathbf{r}'|} \tag{4}$$

$$\mathbb{B} = -\nabla\phi \tag{5}$$

where B_n is assigned on the bottom boundary surface,the photosphere. This method is widely used both in pre-Skylab days (eg., Rust 1972 for loop prominences) and in post-Skylab days (eg., Poletto et al 1975 for soft X-ray loops (Figure 2a, b)). It is seen that a rough agreement is obtained.

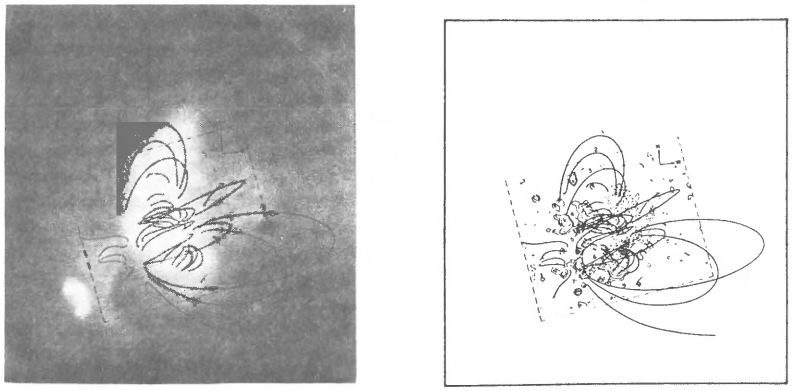

a b

Fig 2 a) X-ray loop structure of Jun 15,1973 observed by AS and E experiment on Skylab. b) Field lines calculated by Poletto et al (1975) using the photospheric magnetic field distribution of that day. (Sorry for bad reproduction of X-ray picture. Original is quite good).

A direct extention of Schmidt's approach to the global case was attempted by Schatten et al (1969), but a more legitimate way in the global case was developed by Altschuler and Newkirk (1969) in spherical harmonic expansion technique,

$$\phi(\mathbb{r}) = R_e \sum \left\{ C_{\ell m} \left(\frac{a}{r}\right)^{\ell+1} + D_{\ell m} \left(\frac{r}{a}\right)^{\ell} \right\} Y_\ell^m(\theta,\varphi) \tag{6}$$

$$\mathbb{B} = -\nabla\phi \tag{7}$$

and the coefficients are fixed by matching the expression with

the observed field given on the inner boundary, the photosphere. Their treatment was in pre-Skylab days, and the comparison with the observation was made with the eclipse or K-coronagraph results in which the structure can only be observed beyond the limb, and the detail of the coronal structure can not be separated and obscure due to the overlap in the projection of the structure on the sky.

In trying to reproduce the X-ray loop pattern obtained by Skylab, Sakurai and Uchida (1977) developed another method based on Biot-Savart's law by replacing the active region flux tube by subphotospheric current in the form of solenoids, and calculating vector potential.

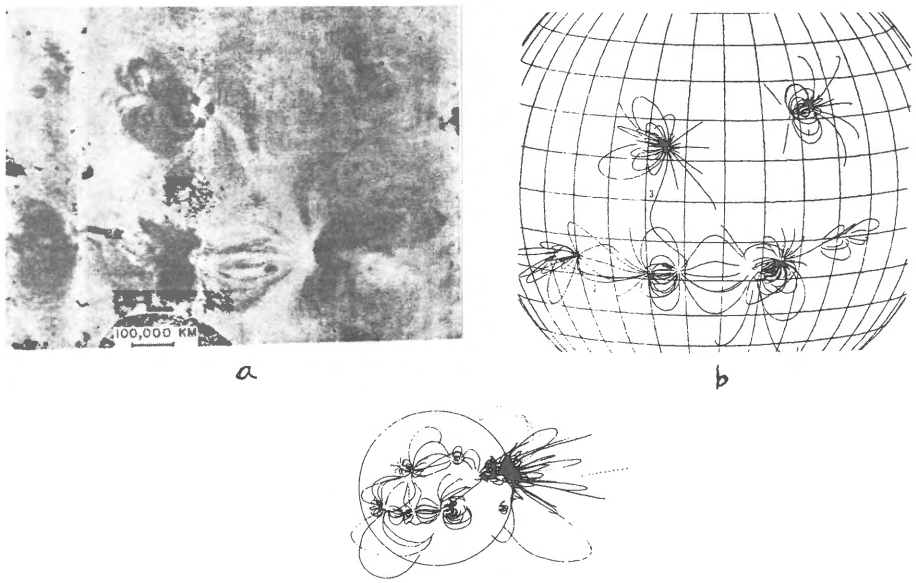

Fig 3 a) Coronal loop structure of Sep 5,1973 observed by NRL experiment on Skylab.
b) Calculated model of the magnetic field lines of the same day by Sakurai and Uchida(1977).
c) The same by Altschuler et al(1977),for the preceding day. (Sorry for bad reproduction of EUV pictures. Original is superb.)

$$A(r) = \frac{1}{c}\int \frac{j(r')}{|r'-r|}\,dr' \qquad (8)$$

$$B = \mathrm{rot}\,A \qquad (9)$$

It may be said that the global-scale features as well as loop structures above active regions are reasonably well reproduced by this model (Figure 3a, b). Altschuler et al (1977) developed their own method to include very high order terms in spherical harmonic expansion, and also tried to reproduce the Skylab result (Figure 3c).

The result of such a comparison using potential field models indicates the following ; (i) the rough structure of the loop-shaped corona can be reproduced already by potential field models, but (ii) marked deviations are often seen especially near the flaring active regions, and (iii) a better fitting of local and global features observed in X-ray is obtained by Sakurai-Uchida method rather than by elaborated extention of Altschuler and Newkirk's method with very many terms of expansion. Items (i) and (ii) suggest that most part of the coronal field is relaxed to the current-free state (the lowest energy state), but at some special part like the neighborhood of the flaring active regions , the deformation of the field is seen, suggesting the presence of the local current in the corona. Item (iii) reflects the fact that the brightest corona is closely related to the active region fields which is difficult to take into account in detail in Altschuler et al's method . Sakurai-Uchida method concentrates attention on strong fields and is advantageous in reproducing the brightest loop structures of the corona which are due to the active region fields.

3.2. Implication of the Deviation from the Potential Field and the Extention to the Model-Fitting by Non-Potential Fields

Potential field in the corona is nothing but the field due to the source current outside the region under consideration, ie, in the invisible subphotospheric layers in our case. Since observations of the photospheric magnetic field at the time of flares generally indicate that there is no appreciable change in the magnetic field observed at the very moment of the flare occurrence (Rust 1972), it is required that the electric current respon-

sible for the releasable magnetic energy available for the flare should preexist in the corona or in the chromosphere . The detection of the presence of such a current in the corona was simply beyond the range of capability of observation before Skylab, but now it is, so to say, made visible by X-ray or EUV observations as the deviation of the coronal magnetic field from the potential field, if we identify the coronal loops with the field-aligned plasma inhomogeneity. Potential field is the lowest energy state (without any current in the corona) for the given distribution of the normal component of the field on the boundary, and the deviation from this is produced by the presence of the coronal current. Naturally, such a current is held only in those cases in which the distortion of the field lines can not be continuously relaxed by the motion in the corona alone. In such cases, the work done on the footpoint of the flux tube by the photospheric motion is stored in the form of excess magnetic energy, or,

$$\Delta W = -\frac{1}{2c}\int \mathbf{A}\cdot\mathbf{j}\, dV \qquad (10)$$

providing the energy of flares (Uchida and Sakurai 1977).

Two fundamental cases of such current configurations widely considered in relation to flares are (a) field-aligned (force-free) current which may be built up, eg , by the twisting at the footpoint of the magnetic flux tubes, and (b) the sheet current which may be produced at the boundary of two regions of plasmas with magnetic fields frozen to them. This occurs at the boundary of plasmas with different pressures (and different field strengths to compensate the difference in pressure) in general. The polarities of the field on both sides of the sheet may be the same, but an important situation appears when the polarities of them are opposite from each other. So-called neutral sheet is a special case of this.

Field-aligned current (a) may be characterized by the helical winding of the loops. Since $\beta \equiv 8\pi nkT/(B^2/8\pi)$ is small in the corona except at the neutral sheet, we deal with this case in terms of force-free field in which the Lorentz force disappears, ie,

$$\mathbf{j}\times\mathbf{B} = 0 \quad , \qquad \mathrm{rot}\,\mathbf{B} = \alpha\mathbf{B} \qquad (11)$$

α = const along the lines of force by its nature, but can vary from a line to another. A constant-α field signifies the one in which α takes a common value for all field lines, and can be tackled with (eg, Woltje 1958). Nakagawa and Raadu (1972) applied this to the sunspot field and claimed that the cyclonic appearance of the fibrils around the sunspots may represent the presence of the current. Levine and Altschuler (1974) formulated

the global constant-α field, and found that the constant field with constant everywhere is too restrictive to reproduce the observation.

Non-constant-α field has been discussed by Sturrock and Woodbury (1967), Barns and Sturrock (1972), Chiu and Hilton (1977) and other people, in the expression using the Euler potentials, but the equation is very complicated and difficult to deal with. Recently, however, Sakurai (1979) has developed a variational method of dealing with this problem. His method is to treat the eneryg integral(the variation of which gives out the Lorentz force equation (10) as the Euler's equation for the minimization in a special case in which other terms are negligible) and minimize the integral by varying the shape parameters (finite element method). Figure 4 shows examples of the results of his calculations of non-constant-α force-free field produced by the motion of footpoints.

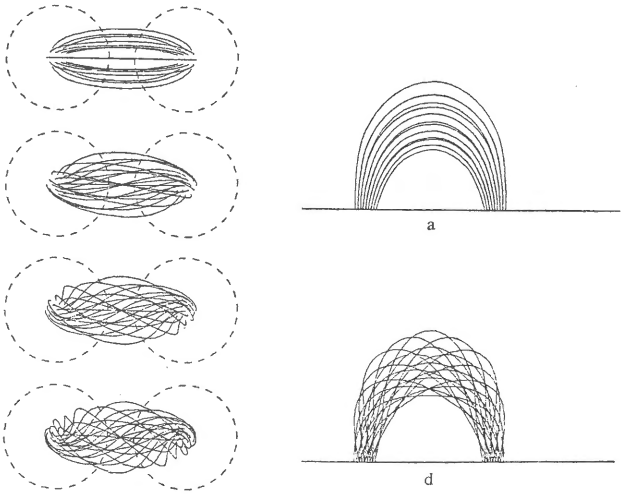

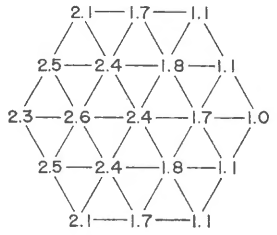

Fig. 4. Model Calculation of non-constant-α field by Sakurai(1979).
a) Magnetic field before and after applying twist motion.
b) Distribution of induced α value inside the spot.

$$\delta W(r) = \delta \int \left\{ \frac{dl_3^2}{8\pi J} + \bar{p}(r) J \right\} d^3u = 0 \qquad (12)$$

$$B = \nabla u_1 \times \nabla u_2 = \frac{dl_3}{J} \qquad (13)$$

$$dl_3 \equiv \frac{\partial r}{\partial u_3} \quad , \quad J \equiv \frac{\partial(x_1, x_2, x_3)}{\partial(u_1, u_2, u_3)} \qquad (14)$$

He also developed another approach in which the current is assigned for each tube and obtained the configuration which minimizes the energy (Sakurai 1980). An example of the result of the calculation is shown in Figure 5.

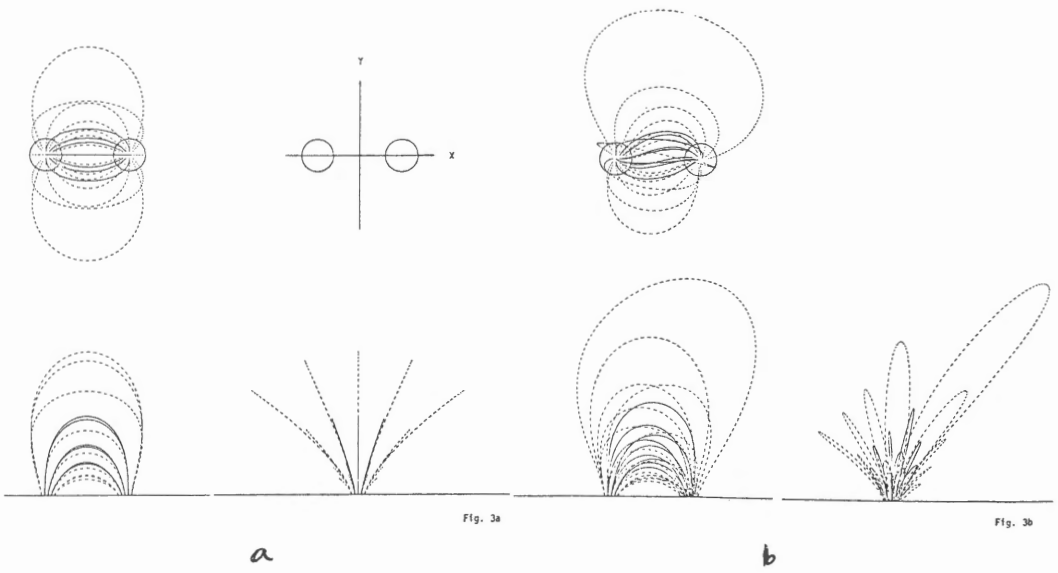

Fig. 5. A result of model computation in which the distributions of $B_n(r)$ and $\alpha(r)$ are given in the region of one(+) polarity in the photosphere. a) Before twisting. b) After twisting. Solid lines are those to which $\alpha(r)$ is assigned and are twisted as the result.

The effect of the sheet current,on the other hand,may be characterized by the "insulation" of the nearby regions of opposite polarities which are otherwise expected to connect to each other. The presence and the drastic change at a flare of such an "insulation" are seen in EUV monochromatic pictures obtained by Skylab. Calculation of the field with sheet current can be done in cases in which the sheet is singly connected . Sakurai and Uchida (1977) calculated the current sheet models and an example of calculation is given in Figure 6.

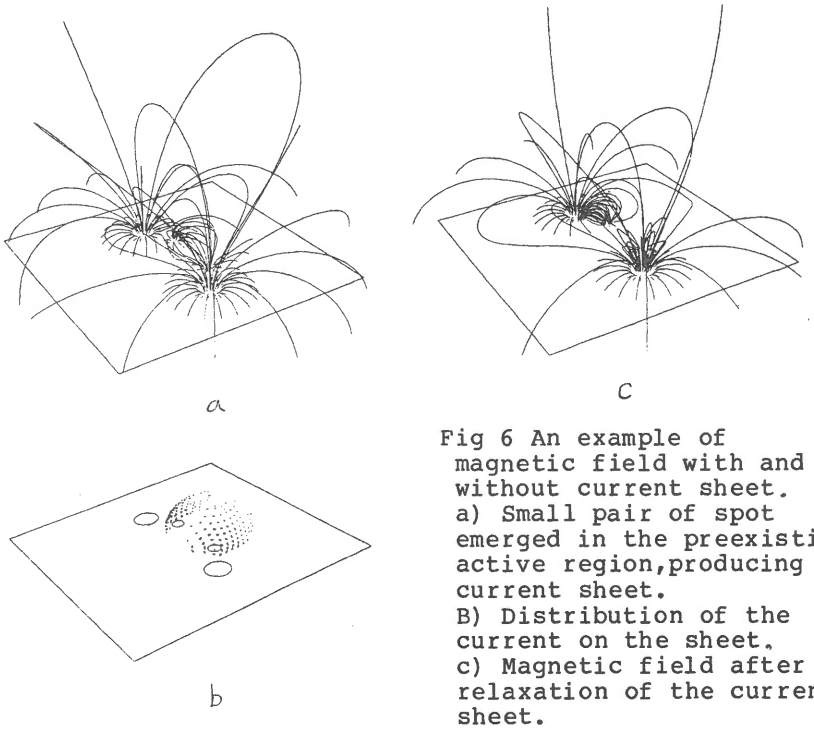

Fig 6 An example of magnetic field with and without current sheet.
a) Small pair of spot emerged in the preexisting active region,producing current sheet.
B) Distribution of the current on the sheet.
c) Magnetic field after relaxation of the current sheet.

Reconfiguration of this type is certainly seen in some flares observed in X-rays or EUV lines (Sheeley et al 1974b). Purely field-aligned current and purely sheet current, however, are idealizations and both may coexist more or less in actual cases. It is, however, important to establish which is the main mechanism of

flare energy storage, in order to pin down the flare mechanism. More observation in X-ray and EUV lines which cover the build-up and release phases of flares is highly desirable.

3.3. Possibility of Direct Geometrical Determination of Magnetic Field

Lastly, a brief remark for the possibility of the direct geometrical determination of the field and current is given. We discussed in the above the parameter-fitting by using models, but it would be better if the field can be calculated model-free. This may in principle be possible if we obtain the three dimensional shape of the loops purely geometrically from the comparison of photographs taken with appropriate time separation (long enough to produce stereo effect but short enough compared with the life of a loop). Three dimensional shape of the loop can be obtained as the intersection of two cylindrical(non-circular) surfaces, each of which contains the loop itself and the projection of it on the solar surface at the relevant time, one being rotated back by the angle corresponding to the solar rotation during the time separation. Computor programs are now being prepared in order to do this from the time sequence of X-ray photographs of AS and E experiment on Skylab.

4. Summary and Discussion

At present, it is still impossible to say that the knowledge about the coronal magnetic field is established. It is still difficult to have decisive information about the coronal magnetic field from radio observations since most of them as they are, involve with other unknown entities of which we have to make some assumption. Compared with these, the method using the geometry of loops observed in X-ray or EUV lines is rather naive one, and the only assumption is that these loops are frozen-in inhomogeneities to the magnetic field. This assumption seems to be safe except for the transiency during the flare time,for example. The state of the matter with this method is pretty far from being complete but there is a hope to do this first in the model-fitting method and gradually in full to determine the current as well as the magnetic field on computors.

References

Altschuler,M.D., and Newkirk,G.,1969, Solar Phys. 9, 131.

Altschuler,M.D. ,Levine,R.H ,Stix,M. , and Havey, J., 1977, Solar Phys.51, 345.

Barns,C.W., and Sturrock,P.A.,1972, Astrophys.J.174, 659.

Behannon,K.W ,1976, in Physics of Solar and Planetary Evironment, ed, Willioms,D.J. (Am. Geophys. Union), p 332.
Chiu,Y.T. and Hilton,H.H.,1977, Astrophys.J. 212,873.
Dulk,G.A., and McLean,D.J.,1978, Solar Phys.57, 279.
Levine,R.H., and Altschuler,M.D.,1974, Solar Phys.36, 345.
Nakagawa,Y., and Raadu,M.A.,1972, Solar Phys.25, 127.
Poletto,G.,Vaiana,G.S.,Zombeck,M.V.,Krieger,A.S., and Timothy,A.F., Solar Phys.44, 83, 1975.
Rust,D.M.,1968, in IAU Symp. No 35,Structure and Development of Solar Active Regions, ed.Kiepenhener, K.O. (D.Reidel),p77.
Rust,D.M.,1972, Solar Phys.25, 141.
Sakurai,T., and Uchida,Y.,1976, Abstract, US-Japan Cooperative Seminar High Eenergy Phenomena in Solar Flare, Tokyo Japan, p V 3.
Sakurai,T., and Uchida,Y.,1977, Solar Phys.52, 397.
Sakurai,T.,1977, Publ. Astron. Soc. Japan, 31, 209.
Sakurai,T.,1980, CFA Reprint No 1316, Harvard.
Schatten,K.H.,Wilcox,J.M. and Ness,N.F.,1969, Solar Phys.6, 442.
Schmidt,H.U.,1964, in NASA Symp. on Physics of Solar Flares, ed. Hess,W.N., (NASA) p 107.
Sheeley,N.R.,Bohlin,J.D.,Brueckner,G.E.,Purcell,J.D., Scherrer, V. and Tousey,R.,1974, Solar Phys.40, 103.
Sheeley,N.R. ,Bohlin,J.D. ,Brueckner,G.E. ,Purcell,J.D., Scherrer,V.,Tousey,R.,Smith,J.B.,Speich,D.M., Tandberg-Hanssen,E.,Wilson,R.M., de Loach,A.C., Hoover,R.B., and McGuire,J.P.,1975, Solar Phys.45, 377.
Sturrock,P.A., and Woodbury,E.T.,1967, in Plasma Astrophysics, ed. Sturrock,P.A.,(Academic Pr.), P155.
Svestka,Z.,Krieger,A.S.,Chase,R.C., and Howard,R., Solar Phys. 52, 69.
Takakura,T.,1967, Solar Phys., 1, 304.
Uchida,Y.and Sakurai,T.,1977, Solar Phys.,51, 413.
Vaiana,G,Krieger,A.S., and Timothy,A.F.,1973 Solar Phys. 32, 81.
Woltjer,L.,1958, Proc. Nat. Acaad. Sci. USA, 44, 489.

AN ANALYTICAL APPROACH TO THE THREE-DIMENSIONAL STELLAR(SOLAR) WIND SOLUTIONS WITH MAGNETIC FIELD

Osamu Kaburaki
Astronomical Institute, Faculty of Science, Tôhoku University, Sendai 980, Japan

1. Introduction

Although more than two dacades have past since Parker[1] predicted the existence of the solar wind, no satisfactory solution to the combined problem of stellar-wind and magnetospheric structures has been obtained yet. The main difficulties seem to be arisen from the following two points.

Firstly, the inclusion of the magnetic field $\mathbb{B}$ and the stellar rotation Ω breaks symmetry. Though in the absence of them the spherically symmetric, therefore one-dimensional, treatment is possible, in the presence of them the three-dimensional treatment is in general required. This difficulty can be reduced to some extent by considering only axisymmetric magnetic fields around a rotation axis, as most researchers do. In our treatment, however, this point is overcome by adopting a coordinate-independent description (i.e. the vector representation) in which the expressions of physical quantities are the same for both aligned- and oblique-rotation cases.

Secondly and this is the most troublesome, the outer boundary conditions can not be known explicitly until the problem is solved. Therefore we use here a kind of successive-approximation method starting from a well known situation. For simplicity, we assume that the stellar magnetization has only a dipole moment μ and that all time variations are due only to the stellar rotation (the quasi-steady condition). The modifications of this dipole magnetic field are investigated in turn which are respectively due to the effects of 1) stellar rotation in the asymptotic regions (the solutions in this approximation are called the asymptotic solutions), 2) stellar rotation in the whole vacuum space (the vacuum solution), 3) corotating plasma around a star (the corotating-plasma solution), 4) inertia of a rotating plasma (the centrifugal-wind solution) and 5) pressure and gravity forces (the stellar wind solution in general).

We have already solved the problems up to the third step. The fourth step is now in progress.

2. Asymptotic Solutions[2)]

The expression is well known for the vector potential $\mathbb{A}_0$ and the magnetic field $\mathbb{B}_0$ produced by a dipole moment μ in a vacuum, which is at rest in an inertial frame. In the first step of the successive approximations, the effects of stellar rotation is considered in two asymptotic regions, the near zone ($r \ll r_L$) and the wave zone ($r \gg r_L$), where r is the radial distance from the center of a star and $r_L = c/\Omega$ is the light radius.

In the near zone, the vector and scalar potentials are obtained from a general relativistic consideration, and it is shown that the Backus term[3)] in the scalar potential results from the transformation law of the potentials between the rest and rotating frames.

In the wave zone, the dipole approximation is used.

The results thus obtained coinside with that of Deutsch[4)] as can be confirmed by writing out all the components in the spherical polar coordinate.

3. Exact Vacuum-Solution[5)]

The effects of stellar rotation are exactly included in the solution by neglecting all sources (the electric charge and current densities) except for the stellar magnetization current. In this approximation the scalar potential can be put equal to zero. All the effects of rotation are expressed in terms of the operators acting on the zero-order solution $\mathbb{A}_0$: they are the rigid-rotation, retardation and radiation operators. This solution reduces in the asymptotic regions to the asymptotic solutions obtained in the previous step, and is the generalization to a general oblique-rotation case of the solutions obtained by some previous authors[6)] in the orthogonal-rotation case ($\mu \perp \Omega$).

The vacuum solution is used[7)] to infer the structure of the neutral sheet (or the polarity-reversal-surface) in the heliomagnetosphere. This is a three-dimensional counter part of the solar sector boundaries.

4. Corotating-Plasma Solution[8)]

In this step of approximation, a corotating plasma sphere of radius b ($b \leqq r_L$) around the star is taken into account. The plasma is assumed to corotate strictly. In reality, since the mass of the plasma is non-zero the centrifugal force drives an outward plasma flow even if other non-electromagnetic forces are negligible. The inertial force, which is approximately given in terms of the gradient of the non-Backus part of the scalar potential, is considered to be balanced by an imaginary force. Thus, instead of solving a dynamical equilibrium with the plasma outflow, we solve only Maxwell's equations for corotating plasma region ($r \leqq b$) and for the outer vacuum space ($r > b$).

The obtained structure of magnetic lines of force is not so drastically different from that in the vacuum case, even in the limit of $b \to r_L$.

5. Centrifugal-Wind Solution

Inclusion of the inertial terms in our consideration yields a formula for the electric field (generalized Ohm's law) such as

$$\mathbb{E} + \frac{1}{c} \mathbb{v} \times \mathbb{B} = \frac{1}{en} (q\mathbb{E} + \frac{1}{c} \mathbb{j} \times \mathbb{B})$$

in a perfectly conducting plasma, where $\mathbb{E}$ and $\mathbb{B}$ are the electric and magnetic fields, $\mathbb{v}$ and n are the velocity and density of the plasma, q and $\mathbb{j}$ are the electric charge and current densities, respectively, and e is the charge unit. The right-hand side of this equation can be rewritten in terms of the inertial terms by using the equation of motion. Generally speaking, the appearence of this term implies the "violation of flux freezing".

Our preliminary analyses[9] strongly suggest the coexistence of closed magnetic lines of force and plasma outflow across them, as in the numerical results of Kuo-Petravic et al.[10].

References

1) Parker, E.N.: 1958, Astrophys. J. 128, 664.
2) Kaburaki, O.: 1978, Astrophys. Space Sci. 58, 427.
3) Backus, G.: 1956, Astrophys. J. 123, 508.
4) Deutsch, A.J.: 1955, Ann. D'Astrophys. 18, 1.
5) Kaburaki, O.: 1980, Astrophys. Space Sci. 67, 3.
6) Endean, V.G. and Allen, J.E.: 1970, Nature 228, 348.
   Ferrari, A. and Trussoni, E.: 1973, Astrophys. Space Sci. 24, 3.
7) Kaburaki, O. and Yoshii, Y.: 1979, Solar Phys. 64, 187.
8) Kaburaki, O.: 1980, Astrophys. Space Sci. in press.
9) Shibata, S., Kaburaki, O. and Okazaki, M.: to be published.
10) Kuo-Petravic, L.G., Petravic, M. and Roberts, K.V.: 1975, Astrophys. J. 202, 762.

WIDE BAND POLARIZATION OF SUNSPOTS

Mitsugu Makita
Tokyo Astronomical Observatory, University of Tokyo,
Mitaka, Tokyo, Japan

1. Observations

The wide band polarization of sunspots was first systematically observed by Leroy (1962). He measured the linear polarization and interpreted it as the differential saturation effect of π and σ Zeeman components. In 1974, Illing et al. (1974a, 1974b, 1975) measured all the polarization components, i.e., Stokes parameters, and found a net circular polarization. Our recent preliminary observation, made at the Okayama Astrophysical Observatory, almost confirms their result. The first two observations used a color or interference filter and put a polarimeter at the prime focus. Ours is made at the coude focus with the use of two polarization compensators (Makita 1970), and with a 10m-spectrograph. A summary is given in table 1.

Table 1. Observations of the Wide Band Polarization of Sunspots

observer & site	spectral range	spatial resolution	remarks
Leroy(1962), Meudon	4400A-4900A (filter)	5 arc sec.	only the linear polarization is measured.
Illing et al.(1974), Mt. Haleakala	5250A-5350A (filter)	4 arc sec.	
Ours, Okayama	5243A-5257A (spectrograph)	6 arc sec. x 3 arc sec.	

The Stokes parameter map of the sunspot thus obtained so far is listed in table 2. Our maps are shown in figure 1. They need some correction for a spatial distortion due to an indirect guiding of the

Figure 1. Stokes Parameter Maps Obtained at Okayama. From top to bottom, white light picture, circular polarization V(solid line shows a positive polarity), linear polarization L(dotted line shows a depression), and direction of the linear polarization, the bar length is equivalent to about 4 arc sec. Broken line is along V=0. Thick line shows the photosphere-penumbra boundary obtained from the intensity record. Comparison of this with the white light picture shows a image distortion of the scanning system. A step of the isopolarization curve is 5.10^{-4} and $2.5.10^{-4}$ for L and V, respectively. The outermost isopolarization curve also corresponds to this value. C shows the disk center direction.

JULY 25, 1979 JULY 27, 1979

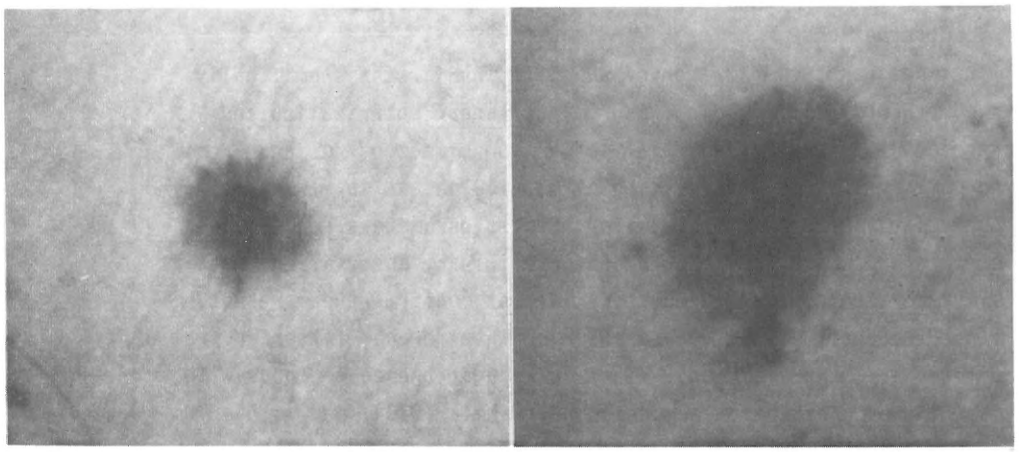

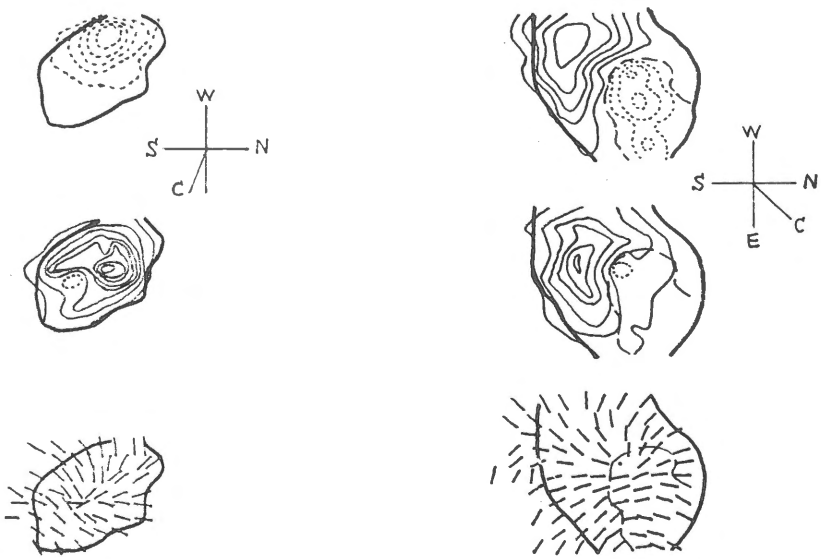

Figure 1. Stokes Parameter Maps Obtained at Okayama. (continued)

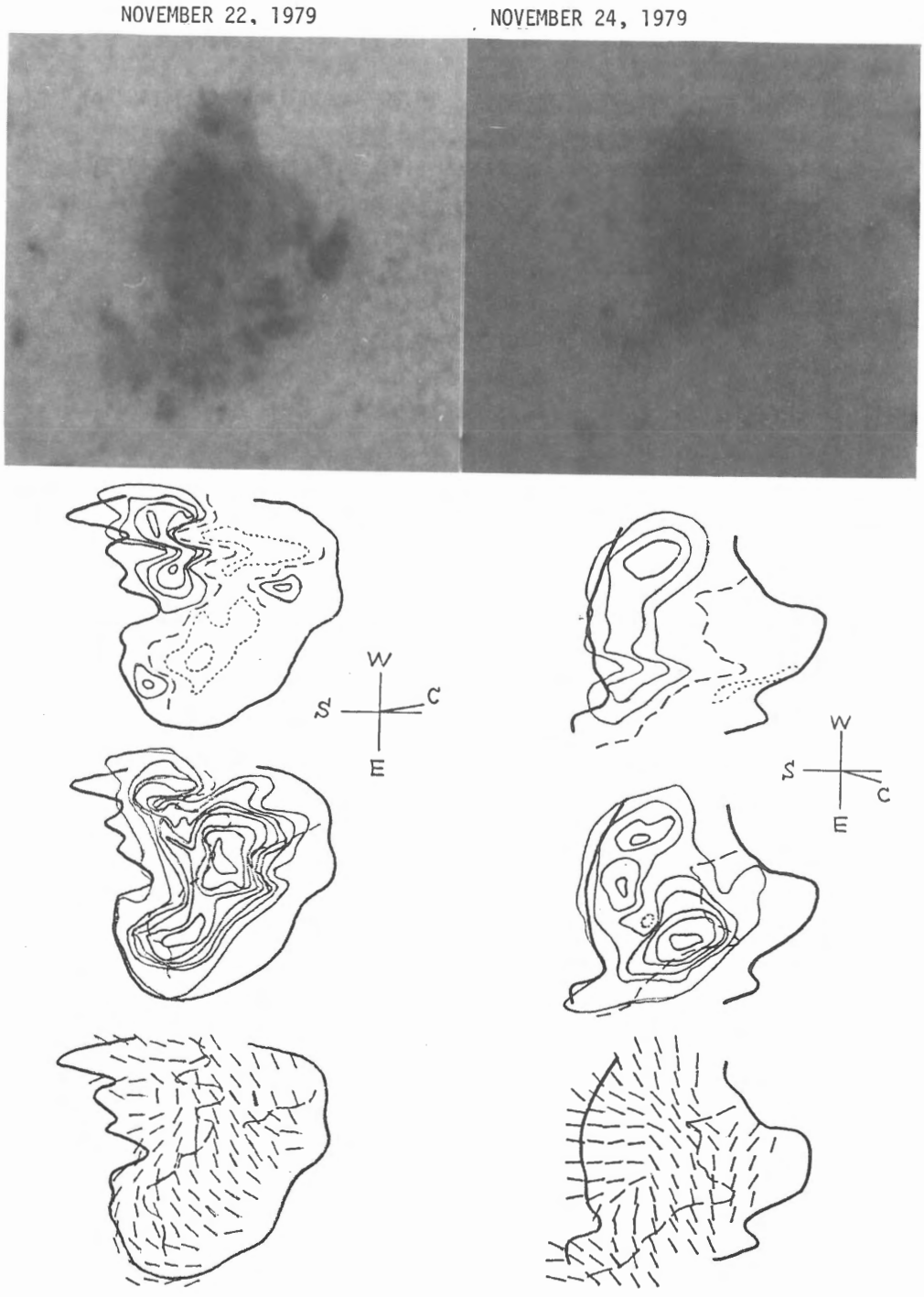

Table 2. Stokes Parameter Map

date	spot no.*	$\sin\theta$**	$\cos\theta$**	remarks
1974 Feb.15 20h(UT)	26p,f	0.44	0.90	Illing et al.(1974b)
21h	21p	0.79	0.61	"
Feb.19 19h	27f	0.37	0.93	Illing et al.(1975) also observed in 5824A-5844A
Mar.26 2h	39p	0.31	0.95	Illing et al.(1974a)
27 2h	"	0.53	0.85	"
27 19h	"	0.67	0.74	"
28 20h	"	0.81	0.58	"
29 2h	"	0.85	0.53	"
29 21h	"	0.93	0.37	"
1979 Jul.25 6h	330	0.40	0.92	see figure 1
27 6h	342p	0.36	0.93	"
Nov.22 4h	562p	0.54	0.84	"
24 0h	"	0.45	0.89	"

* from "Solar Data"(Russian), p: preceding sunspot, f: following sunspot
** θ is heliocentric angle of the sunspot.

solar image by a side telescope, but this is not performed there. For the circular polarization, we adopt the sign convention in radio-wave theory, instead of in optics.

2. Origin of the Polarization

The observed polarization was assumed, by Leroy (1962), to be due to the Zeeman effect of the spectral line. Illing et al. (1974a, 1974b, 1975) also selected the same assumption. Figure 2 shows an example of our observation with and without a mask, put at the spectrograph exit and stopping the light at the strong spectral lines. (The mask should be carefully inserted, since the line wing left uncovered may fairly contribute to the net polarization) This clearly proves that the main polarization source is the strong spectral lines.

The interpretation of the linear polarization was beautifully done by Leroy (1962), therefore, we do not discuss it here. For the circular polarization, Illing et al. (1975) first proposed a joint effect of the

Figure 2. Observed Stokes Parameters of a Sunspot with and without Strong Lines. Broken curves show the observation without strong lines.

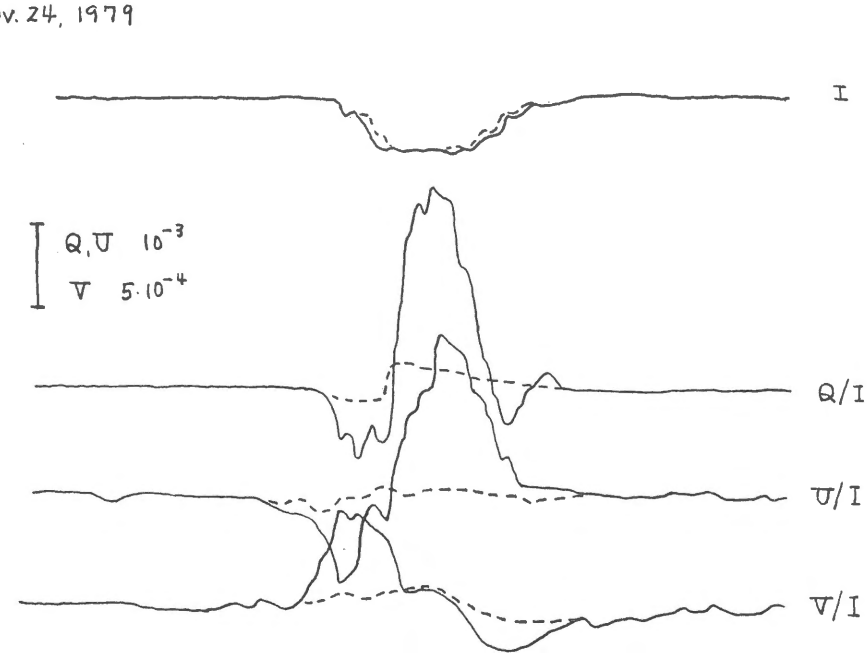

velocity and magnetic field gradients. Since the absorption coefficient of the σ component is symmetric against the line center, the observed net circular polarization implies some kind of asymmetrized effect in the line-forming layers. This is the velocity gradient. In the homogeneous magnetic field, it makes the coupling of the π and σ components asymmetric and causes a differential saturation effect. Under this assumption, the net circular polarization of a single line was estimated by Auer and Heasley (1978) and myself (1975, unpublished), for the atmosphere of the linear source function, $B=B_0(1+\beta\tau)$, and of the constant ratio of the line-to-continuum absorption coefficient, η . Figure 3 gives the result for the magnetic field at the disk center, having the various tilt, ψ , against the line of sight. At ψ =0° and 90°, there is no coupling of the π and σ components and no net circular polarization. The calculated value is at most 2.10^{-3}, just as much as the observed polarization. Accordingly, the strong saturated lines with η =20 must fully occupy the observed wavelength range.

Figure 3. Calculated Net Circular Polarization of a Single Line. The magnetic field is at the disk center and has a tilt ψ against the line of sight. An atmosphere with a linear source function B and a constant ratio η of the line-to-continuum absorption coefficient is assumed. Velocity $v(\tau)$ and Zeeman shift v_H, both normalized by the Doppler width, and the other parameters in the calculation are given in the right side. × shows the polarization when a different parameter, assigned by the arrow, is adopted.

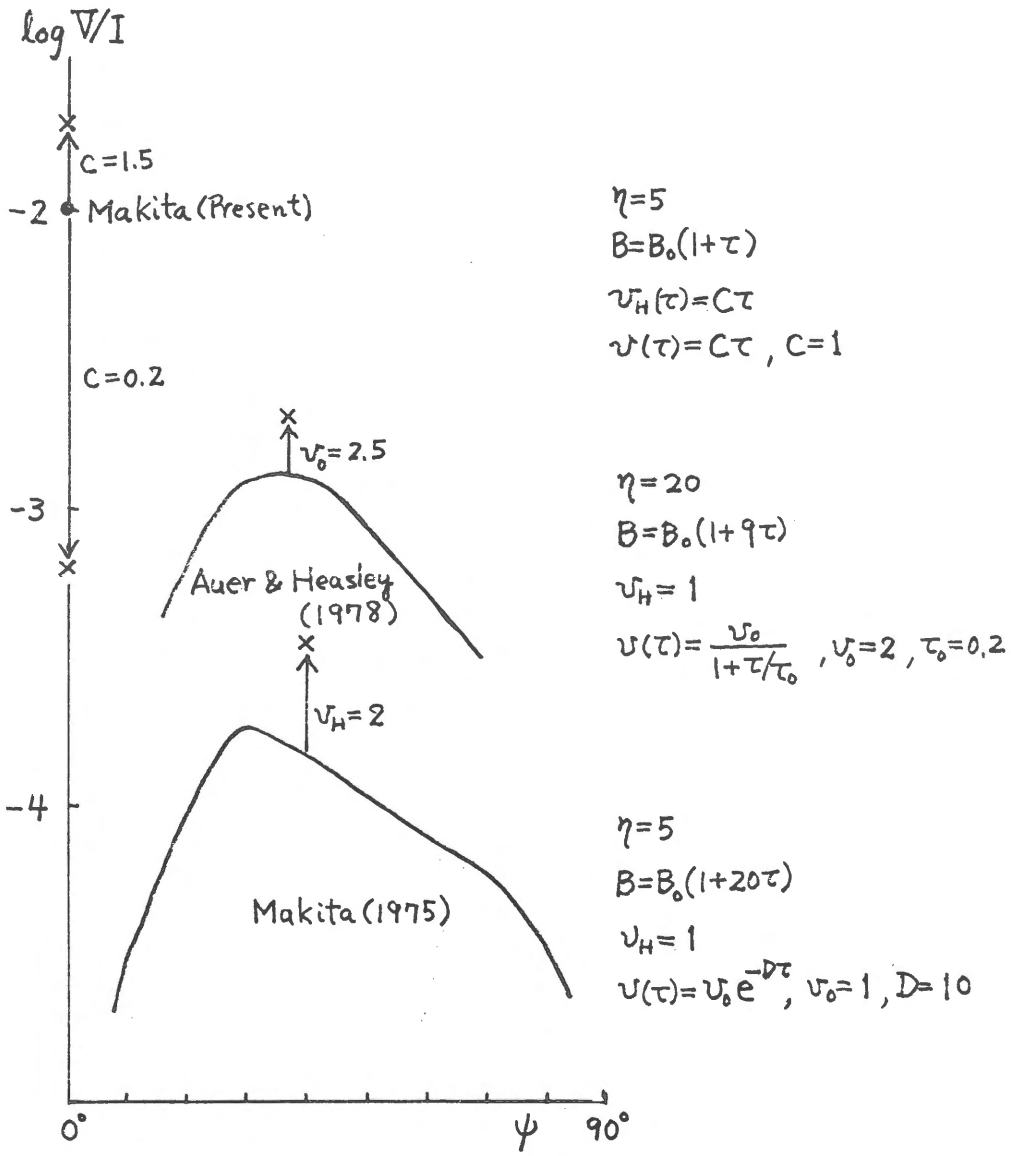

This may not be probable and the other more powerful polarizing mechanism should be considered. Figure 4 shows such an another saturation mechanism, which is along the first proposal by Illing et al. (1975). Suppose the magnetic field is longitudinal and the velocity shift at every depth is equal to the Zeeman shift. Then, one σ component of the absorption coefficient is unshifted and suffers a greater saturation than the other component. A calculation for this case, under the same assumption of the atmosphere, gives the value of 10^{-2}as shown in figure 3. Consequently, it will be reasonable to conclude that both the velocity and magnetic field shifts have to vary within a unit optical depth by a few times of the Doppler width, in order to explain the observed net polarization of 10^{-3}.

Figure 4. Differential Saturation of the Zeeman σ Components. In the case of a longitudinal magnetic field, absorption coefficients at four atmosphere levels (τ_1 , τ_2 , τ_3 , τ_4) are schematically shown. Due to the combined effect of the Zeeman and velocity shifts, one σ component suffers a greater saturation than the other. The resultant spectral line has a non-vanishing net polarization.

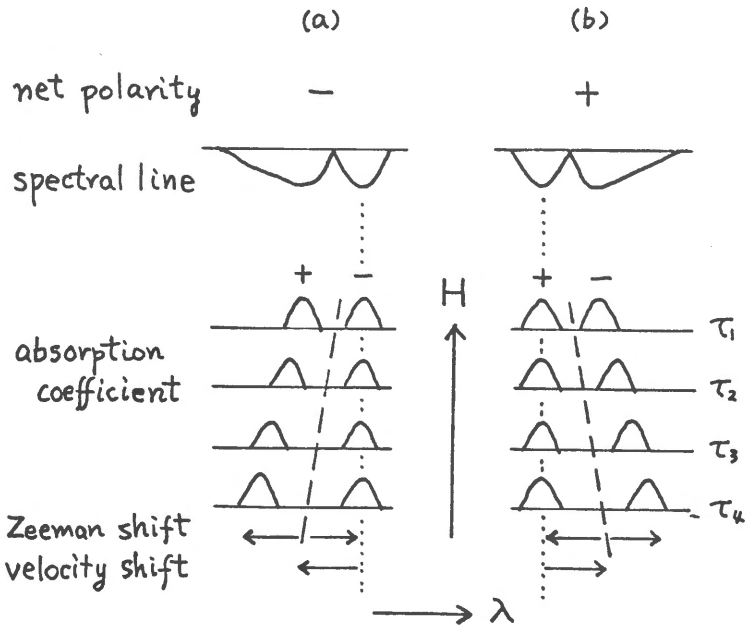

3. Discussion on the Net Circular Polarization

The velocity field in the penumbra is known as the Evershed flow. By St. John's analysis (St. John 1913), it is an outward radial flow from the umbra and its speed increases in deeper layers. If we accept this and consider a sunspot with a positive magnetic polarity, N, the polarity of the wide band observation is expected from figure 4, following the conclusion in the preceding section. (Since the differential saturation effect of σ components is essential, the idea of figure 4 will be applicable to the case of non-longitudinal magnetic field) In the limb side penumbra, both the magnetic line of force and the flow go away from us. The figure 4b shows this, if we reverse the magnetic polarity. Accordingly, a net negative polarization is expected there. In the center side penumbra, with the approaching flow and the positive magnetic polarity, the figure 4a is the case, and the expected net polarity is also negative. Since the umbra is reported to have no measurable velocity (Beckers 1977), its net polarization will be negligible. Consequently, we expect that the net polarity is the same throughout the sunspot and the net polarization is weak in the umbra and at places with negligible longitudinal magnetic field.

The 13 circular polarization maps listed in table 2 are not consistent with the above expectation. They show a strong limb side polarization, and, in the center side, a weak or negligible reverse polarization (ours) or a 'speckle' with the reverse polarity (Illing et al. 1974a, 1974b, 1975). If the limb side polarity is assumed to be principal, the correspondence between the magnetic and net polarization polarities is as given by Illing et al. (1974b) and agrees with our expectation. However, the existence of the opposite polarity in the center side of the sunspot will either force to reconsider the conclusion in the previous section, or demand some complex velocity and magnetic structure, different from that given by St. John (1913).

References

Auer, L.H. and Heasley, J.N. : 1978, Astron. Astrophys. 64, 67.

Beckers, J.M. : 1977, Astrophys. J. 213, 900.

Illing, R.M.E., Landman, D.A. and Mickey, D.L. : 1974a, Astron. Astrophys. 35, 327.

Illing, R.M.E., Landman, D.A. and Mickey, D.L. : 1974b, Astron. Astrophys. 37, 97.

Illing, R.M.E., Landman, D.A. and Mickey, D.L. : 1975, Astron. Astrophys. 41, 183.

Leroy, J.L. : 1962, Ann. d'Astrophys. 25, 127.

Makita, M. : 1970, Ann. Tokyo Astron. Obs. 12, 139.

St. John, C.E. : 1913, Astrophys. J. 37, 322.

THREE-COMPONENT MAGNETIC FIELD OF SUNPOTS

H. kawakami and M. Makita*
Department of Astronomy, University of Tokyo, Bunkyo-ku, Tokyo
* Tokyo Astronomical Observatory, Univ. of Tokyo, Mitaka, Tokyo

Four Stokes parameters of sunspots were observed with the photographic polarimeter fed to the Okayama 65cm solar coude telescope, and the three-component magnetic field was obtained. The Okayama solar coude telescope has two tilting mirrors (the coude mirror and the auxiliary mirror) which affect the polarization of the light from the sun. This instrumental effect should be corrected as shown in figure 1.

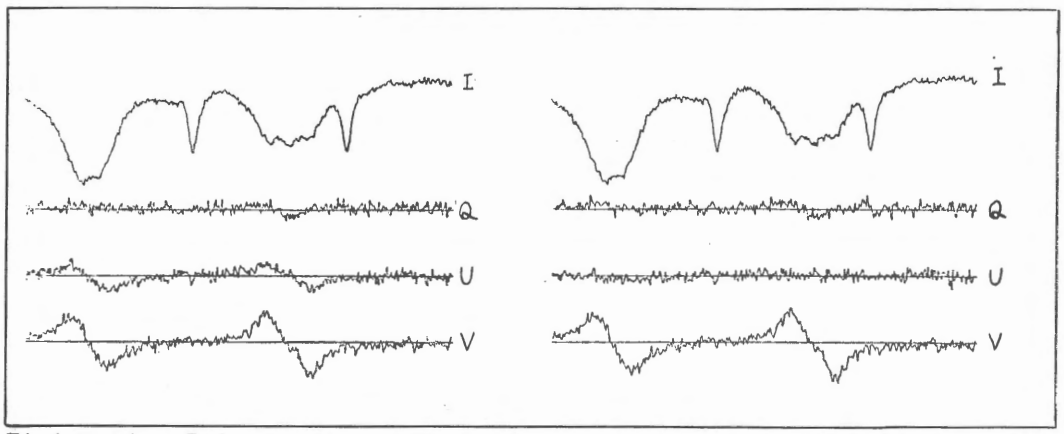

Figiure 1. Polarization effect of the tilting mirrors. Original Stokes parameters are on the left and the corrected ones on the right. Instrumental linear polarization (U) is removed in the right hand record.

The calibration of the instrumental polarization showed, wihtin the photometric accuracy, that the effect of the auxiliary mirror was negligible and the effect of the coude mirror was in good agreement with the calculated one from the alminium optical constants given by Shulz

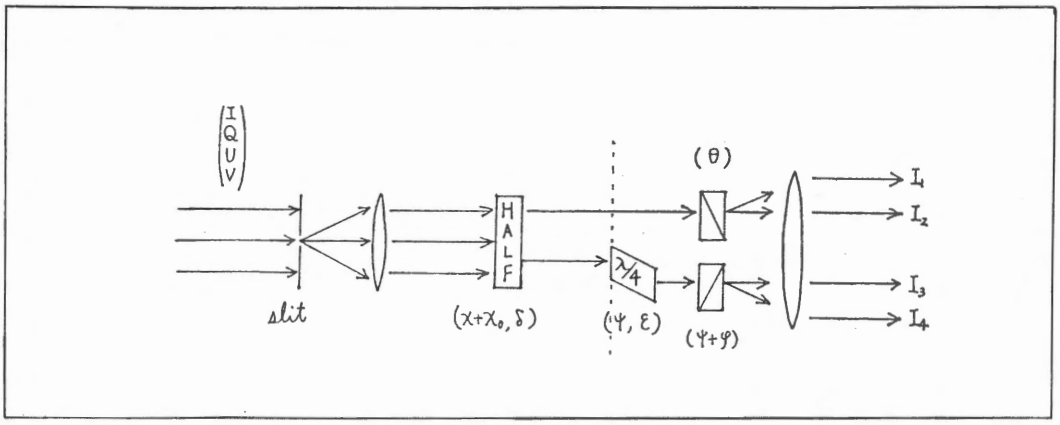

Figure 2. Schematic diagram of the polarimeter optics. A light beam is divided into four beams according to its polarization state. The symbols $(\chi+\chi_0)$, Ψ, $(\Psi+\varphi)$, θ show the direction of the crystal axis of a half wave plate, of a quarter wave retardar and of the Rochon analyzers respectively. And δ is the retardation of a half wave plate and ε is that of a quarter wave retardar. If the polarimeter is well constructed, $\theta=\Psi+\varphi=\chi_0=45^\circ$, $\Psi=0^\circ$, $\delta=180^\circ$, $\varepsilon=90^\circ$.

(1954) . Therefore, the instrumental effect was corrected by this calculation. Figure 2 shows the structure of the polarimeter, which is composed of a half wave plate, the Fresnel rohm as a quarter wave retardar, and the Rochon prism as an analyzer. The light entering the polarimeter is divided into four beams I1,I2,I3,I4 according to its polarization state. If the polarimeter is well constructed,

$$I1=(I-U)/2,\ I2=(I+U)/2,\ I3=(I-V)/2,\ I4=(I+V)/2 \quad (\text{for } X=0^\circ)$$
$$I1=(I+Q)/2,\ I2=(I-Q)/2,\ I3=(I-V)/2,\ I4=(I+V)/2 \quad (\text{for } X=22^\circ 5)$$

where, X is rotational angle of the half wave plate, and the sign of V is defined after the convention of radio wave thory. The calibration of the polarimeter parameters (e.g.,actual retardation of the half wave plate, actual direction of the crystal axis etc.) was made within the photometric accuracy. As seen above, we need two exposures and eight strips of a spectrum, to have a complete set of Stokes parameters. As four beams have different paths, illumination and relative positions among the four strips are different. This difference was corrected with the use of the continuum level and the atmospheric

lines.

A new method by Makita (1979) was taken in order to interpret the polarimetric spectra and determine the three-component magnetic field.

Makita's method assumes that:

(i) Magneto-optical effect is negligible.

(ii) The variation of any physical quantity is small along the layers of line formation.

(iii) The line profile can be divided into symmetry part and asymmetry part, the latter can be dealt with separately, following to E. Landi Degl'Innocenti and M. Landi Degl'Innocenti (1977) .

Assumption (i) is expected ,if the polarization degree is not so high. It implies U Should be zero at every wavelength, when a coordinate parallel to the azimuth of magnetic vector is taken. This transformation from the observing coordinate is performed as follows,

$$Q' = Q\cos 2\varphi + U\sin 2\varphi \quad (=\sqrt{Q^2+U^2}) \tag{1-1}$$

$$U' = -Q\sin 2\varphi + U\cos 2\varphi \quad (=0) \tag{1-2}$$

The linear polarization in the new coordinate, Q', is obtained from the first equation (see in the parenthesis) , and the azimuth of the magnetic field vector,φ, is derived from the second equation, since U' should vanish. Hereafter we omitt the prime from Q' and U'. The analytic solutions of the polarization transfer equation, W1,W2,W3, have relations with the observing quantities,I,Q,V as follows.

$$W1 = I + (Q\sin\Psi + V\cos\Psi) \tag{2-1}$$

$$W2 = I - (Q\sin\Psi + V\cos\Psi) \tag{2-2}$$

$$W3 = Q\cos\Psi - V\sin\Psi = 0 \tag{2-3}$$

where, Ψ is a known function of v,VD,a,VH,Ψ, and v is the wavelength deviation from the line center normalized by Doppler width VD, a is a damping constant normalized by VD, VH is Zeeman split of -component normalized by VD, and Ψ is the tilt of the magnetic field vector to the line of sight. As W3 is zero at every wavelength, $(Q\sin\Psi+V\cos\Psi)$ reduces to $\sqrt{Q^2+V^2}$. We can calculate W1 and W2 using only the observable quantities I,Q,V. As the analytic solutions, W1 and W2, have the same form except for the absorption coefficient (see Makita eq.(2.12)), the multiplet method is applied to W1 and W2.

$$\text{If } W1(v1)=W2(v2), \quad \text{then } \alpha 1(v1;VD,a,VH,\ )=\alpha 2(v2;VD,a,VH,\ ) \tag{3}$$

where, $\alpha 1$ and $\alpha 2$ are the absorption coefficients of W1 and W2 respectively, and both are the known function of v,VD,a,VH,Ψ. The multiplet method is also applied to W2 of two lines belonging to the same multiplet number.

$$\text{If } W2(v2)=W2'(v2'),\quad \text{then } \alpha 2(v2;Vd,a,VH,\Psi)=\alpha 2'(v2';VD,a,VH,\Psi) \tag{4}$$

where, the prime means the different line. The condition of eq.(4) enable to obtain VD,a for the case of a longitudinal magnetic field. Eq.(2-3) and (3) is applied to the line 6302.5 Fe which has Zeeman g-factor 2.5, and eq.(4) to this line and the same multiplet line 6301.5 Fe. Actually, we modify the eq.(3) and eq.(4) in order to treat every conditional equation eaqually and (O-C) of the observing quantities directly. Consequently, the parameters VD,a,VH,Ψ are determined by the least square method using the following conditional equations.

$$Q\cos\Psi - V\sin\Psi = 0 \qquad \text{for } \lambda 6302.5 \tag{5-1}$$

$$(\partial W2/\partial v\,|\,v2^0)(v2-v2^0)=0 \qquad \text{for } \lambda 6302.5 \tag{5-2}$$

$$(\partial W2'/\partial v\,|\,v2^{0\prime})(v2'-v2^{0\prime})=0 \qquad \text{for } \lambda 6301.5 \text{ and } 6302.5 \tag{5-3}$$

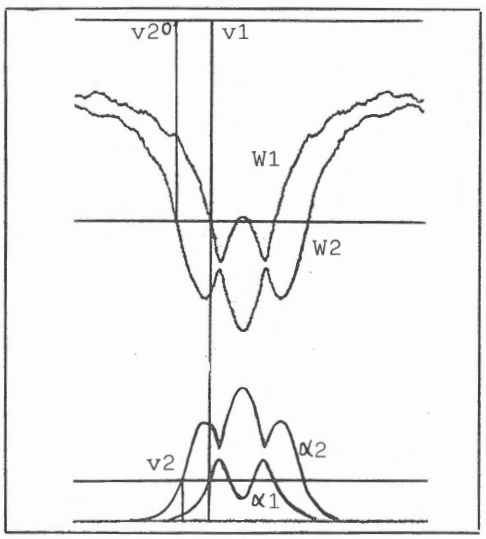

Figure 3. Application of the multiplet method. The upper is spectral line and the lower is absorption coefficient. We take v1 at first, then v2 and v2 are derived from the relations,
$W1(v1)=W2(v2^0)$ and $\alpha 1(v1)=\alpha 2(v2)$.
Parameters VD,a,VH,Ψ are determined so as to minimize the difference between $v2^0$ and v2 for all the different v1.

The meaning of v2 and $v2^0$ are shown in figure 3. In the eq.(5-3), the ratio of the gf value of the two lines was assumed to be 3, which is given by LS coupling assumption.

The validity of Makita's method was investigated by the residual error of U and eq.(5-1), (5-2) and (5-3). In most case it is within the photometric accuracy. Following the above procedure, two sunspots were studied. One is an active sunspot in which several large flares occurred, and the other is a stable unipolar sunspot which lasted 7 rotations. We should note that there exists an ambiguity caused by the two branch of φ and $\varphi+\pi$. The selection of this branch is carefully done by considering the reasonable spatial distribution of the magnetic vector.

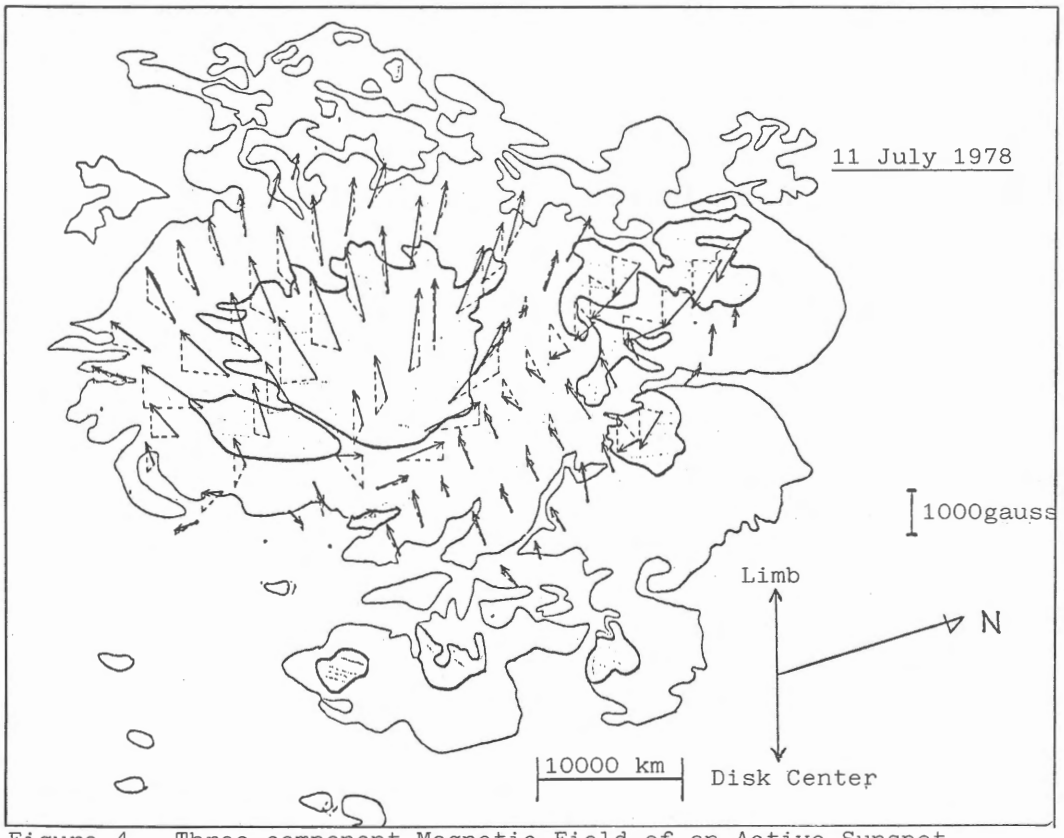

Figure 4. Three-component Magnetic Field of an Active Sunspot. solid lines represent the magnetic vector, and broken lines its vertical and parallel components to the solar surface,respectively. The lenght of the line shows the projection of the above three vectors to the line of sight. Vertical of the solar surface inclined by 45 .

INTERPRETATIONS OF SIMULTANEOUS OBSERVATIONS OF HIGH RESOLUTION SPECTRA OF CaII OVER A SUNSPOT UMBRA

Hong Sik Yun
Department of Astronomy, Seoul National University, Korea
Herbert A. Beebe and Wayne Baggett
Department of Astronomy, New Mexico State University, U.S.A.

1. Introduction

The central emissions of CaII H and K lines over sunspots have been measured by several workers. A comprehensive summary of these observations is given by Kneer and Mattig (1978). Mattig and Kneer (1978) demonstrated that sunspot chromospheres exhibit fine structures in the H and K lines. These structures indicate that the umbral chromospheres differ strongly from one region to another, even within a spot. Mattig and Kneer also noted that the profiles of the H and K lines vary with time on a relatively short time basis, implying that some time-dependent dynamical phenomena are occurring in the sunspot chromospheres. These findings lead us to believe that for the determination of the thermal structure of sunspot chromospheres, simultaneous observations are mandatory to avoid the dynamical disturbance influencing our observed spectra. In order to cover a wider range of depths and for completeness of chromospheric modellings, it is desirable to take into account all of the strong lines of CaII. Spectral features of CaII lines were observed simultaneously over a sunspot umbra (SPO 5007) by means of Sacramento Peak Observatory's HIRKHAD program (Beckers, 1972) with the Echelle spectrograph at the Vacuum Tower Telescope. The observed spectra of CaII H, K, λ8542 and λ8498 have been scanned by the SPO's fast microphotometer and reduced for theoretical interpretations. In the present study we examined only a specific region of the umbra which is thought to be coolest over the spot.

2. Observed Profiles

The sunspot we observed is a round, single spot (SPO 5007, December 18, 1979) whose diameter of the umbra is about 15 seconds of arc. About 3000 gauss is estimated from the Zeeman splitting of Fe I λ6303 with about 0.16Å.

The reduced profiles of CaII H, K, λ8542 and λ8498 lines sampled over the coolest region of the umbra are shown in Fig. 1. In Fig. 1a the dots represent a typical penumbral profile of CaII K, where it is compared with the umbral profile. In taking these umbral spectra, we scanned the umbral region spatially 1 seconds

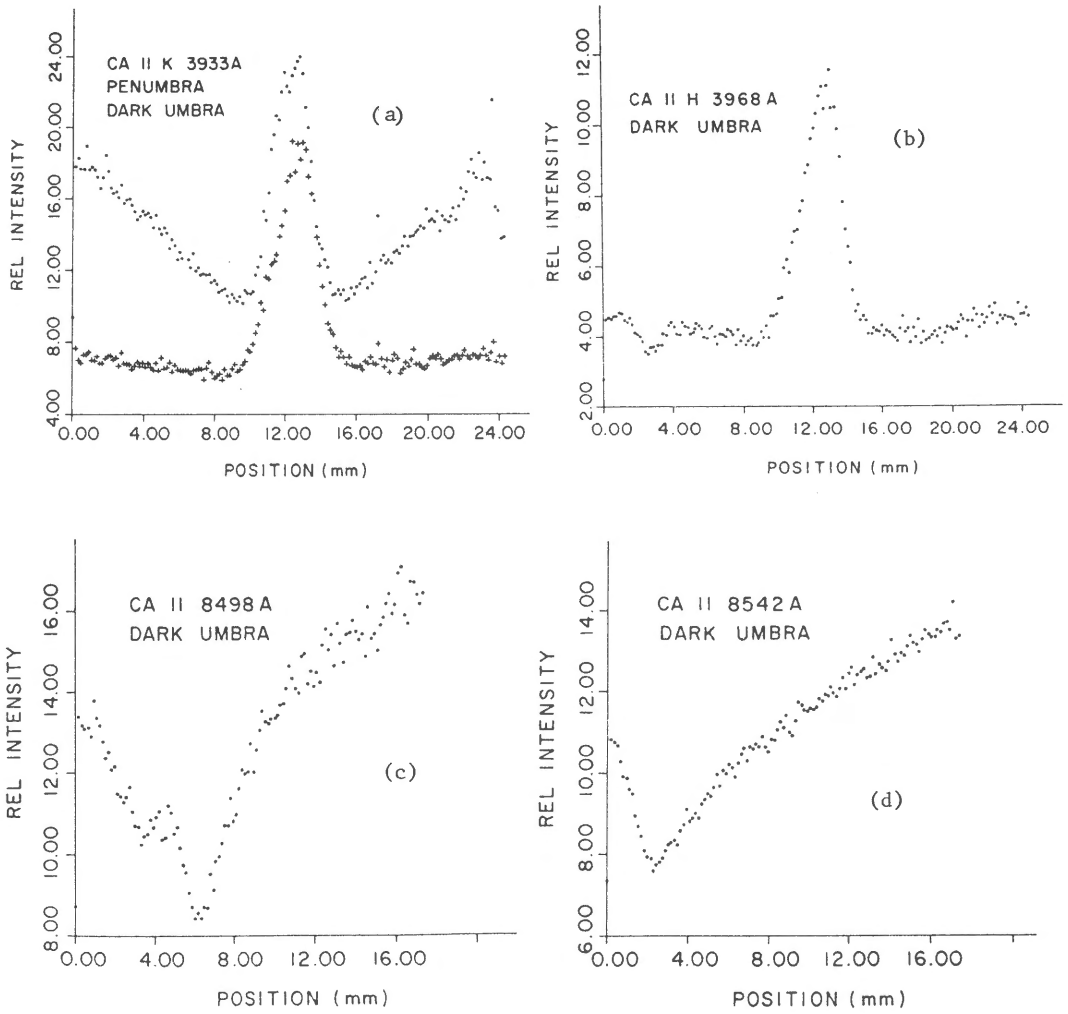

Fig. 1 The reduced profiles of (a) K (b) H (c) λ8498 (d) λ8542 expressed in relative intensity units. The scan position is given in mm from the beginning of the scan.

of arc apart. We blocked the entire spot and took the spectra of the blocked spot in order to estimate the amount of the scattered light inside the spectrograph.

3. Interpretation of observations

In order to explore the thermal structure of our umbral chromosphere, we adopted a frequently used empirical approach. In this approach one sets up the run of temperature and microvelocity with column mass density and then a self-consistent model of umbral chromosphere in hydrostatic equilibrium is constructed by solving the equation of statistical equilibrium of hydrogen. Making use of

this model, theoretical line profiles are computed by solving the non-LTE line formation problem and the computed profiles are compared with the observations. If the agreement between the observations and the calculation is not satisfactory, the model is perturbed in such a way to produce a closer agreement between the theory and the observations. In the present calculation, we used a computational program HCODE by Shine (1975) to solve the statistical equilibrium of hydrogen, and, for the computation of CaII line profiles, we employed another program deduced by Auer et. al. (1972). The model atom is assumed to consist of 3 levels plus continuum for hydrogen and 5 levels plus continuum for CaII, respectively. The values of the cross sections for collisional and radiative processes were adopted from Shine et. al. (1974). The abundance of Ca is taken to be 2.14×10^{-6}.

The optimum temperature-column mass density relation for the region we selected over the umbra is given in Fig. 2, where the column mass density near the top of the atmosphere was found to be $m_o = 5 \times 10^{-5} gm/cm^2$. In this figure

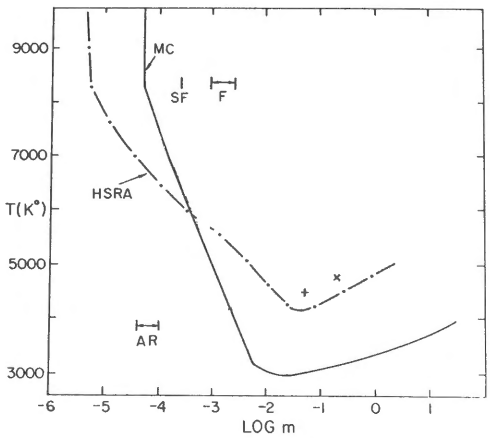

Fig. 2 Temperature distribution T(m) for a typical sunspot umbra as deduced from observed CaII H, K and λ8498. The cross (x) refers to the location of temperature minimum for flares (Machado et. al. 1975) and the dagger (+) for active region (Shine et. al. 1974). "F" and "AR" refer to the range in which the temperature gradient increases rapidly. (SF = Subflares)

the location of the temperature minimum for flares (Machado et. al. 1975; indicated by x) and for active regions (Shine et. al. 1974; indicated by +) are included for comparison. Fig. 3 shows the computed intensity profiles of H, K and the infrared λ8498, which are compared with the observed profiles. Our observed profiles of H and K do not show reversals, but the calculated profiles inevitably do show them. So, we invoke macroturbulence of 5km/sec as a simulation of large scale dynamic processes. The computed infrared line shows a mild emission core, which also disappears with the convolution of macroturbulence. The temperature minimum of our umbral atmospheres is found to be about $3000^{o}K$.

The authors wish to thank Professor W. Mattig for his kind advice on sunspot observations at the Sacramento Peak Observatory and Dr. J. Zirker, the Director for the use of observing facilities. This work was supported by SNU-AID program.

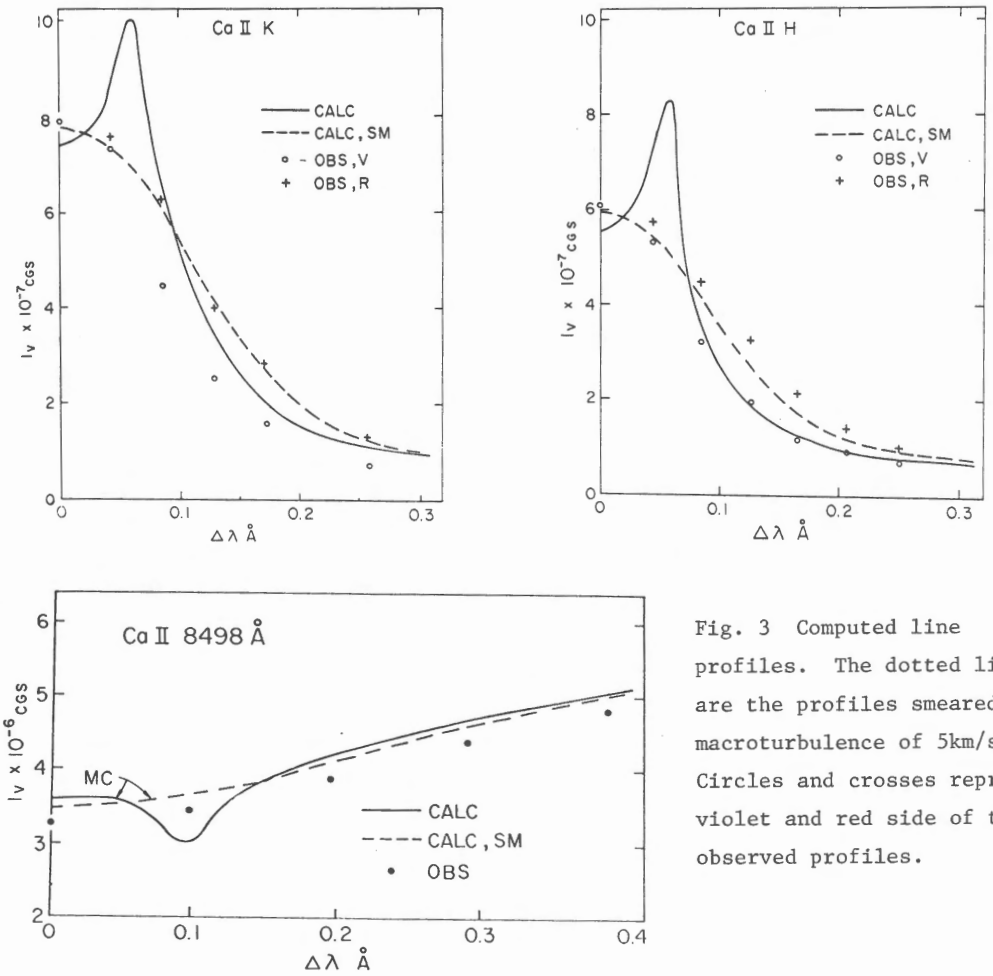

Fig. 3 Computed line profiles. The dotted lines are the profiles smeared with macroturbulence of 5km/sec. Circles and crosses represent violet and red side of the observed profiles.

REFERENCES

Auer, L.H., Heasley, J.N., Milkey, R.W.: 1972, Kitt Peak National Observatory Contribution No. 555

Beckers, J.N., Mauter, H.A., Mann, G.R.: 1972, Solar Phys., 25, 81

Gingerich, O., Noyes, R.W., Kalkofen, W., Cuny, Y.: 1971, Solar Phys. 18, 347

Kneer, F., W. Mattig: 1978 Astron. Astrophys. 65, 18

Machado, M.E., Linsky, J.L.: 1975, Solar Phys. 42, 385

Mattig, W., Kneer, F.: 1978, Astron. Astrophys. 65, 11

Shine, R.A., Linsky, J.L.: 1974, Solar Phys. 39, 49

Shine, R.A.: 1975, Private Communication

PRELIMINARY OBSERVATION ON THE GLOBAL ENERGY BALANCE OF SUNSPOT AND PHOTOSPHERIC FACULAE

T. Hirayama
Tokyo Astronamical Observatory
University of Tokyo

The following problems are treated in this report : first whether the missing energy flux of the sunspot appears as the extended bright ring surrounding it and secondly whether the excess energy flux in the active region represented as the photospheric faculae is compensated by the extended dark region surrounding the active region, if it exists at all.

For this purpose we used white-light photographs (5300A) of the Sun taken at Mitaka for routine observations (seven plates of 10cm solar diameter) and at Mt. Norikura (five plates of 2cm solar diameter). We measured the whole disk in 250 x 250 arrays and subtracted for limb darkening.

To search for the extended bright ring around the sunspot (EBR) we averaged the excess intensity over concentric rings surrounding a selected spot. The result shows that some spots do have EBR with the excess intensity of 0.5-0.8% near the penumbral border which decreases to the value of 0.1-0.2% at the distance of 10-15 $\times 10^4$km from the center of big spots. Beyond this distance it becomes impossible to determine the excess intensity because of the large scale inhomogeneity of the emulsion. These excess intensity distribution can be converted to the total energy of EBR using the relationship between the monochromatic flux and the total flux from the radiative equilibrium models of Kurcz(1969) where the grid of models with different effective temperatures for the same surface gravity is given and $\Delta\pi F / \pi F = 0.81 \times \Delta\pi F_\lambda / \pi F_\lambda$ can be deduced. The total energy flux of EBRs is found to be 0.3-1.2 x 10^{29}erg/s. Missing flux of the sunspot is, for example, about 1.3 x 10^{29}erg/s for the spot of diameter of 3×10^4km. Whether the EBR does really compensate the missing energy is critically dependent on the precise determination of further extended regions than our limit of $10\text{-}15\times10^4$km.

Some other spots, however, did not show any enhancement or revealed only marginal one even in the immediate vicinity of the penumbra. Interesting examples are given for two cases, April 10, 1980 and May 27, 1980 in which solar constant measurements by the SMM satellite showed 0.2-0.3% depression in the total solar

energy flux received from the earth, compared with the averaged value (Willson and Hudson, 1980). For these two plates we could only deduce the average excess intensity distribution for groups of big spots because big spots are aligned closely together and it is not possible to determine the excess intensity from a single concentric ring because of overlapping. In case for May 27th it shows that the excess brightness is less than 0.2% even in the neighborhood of the penumbra and it is consistent with the SMM solar constant measurement. The case for April 10 shows slight emission near the spot but because of the inhomogeneity of the emulsion the clear-cut conclusion was not reached.

Now we turn to the problem of the total energy balance of photospheric faculae : Active regions which do not contain large spots have been selected and the measured data are represented as the function of position angle and the radial distance from the disk center. The total excess energy from the facular region was, then, estimated using the known center-limb contrast of facular granules and the relation between the monochromatic flux and the total flux. It ranges from 1.5×10^{28}erg/s to 6×10^{29}erg/s and, as would be expected, the larger the Ca^+ plage area ($S(Ca^+)$ in $2\pi R^2 \cdot 10^{-6}$), the larger the total excess flux (E in erg/s) : $\log S(Ca^+) = 0.6 \times \log E - 14.2$. Scatter around this relationship is quite large, amounting to ± 0.6dex. Next in order to search for the extended dark region around the active region the curvature of the intensity distribution of adjacent quiet region along the position angle was inspected. If this intensity curve is concave towards the facular region it means there exists dark region and if convex, vice versa. The result indicates that the characteristic distance of the dark region must be larger than 35000km if we alow 95% statistical significance for the distribution of the curvature for fifty active regions. Or simply we did not detect the dark regions in the present investigation.

If we suppose that the facula is truely excess emitter and if we use the relationship between the Ca plage area and excess facular energy, we can conclude that the missing flux of sunspot might be balanced by the excess facular flux. And the SMM result does not prove that the sunspot energy flux is really missing since the satellite does not receive most of the excess facular flux of active regions around disk center. There are two possibilities in interpreting the present problem : (a) Sunspot and facular energy flux are independent and either they are balanced separately over very large area or they are not balanced because of the long time scale of convective motion if they are seated below the photosphere deeper than 40,000km (b) Both energy flux are closely interrelated in the sense that the energy flux from sunspot is converted to the facular energy flux in the convection zone. In this case (b), problem is how to interpret the big, long-lived facular regions without spots.

DISCUSSION OF THE SEMI-EMPIRICAL DETERMINATIONS OF THE OPTICAL DEPTH OF CHROMOSPHERE-CORONA TRANSITION C IV LINES

J.-C. Pecker[1], S. Dumont[1], Z. Mouradian[2], and E.G. Chipman[3]

[1] Collège de France, Paris

[2] Observatoire de Paris, Meudon

[3] Nasa, Washington

From the emission ratio of two lines of a doublet (such as the C IV 154.8 and 155.1 nm lines) or from the center-to-limb variation of a single line, one can extract the effective optical depth of the responsible layers. However, these deductions depend heavily upon the implicit or explicit assumptions made in the derivation. Two methods were used to analyze C IV lines observed with the LASP spectrometer aboard the OSO-8 satellite (see Bruner et al., 1977).

The correct expression of the measured intensity, at a given point on the profile, for one single line is :

$$I = \int_0^{\tau} S\, e^{-t} dt \qquad (1)$$

where τ is the optical depth of the emitting layer along the line-of-sight at any point of the spectral line profile. In a first approximation, the gradient of the physical quantities being steep and the depth τ being considered as corresponding to a narrow layer, one generally assumes S to be constant within the layer. Thus, the approximative form of Equation (1) may be written :

$$I = S\,(1 - e^{-\tau}). \qquad (2)$$

i) The doublet method essentially assumes that the two lines have the same source function. The ratio of the oscillator strengths of the two lines is $f_2/f_1 = 2$ in the case of the doublet C IV. Hence, τ_1 being the central optical depth for the weaker of the two lines (155.1), one may write :

$$\tau_1 = -\ln (2K - 1) \quad \text{and} \quad \tau_2 = 2\tau_1 \qquad (3)$$

where K denotes the quantity $I_2/2I_1$. I_2 and I_1 are the central intensity of lines 2 (λ154.8) and 1 (λ155.1).

An average value K = 0.875 was obtained for active areas (A), and 0.80 for the

quiet areas (Q), which, respectively, correspond to $\tau_1 = 0.29$ (A) and $\tau_1 = 0.51$ (Q) for the fainter component of the doublet C IV. The error bar is estimated to be of the order of $\Delta K = 0.2$ for the active areas and 0.35 for the quiet ones.

In this determination, we have combined results from all points of the solar disk. The two samples are indeed too small for a systematic differential study as a function of μ. The optical depths determined in this way shall hereafter be denoted by the single prime sign : τ'

ii) The center-to limb variation of a single line allows a determination of the optical depth, provided that the geometry is assumed to be essentially that of concentric spherical layers. The expression of the ratio of the line center intensities at two different locations on the solar disk is, thus, equal to :

$$I_o(\mu)/I_o(\mu=1) = (1 - e^{-\tau_0/\mu}) \; / \; (1 - e^{-\tau_0}) \qquad (4)$$

for $\mu \geq 0.2$, where the index o designates the quantities relative to the line center. Expression (4) does not depend upon the source function S, but (as for Equation (3)) S is assumed to be constant within the emitting layer ; the Doppler width is also assumed to be constant.

We obtained, for the 155.1 nm line, an optical depth at line center of 0.5 for active areas and 0.7 for quiet ones. The optical depths determined in this way shall hereafter be denoted by the double prime sign : τ''_o.

Some authors have also used the ratio of the integrated intensities, the integration being performed over the line profile such that :

$$I(\mu)/I\ (\mu=1) = \int_{-\infty}^{+\infty} (1-\exp(-\frac{\tau_0}{\mu} e^{-x^2}))dx \; / \; \int_{-\infty}^{+\infty}(1-\exp(-\tau_o e^{-x^2}))dx. \qquad (5)$$

According to Roussel-Dupré et al. (1979), who used this method, the ratio has the same form as Equation (4), where the indices o are suppressed ; then, τ (the "integrated depth") is equal to $k\tau_o$, and, according to the same authors, $k = \sqrt{\P}$. Actually, this is slightly incorrect ; a complete determination shows that k is indeed a function of τ_o/μ and the values of k differ from the denominator to the numerator. The net effect of this on the use of the ratio of integrated intensity is, actually, that they obtained, for the 139.3 nm line of Si IV, a value of τ closer to τ_0 than to $\tau_o\sqrt{\P}$. Although the use of Equation (5) presents no difficulty, we found

it more convenient to use Equation (4) and the ratio of line center intensities.

iii) Both of the above determinations make use of certain hypotheses, and we will now assess their validity to our particular problems.

A given model corresponds to a certain value of the optical depth τ_o of the emitting layer in line 1 (155.1 nm), for instance. Simulated profiles of lines 1 and 2 can be computed and, then, τ_o' and τ_o'' may be determined from them. A comparison is thus possible and allows us to test the method of determination of τ_o' and τ_o''.

The computed profiles on various μ give, with method (i), K values which lead to different τ_o', the best one being obtained with profiles near the limb. If we take the average of K on the disk, the value obtained for τ_o' differs from τ_o (true optical depth) by about a factor of 2. Numerical experiments have shown that this discrepancy is associated with the fact that the ratio S_2/S_1 differs from unity, even if only by a few percentage points. The error made in the computation of τ_o' by assuming this ratio to be equal to unity is important when the optical depth is small, i. e., near the center of the disk, since the simulations are made assuming spherical symmetry.

Method (ii) yields a value of τ_o'' that differs from τ_o by as much as 30 % (using either Equation (4) or Equation (5)). Note that the simulated profiles were computed in a spherically symmetric atmosphere.

iv) Conclusion. If used for observed profiles, both methods (i) and (ii) give approximatively the same optical depths τ_o' and τ_o'' ; the discrepancy can be explained with the influence of the fine structure of the solar atmosphere, i.e. some departure from spherical symmetry. Indeed the method (ii) must give an higher value of the optical depth than the true one if the atmosphere is heterogenous. Let us remind that both methods can be applied only to optically thin lines.

References

Bruner, E.C., Chipman, E.G., Lites, B.W., Rottman, G.J., Shine, R.A., Athay, R.G., and White, O.R., 1976, Astrophys.J.,210, L97.

Roussel-Dupré, Francis, M.H. and Billings, D.E., 1979, Month. Not. Roy. Astr. Soc., 187, 9.

THE MAGNETIC FIELD FLUX IN FACULAR REGIONS

Z. Mouradian[1], G. Chapman[2], S. Dumont[3], Ch. Fang[1,4], Y. Feng[1,5], J.C. Pecker[3]

1 Observatoire de Paris-Meudon

2 California State University, Northridge, USA

3 L.A.T. College de France

4 Université de Nankin, Chine

5 Observatoire de Yunnan, Chine

1. Introduction

The solar magnetic field ($\vec{B}$) is usually studied by observation of the value of the line-of-sight component ($B_{\parallel}$), (Harvey, 1977). In the present note we give preliminary results of another approach ; the study of the flux of the line- of-sight component (ϕ) of magnetic structures. Our study is statistical.

2. Data

To carry out this investigation, we used observations taken with the Kitt Peak magnetograph (Pecker et al., 1977). Maps (512" x 450") of $B_{\parallel}$ were obtained with the FeI λ 868,86 nm line and with an observing aperture of 1" x 1". The spatial resolution was about 1",5 to 2",5. We measured the flux (ϕ) of the magnetic structures limited by the isogauss 25, where

$$\phi = \int_S B_{\parallel} \, dS \qquad \text{for } B_{\parallel} \geqslant 25 \text{ gauss}$$

The surface (S) of the structures is between 6 and 2000 " x " The experimental error is less than 10 gauss for the given aperture.

3. Results

For each magnetic structure, we measured the flux (ϕ) through the surface (S) and obtained an empirical relation of the forme

$$\log \phi = c + d \log S \qquad (1)$$

The figure shows an example for the center of the solar disk. Two conclusions may be drawn : i) there is no basic difference between the magnetic field in faculae

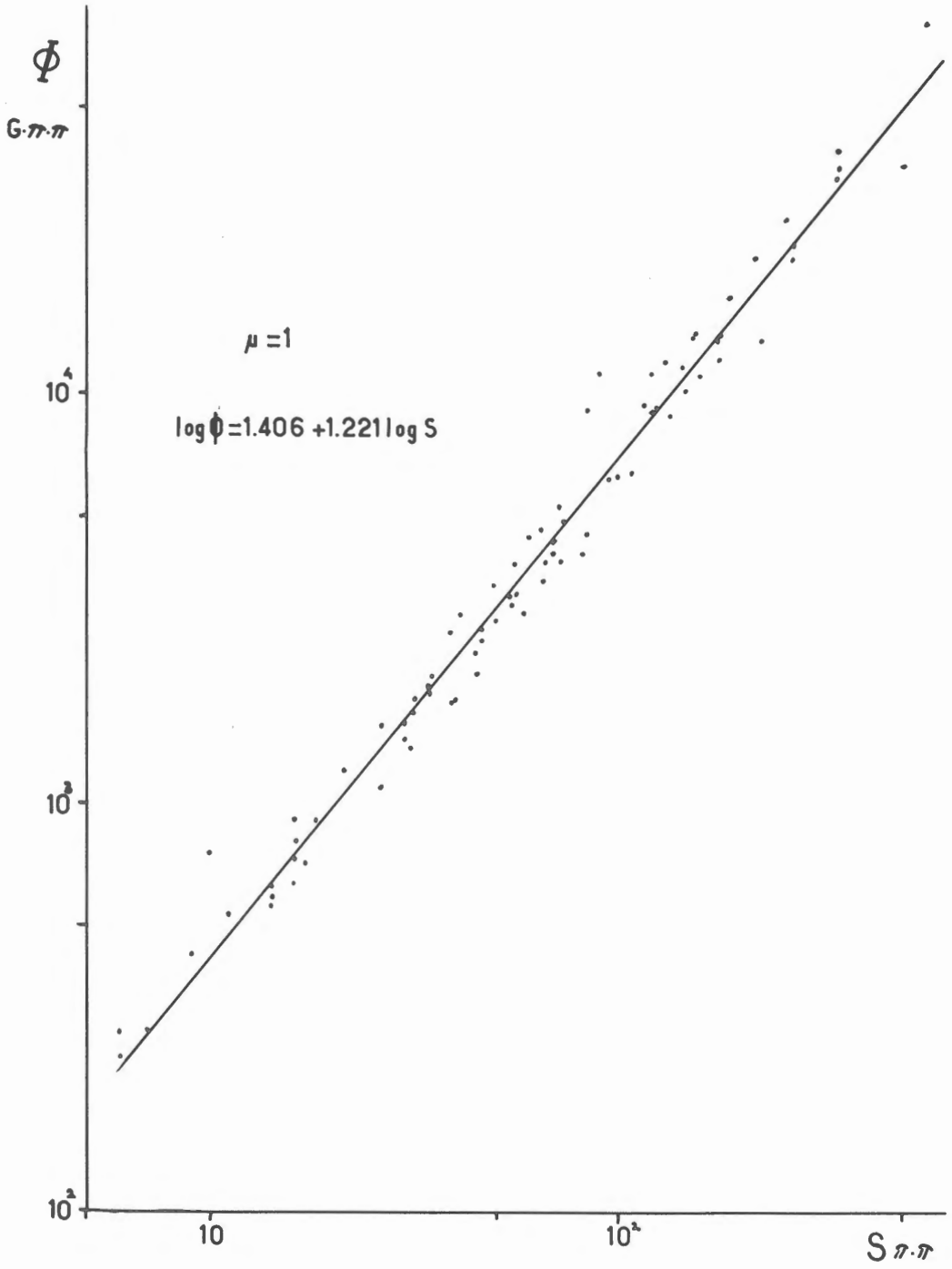
Φ
G·π·π
μ =1
log Φ=1.406 +1.221 log S
10⁴
10³
10²
10
10²
S π·π

and in plages, and ii) a very strong relationship exists between the flux of $B_{\parallel}$ and the occupied surface.

In our study, we do not take into account sunspots and pores, or peculiar regions such as bright X points, etc.

The relation (1) remains valid over the whole solar disk, only the constants changing :

μ	$\Delta\mu$	N	c	d	r	σ
1	1 -0.97	83	1.406	1.221	0.992	0.072
0.71	0.88-0.37	79	1.421	1.275	0.984	0.082
0.60	0.71-0.48	45	1.529	1.139	0.990	0.063
0.35	0.47-0	27	1.488	1.164	0.992	0.050

In the table, N represents the number of measured structures, r is the correlation coefficient and 6 is the standard deviation.

Two corrections can be applied to the relation (1) ; the first is a correction for the seeing influence and the second is for the influence of choice of the boundary of the structure, i.e. $B_{\parallel} \geqslant 25$ gauss, instead of the isogauss curve $B_{\parallel} = 0$.

The effect of the image quality is studied in two successive observations of the same region, one with good seeing and the other with bad seeing. The results show a "tilt" of the logarithmic relationship between ϕ and S, when the seeing is bad.

IQ	N	c	d	r	σ
good	63	1.399	1.228	0.997	0.061
bad	90	1.397	1.317	0.987	0.087

From the relation (1) and an examination of the choice of contours, we see an important change in the value of the c constant. The relation (1) becomes :

$$\log \phi_c = 0.34 + 1.44 \log S \qquad (2)$$

This is the true relationship between ϕ and S for the center of the solar disk. From the relation (2) we can compute the flux through a surface of 5" x 5" as done

by Wiehr (1979) for the Fe I λ 525,02 nm line. In the present study, we obtained a value of 1.2 10^{18} Mx, which is half of the value obtained by Wiehr. This discrepancy can be explained by the fact that the two sets of observations were performed for different lines.

We would also point out that the Meudon observations give the same relation (1) and same constants, even when the technique of observation and the spectral lines used are entirely different.

REFERENCES

Harvey, J. : 1977, Highlights in Astronomy, Vol. 4, Part II, 223.

Pecker, J.C., Dumont, S., Mouradian Z., Chapman, G.A. : 1977, Proceeding of the November 7-10, 1977 OSO-8 Workshop, Univ. of Colorado, 172.

Wiehr, E. : 1979, Astron. Astrophys. 73, L19.

CORONAL MAGNETIC FIELDS AND FORBIDDEN EMISSION LINE POLARIZATION

David E. Rees
Department of Applied Mathematics,
University of Sydney, N.S.W. 2006, Australia

1. Introduction

It is generally assumed that the morphology of the solar corona as seen, for example, in white light provides a map of the coronal magnetic field. Not only are coronal structures such as loops and streamers strongly suggestive of magnetic fields, but also on theoretical grounds one expects the field to be frozen into the highly ionized coronal plasma. A standard test of the morphology hypothesis is to extrapolate from photospheric field measurements into the corona by means of a potential field calculation (Altschuler and Newkirk, 1969). However, as noted by Picat et al. (1979), such calculations yield only a rough fit to the white light corona. Some crude estimates of the orientation of coronal magnetic fields also can be obtained from polarization measurements of radio bursts (e.g., Kai, 1970).

At present the most direct technique for inferring the direction of the coronal magnetic field is by observations of forbidden line polarization. The first substantial application of this method was by Charvin (1965). The most recently published data are by Arnaud (1977) and Picat et al. (1979) using the so-called green line Fe XIV 5303Å and by Querfeld (1977) using the Fe XIII 10747Å line. House (1977) reviews earlier work. All these observations were ground-based, the measurements being limited to heights $\lesssim 1.5\ R_\odot$. Observations are now being made to heights $\gtrsim 1.7\ R_\odot$ by the High Altitude Observatory Coronagraph/Polarimeter on the Solar Maximum Mission Satellite. House et al. (1980) report detection of green line emission out to $3.2\ R_\odot$.

As a prelude to the analysis of data from the HAO/CP experiment, a detailed study of the formation of green line polarization has been carried out following the theoretical work of Sahal-Bréchot (1974) and House (1977). The rest of this article outlines some of the essential features of the theory and reports on progress and goals. The work has been done in collaboration with Drs. L. House

and C. Querfeld, and a full account is in preparation.

2. Theory of Green Line Polarization

The central problem in modelling coronal emission line polarization is to solve the statistical equilibrium equations for the magnetic sublevel populations of the coronal ion. The green line is formed in the $3s^2 3p$ ground configuration of the ion as a $^2P_{3/2} \rightarrow {}^2P_{1/2}$ transition. Polarization in the line arises because of the inequality of the sublevel populations of the $^2P_{3/2}$ excited state. This inequality is due to the anisotropy of excitation by radiation from the photosphere. Depolarizing collisions within the ground configuration, as well as electron collisions to excited configurations followed by cascades, tend to equalize these populations.

The full details of the method of solution of the equations of statistical equilibrium are given by House (1977). We applied his method to the 9-level (34-sublevel) model Fe XIV ion illustrated in Figure 1. Table 1 summarizes the sources of atomic data used to calculate the various transition rates. We neglected radiative absorption from the ground to excited configurations, radiative rates between sublevels of any given term, electron depolarization rates and all rates between terms in excited configurations.

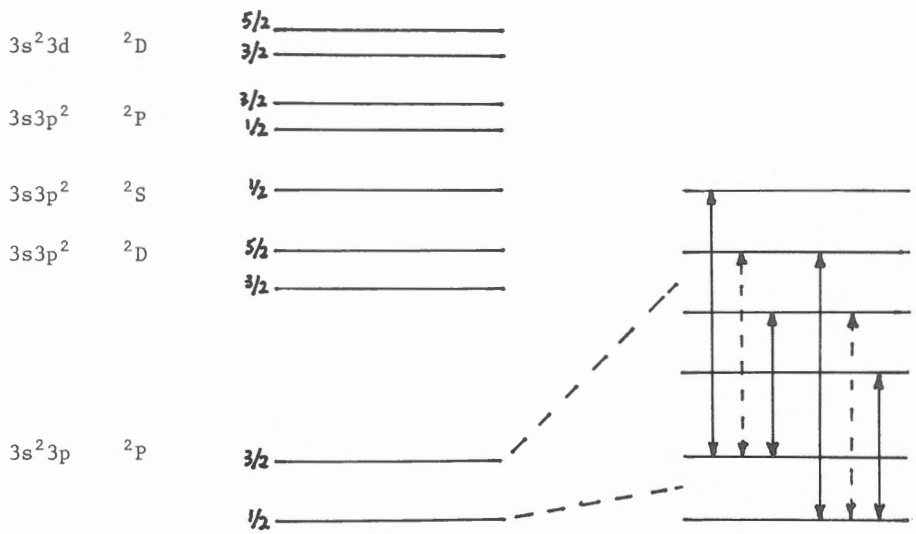

Figure 1. Energy levels of model Fe XIV ion. Details of magnetic sublevels and Zeeman transitions are shown only for the ground configuration.

Table 1.

	Within Ground Configuration	Ground-Excited Configurations
Spontaneous Decay	Krueger and Czyzak (1965)	Blaha (1971)
Radiative Absorption	Radiation Temp. 6275K	Neglected
Electron Excitation	Petrini (1970)	Blaha (1971)
Proton Rates	Landman (1975)	Neglected

Our initial calculations have concentrated on testing the sensitivity of the sublevel populations and emergent polarization to collisions, magnetic field configuration and thermodynamic structure. One of our primary aims has been to improve the efficiency of the calculations which are very time-consuming especially if line of sight integration effects are included. Querfeld (priv. comm.) has recently derived a convenient numerical fit to the solutions of statistical equilibrium equations, giving specifically the sublevel populations of the $^2P_{3/2}$ state of the ground configuration.

The observed polarization is related in a highly non-linear fashion to the three-dimensional coronal structure. The inverse problem of deducing magnetic field directions directly from data poses considerable uniqueness difficulties. The above simplified fit will play an important role in the development of a fast deconvolution method. For the moment, however, we are concentrating on model calculations in order to gain insight into the best way to attack this inverse problem.

3. Goals

It is envisaged that this theory will be used in routine analysis of the HAO/CP green line data to derive the magnetic field structure in coronal features. Since electron densities are required to calculate polarization, the analysis will need to be concurrent with deconvolution of polarization observations in the broad band continuum. A further complication is worth noting: the line polarization is preferentially radial, while the continuum polarization is tangential to the limb.

Our intention is to test directly whether indeed the morphology of dense structures follows the coronal magnetic field and to assess the accuracy of potential field calculations. This program should be quite feasible for long-lived

coronal structures. Ideally one would like to be able to measure field directions in coronal transients as well. However, integration times necessary to obtain green line data pose serious difficulties here. Certainly it will be of great interest to study the magnetic structure before and after the passage of a transient.

References

Altschuler, M.D., and Newkirk, G.A., Jr.: 1969, *Solar Phys.* 9, 131.

Arnaud, J.: 1977, *Lund Obs. Rept.* 12, 137.

Blaha, M.: 1971, *Solar Phys.* 17, 99.

Charvin, P.: 1965, *Ann. Astrophys.* 28, 877.

House, L.L.: 1977, *Astrophys. J.* 214, 632.

House, L.L., Wagner, W.J., Hildner, E., MacQueen, R.M., Sawyer, C., and Schmidt, H.U.: 1980, *Astrophys. J. Letters*, in press.

Kai, K.: 1970, *Solar Phys.* 11, 456.

Krueger, T.K., and Czyzak, S.J.: 1965, *Astrophys. J.* 144, 1194.

Landman, D.: 1975, *Astron. Astrophys.* 43, 285.

Petrini, D.: 1970, *Astron. Astrophys.* 9, 392.

Picat, J.P., Felenbok, P., Fort, B. et Groupe 'Caméra Electronique': 1979, *Astron. Astrophys.* 75, 176.

Querfeld, C.W.: 1977, *Lund Obs. Rept.* 12, 109.

Sahal-Bréchot, S.: 1974, *Astron. Astrophys.* 36, 355.

SMALL-SCALE UNRESOLVED SOLAR MAGNETIC FIELDS

Elizabeth Ribes and Meir Semel
D.A.S.O.P., Observatoire de Meudon

ABSTRACT :

We review briefly the various observations showing the unresolved nature of the small-scale solar magnetic fields. The horizontal scale-length of these magnetic elements is only a fraction of one arc second (< 0"2). The observed average field strength is weak (from 20 gauss up to a few hundred gauss) and the true field strength should be higher. But the high value (> 1500 gauss) inferred by the observers is model-dependent. The magnetic models of atmosphere they used contain many crude assumptions : the neglect of the vertical variations of the physical parameters with height, the "dynamically thin tube" assumption, the neglect of velocities, even subsonic, etc...

We propose a self-consistent hydromagnetic model of magnetic flux tubes. The observed downdraft provides a mechanism for the facular heating by transporting an excess of entropy (the excess is between the magnetic tube and outside) from the chromospheric layers down to the photosphere. Two different Bernoulli solutions are studied :

- the critical solution C_1 exhibits a temperature excess of 1000°K localized in the upper photosphere and a downdraft decelerating with increasing depth. The magnetic field strength at the base of the photosphere is low (300 gauss, for an "optically thin" tube (model 1) up to 800 gauss if we allow an empirical departure from the "optically thin" assumption (model 2)). This solution seems to be more appropriate to the upper levels of the photosphere or to the chromosphere .

- the other family of solutions predicts an excess of temperature which can explain the center-to-limb effect of the continuum facula. The magnetic field strength at the base of the photosphere does not exceed 1300 gauss. The flow is adiabatic, accelerating rapidly inwards. The theoretical velocity of 7 km s^{-1} obtained at the base of the photosphere can be substantially reduced if the bright facula has the dimensions of filigrees.

We suggest that a realistic picture of the small-scale magnetic fields will be obtained by the particular Bernoulli solution which behaves thermodynamically as the critical solution in the upper layers and becomes adiabatic in the lower layers.

INTRODUCTION

For the last decade, many attempts have been made to understand the physics of the small-scale solar magnetic fields. The magnetic elements beeing unresolved with the present telescopes, the interpretation of the averaged quantities observed requires the elaboration of magnetic models. Hydrostatic solutions (with radiative equilibrium) have been extensively used and lead to a strong field strength (> 1500 gauss) at the base of the photosphere. However, the presence of a flow, even subsonic, has a considerable importance : it carries the thermal energy which controls the temperature and the temperature affects back the dynamics. This coupling will modify deeply the magnetic structure. Consequently, the hydrodynamical situation is very different from the hydrostatic one. Since the interpretation of unresolved observations is not unique, we cannot exclude the possibility for the two types of solution to exist in the unresolved fine structures.

In this paper, we first review some observations showing that the small-scale fields are unresolved (part A). Then, we point out the difficulties to interpret the "averaged" observations with the help of too simple assumptions (part B). Finally, we propose a new heating mechanism for the magnetic tubes with various thermodynamical conditions for the fluid (part C). This mechanism is valid throughout the solar atmosphere, but in the present stage, the results are rather qualitative and should be considered as a step towards a better understanding of the solar network.

A) OBSERVATIONAL EVIDENCE FOR THE UNRESOLVED NATURE OF THE SMALL-SCALE FIELDS.

Simultaneous observations of several photospheric lines with a magnetograph (Harvey and Livingston (1969) ; Frazier and Stenflo (1972, 1978) ; Wiehr (1978) ; Semel (1980 b)) showed a very significant incoherence in the measured magnetic field, both in faculae and network. The ratios of the magnetograph signals for two given lines were also found to be constant and independent of the observed field strength. At first, Harvey and Livingston attributed this incoherence to a line weakening caused by an excess of temperature. For a weak field, the magnetograph signal is proportional to the slope of the line profile. If this slope is sensitive to the temperature, then the magnetograph signal is sensitive to the temperature as well.

However, these authors observed a broadening in the faculae larger than in the quiet photosphere, for the 5250.2 Å line of Iron I. They interpreted the broadening as a manifestation of a magnetic turbulence corresponding to about 500 gauss.

It is known that the magnetograph saturation e.g., the non linear response of the magnetograph for strong Zeeman displacements could explain partly the incoherence of the magnetograph measurements. By measuring two lines with different Landé factor (g), hence with different magnetograph saturation, a one kilogauss field was necessary to explain the ratio of the magnetograph signal for these 2 lines. By assuming a large scale distribution of magnetic field, Stenflo deduced the amplitude of the peak of 2 kilogauss. The constancy of the magnetograph signals' ratios for the two lines and the non-dependence with the field strength was an argument in favor of a "unique" magnetic structure (Frazier and Stenflo, 1972).

Similar observations have been carried out by Frazier (1974) and Wiehr (1978) with three lines. Wiehr found the magnetic structure was not unique and the field strength could range from 1200 gauss to 2500 gauss, both in active regions and in the network.

Harvey and Hall (1975) observed an infra-red line at 1,5 μ. This choice of the wavelength is particularly advantageous because the Zeeman displacement (proportional to λ^2) is much larger than the Döppler broadening (proportional to λ). The observed profiles of the circular polarization, that is the Stokes parameter V, shows peaks corresponding to a field strength of 1500 gauss and a Döppler shift yielding 1.6 Km s^{-1}.

Other types of observations are also suggesting that the magnetic field could be concentrated and probably strong.

The filigrees observed by Dunn and Zirker (1973) have dimensions much inferior to 1 arc second. If the magnetic field is concentrated in the filigrees, it should be very strong.

The line gaps observed by Sheeley (1967) with a very good seeing might be explained by a Zeeman weakening, as well. Wilson (1971), Rees (1973), Chapman (1977) elaborated facular models from these data. In general, no model could fit with all observed line weakenings. The field strength proposed by Chapman is about 1800 gauss at $\tau_{5000} = 1$ in the magnetic tube. His model does not fit with strong lines and non L.T.E. effects are invoked to be the main reason.

Simon and Zirker (1974) obtained spectra with excellent spatial resolution. They looked for the smallest magnetic structure to fit with the filigrees. They found that the magnetic field covers an area much larger than the filigrees'. For many cases, the magnetic intensity was weak. If Stenflo's conjecture is correct, namely the field distribution is the same for all structures and strong, the magnetic

elements observed by Simon and Zirker consist of clumps of flux tubes.

Another confirmation of the unresolved nature of the magnetic field was obtained by Semel (1980 b) using 12 lines recorded simultaneously (1980 a). The incoherence between the magnetic field intensities deduced from each of these lines proves that the magnetic field is unresolved, and the line weakening is spatially correlated with the magnetic field.

In conclusion, *the magnetic structure is obviously unresolved.* The horizontal scale length is inferior to the best resolving power of the present observations, only a fraction of one arc second. *The strength of the magnetic field is certainly much higher than what we observe.* The estimations are : 1800 gauss (Chapman), 2000 gauss (Frazier and Stenflo), 1600 gauss (Harvey), > 1500 gauss (Wiehr). Besides, it is very likely that a *downdraft accelerating with increasing depth exists in the magnetic tube* (Giovanelli and Slaughter, 1977).

B) CRITICAL REVIEW OF THE INTERPRETATIONS OF OBSERVATIONS.

We should keep in mind that the observed magnetic field is usually small, at least one order of magnitude less than what the strong values generally claimed. *The reduction of the data is more or less model dependent. The assumption of a "thin" magnetic tube is always used.* In particular, the curvature of the lines of force is neglected and the Laplace forces are reduced to the magnetic pressure only, as follows :

$$(P_{gaz} + B^2/8\pi)_{in} = (P_{gaz})_{out} \qquad (1)$$

this sets a constraint on the maximum field strength and its variation with height. Although the line formation calculations are considerably easier with such an assumption, we may question its validity. A priori, we would expect that the lateral dimension of a thin tube is much smaller than the vertical scale height variations. Assuming a tube of 260 km diameter, the magnetic pressure scale height is half the diameter and is the same as the external gaz pressure scale height (130 km). So, *we cannot neglect the variation of both geometry and physical quantities with height.* Moreover, in the frozen field assumption, the presence of a downdraft increasing with increasing depth will make the variation of the magnetic scale height even more rapid, for continuity reasons (B is proportional to ρu). The magnetic field scale height will be much smaller than in the hydrostatic case. Then, the interpretations of observations become questionable if the variations of the physical parameters with height are not taken into account.

For example, Frazier and Stenflo (1978) measured the brightness, the velocity and the polarization in two lines simultaneously. While the polarization was in favor of a strong field, velocity and brightness were in favor of a weak field. There was no way to explain all the obervables. It is very likely that the difficulties in interpreting their data come from the neglect of height variations and the assumption of a too simple distribution of the physical parameters. A more sophisticated model including height variation is necessary.

Wiehr (1979) made an experiment to find out what is the limit flux coming out of a bright facular point. Observing the 5250.2 Å line with an aperture of 4" by 4", the measured field was found to be either higher than 20 gauss or within the noise. If there is a limit flux, the magnetograph signal should be inversely proportional to the magnetograph aperture. In fact, Wiehr found an increase of the magnetograph signal when decreasing the aperture, but not in the expected ratio. The concept of limit flux in a concentrated magnetic field is, therefore, questionable.

Chapman's model (1977) includes a height variation of the magnetic field, but he has neglected the observed velocities. He assumes several empirical models to explain the excess of temperature observed in facular regions. He considers different field intensities and the percentage of the area occupied by the magnetic tubes. He found that the best solution is obtained for his model 7 B 13, giving a temperature excess of 1000°K, a magnetic field strength of 1800 gauss at $\tau_{5000,\ facula} = 1$. This depth is 165 km below the level $\tau_{5000} = 1$ in the H.S.R.A. reference atmosphere. However, not all the lines he observed could fit the model adopted;out of 10 lines, 4 gave a too strong or a too weak field and were rejected on the grounds that these strong lines were influenced by non L.T.E. effects. We think that Chapman's approach may give good temperature models but is not adequate to determine the magnetic field strength.

To illustrate this, let's consider the two lines 5250.2 Å and 5247.1 Å belonging to the same multiplet of Iron I. The profiles of the two lines are practically identical in the quiet photosphere. In faculae, they are substantially weakened but the difference in their profiles is still very small, in spite of quite different Landé factors (see Fig. 7 a of Chapman (1977)). So, the temperature excess is the main cause of the line weakening and the contribution of the Zeeman effect is small. Therefore, all the uncertainties involved in the model calculated by Chapman (abundance, oscillator strength, microturbulence, temperature excess etc...) will affect heavily the small difference between the two weakened lines. As a result, the determination of the magnetic field is difficult.

Spruit (1976) studies a magnetostatic solution of axially symetric flux tubes and calculates the energy balance of these tubes. The interior pressure is lower than the outside pressure, according to equation (1). He explains the excess of brightness in the continuum faculae by the fact that one is seeing the walls of the tube, for an heliographic angle $\theta > 0$ (see Fig. 1).

Fig. 1 : MODEL OF MAGNETOSTATIC FLUX TUBE (SPRUIT, 1976)

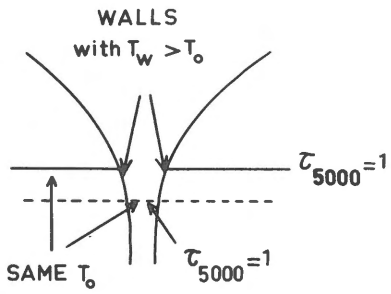

We can summarize some of our objections to the present picture :

1) The actual resolution of the telescopes cannot isolate the walls of Spruit's model. On the other hand, the observations indicate an excess of flux coming out from facular regions. Spruit assumes that the excess of flux observed in the magnetic tube has been radiated laterally through the walls from the surrounding regions. But his assumption does not seem to be supported by the observations (the bright facula does not appear to be surrounded by a dark ring). The origin of the excess of flux and the flux conservation are fundamental problems which should be carefully studied.

2) Can we really assume so much brightness excess from the walls ? Spruit assumes that the walls have no thickness and the effective temperature for the outflow radiation from the wall is the same outside the wall. In reality, the walls have a finite thickness and the energy transfer through it will give a temperature gradient and a reduced temperature for the wall.

3) He estimates the energy transport through the walls by using the approximation of the diffusion equation. This approximation is valid for an optically thin tube.

Below $\tau = 1$, the tube is thick, therefore the source function is overestimated.

In short, the radiative transfer through the walls requires a much more complicated treatment than the approach made by Spruit. It is very likely that a more rigourous treatment of the radiative transfer, even one-dimensional, would fail to fit with the observations of the continuum faculae. In any case, Spruit's mechanism is restricted to the low photosphere and does not explain the heating of the chromospheric faculae.

C) HYDROMAGNETIC APPROACH FOR THE SOLAR SMALL-SCALE FIELDS.

There are observational and theoritical motivations to look for a magnetohydrodynamic solution of the solar magnetic flux tubes.

1) The stability analysis of a thin magnetic tube in hydrostatic equilibrium indicate that the magnetic field necessary for stabilizing the tube should exceed 1800 gauss at $\tau_{5000} = 1$ (Unno and Ando, 1979), which means an almost empty tube. *Below this value, the tube is convectively unstable and a flow will set in.* From thermodynamical considerations, a downdraft is more plausible (Ribes and Unno, 1976).

2) *The observations indicate the presence of velocities in the magnetic tube* (Frazier, 1970 ; Harvey and Hall, 1975 ; Giovanelli and Slaughter, 1977 ; Frazier and Stenflo, 1978). The downdraft is accelerating with increasing depth, showing a rapid increase in the inner photosphere.

3) *Solutions with non-zero velocities are quite different from those with zero velocities* (Unno, 1980).

On one hand, the necessity of keeping the mass flux constant makes the hydrostatic models highly inconsistent with velocities, even small. Giovanelli (1977) suggests that the matter can move across the lines of force near the temperature minimum and below. Therefore, the relation $B \propto \rho u$ needs not to be satisfied. Hovewer, the process requires the cross-section of the tube to be small. In the upper photosphere, the lines of force have already spread out and the inflow of matter will be restricted to the skin of the magnetic tube. So, in our model, we still keep the field "frozen" and we let the magnetic configuration open fast enough to satisfy the mass conservation.

On the other hand, the presence of velocities affect considerably the energy balance through the transport of entropy. In the hydrostatic case, the balance is between emission and absorption of radiation. In the hydrodynamical case, the term

of entropy should be added. An enhanced emission is necessary to compensate the entropy excess transported by the downdraft. The resulting temperature excess is significant in the upper layers where opacity and density are low.

To illustrate this basic difference, we discuss now a hydromagnetic model of solar faculae (Unno and Ribes, 1979). We consider a "thin" magnetic tube embedded in the photosphere. The basic equations governing the flow in the tube are given by :

$$P + B^2/8\pi = P_R \tag{1}$$

$$\rho\, u\, \sigma = C_1 \tag{2}$$

$$B\, \sigma = C_2 \tag{3}$$

$$\frac{d}{dZ}\left(\frac{u^2}{2}\right) + \frac{1}{\rho}\frac{dP}{dZ} + g = 0 \tag{4}$$

$$T\, u\, dS/dZ = \frac{1}{\rho}\nabla.F = 4\,\pi(K_P\, B - K_J\, J) \tag{5}$$

where ρ, T, S, u, σ, B, J, F, K_P, K_J, C_1, C_2 and g denote the density, the temperature, the specific entropy, the downdraft speed, the cross section of the tube, the integrated source function (black body), the integrated mean intensity, the radiative flux, the Planck-mean absorption coefficient, the mean absorption coefficient weighted by the specific mean intensity, the mass flux, the magnetic flux and the gravity respectively. The flow is driven by the difference between the gravity and the pressure gradient.

The equations are coupled and a general solution is difficult to obtain. So, we proceed as follows :

1) First, we assume an entropy (or a temperature) distribution (Fig. 2) as a solution of the energy equation (5) and we solve the Bernoulli flow (that is, the flow along the lines of force, equations 1 to 4) for the density, the pressure and the velocity as a function of height.

2) Then, we check the consistency of the energy equation. The best fit is obtained by adjusting the free parameters of the analytical function which describes the entropy distribution.

the general Bernoulli flow is characterized by two critical solutions C_1 and C_2

passing through the singular point, and four families of solutions (a, b, d, e) (Fig. 3). We have eliminated the critical solution C_2 and the families b and e which are restricted to the deep layers where our assumption of a thin tube, without viscosity etc. are not valid. The family a does not connect sufficiently distant layers and has been disregarded too.

The critical solution C_1 exhibits the following properties (see Fig. 4) : *the flow speed is large,* although *subsonic*, at the top of the photosphere and *decelerates rapidly with increasing depth.* This is in contradiction with Giovanelli and Slaughter's observations (1977) of a downdraft accelerating inwards. *A temperature excess of 1000°K is localized in the upper photosphere*, in agreement with the line weakenings. But there is a significant difference for the continuum center-to-limb variation as observed by Müller (1975). *The magnetic field strength is low* : at $\tau_{5000} = 1$, *300 gauss for an optically thin tube* (model 1), *up to 800 gauss if we allow a departure from the opticelly thin assumption* (model 2) (the departure is parametrized by a dilution factor which varies empirically from 1 (at $\tau = 1$) up to 1.5 at $\tau = 0.01$). The corresponding magnetic scale heights are 340 km and 500 km respectively.

These models (1) and (2) describe a new self-consistent heating mechanism necessary to explain the brightness enhancement of faculae, in the lines as well as in the continuum. It is the competition between the excess of entropy transported by the downdraft and the radiation loss. The two models presented above underline the role of the dilution factor. However, the infinitesimally thin tube model (n° 1) seems to fit more with the characteristics of the chromospheric faculae and do not explain the main properties of the photospheric faculae. In particular, a relevant solution should approach the upper branch of the critical solution C_1 and differ from it in the lower levels. Among the d-type solutions, there is one which seems to fulfill the requirement (see d_{Fac} in Fig. 3). Since the thermodynamics in the lower photosphere is unknown, we approximate it by a polytropic law, as follows :

$$P = k \rho^{\Gamma} \qquad (7)$$

where Γ is the polytropic index. Moreover, we decide to put more weight on the recent photospheric observations, namely, the distribution of velocity reported by Giovanelli and Slaughter (1977), the continuum center-to-limb variation (Müller, 1975 ; Hirayama, 1978) and a strong field.

The Bernoulli flow is reduced to two equations :

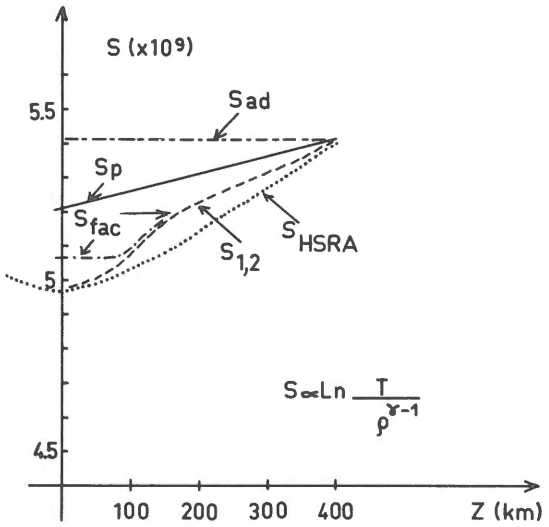

Fig. 2 : represents various possible thermodynamical behaviours of the fluid in a magnetic tube.

A realistic entropy distribution for the facula (S_{FAC}) is probably the combination of the chain line (adiabatic flow) with the dashed line (Models 1 and 2).

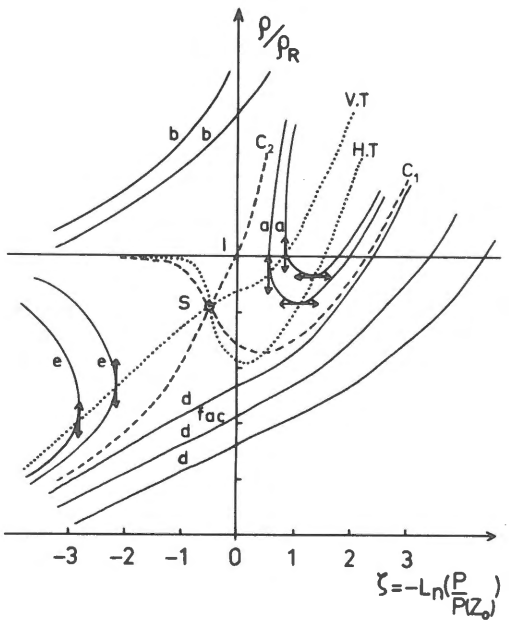

Fig. 3 : shows the different Bernoulli solutions for a given entropy. Note that there is a particular d-type solution (d_{fac}) which approaches the critical solution C_1 in the upper layers and diverge from it in the low photosphere.

$$\frac{u^2}{2} \rho^2 \left[P_R - P\right]^{-1} = \text{Constante} \qquad (8)$$

$$\frac{u^2}{2} + \Gamma \left(\Gamma - 1\right)^{-1} \frac{R}{\mu} T + gZ = \text{Constante} \qquad (9)$$

By inspection of equation 8, $\rho^2 u^2$ should increase rapidly inwards to allow a strong magnetic pressure on the other hand, the equation of motion (9) shows that a large variation of the gravitational potential gZ should be balanced either by a rapid increase of u^2 or by the second term representing a kind of potential energy. The T(Z) relation from Müller requires Γ to be close to unity, but the gaz pressure decreases too rapidly inwards with a resulting low magnetic field. So, a strong field requires Γ to be close to the adiabatic value. The characteristics of the d-type adiabatic steady flow are illustrated in Fig. 4 : *the magnetic field strength is about 1300 gauss* at $\tau_{5000} = 1$ and diverges rapidly, with a scale height of 110 km. The *flow is nearly adiabatic* and *accelerates downward up to 7 km* s^{-1}. This value is 4 times larger than the velocity observed by Harvey and Hall (1975). However, if the bright faculae have the dimensions of the filigrees (200 km or less), the temperature excess at $\tau_{5000} = 1$ is still important (Koutchmy, 1977). A temperature excess of 1700°K at this depth would reduce the theoritical flow speed down to 2 km s^{-1}. *Our parameter fitting is approximate because the interpretations of observations are uncertain.* Nevertheless, we can understand, at least qualitatively, the heating of faculae by the thermodynamical behaviour of the fluid.

CONCLUSION

The observations have shown that the magnetic field in the faculae and in the network is unresolved, with a lateral dimension of 200 km or less.

The vertical scale height variations are even smaller and cannot be neglected.

A downdraft is observed and provides a consistent mechanism for the facular heating by transporting the entropy excess from the chromospheric layers. A three dimensional radiative transfer is necessary to proceed in our investigations. The energy balance should also include the wave generation and dissipation. The stability of steady flows is another problem worth investigating.

Where and why the magnetic field is concentrated is a very intriguing problem which is not considered here. But very likely, the concentration is conditioned by the convection zone, and the observable layers play a rather passive role in this context.

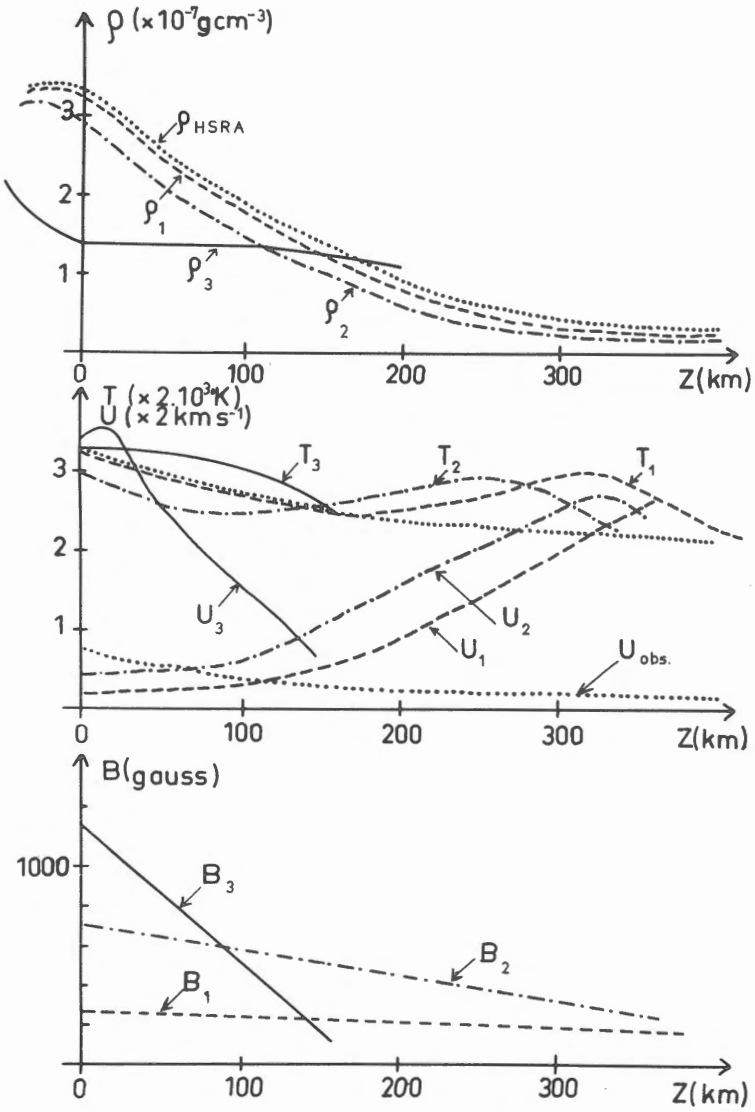

Fig. 4 : summarizes the variations of the physical parameters (S, T, u and B) with height, for the various hydromagnetic models refered by the indices 1, 2 and 3. Also, is represented the H.S.R.A. model, for comparison.

REFERENCES :

CHAPMAN M. : 1972, Solar Phys. 26, 299.

CHAPMAN M. : 1972, Ap. J. supplement series 33, 35.

DUNN R.B., ZIRKER, J.B. : 1973, Solar Phys. 33, 281.

FRAZIER E.N. : 1970, Solar Phys. 14, 89.

FRAZIER E.N. : 1974, Solar Phys. 38, 69.

FRAZIER E.N., STENFLO J.O. : 1972, Solar Phys. 27, 330.

FRAZIER E.N., STENFLO J.O. : 1978, Astron. Astrophys. 70, 789.

GIOVANELLI R.G. : 1977, Solar Phys. 52, 315.

GIOVANELLI R.G., SLAUGHTER C. : 1977, Solar Phys. 57, 255.

HARVEY J., LIVINGSTON W. : 1969, Solar Phys. 10, 283.

HARVEY J., HALL D. : 1975, Bull. Am. Astron. Soc. 7, 459.

HIRAYAMA T. : 1978, Plub. Astron. Soc. Japan 30, 337.

KOUTCHMY S. : 1977, Astron. Astrophys. 61, 397.

MÜLLER R. : 1975, Solar Phys. 45, 105.

RIBES E., UNNO W. : 1976, Astron. Astrophys. 53, 197.

SPRUIT H.C. : 1976, Solar Phys. 50, 269.

REES D. : 1973, Thesis (University of Sydney).

SEMEL M. : 1980a, Astron. Astrophys., in press.

SEMEL M. : 1980b, Astron. Astrophys., in press.

SHEELEY N.R. : 1967, Solar Phys. 1, 171.

SIMON G.N., ZIRKER J.B. : 1974, Solar Phys. 35, 331.

UNNO W., RIBES E. : 1978, Astron. Astrophys. 73, 314.

UNNO W., ANDO H. : 1979, Geophys. Astrophys. Fluid Mech. 12, 107.

UNNO W. : 1980, Proceedings of the seminar "The sun as an active star", Tokyo.

WIEHR E. : 1978, Astron. Astrophys. 69, 279.

WIEHR E. : 1979, Astron. Astrophys. 73, 219.

WILSON P.R. : 1971, Solar Phys. 21, 101.

MORPHOLOGICAL AND DYNAMICAL PROPERTIES OF MAGNETIC BRIGHT POINTS IN THE QUIET PHOTOSPHERE.

Richard Muller
Observatoire du Pic du Midi - France

Introduction.

Observations in photospheric lines reveal that many small bright points are present on the quiet surface of the sun, at the photospheric level. They have a tendency to concentrate at the vertices of several supergranular cells (fig.1), but a few points are present, in the cells'interior. In active regions the large concentration of bright points gives the well known filigree aspect (fig.2).

It has been shown that strong magnetic fields, concentrated in small tubes, are associated to the photospheric bright points. These elementary magnetic fields seem to take a proeminent part in a number of solar phenomena.

Observations

The dimension of the photospheric bright points is at the limit of resolution of the best ground based instruments. For this reason, though they were discovered, at Sacramento Peak Observatory in the early seventies, their morphological and dynamical properties are still very poorly known. Their knowledge is, however, essential if we want to be able to understand, on the one hand, the magnetic field concentration phenomenon, and, on the other hand, solar features like filigree, faculæ , sunspots, spicules, which result from the interaction of magnetic field with convection. Magnetic, bright points, perhaps take a proeminent part in the production of flares,too.

With the 50 cm refractor of the Pic du Midi Observatory, I recently obtained the first time series - one hour long - which permits the study of the evolution of photospheric bright points. The observations consist in photographs taken quasi-simultaneously in the K line of ionized calcium, where the points appear bright, and in the continuum. (For instrumental reasons I now use a 10 Å broad filter centered at 4308; near this wavelength many iron lines are present). The photographs are spaced by about thirty seconds and the spatial resolution was sufficiently high (that is 0.3" or better) during about one hour.

Statistical properties

Photospheric bright points are distributed over all the quiet surface of the sun (fig. 3) :

- in the form of single points in 33 percent of cases
- in the form of pairs in 32 per cent of cases (I call a pair an association of two points separated by less than 1"5).
- in the form of concentrations of three points or more in 35 per cent of cases.

There are about 2 points in a square of 10 arc sec.

The figure 4 is a histogram of measured dimensions of photospheric bright points. It shows that 82 % of points are of observed dimensions smaller than 0.5" and that 95 % of them are of dimensions smaller than 1".

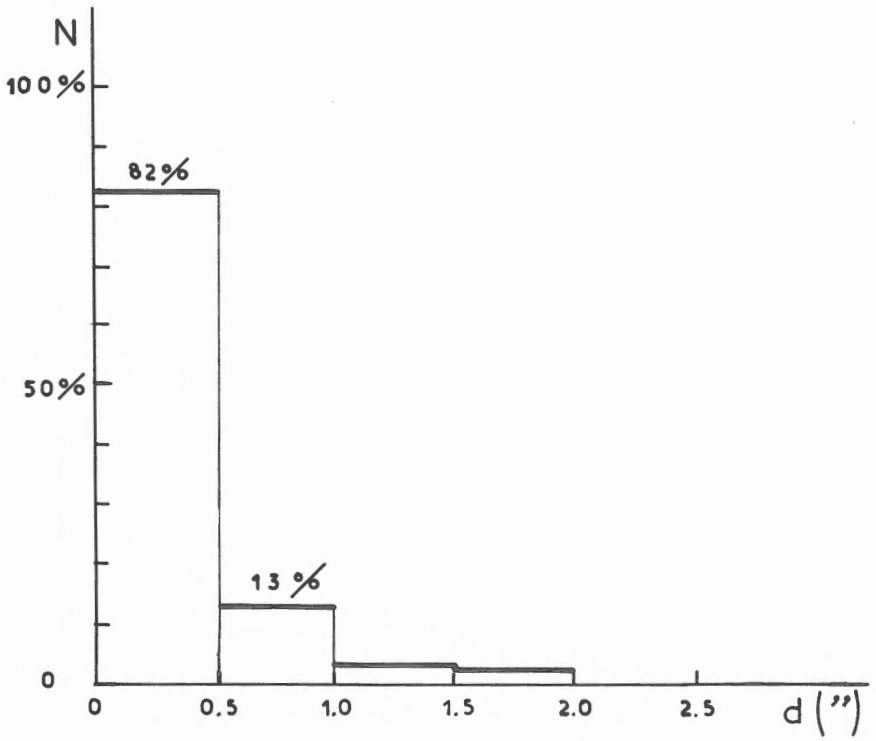

Figure 4.

Histogram of measured dimensions of photospheric bright points.

Bright points dynamical behaviour

As a first step of a more extended work I am studying the behaviour of single bright points in quiet regions. The results presented here are not of great statistical significance because at the moment I have studied the evolution of a few points only. Nevertheless they already clearly show the dynamical behaviour of bright points in quiet regions.

Bright points do not appear anywhere with respect to the granular network, but at the vertices of several granules (never in granules nor in spaces between two granules only).

The lifetime ranges from 12 or 35 min.,and has a mean value of 25 min. (it is not as short as a few min. as estimated previously).

In the K line the points appear bright for a few minutes only, ten minutes at most.

After the brightening the points fade away slowly in intergranular spaces.

Four out of the eleven bright points studied have a remarkable behavior : they first grow longer, become unusually bright in the K line and separate in two fragments. After the separation both points evolve independently. A careful examination of the separation process gives the impression that the points really split. But at that time I cannot reject another possibility : the appearance of a new point very close from the first one.

It appears that the pairs of points result either from the fragmentation of one element, or from the appearance of a new point near an old one. Each element of a pair evolves independently from the other.

Physical consequences

The results presented here show that the bright points and then the associated magnetic tubes, appear in the photosphere in regions of strong downdrafts that probably the vertices of several granules are. The relatively short lifetime and the tendency to split, if confirmed, show that they are rather unstable features. We can already mention some possible implications of these new results :

Downdrafts favour the appearance and concentration of photospheric magnetic fields. This confirms previous observational and theoretical results. At the vertices of several granules a helical downdraft take perhaps place and may generate a magnetic field like in the "battery process" described by W. Unno in his communication.

Recent theories of formation and decay of sunspots are based on a strong stability of magnetic tubes; this does not seem to be the case.

The concentration of bright points at the vertices of supergranules is

usually explained by an outward migration of magnetic tubes, emerged in cells interior, due to horizontal convective flow. But this process requires long lived features. Our results suggest another explanation : vertices of supergranules simply are regions of strong drawndrafts (where supergranular downdraft is added to granular downdraft) propicious to the appearance of photospheric bright points.

The lifetime of the bright phase of a photospheric point is about 5 min. This is just the lifetime of spicules. This may suggest, like Shibata has proposed in his communication, that spicules are constructed by the appearance of a photospheric bright point.

The results presented here are deduced from a study of single bright points in the quiet photosphere. This study is the first step of a more extended work which will include the study of bright points in active regions and at various positions between the center of the disk and the limb. Required observations are already available. It appears also from these results that it will be very important, for the understanding of the appearance and the concentration of photospheric magnetic field, to measure downward velocity at the vertices of several granules and to compare it to the velocity in intergranular spaces, both in the interior and at the vertices of supergranular cells.

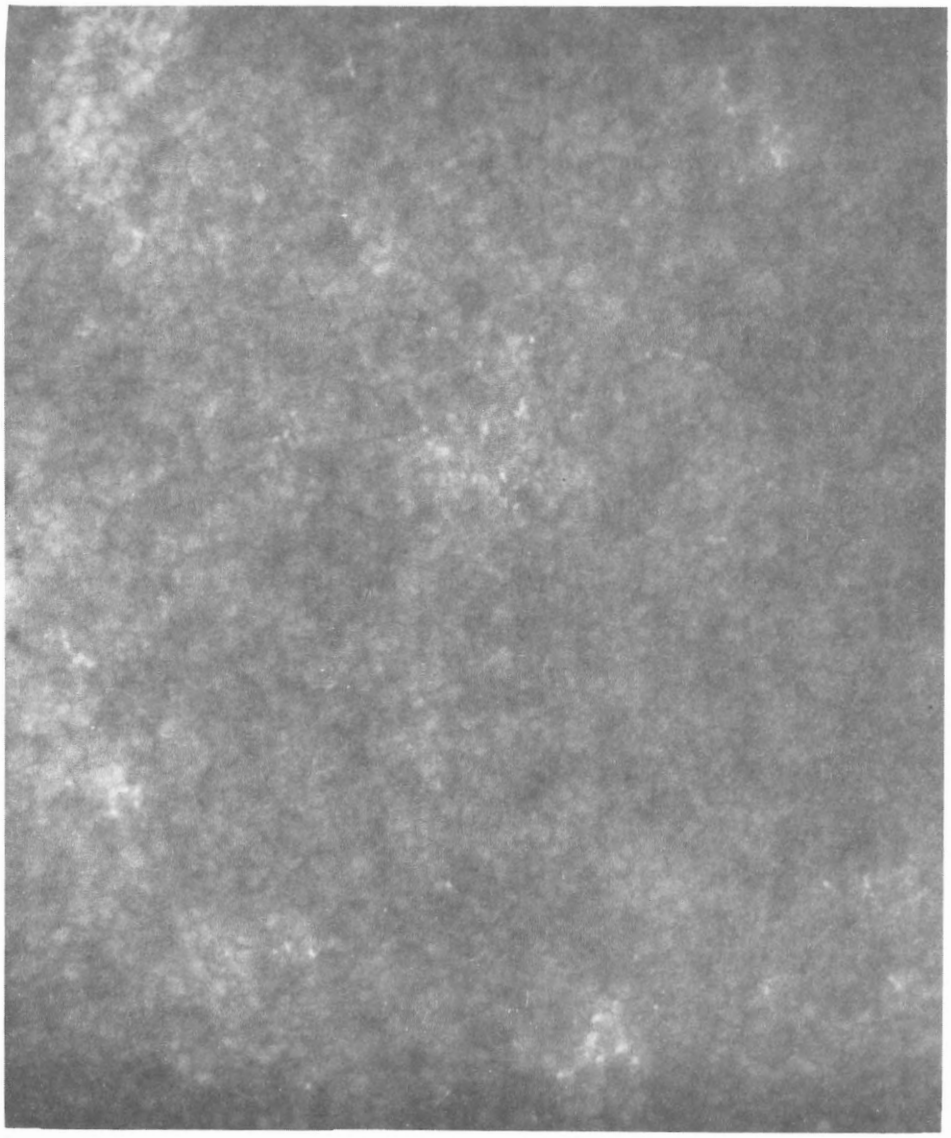

Figure 1. Bright points in the quiet photosphere visible through a 13 Å wide filter centered on the Ca II K 3933 Å line. They outline the supergranular cells. July, 19, 1975. 1 mm = 0"7

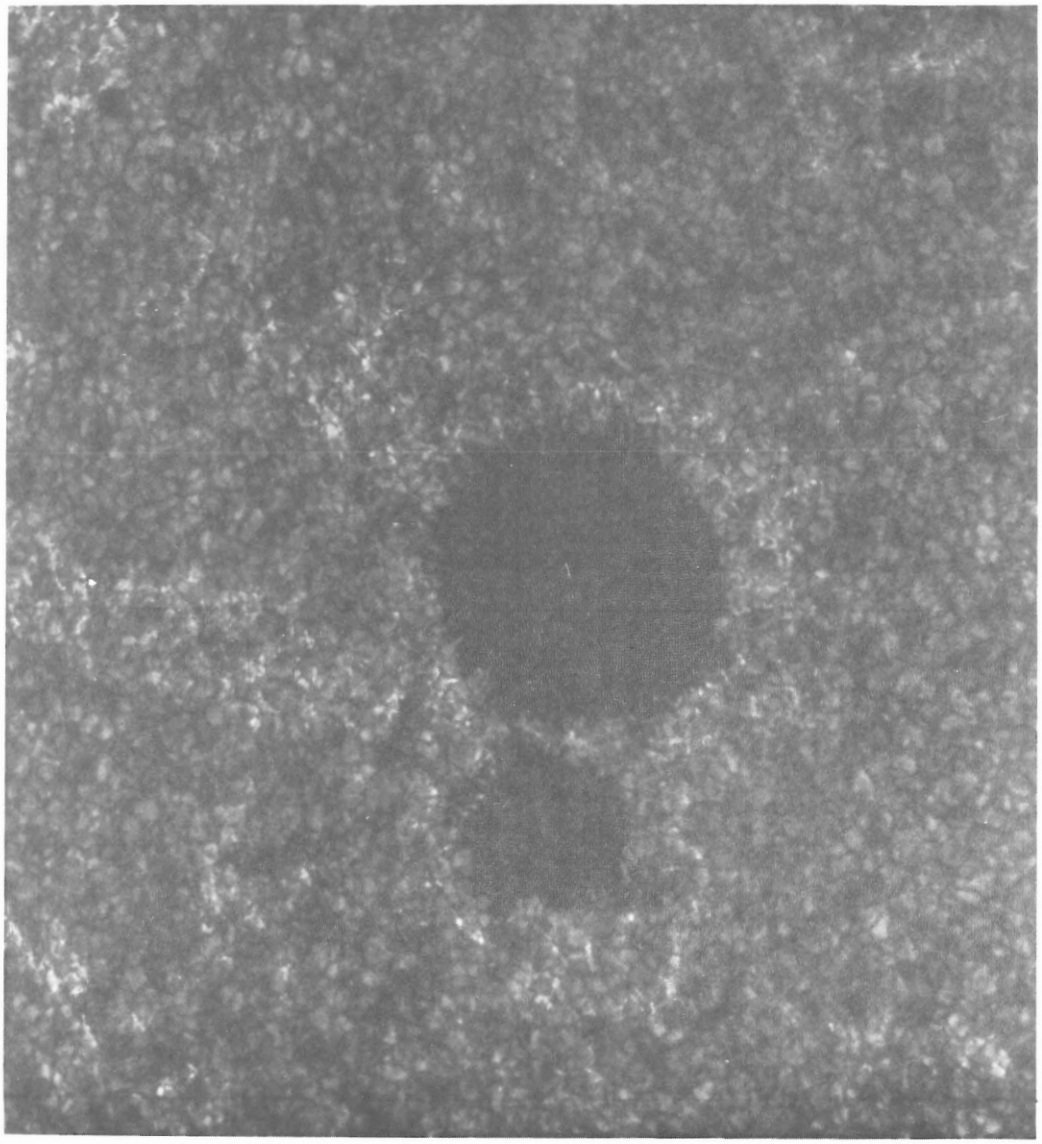

Figure 2. Bright points around a sunspot visible through a 10 Å wide filter centered at 4308 Å. June, 3, 1980. 1 mm = 0"7.

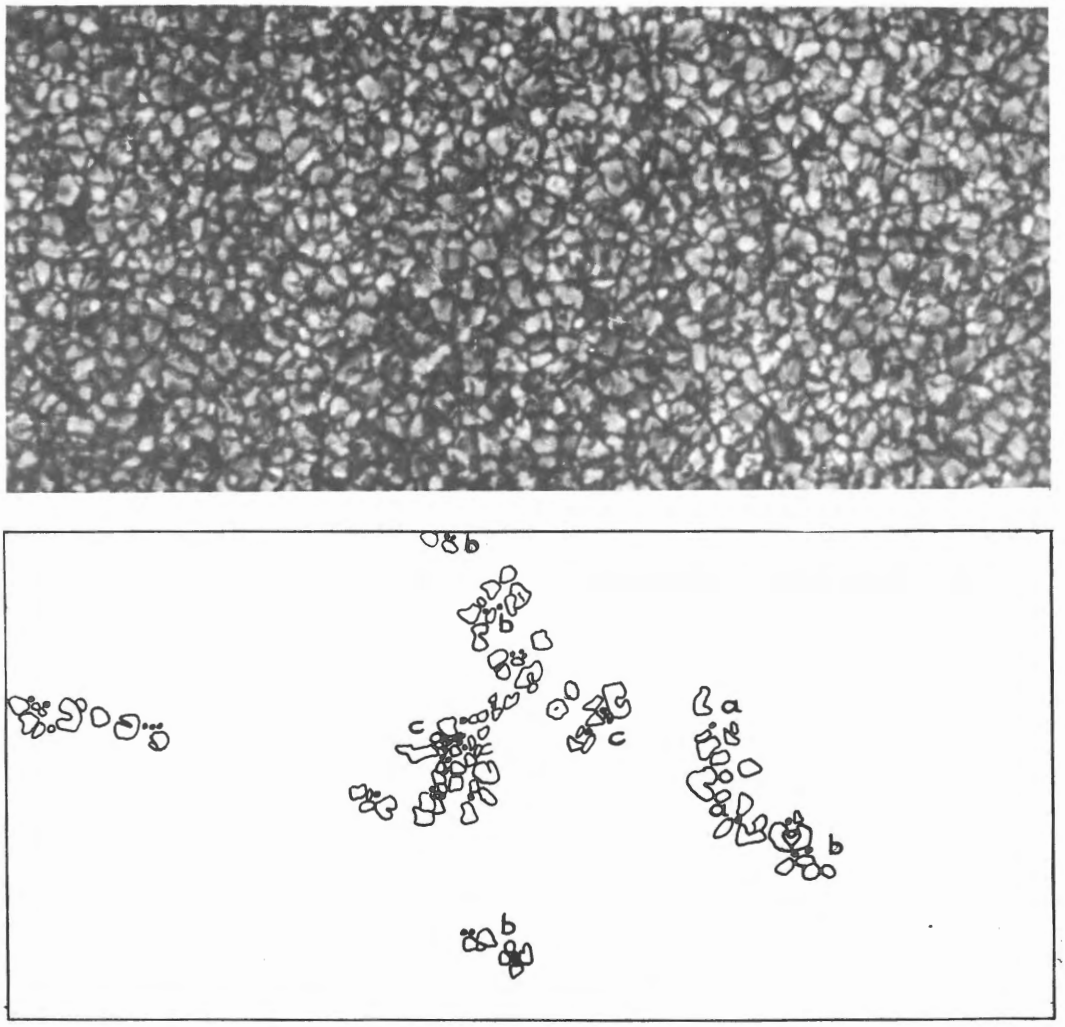

Figure 3. Bright points as visible in the continuum. a : single point; b : pairs of points; c : groups of points. June, 9, 1978. 1 mm = 0"65.

OBSERVATIONAL TEST FOR HYDRODYNAMICAL MODELS OF SOLAR FACULAE.

M. Semel and E. Ribes
D.A.S.O.P. Observatoire de Meudon
D. Rees
Department of Applied Mathematics, University of Sydney

In an earlier paper (Unno, Ribes, 1979), the thermodynamics was added to the M.H.D. equations in order to provide a heating mechanism for the solar network. Various thermodynamical situations were considered, leading to 3 models with the following characteristics :

Model n° 1 :

Describes the steady Bernoulli flow for an "*infinitesimally thin*" tube : the flow decelerates with increasing depth, a temperature excess of 1000°K is localized in the upper photosphere and the magnetic field strength at $\tau = 1$ is of the order of 300 gauss.

Model n° 2 :

Differs from model n° 1 only by the dilution factor. The tube is *no longer optically thin*. The dilution factor W was chosen rather arbitrarily since the 3 dimensional transfer was not solved (W = 1 at $\tau = 1$, and increases by 50 % at the top of the photosphere) the magnetic field strength is stronger at $\tau = 1$ ($\approx$ 800 gauss).

Model n° 3 :

Describes an ADIABATIC steady flow and is more relevant to the deeper layers. The flow accelerates very rapidly with increasing depth (from 0.5 Km s^{-1} at the top of the photosphere up to 7 Km s^{-1} at $\tau = 1$). The temperature excess is localized at $\tau = 0.5$. The magnetic field has a strength of 1300 gauss at $\tau = 1$ and diverges very rapidly with height (magnetic scale height = 110 Km).

In this paper, we report results of LTE line formation calculations performed for these hydromagnetic models. The calculations were restricted to the axis of the magnetic tube located at the disc center where the magnetic field is longitudinal. All the lines were approximated by Zeeman triplet.

The main results are as follows :

1) Weakening in the lines, as a function of the Agf value (Abundance times Landé factor times oscillator strength) and as a function of the potential excitation.

- We have made a curve of growth for 4 lines of neutral Iron (Fig. 1a, b, c). We found that the weak lines weaken more than the strong lines. Both temperature excess and velocity gradients reduce the saturation in the lines and increases the slope of the curve of growth. This is in good agreement with the magnetic field observations made by Semel (1980) and by Shimizu et al. (1981). An excess of temperature has the tendancy to weaken the lines of neutral iron. But for strong lines, the combined effect of velocity gradients and temperature excess may result in an increase of the equivalent width. We should note that in general, an enhanced brightness in the core of the lines (weakening) is possible even if the equivalent width increases (probably because ΔT, B and $\frac{dV}{dZ}$ contribute all to the weakening in the line center).

- The effect of the potential excitation is clearly seen in Fig. 1a, b, c when comparing 2 lines with the same equivalent width. The weakening is larger for lines with a lower potential excitation.

2) Net circular polarization (N.C.P.)

Our computations indicate a net circular polarization (N.C.P.) in the lines. This phenomenon is the result of the presence of both velocity and magnetic field gradients (ILLING et al. 1975 ; MAKITA, 1980). Fig. 2a, b, c shows that the N.C.P. increases with the Landé factor and varies with the three models. In particular, note that the sign of the N.C.P. for model n° 3 is opposite to that of the models n° 1 and 2 : this is due to the opposite sign of the flow velocity gradient. Future observations of the net circular polarization may be a good test for hydromagnetic models.

3) Continuum enhancement.

When the 3 models were elaborated, a constraint of no temperature excess at $Z = 0$ ($\tau_{HSRA} = 1$) was applied for two reasons. First, observers claimed that the

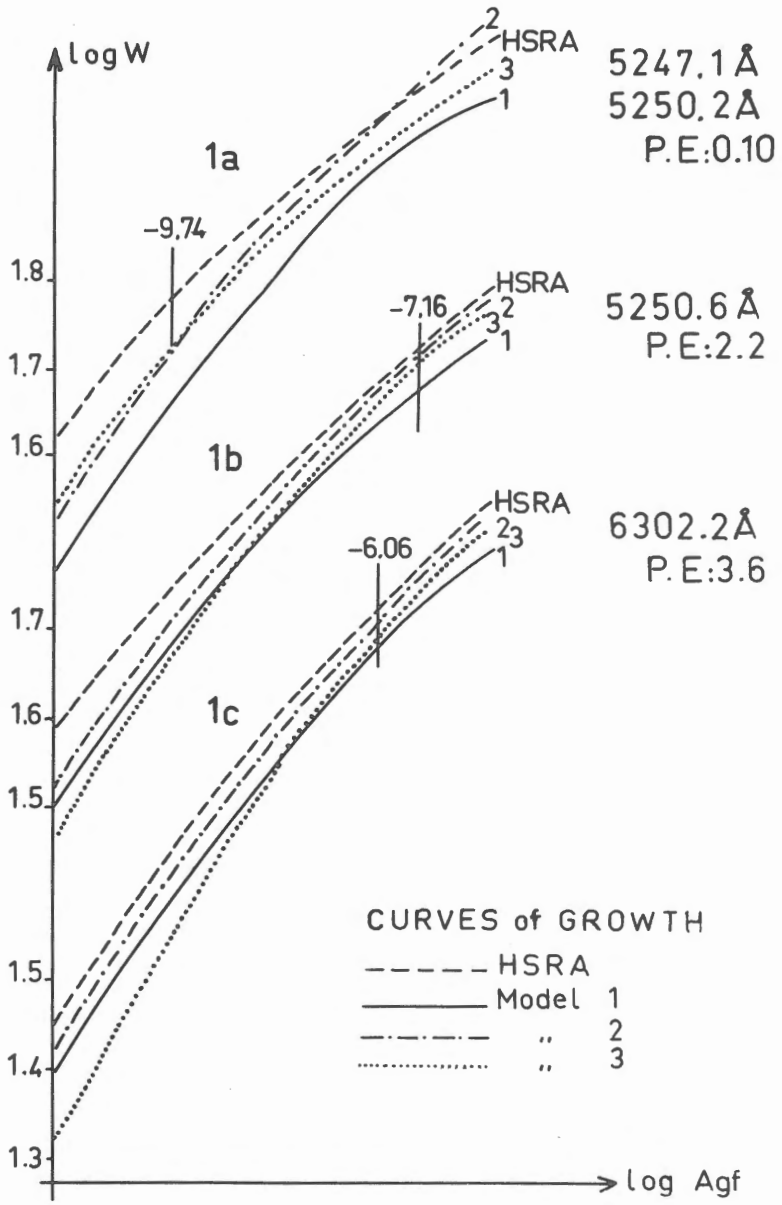

Fig. 1a, b, c represents the curves of growth for iron lines in the 3 models and in the H.S.R.A. reference atmosphere. The adopted log Agf value for the respective lines are :

- 9.74 (5247.1 Å and 5250.2 Å), - 7.16 (5250.6 Å) and - 6.06 (6302 Å).

faculae were not visible in the continuum at the disc center. Second, at this level, the opacity is high and the radiative losses become significant. Therefore, a small temperature excess could be sufficient to balance the excess of entropy transport. However, our computational results indicate an excess of the continuum brightness, as seen in Table 1. This is not in contradiction with the constraints mentioned above : the continuum in the magnetic tube is emitted at lower geometrical depth than $\tau_{HSRA} = 1$, and, therefore, at higher temperature.

As this stage, we should recall that all our calculations were made along the axis of the magnetic tube. We can estimate the apparent continuum enhancement if we know, at least, the cross-section of the magnetic tube. At $\tau = 1$, the cross-section can be extremely small (Koutchmy 1977). Thus, even if a brightness is not observed in the continuum, it may not be negligible and the problem of the enhancement of the facular continuum is still open (Rees, thesis 1973).

CONCLUSION.

The line formation calculations show how the lines are affected by the various physical conditions (temperature excess, velocity distribution, density etc...) in the faculae. They can be used eventually as a test for theoretical models. The predicted weakening for the 4 lines is qualitatively in agreement with observations. Future observations of the net circular polarization will be useful to indicate the presence of velocity gradients. Although the observations don't show any significant brightness excess in the continuum faculae, model 3 cannot be rejected in spite of the results in Table 1. The contradiction may disappear with very high resolution observations.

The three models differ by their thermodynamics. None of the 3 models is completely satisfactory because none of the 3 thermodynamical situations is valid throughout the photosphere and chromosphere. For the low chromosphere we suggest the model n° 1 as representative, for the deep photosphere, the adiabatic flow model (model n° 3) and in between the model n° 2. The next step will be to solve the Bernoulli flow with a combined thermodynamical situation.

TABLE 1

CONTINUUM	ENHANCEMENT		
	Model 1	2	3
5250 Å	4 %	16 %	55 %
6302 Å	1 %	13 %	46 %

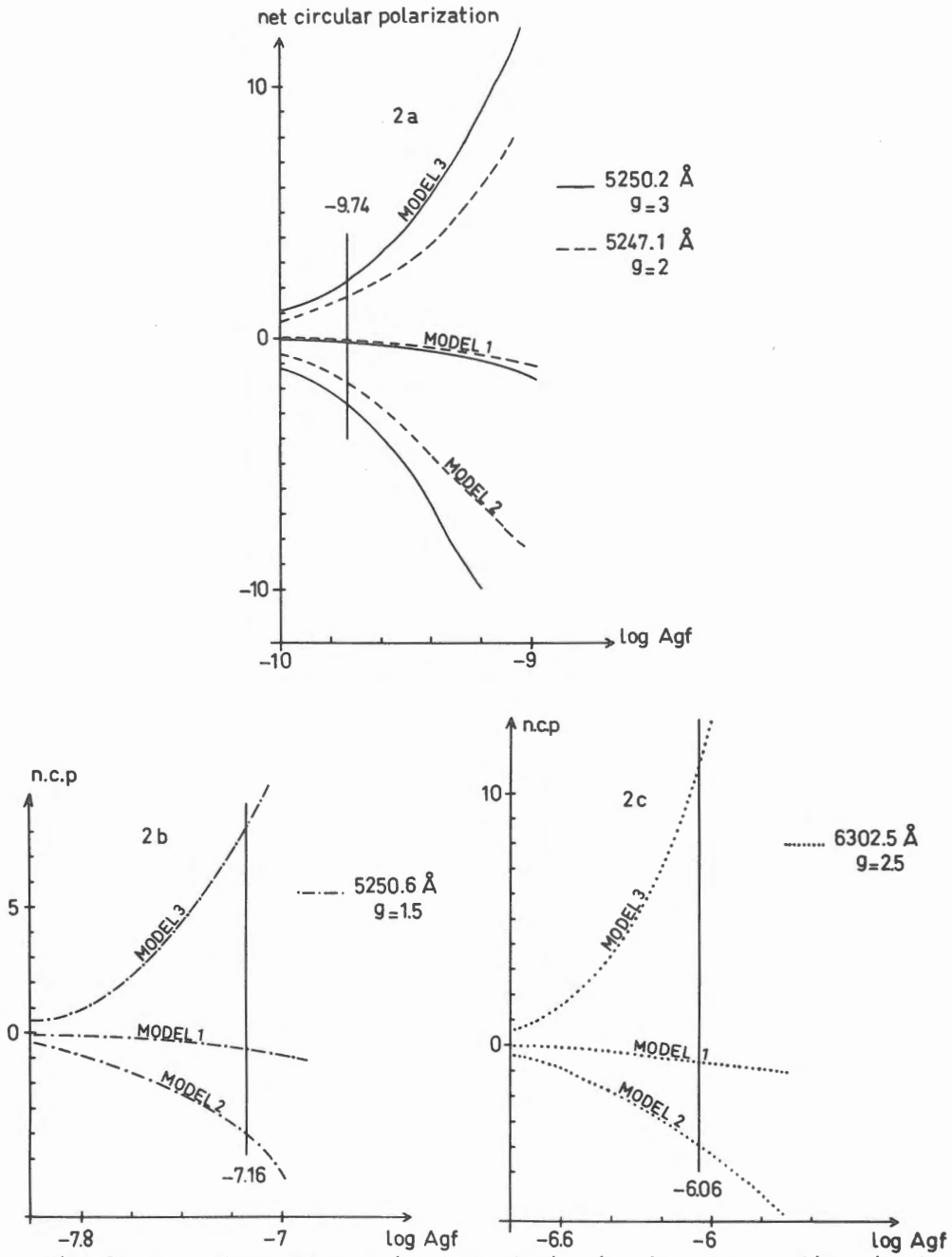

Fig. 2a, b, c shows the net circular polarization for the Iron lines in the 3 hydromagnetic facular models.

REFERENCES.

KOUTCHMY S. : 1977, Astron. and Astrophys., 61, p. 397.

ILLING R.M.E., LANDMAN D.A., MICKEY D.L. : 1975, Astron. and Astrophys., 41, 183.

MAKITA M. : 1980, private communication.

REES D. : 1973, thesis.

SEMEL M. : 1980, Astron. and Astrophys. in Press.

SHIMIZU I., HIEI E., SEMEL M. : 1981, in preparation.

UNNO W., RIBES E. : 1979, Astron. and Astrophys. 73, 314.

MASS BALANCE AND MAGNETIC STRUCTURE IN QUIESCENT PROMINENCES.

Jean-Louis LEROY
Observatoires du Pic du Midi et de Toulouse
65200 Bagnères-de-Bigorre FRANCE

Abstract

We discuss implications for prominence models of the apparent downward motions which are frequently observed at the limb. Both the reality of these motions and the value of the material density in prominences are presently subject to a great uncertainty so that firm conclusions about the mass balance of prominences can hardly be reached.

As a consequence it is not still clear whether quiescent prominences need a more or less permanent mass supply like that which is assumed in siphon-type models or if quasi-static models of the Kippenhahn and Schluter family are sufficient to explain the overall stability of the prominence phenomenon. It is concluded that coordinated determinations of several physical parameters (magnetic and velocity fields; electron density) in the same prominences are wanted to allow a progress on this critical problem.

1 - Introduction

Two years ago was held at Oslo a Colloquium devoted to solar prominences : as progress of our knowledge has not been specially fast since the meeting it is clearly useless to repeat here all the conclusions which were reached at this occasion. Rather I want to discuss a more limited question, although it has implications in many parts of the physics of prominences, which is the problem of mass balance in quiescent prominences. One cannot claim that this is now the only important unknown question on the topics but, as we shall see, a better understanding of the mass balance would immediately help to choose between the various prominence models which are presently under discussion.

2 - Static and dynamical mass balance in prominences

Everybody has in mind beautiful Hα pictures of quiescent prominences where the general blade shape as well as the filamentary structure are well visible.

An important point we shall have to discuss is that quiescent prominence movies display an apparent slow downflow of material visible in Hα. One must stress that this is an apparent motion as seen on the plane of the sky, not a motion derived from a Doppler analysis.

Another fundamental point which is well known (Koutchmy, 1977) is the peculiar location of quiescent prominences in the corona where they are very frequently seen at the bottom of streamers. Most striking is the fact that they are often surrounded by a dark cavity and by arches which have been known for many years (Kawaguchi, 1967; Saîto and Tandberg-Hanssen, 1973). The dark cavity has been generally interpreted as a proof of the "condensation" of coronal matter into a prominence and we meet there what can be called the "static mass balance problem" when we try to compare the mass available from a cavity and the mass necessary to build up a prominence.

One starts with the results of spectroscopic diagnostic. As which concerns the density, in which we have presently most interest, the possible range is still spread over nearly two orders of magnitude (Hirayama, 1979; see table 3) this scatter being due either to inaccurate determinations or to real variations among different prominences. Useless to say this uncertainty on the actual value of the density will hamper all the following analysis on mass balance.

Once one has derived the electron density, the ionization of hydrogen and the filling ratio, it is possible to derive an average mass Mp for a quiescent prominence which is found to be of the order of 10^{16} g. Note that this is not a negligible part of the total coronal mass (3×10^{17} g) so that the mass balance in prominences may be a point of interest for the more general problem of the coronal mass balance.

It is also possible to estimate the mass Mc which has become available after the depletion of a coronal cavity (Saîto and Tandberg-Hanssen, 1973) and it turns out that Mp >> Mc which raises two questions : whence comes prominence material ? What is the nature of the cavity-prominence association, if any ?

The situation remains confuse if we switch to what can be called the "dynamical mass balance problem" which is related to the apparent downflow of prominence material as seen on Hα movies. That this effect is conspicuous is proved by the fact that this apparent motion was taken many years ago as a criterium for prominence classification by Menzel and Evans (1953). Recent careful studies by Engvold (1976) show that one can adopt a figure around 1 - 10 Km/s for the apparent downward velocity and eventually one is left with the following dilemma : either it is considered that these are real material motions, because it is not so easy to explain the observations by variations of excitation or ionization of prominence

matter. Therefore one finds that the whole prominence will be emptied in some hours. As a matter of fact the figure of 5 hours was quoted by Anzer (1979) at one of the Oslo concluding workshops. Or one considers that the real material motions are not systematically downwards, and this point of view is supported by Doppler studies of filaments on the disc, specially by the recent observations of Martres et al (1980) who find no systematic downward velocities. In that case the material loss by a prominence is very slow and could be counterbalanced by the matter injected into the corona at the time of Disparitions Brusques (Engvold, 1980). But more Doppler studies of filaments on the disc are necessary before any conclusion (Kubota, 1980).

Both wide range of derived prominence density and uncertain signification of apparent downward motions make possible very different conclusions about the time lapse sufficient to empty a prominence : by contrast with the figure of 5 hours mentioned previously you can read that, at another workshop of the Oslo Colloquium Maltby (1979) suggested a time lapse of the order of 10 days... Such an uncertainty obviously has important consequences on prominence models !

3 - The mass-balance in some prominence models

Having in mind the idea that prominence material must be renewed within some hours some authors have felt it impossible to find enough available matter in the neighbouring corona and have been led to siphon-type models whose the first famous example was given by Pikelner (1971).

Recently there has been a lot of investigations concerning the magnetic stability and the thermal equilibrium in coronal arch structures with specific models of quiescent prominence by Ribes and Unno (1980) and by Uchida (1980). Concerning this family of models one can make three remarks : it is the only type of prominence model in which one can see clearly the origin of prominence material; but it postulates a magnetic configuration with a central dip which has not been observed clearly in the corona (Serio et al., 1979); and, finally, when the prominence is formed the type of support which is invoked is of the type of the classical Kippenhahn and Schluter model which will be considered later.

Although the model put forward by Pneuman (1972) does not invoke siphon mechanism its analysis could probably be extended to the case where material is supplied from below. The interest of Pneuman's work is to show that the existence of prominences at the bottom of streamers and the occurence of coronal cavities could be a natural consequence of density and temperature adjustments to satisfy energy and mass balance conditions at the bottom of a streamer. In such a view a quiescent prominence is usually formed in a generally bipolar magnetic configuration

(see figure 2 and 6 in Pneuman's paper).

In the case where we need alittle material to make up a prominence, because it is emptied very slowly, different authors have studied the possible occurence of thermal instabilities in specific regions of the corona where prominences would "condense". By contrast with the bipolar magnetic geometry assumed by Pneuman, Kuperus and Tandberg-Hanssen (1967) consider the neutral sheets which might appear over neutral lines of the photospheric field and show that they cannot remain in thermal equilibrium so that matter starts cooling which could ultimately result into the formation of a prominence (figure 4 in Kuperus and Tandberg-Hanssen paper).

4 - The prominence-corona association

Before any comparison between measured magnetic field and the configurations forecasted by Pikelner, Pneuman and Kuperus (to quote only these three main families of models) one can notice that the corona-prominence association should be different in these three cases so that there could be already observational tests based upon morphological properties which could help to choose the most likely model (but differentmechanism giving cool prominences in the hot corona can simultaneously be at work in the solar atmosphere !). Unfortunately observational data do not seem to give, up to now, a consistent idea of the prominence-corona association : for instance Fort and Martres (1974) have shown that coronal arches surrounding a prominence are more nearly parallel than perpendicular to the long axis of the prominence and that the classical view of a coronal cavity thought as a tunnel observed edge-on is not often consistent with the real geometry of the filament; thus even a model like Pneuman's which, at first glance, seems to be able to explain the observed corona-prominence association, would probably require deep geometrical modifications.

On the other hand, the observation of X-ray arches over neutral lines has been taken as an argument against the magnetic configuration assumed in the Kuperus-Tandberg-Hanssen model (Mc Intosh et al., 1976, Sheeley, 1979) but one must admit that X-ray arches are not very conspicuous in the vicinity of quiescent prominences and that they are generally observed much higher. We have already mentioned that no central bending of coronal arches has been observed on X-ray pictures (Serio et al., 1979) which does not support a geometry of the type chosen by Pikelner.

A fundamental test which bears directly on the mass balance problem would be to try to observe ascending motions in the vicinity of filaments (on the disc) for radiations corresponding to intermediate stages of ionization. Although some indications of this type have been provided by OSO 8 (Lites et al., 1976) this question

certainly deserves much more attention. Ground-based observations at the limb can also bring useful information about the "prominence tails" which may be the most important part of the corona-prominence interface as which concerns the mass balance problem (Kawaguchi and Oda, 1972). One remembers, for instance, the evidence for occasional large horizontal velocities found by Engvold et al. (1978) at the edge of some prominences.

5 - The magnetic support

Another way to attack the mass balance problem in quiescent prominences is to make it clear whether the prominence material can be kept in mechanical and thermal equilibrium in the lower corona, which would correspond to static models, or if we are observinga more or less continuous dynamical process. The physical parameter which has a critical role at this step is magnetic field in which prominence material is embedded. Therefore prominence models had to consider the support of cool matter which can be explained in several ways. It has already been mentioned that in the Pikelner model the material support is of the type early proposed by Kippenhahn and Schluter (1957). As a matter of fact more or less similar models have also been put forward (Tandberg-Hanssen, 1974) but the Kippenhahn and Schluter model still remains after 25 years one of the most successful and it has been the subject of detailed investigations including stability analysis (Anzer, 1969).

An interesting question, in view of the apparent downward motion in prominences, was to know whether the horizontal magnetic configuration which is foreseen in the Kippenhahn and Schluter model can keep material in strict static equilibrium or if slow vertical motions are allowed. Mercier and Heyvaerts (1977) have shown that the relative downward diffusion of neutral atoms is negligible but that, taking into account the Joule dissipation in subphotospheric regions of the currents which are pervading the prominence, one can explain downward velocities of some hundreds of meters per second.

The Kippenhahn and Schluter type of support is likely to be efficient also in the magnetic configuration considered previously in the case of the Pneuman model. On the opposite in the case of the Kuperus and Tandberg-Hanssen model the description of the prominence support takes into account the boundary condition set by the photosphere. Van Tend and Kuperus (1978) argue that the direction of the current in the Kippenhahn and Schluter model leads to unstable filament currents and they postulate a current in the opposite direction. But therefore the Lorentz force due to the ambiant magnetic field would be downwards and the support of cool material must be due to another mechanism. According to Kuperus and Raadu (1974) the global effect of the photosphere can be represented by a photospheric current

flowing antiparallel to the prominence filament current which gives a force upward with the right order of magnitude (cf. figure 2 in their paper). Further investigations on this topics have been made recently by Lerche and Low (1980 a and b.).

Obviously, the axial current along prominence long axis modifies the initial ambiant coronal field. Anzer and Tandberg-Hanssen (1970) have computed the resulting lines of force for increasing values of the current in a Kippenhahn and Schluter configuration. As it is probable that there is a component of the background field along the prominence long axis, lines of force are actually helices. Therefore we get a field configuration which would explain the often mentioned spiral-like structures in prominences (Rompolt, 1975); such a situation certainly exists in erupting prominences but it can also been argued (Malville, 1976; Stenflo, 1979) that in quiescent prominences at rest spiral lines of force with subtelescopic structure are also existing.

Another point which has become clear in the recent year is that the magnetic vector makes a small angle with the prominence long axis instead of being directly across the filament like in the original Kippenhahn and Schluter work. This shear appears to be intimately linked to the thermal equilibrium of the prominence as it has been clearly shown ina recent investigation by Milne et al. (1979). These authors have shown that in a generally horizontal magnetic configuration cool material can exist only for a narrow range of values of β (the ratio of kinetic to magnetic pressure) and α (the angle between the field vector and the prominence long axis); see figure 9 in the paper of Milne et al. Modifying the heating function it is possible to produce solutions for less stringent values of α and β but there is always a limit $\beta < 0.8$ and $\alpha > 7^\circ$ for the existence of prominences.

6 - Observed versus forecasted magnetic structures

This problem has been discussed (Anzer, 1979) during one of the concluding workshops of the Oslo Colloquium. Although the result is slightly disappointing, because observations do not seem to be sufficient to retain already a single model, it is interesting to follow the résumé written by Anzer (see figure 1 in his paper) .

Models of the Malville's type with large helical structures do not fit observations except in destabilized erupting prominences (see Tandberg-Hanssen, 1979, figure 4). Butpresent magnetic field measurements cannot discard the possibility of helical structures along the horizontal long axis prominences if the diameter of helices is below the resolving power of instruments ($\simeq$ 2000 Km). On the other hand observations seem to exclude structures like vertical helices which would have been more intuitive in view of the limb appearance of prominence ...

The Kuperus and Tandberg-Hanssen model has some features which do not fit observations : 1) the field is far from being horizontal 2) the transverse field strength is probably smaller than observed (Raadu, 1979) 3) the shear of lines of force does not seem to be easy to understand 4) the field polarity in prominence material should be opposite to the field polarity in the neighbouring photosphere.

Rust (1979) has emphasized that such was not the case and that he had always observed field polarities identical in the photosphere and in the prominence. My own feeling was the same at the beginning of investigations on the Hanle effect but I believe now that there are at least some cases where the field in prominences has a polarity oppositeto the photosphere : actually as the field vector is nearly along the prominence long axis it is rather difficult to ascertain experimentally what is the polarity of the field in prominences. This point which seems critical for the choice of the most probable prominence model certainly deserves further observational work.

Eventually, and even with some confusion about the question of the field polarity, it seems to me that present magnetic field measurements are more often consistent with the Kippenhahn and Schluter model than with the other one, but this opinion must not be taken as a definitive conclusion. In this connexion I have tried to compare some of the results of Milne et al(1979) with my recent measurements : first one can notice that the strength of the prominence field is now well known (Leroy, 1979, see figure 9) and that the agreement between Zeeman and Hanle method (Sahal-Bréchot et al., 1977) is excellent. As for the angle α between the magnetic vector and the prominence long axis I have obtained recently good data concerning prominences of the polar crowns which confirm that α is around 25° for these objects while it is somewhat smaller for prominences inside active regions. This is well consistent with the requirement that $\alpha > 7°$ (Milne et al. 1979), but one must remember that the observations would be identical for an unresolved horizontal helical field of subtelescopic scale with a pitch angle of about 35°. At last I have given on figure 1 the repartition of B_T which is the supporting component of the field, perpendicular to the prominence axis (figure 1 refers again to prominences of the polar crowns). Following Milne et al. there must be the condition

$$\beta < 0.8 \text{ i.e. } kNT < 0.8\ B_T^2 / 8\pi$$

or

$$Ne < 1.1 \times 10^{10} B_T = Ne \text{ max} \quad (\text{for } N \simeq 2.5 \times Ne)$$

Thus the upper scale of figure 1 shows the maximum value Ne max which can be supported by the field B_T.

If one retains low values of Ne like those which have been computed recently

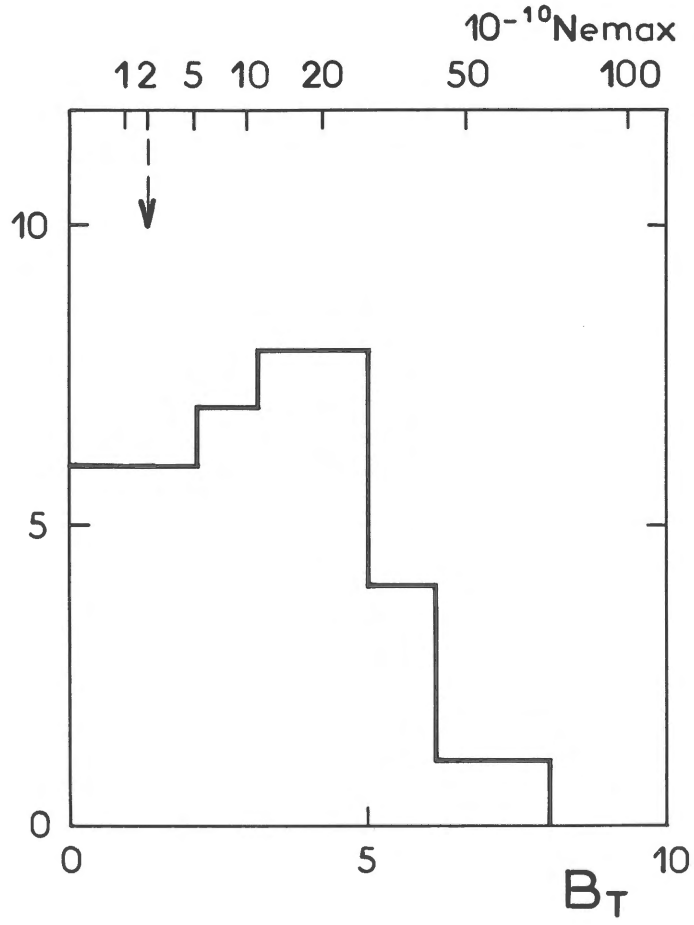

Figure 1.

Repartition, for a sample of 41 prominences of the polar crowns, of measured values of B_T (lower scale) : B_T is the component of the magnetic vector across prominence long axis, expressed in Gauss. The upper scale gives the corresponding values of Ne max defined following the equality :

$$kNmaxT = 0.8 \times B_T^2 / 8\pi \quad \text{with Nmax} = 2.5 \times \text{Ne max.}$$

by Heasley and Milkey (1976; see model c 1) and seem to fit quite well spectroscopic data, it is seen that the magnetic support is generally much larger than necessary according to figure 1; therefore the prominence magnetic field is probably not far from a force-free configuration.

7 - Conclusion

If we cannot find presently a model which fits completely magnetic observations it may be that models have not included something essential and the fine structure of prominences has often been mentioned at this stage. Together with the problem of geometrical fine structure one has to deal with a question of life time of prominence material : it is true that a given neutral line can remain the seat of prominence appearance during several months and it is true that a given prominence can last several weeks. But when one is observing with better resolving power it becomes clear that the lifetime of individual knots or threads is much smaller, of the order of 10 minutes only (Engvold, 1976). Therefore it may be erroneous to search prominence models in which cool material can reach mechanical as well as thermal equilibrium and one can be tempted to think towards dynamical models as Priest and Smith (1979) have recently proposed it (see figure 8 in their paper). I don't know whether one can explain theoretically heating or cooling times of only several minutes but, from the experimental point of view the idea of a quiescent prominence as a medium in always evolving thermal state, within a generally favorable magnetic configuration, would nicely fit many observations. Such a point of view would also modify drastically some topics linked to the mass balance problem that we have discussed previously.

From the observers side much remains to be done and it seems to me that the most essential requirement would be now to recover, for a given prominence, a complete set of data concerning the electron density, the velocity field and the magnetic configuration. This aim is not impossible to reach if several observatories are involved in such an endeavour. On the other hand, further researches on the shape of coronal structures in the vicinity of prominences are much wanted : they should be undertaken in future space experiments with help of EUV images corresponding to various excitation stages and having as good as possible spatial resolution.

References

Anzer, U., 1969, SolarPhysics, 8, 37

Anzer, U., 1979, I.A.U. Colloquium n° 44, 322

Anzer, U., 1979, I.A.U. Colloquium n° 44, 324

Anzer, U., Tandberg-Hanssen, E., 1970, Solar Physics, 11, 61

Engvold, O., 1976, Solar Physics, 49, 283

Engvold, O., Malville, J.M., Livingston, W., 1978, Solar Physics, 60, 57

Engvold, O., 1980, I.A.U. Symposium n° 91, in press

Fort, B., Martres, M.J., 1974, Astron. Astrophys. 33, 249

Heasley, J.N., Milkey, R.W., 1976, Ap.J., 210, 827

Hirayama, T., 1979, I.A.U. Colloquium n° 44, 4

Kawaguchi, I., 1967, Solar Physics 1, 420

Kawaguchi, I., Oda, N., 1972, private communication

Kippenhahn, R., Schluter, A., 1957, Z. f. Ap., 43, 36

Koutchmy, S., 1977, in Illustrated glossary for solar and terrestrial physics, Bruzek and Durrant editors, D. Reidel, Dordrecht, Holland; p. 39

Kubota, J., 1980, This Colloquium

Kuperus, M., Tandberg-Hanssen, E., Solar Physics, 1967, 2, 39

Kuperus, M., Raadu, M.A., 1974, Astron. Astrophys., 31, 189

Lerche, I., Low, B.C., 1980a,Solar Physics, 66, 285

Lerche, I., Low, B.C., 1980b,Solar Physics, 67, 229

Leroy, J-L., 1979, I.A.U. Colloquium n° 44, 70

Lites, B., Bruner Jr., E.C., Chipman, E.G., Shine, R.A., Rottman, G.J., White, O.R., Athay, R.G., 1976, Ap.J., 210, L 111

Mac Intosh, P., Krieger, A.S., Nolte, J.T., Vaiana, G., 1976, Solar Physics, 49,57

Maltby, P., 1979, I.A.U. Colloquium n° 44, 332

Malville, J.M., 1976, Solar Physics, 50, 79

Martres, M.J., Mein, P., Schmieder, B., Soru-Escaut, I., 1980, submitted for publication

Menzel, D.H., Evans, J.W., 1953, Convegno Volta 11, 19

Mercier, C., Heyvaerts, J., 1977, Astron. Astrophys., 61, 685

Milne, A.M., Priest, E.R., Roberts, B., 1979, Ap.J., 232, 304

Pikelner, S.B., 1971, Solar Physics, 17, 44

Pneuman, G.W., 1972, Ap.J., 177, 793

Priest, E.R., Smith E.A., 1979, Solar Physics, 64, 267

Raadu, M.A., 1979, I.A.U. Colloquium n° 44, 172

Ribes, E., Unno, W., 1980, Astron. Astrophys. in press

Rompolt, B., 1975, Acta Universitatis Wratislaviensis n° 252,55
Rust, D.M.,1979, I.A.U. Colloquium n° 44, 172
Sahal-Bréchot, S., Bommier, V., Leroy, J-L., 1977, Astron. Astrophys., 59, 223
Saïto, K, Tandberg-Hanssen, E., 1973, Solar Physics, 31, 105
Serio, S., Vaiana, G.S., Godoli, G., Motta, S., Pirronello, V., Zappala, R.A., 1978, Solar Physics, 59, 65
Sheeley, N.R., 1979, I.A.U. Colloquium n° 44, 172
Stenflo, J.O., 1979, I.A.U. Colloquium n° 44, 79
Tandberg-Hanssen, E., 1974, Solar Prominences, 60; D. Reidel Publ. Comp.
Tandberg-Hanssen, E., 1979, I.A.U. Colloquium n° 44, 161
Uchida, Y., 1980, This Colloquium
Van Tend, W., Kuperus, M., 1978, Solar Physics, 59, 115

MOTIONS AND OSCILLATIONS IN FILAMENTS

J.M. Malherbe, M.J. Martres, P. Mein, B. Schmieder, I. Soru-Escaut
Observatoire de Paris-Meudon

Abstract

Radial velocities observed in quiescent filaments show that :

1 - long living motions seem to be mainly upward and vertical

2 - chromospheric oscillations are strongly reduced in filament material.

1. Data

Results presented here have been obtained with two kinds of data :

a) H_α pictures from the 9-channel MSDP operating at the Meudon solar tower. This instrument will be described in more details during the last session of this meeting. It is equivalent to 9 monochromatic filters used simultaneously and centered at $H_\alpha \pm n \times 0.30$ Å ($n = 0, 1, 2, 3, 4$)

b) H_α patrols with the Meudon 3λ-heliograph ($H_\alpha \pm 0.75$ Å).

2. Long living motions in quiescent filaments

H_α patrol observations covering 170 hours and corresponding to 34 cases of various latitudes, longitudes and distances to active regions, have been analysed. Comparison between visibility of filaments in the blue and red H_α-wings ($\pm$ 0.75 Å) provides the sign of radial velocity. We assume that dark filaments correspond to source-functions decreasing upwards, so that velocity and Dopplershift have the same sign. Data have been divided into 3 parts, according to the center-limb location (Θ-value). Fig. 1 shows the relative times corresponding to the following situations : blue shifts only are observed (B), red shifts only (R), blue and red shifts observed simultaneously in different regions (B+R), no shift (0). We can see that :

a) blue shifts are always dominating near the center, which indicates that motion are mainly upward. This result seems to be conflicting with proper motions observed at the limb, unless the regions of line formation correspond to quite different locations inside prominences. More detailed observations are needed. So far, velocity maps provided by MSDP in a few cases seem to confirm

our result.

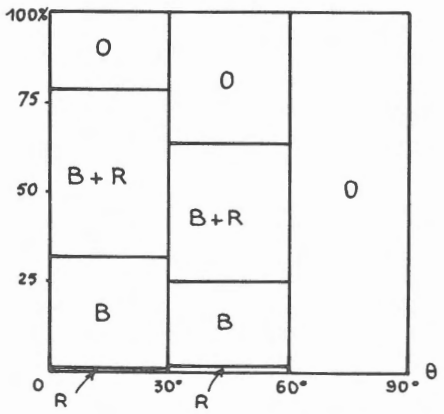

Fig. 1 - Normalized observing times corresponding to occurrence of blue (B) and red (R) shifts, versus center-limb location of filaments

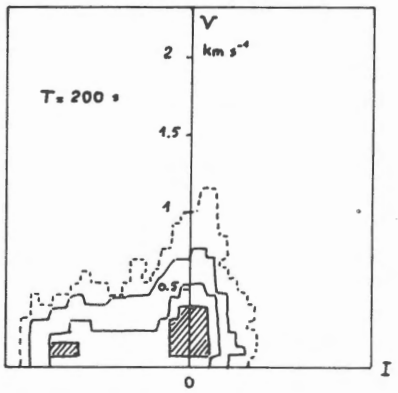

Fig. 2 - Histogram of oscillation amplitude (period 200 s) versus average intensity ($H_\alpha \pm 0.30$ A), in filament and neighbouring chromosphere.

3. Oscillations in quiescent filaments

A time sequence of MSDP pictures has been obtained on July 17, 1979, on a filament located at N36 W20. The duration was 720 s. Dopplergram and intensity maps have been computed with a 60 s time-step. A shorter sequence (420 s) was analysed every 30 s. "Steady" flows and "oscillatory" motions have been investigated by Fourier transforms on the total observed field (1' x 6') with a spatial resolution of 1 arc second. Of course, long periods cannot be discriminated from real steady flows, but 3 min or 5 min oscillations can easily be separated. The results can be summarized in the following way :

a) "Steady" flows are fast only in some localized regions, near the edges of dark material. Average values over the whole filament confirm the general trend observed previously (upward velocities).

b) Oscillations appear to be weak inside the filament. Fig. 2 shows an histogram of oscillation amplitude versus average intensity (whole field of view, 600 s sequence) for periods around 200 s. Dark regions of the filament

are located at the left of the diagram, and correspond to smallest amplitudes. This behaviour can be checked on amplitude maps : oscillations seen to avoid the regions where the filament lies. Analyses have been performed for two different distances from H_α center ($\pm$ 0.30 and $\pm$ 0.60 Å). The oscillation amplitude decreases towards the line center. It could be possible that the material velocity amplitude is nearly zero inside the filament, and that residual Dopplershifts are due to superimposed chromospheric motions, if the dark material is not optically thick. This result is very consistent with efficient reflection of acoustic waves at the top of the chromosphere, and with a very small leakage of acoustic flux into the corona.

4. Active region filaments

Time sequence of MSDP observations have also been obtained for active region filament. Preliminary analysis in one case shows that higher velocities are present. Weak oscillations can also be detected. As expected, they correspond to lower frequencies. Fourier analysis is more difficult to interpret because of sporadic motions connected with magnetic field evolution. In other respects, the shape of some function should be known in order to deduce velocities from Dopplershifts, especially in neighbouring bright regions.

REFERENCES

- Martres, M.J., Mein, P., Schmieder, B., Soru-Escaut, I., 1980, Solar Phys., in press.
- Malherbe, J.M., 1980, DEA d'astrophysique, Rapport de stage.

A Model of Magnetic Field and Mass Flows in Dark Filaments

by

Yutaka Uchida
Tokyo Astronomical Observatory
University of Tokyo, Mitaka, Tokyo

Abstract

A model of magnetic field in the dark filament having a "neutral sheet" in $B_\perp$ (the field component perpendicular to the polarity reversal line in the photosphere) is obtained by solving the equation for the magnetostatic equilibrium. The apprearance of the "neutral sheet" structure is due to the assumed (line-) quadrupole component in the photospheric magnetic field distribution, and, from the standpoint of view of the neutral sheet hypothesis of flares, it is favorable in explaining the fact that the dark-filament disappearance is connected to the occurrence of flares. Further,possible mass-flow is examined in the derived magnetic field configuration in order to explain the steady supply of mass for the downflow across the height of the prominence. It turns out that there is a steady Bernoulli flow solution which first increases its velocity towards the top of the loop and then diminishes its velocity on approaching the "neutral sheet" region, explaing the slow downflow observed in the prominences.

1. Introduction

A dark filament is an elongated, thin partition-like object (length $\simeq$ (1 - 2) x 10^5 km, width $\simeq$ a few x 10^3 km, height$\simeq$ (2 - 5) x 10^4 km) lying over the polarity reversal line of the photospheric magnetic field (McIntosh 1972). When seen from above, it is consisted of thin threads along the length of the structure with centipede-leg type features on both sides of it. Thin threads are also observed when seen on the limb (or seen from sideward) with a continuous downflow along them (Engvold 1976).

A dark filament is thus considered to be a structure due to magnetic field which suspends the material against gravity, and many theoretical models for the magnetoplasma equilibrium have been proposed to explain the observed characteristic features of it (Bhatnager et al 1951, Dungey 1953, Brown 1958, and so on. See Tandberg-Hanssen 1974 for review). One of the most widely discussed modelds among them is Kippenhahn and Schluter's model

(1957). It is a model in which the mass is suspended by a sagged magnetic field lines and a thin partition-like structure is considered as the locus of the lowest points on the similarly sagged group of lines of force at which low temperature mass is sedimented with a short scaleheight.

Kippenhahn-Schluter model, however, deals with sagged field lines locally, and actually the sagging is due to the specification of the boundary value of B_z/B_x . In actuality, if we consider that the lines of force above the polarity reversal line of the photospheric magnetic field is convex, there is no way for the mass pile-up to start because it is not possible to suspend the mass on the top of the convex field lines. The production of the dip, on the other hand will be appreciable only after the amount of the loaded mass at the top of the loop reaches an appreciable amount. In other words, the mass slides down and can not stay at the top to sag the lines of force if it is initially convex. Another difficulty with K-S model may be the fact that there is a steady downward mass flow observed across the height of the dark filament, but K-S model does not have a drainage installed in it. The mass down-flow suggests that the mass of the dark filament is replaced in every several hours, and that there should be a supply of the mass either from the surrounding corona, or from the chromosphere by some special means. The former, however, is difficult because it means a mass flow across the field lines as long as we consider the thread-like structure as representing the field lines. In the latter line, the mechanism proposed by Meyer and Schmidt (1968) for the flow in coronal loop was applied to the present problem of the mass supply to the dark filament by Pickelner (1971). Pickelner's model, however, has no drainage again and does not explain the down-flow in the steady state.

Our model to be discussed here explains the observational characteristic features of the dark filament described at the begining of this section, as well as its relation to the polarity-reversal lines, and gives naturally an explanation for the flows down across the prominences (dark filament seen on the limb). In section 2 we describe the solution for the magnetoplasma equilibrium (Uchida and Jockers 1977, 1981), and in section 3 we discuss the result of the calculation of the flow induced in the structure by syphon mechanism (summary of the work done by Uchida and Tsuneta 1978, 1981). Discussions are given in section 4.

2. A Solution for the Magnetoplasma Equilibrium

Uchida and Jockers' (1977) solved the equation for the equilibrium of magnetoplasma under constant gravity,

$$\frac{1}{c}\, j \times B - \nabla p + \rho g = 0 \,, \quad j = \frac{c}{4\pi} \mathrm{rot}\, B \tag{1}$$

for quasi-three dimensional configuration (the field has three components but does not depend on one coordinate, say, y along the polarity-reversal line in the photospheric magnetic field). In this case, B is expressible by two variables, φ and $B_{\parallel}(\parallel y)$ as

$$B = \left(\frac{\partial \varphi}{\partial z} \,,\; B_{\parallel} \,,\; -\frac{\partial \varphi}{\partial x} \right) \tag{2}$$

and it can be shown that the problem reduces to solving

$$\nabla_{\perp}^2 \varphi + \frac{1}{2} \frac{d}{d\varphi} \left\{ B_{\parallel}^2(\varphi) + 8\pi p_0(\varphi) e^{-z/z_s} \right\} = 0 \tag{3}$$

where $\nabla_{\perp}^2 \equiv \partial^2/\partial x^2 + \partial^2/\partial z^2$, $z_s \equiv RT/g$ and $B_{\parallel}$ is required to be the function of φ alone from the force balance along y-axis, and p_0 is the pressure at z = 0 which may be the function of φ. The pressure assigned according to the boundary condition at the base now distributes hydrostatically along the magnetic tubes of force protruding in the corona.

In order to avoid the difficulty of convex field lines in supporting the cold mass loaded upon them, Uchida and Jockers introduced a quadrupolar component in the distribution of photospheric magnetic field. This introduces the possibility for a "neutral sheet" (in $B_{\perp}$) to appear right above the polarity reversal line and also gives rise to a dip to the otherwise convex field pattern. It is rather surprising that the neutral sheet structure has never been considered in the context of the dark filament models while the disappearance of the dark filament is known to be related to the occurrence of flares and the neutral sheet hypothesis has been discussed as a likely mechanism of flares during the last twenty years. Our dark filament model is the one which is intrinsically related to a "neutral sheet" (in and $B_{\perp}$) and its relation to flares is discussed in Uchida and Sakurai (1980) and in Uchida (1981). As for the distribution of $B_{\parallel}$ and p_0 , we assume

$$B_{\parallel} = B_{\parallel 0} \exp\left\{ -\frac{(\varphi - \varphi_c)^2}{\sigma_{B_{\parallel}}^2} \right\} \tag{4}$$

and

$$p_0 = p_{0c} + p_{0c} \exp\left\{ - \frac{(\varphi - \varphi_c)^2}{\sigma_p^2} \right\} \qquad (5)$$

as an example in the calculation.

We solve equation (3) by using an extended version of Jockers' code with Marder and Weitzner's relaxation scheme, which was used for the force-free field case (Jockers 1978). The result is shown in Figure 1 and the central part of it having the centipede-leg like feature is shown in Figure 2. It is seen in Figure 1 that our model indeed has a thin vertical "neutral sheet" of $B_\perp$ right above the polarity reversal line of the photospheric magnetic field, and the effect of relatively small $B_\parallel$, dominates in this sheet of vanishing $B_\perp$, and field lines shows a strong tendency of aligning along the y-axis in the sheet. The lines of force, all of which would be convex without the quadrupolar component in the photospheric field distribution, are now deformed to have sagged part as well as sheet structure, due to the introduction of the quadrupolar distribution of the field near the polarity reversal line.

3. Supply of the Mass by Steady Flow

Although the solution shown above is that for a static equilibrium and no mass-flow is installed in it, we may discuss the mass-flow in the configuration without deforming it too much, since $\rho v^2/2 \ll B^2/8\pi$, and $\mathcal{R}\rho T \ll B^2/8\pi$ even in the sheet. Thus, we consider the magnetic tubes of force as fixed pipes and write hydrodynamic equations in them. We have for steady flows,

$$\frac{1}{A}\frac{d}{ds}(AB) = 0 \qquad (6)$$

$$\frac{1}{A}\frac{d}{ds}(A\rho u) = 0 \qquad (7)$$

$$\rho \frac{du}{ds} = -\frac{dp}{ds} - \rho \frac{GM}{r^2}\frac{dr}{ds} \qquad (8)$$

$$\frac{1}{A}\frac{d}{ds}\left[A\rho u\left(\frac{u^2}{2} - \frac{GM}{r} + \frac{5}{2}\mathcal{R}T\right) - AK\frac{dT}{ds}\right] = Q - \rho^2\Phi \qquad (9)$$

where A(s) is the crosssectional area of tubes of force, and s is the length measured along them. A(s) is related to the magnetic field strength, B(s), as AB = const, and is given from the model

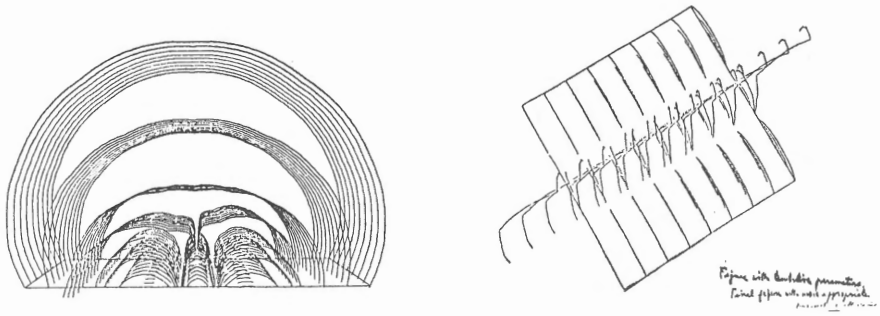

Fig. 1. A solution for the magnetic field in dark filaments. Quadrupolar component in the photospheric magnetic field distribution introduces a "neutral sheet" (neutral sheet in $B_\perp$) above the central polarity reversal line.

Fig. 2. A part of the structure of the field configuration of Figure 1. Field lines are stretched along the neutral sheet of $B_\perp$, because even comparatively weak $B_{//}$ dominates in the sheet where $B_\perp = 0$.

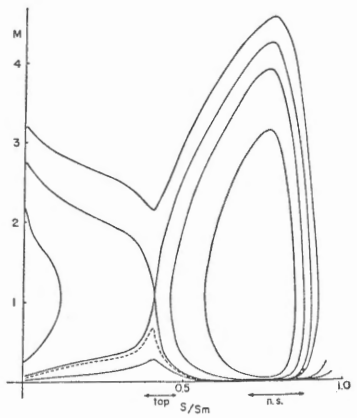

Fig. 3. s-M diagram for the steady polytropic flow. The solution fulifilling the condition that the flow slows down and condenses on approaching the sheet region is the one shown in dotted curve, staying subsonic all the way. The flow is accelerated and has a maximum velocity near the top of the loop and then diminishes its velocity.

in section 2. Other notations are as usual.

If we first assume a polytropic gas for simplicity, equations(9) is replaced by $p\rho^{-\alpha}$ =const, and equations (7) and (8) are integrated parallel to the solar wind case (cf. Kopp and Holtzer 1976) to give

$$M^{\frac{4}{\alpha+1}} + \frac{2}{(\alpha-1)M^{2\frac{\alpha-1}{\alpha+1}}} = \left\{ M_0^{\frac{4}{\alpha+1}} + \frac{2}{(\alpha-1)M^{2\frac{\alpha-1}{\alpha+1}}} \right\} \frac{f(s)}{f_0} \qquad (10)$$

$$f(s) = \left\{ A(s) \right\}^{2\frac{\alpha-1}{\alpha+1}} \frac{E' - gh(s)}{E'} \qquad (11)$$

$$E' = \frac{u^2}{2} + \frac{5}{2}\mathcal{R}T \qquad (12)$$

The s-M diagram for a typical tube of force passing the sheet is shown in Figure 3.

It shows that the diagram is very much different from that of the solar wind case due to the area-variation effect and to the effect of the change in the effective gravity along the path, even changing signs with respect to the flow direction. Appropriate solution for our case is in the subsonic branch all the way, and the velocity change along the path, increasing near the highest part of the path and decreasing again in the sheet region, is favorable in explaining the observation.

The assumption of polytropic gas is equivalent to assuming heat sources and sinks distributed along the path in a very artificial way, and also has a restriction that the range of the allowed variation of T, for example, is not wide enough to cover the variation of the temperature expected in reality. Thus we have to recouse to numerical integration of equations (6) through (9) by adopting appropriate expression for $\mathcal{Q}$ and Φ . Figure 4 is the s-M diagram corresponding to Figure 3, and Figures 5 through 7 are u, ρ and T as functions of s . Now, for example, the temperature can fall to lower value with a higher value of density which can not be attained in the polytropic case due to the restriction of polytropic relation.

Interpretation of the results of the calculation may be as follows. From these figures, it is seen that the flow deviates very much from the polytropic case when the radiative cooling becomes effective. The temperatrure falls very much more than what the polytropic relation allows, and the velocity decreases also due to the increase in the density. All these take place when the flow approaches the sheet region. For a given tube of

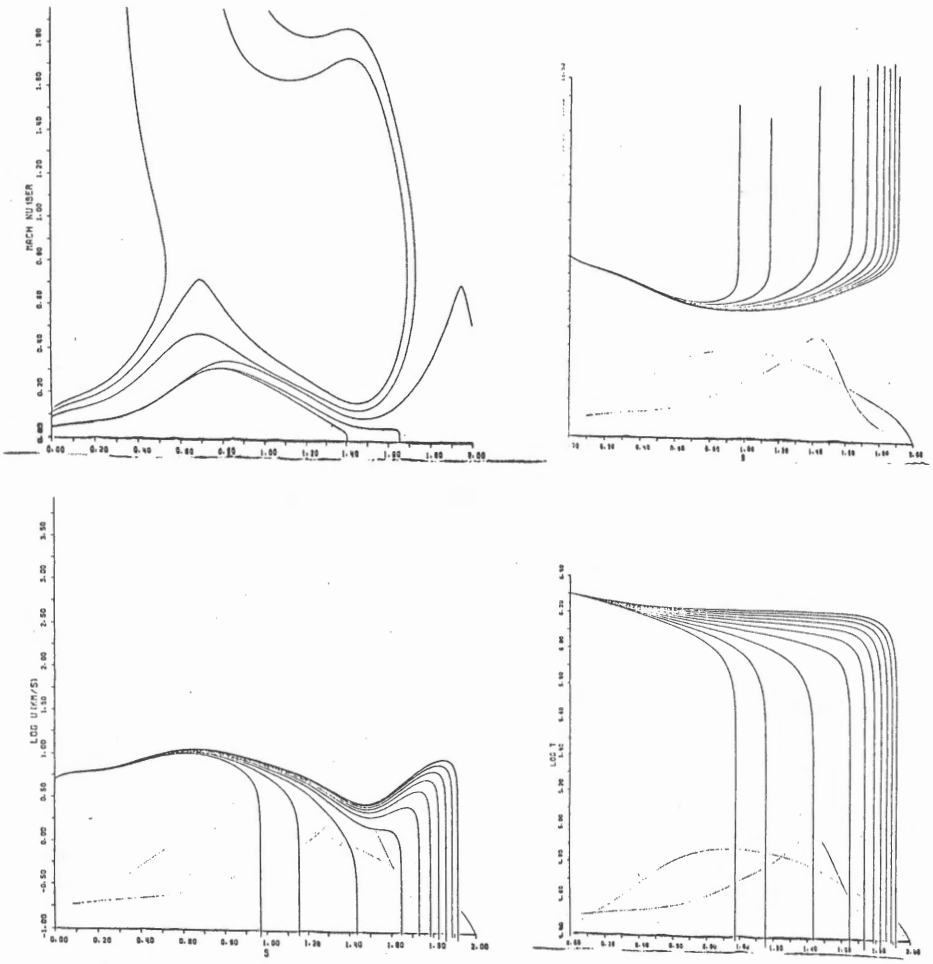

Fig. 4. Steady flow under more realistic conditions of energy exchange. s-M diagram corresponding to Figure 3.
Fig. 5. The velocity variation along the path.
Fig. 6. The density variation along the path.
Fig. 7. The temperature variation along the path.

force, the condition at the starting point (eg , the velocity, when the temperature and the density there are given) is selected out as in the Parker-flow of the solar wind case. The kinetic energy and enthalpy fluxes converts into each other, and if we put too large an inflow, the temperature of the gas gets too high when the kinetic energy is converted into enthalpy before radiative cooling region in and near the sheet is reached, because the excess heat is conducted backward to the starting point which is taken to be in the low corona at the outer footpoint of the flux tube.

Our conclusion is that there is a condition in the subsonic branch in which the flow velocity first rises to a considerable value but slows down again nicely towards the sheet region with high condensation rate and with a decreased temperature as low as 10^4 K, and reproduces the observed slow down-flow of the cool prominence material.

4. Summary and Discussion

Details of the calculation of the equilibrium field configuration and flows in it, together with interpretations of the results of calculations, may be found elsewhere as indicated. Here we summarize them as follows :

We propose a possible equilibrium configuration of magnetoplasma, which has a neutral sheet in $B_\perp$ (with $B_\parallel$ field lying in the sheet) caused by the quadrupolar component in the distribution of the photospheric field, as a possible field configuration in dark filaments. Morphological properties of the dark filament (thin partition-like structure over the polarity reversal line with fine threads along it and centipede-leg like feature on both sides) is pretty well reproduced. We consider the possibility of driving a steady flow in it by syphon mechanism (such a flow can take place without disturbing the equilibrium configuration too much). It is not possible for this mechanism to operate between two equivalent points of a symmetrical loop, but in the present case, the flow is caused between the outer and inner footpoints of the field lines on one side of the sheet, and the thermal expansion flow is driven by the pressure difference between the corona above the outer footpoint and the cooled prominence material which is drained down to the inner footpoint. In our picture, therefore, the mass down-flow observed in prominences is supplied from the low corona on the onter foot of the loop. The mass-flow passes through the top part of the loop with the highest velocity and then, on approaching the sheet region, it condenses through the radiative cooling and its velocity diminishes to reproduce the observed slow down-flow. Thus, it seems that our picture may provide a possible model for dark filaments.

References

Bhatnagar,P.L.,Krook,M ,and Menzel,D.H ,1951,in Report of Conf. on Dynamics of Ionized Media, Univ. College, London.

Brown,A.,1958,Astrophys.J.,128,646.

Dungey,J.W.,1953 Month. Not. Roy. Astron. Soc.,113,180.

Engvold,O.,1976, Solar Phys. 49, 283.

Jockers,K.,1978, Solar Phys. 56, 37.

Kippenhahn,R.,and Schluter,A.,1957,Zeit.Astrophys,43,36,

McIntosh,P.S. ,1972 in Solar Activity Observations and Predictions, eds. McIntosh and Dryer (MIT Press).

Meyer,F.,and Schmidt,H.U.,1968,in IAU Symp.No 35, Structure and Development of Solar Active Region, ed.,K.O.,Kipenhener (D.Reidel).

Pickelner,S.A.,1971,Solar Phys.17,44.

Uchida,Y. and Jockers,K.,1977,Abstract, Ann.Meeting of the Astronomical Society of Japan.

Uchida,Y. And Jockers,K.,1981, in preparation.

Uchida,Y.,and Sakurai,T.,1980, in Solar Flares, ed. Sturrock (Univ. Colorado Press).

Uchida,Y.,and Tsuneta,S.,1979, Abstract, Ann.Meeting of the Astronimcal Society of Japan.

Uchida,Y.,and Tsuneta,S.,1981,in preparation.

Uchida,Y.,1981,IAU Symp. No91, Solar and Interplanetary Dynamics, ed. Tandberg-Hanssen and Dryer (D.Reidel).

Tnadberg-Hanssen,E.,1974, Solar Promineces,(D.Reidel).

The Vertical Motion of Matter in Quiescent Prominences

Jun Kubota
Kwasan and Hida Observatories, University of Kyoto, Kyoto 607

In order to understand the problem of mass balance in quiescent prominence and its evolution, it is important to know the velocity of vertical motion of matter. We have been securred spectroscopic observations of dark filaments and studied the vertical motion of matter by measuring the wavelength shift in the CaII K line at various portions in the dark filament appeared near the disk center.

Observations were made at the Kwasan Observatory with the horizontal solar telescope and the spectrograph and also at the Hida Observatory with the domeless telescope and the horizontal spectrograph. Spectra of the CaII K line were taken with a mean dispersion of 0.3Å/mm, by setting the entrance slit of spectrograph on the various portion of the image of the filament at the prime focus of the telescope. Microdensitometric tracings of the spectra were made along the direction of dispersion within a range of ±10Å from the K line center, and then, the profile of the K line and the relation between measured distance from standard line(x) and the wavelength were obtained.

The theoretical profile of the CaII K line in a homogeneous cloud model can be expressed by assuming constant source function throughout the cloud; $I_\lambda = I_b \exp(-\tau_\lambda) + S[1 - \exp(-\tau_\lambda)]$, where $\tau_\lambda = \tau_0 \exp[-\{(\Delta\lambda - \lambda v/c)/\Delta\lambda_D\}^2]$ and I_b is the background intensity from underlying chromosphere, τ_0, the optical thickness of the cloud at the K line center, v , the velocity of the cloud against the photosphere along the line of sight. The contrast function is defined as $C(\lambda)=(I_b-I_\lambda)/I_b$. We estimated the profiles of the CaII K line and the contrast function in the model cloud in a range of τ_0 from 1 to 5 and of v from 0.5 to 10km/s. Here I_b is taken from the White and Suemoto's measurements(1968). For v<2km/s and

$\tau_0<5$, however, our estimated contrast function does not show distinct maximum. Without knowing real τ_0 in the dark filament, therefore, the estimation of the velocity by the contrast function method may lead to noticeable errors. Our observed profiles of the CaII K line in the dark filament are compared with the estimated ones for various v and τ_0 combinations.

When $\tau_0<2$, the intensity of the CaII K line in the dark filament is much affected by the background radiation. Moreover, if the filament is composed of fine threads of matter, the background radiation from underlying chromosphere would partly pass through the filament and change the intensity of the K line we observed. The minimum intensity in the profile of the K line, I_M , is nearly equal to the source function in the filament, when τ_0 is sufficiently large and I_M is scarcely affected by the background radiation. The excitation temperature of the CaII K line in the quiescent prominence is about 3800K in general. Thus we used the observed profile of K line in which $I_M \simeq S = B(3800)$ is fulfilled for this study. The shift of the CaII K line in the dark filament against the photospheric and chromospheric lines is carefully measured by interpolation with the x vs. λ curve. Then the vertical velocity of matter can be obtained within a range of error of 0.5km/s.

Figure 1 gives histograms of vertical velocity measured in three dark filaments(A: September 3, 1972, B: August 22, 1979 and C: August 11, 1980). The average values of velocities in each filaments are 0.8, 1.4 and -0.2km/s respectively(Minus sign designates upward motion). The downward motion is predominant in A and B filaments, while both downward and upward motions are detected in C filament. The difference of average velocities in these filaments may be due to the evolutional effect; The C filament was young, while others(A and B) were in the middle and old stages in their evolution(Fraunhofer Solar Map and Solar Geophysical Data).

The large velocity(v>4km/s) is detected in some portions of every filaments. Maltby(1976) also obtained large velocity in several portions of filament from his monochromatic observations in Hα light. However, we still can not clarify the relation between the existence of such large velocity and the spatial structure of the dark filament; such as foot, head etc.

The time required for the exchange of total matter in the

filament with newly supplied one from surrounding corona is estimated to be 595 minutes(10 hours), when the height of quiescent prominences is 5 x 10^4km and the downward velocity is 1.4km/s.

References

Maltby, P ; 1976, Solar Phys., 46, 149.
White, O. R., and Suemoto, Z.; 1968, Solar Phys., 3, 523.

Fig. 1

Histograms of vertival velocity in three dark filaments.
A: September 3, 1972, B: August 22, 1979, C: August 11, 1980.

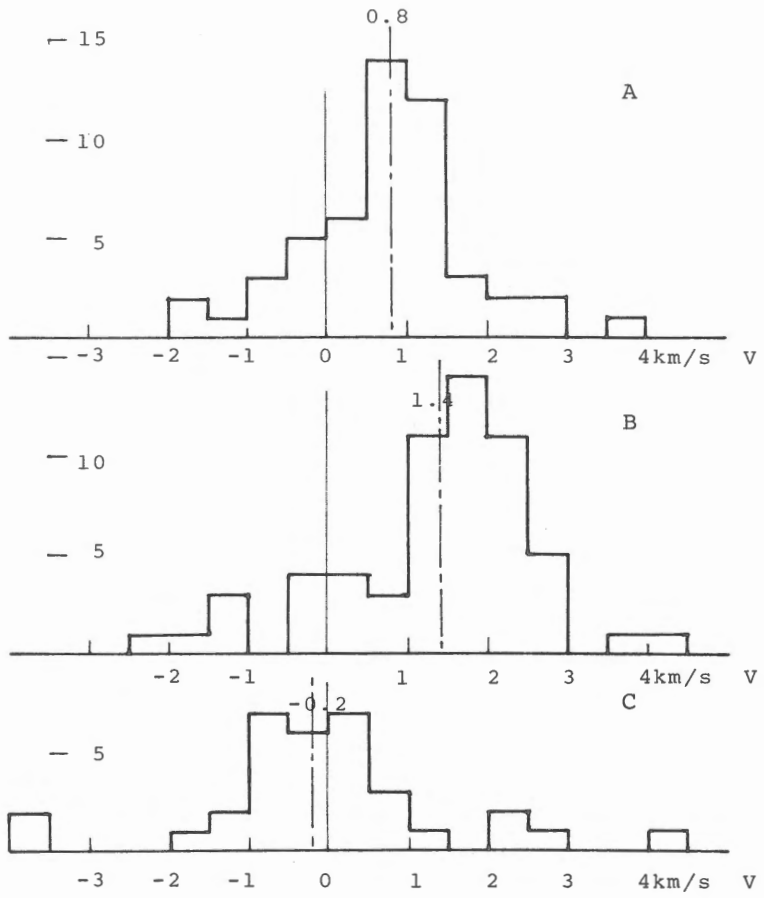

LYMAN CONTINUUM OPTICAL DEPTH OF PROMINENCES DERIVED FROM EUV SPECTROHELIOGRAMS

Mitsuo Kanno
Hida Observatory, University of Kyoto

The two-dimensional distribution of the optical depth at the Lyman limit, τ_H, in three hedgerow prominences (P23, P28A, and P42) is derived from simultaneous spectroheliograms (5"x5" resolution) of C III λ977, Ly C λ896, and O IV λ554 observed with the Harvard experiment on Skylab.

We assume a multiple-slab model for the prominence. In this model the prominence is viewed as consisting of a number of cool ($T < 10^4$K) and identical slabs embedded in the hot ($T \approx 10^6$K) corona; at the surface of each slab is a transition zone of intermediate temperature. Then the observed intensity of C III λ977 and O IV λ554 will be

$$I(\text{C III}) = 2NI_{\text{C III}}, \tag{1}$$

and

$$I(\text{O IV}) = I_{\text{O IV}}\left[1-e^{-N\tau_1}+2\sum_{n=1}^{N} e^{-n\tau_1}\right]. \tag{2}$$

Here $I_{\text{C III}}$ and $I_{\text{O IV}}$ are the intensity of C III λ977 and O IV λ554 emitted by the transition zone at each surface of the slabs, N is the number of the slabs in the line of sight, and τ_1 is the optical depth of one slab in the Ly C at 554 Å.

We now assume that the total optical depth $N\tau_1$ is finite, but that the number of individual slabs is very large; i.e. the hot and cold regions of the prominence are intimately mixed. In the limit where N approaches infinity, we have

$$R \equiv \frac{I(\text{C III})}{I(\text{O IV})} = \frac{I_{\text{C III}}}{I_{\text{O IV}}} \frac{\tau_H(\lambda_1/\lambda_H)^3}{1-e^{-\tau_H(\lambda_1/\lambda_H)^3}}, \tag{3}$$

where $\lambda_1 = 554$ Å and $\lambda_H = 912$ Å. We note that the assumption $N \to \infty$ gives a lower limit for the optical depth. If the number of the slabs in the line of sight is greater than five, then the error in τ_H is less than 20%.

Now we can determine τ_H from Equation (3) using the observed intensity ratio R, provided that the ratio $I_{\text{C III}}/I_{\text{O IV}}$ is known. In order to determine $I_{\text{C III}}/I_{\text{O IV}}$

empirically for each of the prominences we use the Ly C spectroheliograms. Assuming the source function of the Ly C to be constant with depth and position in a prominence, we have the intensity of the Ly C at λ896,

$$I(\text{Ly C}) = S_{\lambda_c}[1-e^{-\tau_H(\lambda_c/\lambda_H)^3}], \tag{4}$$

where S_{λ_c} is the source function of the Ly C at λ_c = 896 Å. From Equations (3) and (4) we have

$$\frac{d[\log I(\text{Ly C})]}{d[\log R]} = \frac{\tau_H(\lambda_c/\lambda_H)^3}{e^{\tau_H(\lambda_c/\lambda_H)^3}-1} \cdot \frac{e^{\tau_H(\lambda_1/\lambda_H)^3}-1}{e^{\tau_H(\lambda_1/\lambda_H)^3}-1-\tau_H(\lambda_1/\lambda_H)^3}. \tag{5}$$

The gradient $d[\log I(\text{Ly C})]/d[\log R]$ is independent of $I_{\text{C III}}/I_{\text{O IV}}$ and S_{λ_c}. For large τ_H (or R) the gradient has a value $\approx$0; it reaches a value of unity at τ_H = 2.46 and then rapidly increases with decreasing τ_H (or R) for $\tau_H < 2.46$. The value of R at which the gradient becomes unity (R_1) will be found from a diagram of log I(Ly C) vs log R plotted for a number of positions in a prominence. Then we can find the numerical relation between τ_H and R, that is, the value of $I_{\text{C III}}/I_{\text{O IV}}$ for the prominence.

Figure 1 displays I(Ly C) as a function of R on a logarithmic scale for the three prominences. The points in Figure 1 are restricted to heights greater than 10" above the limb in order to avoid effects of chromospheric structures such as spicules, fibrils, and network walls along the line of sight. In Figure 1 we have illustrated theoretical curves (dashed lines) derived from Equations (3) and (4),

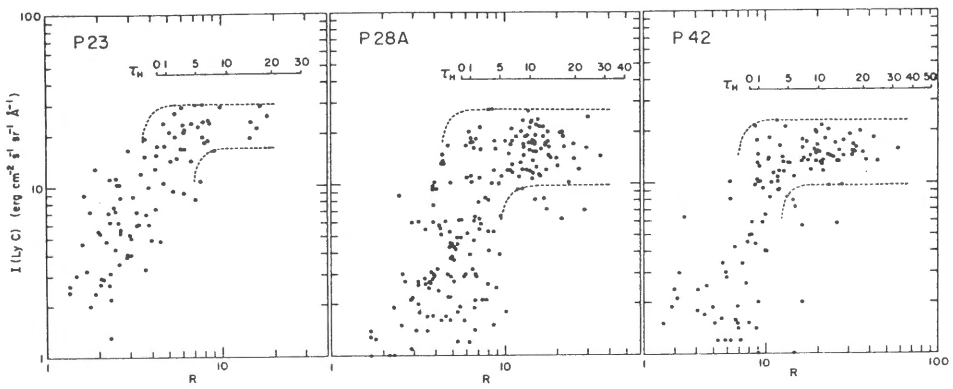

Fig. 1. Intensities of the Ly C at 896 Å as a function of R.

but choosing the parameters $I_{C\,III}/I_{O\,IV}$ and S_{λ_C} arbitrarily, so as to place the curves at locations corresponding to the outer and inner envelopes of the points for each prominence. From these curves we found a possible range of R_1. Given that the geometric mean of R_1 corresponds to $\tau_H = 2.46$, we can derive $I_{C\,III}/I_{O\,IV}$ for each prominence. These values for $I_{C\,III}/I_{O\,IV}$ can then be used with Equation (3) to calculate τ_H as a function of R. The latter relationships are given in Figure 1.

It is interesting that the three prominences have different values of $I_{C\,III}/I_{O\,IV}$: 4.3, 5.7, and 8.1 for P23, P28A, and P42, respectively. This may be due to differences in the structure of the transition zone of the prominence threads and of the region between the threads. On the other hand, Figure 1 shows a number of points which have values of R less than the lower limit $R_{min} = I_{C\,III}/I_{O\,IV}$ predicted by this simple model. The points in question correspond to the positions near the edges of the prominences, rather than near their centers. In location near the edge of the prominence the slit filling factor for the Ly C emitting threads and their transition zones may be considerably less than unity. If we postulate the existance of hot ($T > 10^{5.5}$K) material between the threads, then this material would emit considerable O IV (log $T_{max} = 5.25$) compared to C III (log $T_{max} = 4.95$). This results in $R < R_{min}$ for the positions near the edges of the prominences. In determinimg τ_H we assume that the positions with $R < R_{min}$ are optically thin in the Ly C ($\tau_H < 1$).

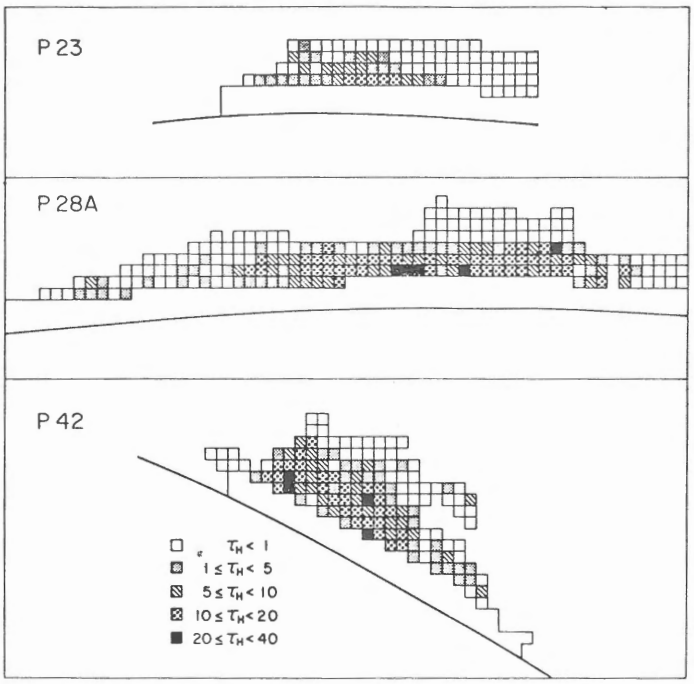

Fig. 2. Two-dimensional distribution of τ_H.

Figure 2 shows the two-dimensional distribution of τ_H for the three prominences at heights greater than 10" above the limb. A square in Figure 2 represents an area of 5"x5" ($\approx$3650x3650 km^2). The value of τ_H varies over a wide range at positions even in a single prominence. At the central part of the prominences where the opacity is largest τ_H reaches a maximum value of 30 to 50 for the three prominences when correction is made for the self-absorption effect of C IIIλ977. In general τ_H decreases with height in the prominences. Most positions near the outer boundary of the prominences are optically thin in the Ly C ($\tau_H < 1$).

PRE-FLARE EVOLUTION AND THE BEGINNING OF FLARES

Eijiro HIEI
Tokyo Astronomical Observatory

1. Introduction

A solar flare is one of the most prominent phenomena of the active Sun, and is still not known why and how it occurs. A flare occurs mostly in an active region. An evolutionary change of an active region, persumably due to the effect of the magnetic field, convection and circulation of the Sun, may prepare an environment of flare occurrence, but the characteristics of the environment, which inevitably lead to flare occurrence, are not known.

The study of pre-flare state is important to understand the storage of the free energy necessary for a flare and the developments that lead to the energy release of the flash phase. If flare occurrence could be predictable, flare mechanisms would be thoroughly studied. The prediction, however, needs knowledge of the flare mechanisms. Lack of the knowledge forces us to do patient works on the pre-flare state.

2. Environment of pre-flare state

One of the pioneer works on the environment of flare occurrence was made by Martres et al. (1971, 1974, 1977a). They studied characteristics of an active region with and without flare activity. Almost no flare activity is seen in an active region where an $H_{//}=0$ line crosses area of the same sign of velocity field or a normal Evershed velocity is observed. If the magnetic configuration of an active region becomes complex due to the existence of a parasitic polarity, inclusion, or juxtaposition of two active centers, the probability of flare occurrence becomes high. Flares occur at locations where an $H_{//}=0$ line crosses a $V_{//}=0$ line, which points towards the disk center. Such velocity fields suggests a kind of vortex motion. Unno et al.(1980) have considered vortex motion as wake formation behind a spot group and studied on evolutionary change of an active region due to the dynamo action in the photosphere.

Harvey and Harvey (1980) also found that i) flaring level is high when

velocity pattern is complex, and ii) an $H_{//}=0$ line and a $V_{//}=0$ line cross in some events, but in most of flare events both lines are roughly parallel, each separating 3 to 8 arc seconds.

The free energy necessary for a flare is considered to be stored in stressed magnetic field in the corona, but the fields and currents are not yet observed. Tanaka (1980) tried to estimate pre-flare energy stored in stressed magnetic field from shear motion of spots in McMath 13043 active region on June 28-July 10 1974, and found a good relation between the stored energy due to the shear motions and the radiated energy of the flares.

3. Pre-flare enhancement

The pre-flare coronal enhancement of an active region commonly occurs (Svestka, 1975). The region of the gradual enhancement in the flaring region is not always in the same loop or loops which are later most enhanced during the flare (Sturrock, 1979).

Not all flare exhibit precursor phase in x-ray, but at least 80% of all flare-associated soft x-ray bursts have measurable precursors which begin about 2 min. earlier than the onset of a flare, on the average (Thomas and Teske, 1971).

From Skylab data Vorpahl et al. (1975) found that in many cases the flare core could be seen several minutes before the flare actually started, but Kahler and Buratti (1976) reported that the region of x-ray brightening prior to several minutes before the onset differed from that of the following flare. Gradual heating or energy release may occur before the more catastrophic event takes place, but the brightening loop may move during the course of flaring event.

Kundu (1965) reported that the gradual increase in intensity of 3cm radio sources of S-component, probably due to energy build-up in an active region, was observed prior to flare start. Kai (1980) has also observed pre-flare enhancements at 17GHz about 20 min. before bursts.

Filament activations such as darkening, slow outward expansion, or fragmentation are detected several min. to one hour before a flare starts (Martin and Ramsy, 1972). At least 82% of flares are preceeded by $H\alpha$ off-band pre-flare activity of filament (Martres et al., 1977b). Two ribbon flares are sometimes observed at disparitions brusques.

Velocity field associated with a flare was observed at and after its maximum phase (Yoshimura et al., 1971). The velocity is higher (1.5km/s) at the lower photosphere and zero at the chromosphere. If the velocity is horizontal, the velocity would be explained as a vortex motion around a bright point of the flare. Blue-shifted velocity changes in the photosphere of 0.3 to 1km/s were observed

in localized area adjacent to the flaring element (Harvey and Harvey, 1976). The change in velocity began about 10-15 min. prior to flare start, reached maximum near or at flare maximum folowed by a slow decrease. A similar but smaller change was observed in H_{α} velocity.

Data on magnetic and veloctiy fields with high time resolution and good spatial resolution are needed for understanding the environment of flare occurrence, and also data from both ground-based and space observations are needed for knowing the accumulation of free energy necessary for a flare.

References

Harvey, K.L. and Harvey, J.W., 1976, Solar Phys., 47, 233.

Harvey, K.L. and Harvey, J.W., 1980, Solar-Terrestrial Predictions Proceedings, ed. R.F. Donnelly, 3, C-41.

Kahler, S.W. and Buratti, B.J., 1976, Solar Phys., 47, 157.

Kai, K., 1980, in preparation.

Kundu, M.R., 1965, Solar Radio Astronomy, Interscience Publ., p583.

Martin, S.F. and Ramsey, H.E., 1972, Solar Activity, Observations and Predictions, ed. P.McIntosh and M. Dryer, p371.

Martres, M.-J., Soru-Escaut, I., and Rayrole, J., 1971, Solar Magnetic Fields, ed. R. Howard, p435.

Martres, M.-J., Rayrole, J., Ribes, E., Semel, M., and Soru-Escaut, I., 1974, Flare-related Magnetic Field Dynamics, Boulder, Colorado, p333.

Martres, M.-J., and Soru-Escaut, I., 1977a, Solar Phys., 55, 225.

Martres, M.-J., Soru-Escaut, I., and Nakagawa, Y., 1977b, Asron. Astrophys., 59, 255.

Sturrock, P.A., 1979, Solar Flares, Colorado Univ. Press.

Svestka, Z., 1975, Solar Flares, Reidel Publ. Co.

Tanaka, K., 1980, Solar-Terrestrial Predictions Proceedings, ed. R.F. Donnelly, 3, C-1.

Thomas, R.J. and Teske, R.G., 1971, Solar Phys., 16, 431.

Unno, W., Tanaka, K., and Semel, M., 1980, in preparation.

Vorpahl, J.A., Gibson, E.G., Landecker, P.B., Mckenzie, D.L., and Underwood, J.H., 1975, Solar Phys., 45, 199.

Yoshimura, H., Tanaka, K., Shimizu, M., and Hiei, E., 1971, Publ. Astron. Soc. Japan, 23, 443.

A SPATIAL DESCRIPTION OF AN ELEMENTARY ERUPTIVE PHENOMENON (EEP)

M.J. Martres, Z. Mouradian, I. Soru-Escaut
Observatoire de Paris-Meudon

1. Introduction

Classically, a flare is considered to be a sudden increase of the brightness in the chromospheric lines. An attentive study of this phenomenon shows that the brightness increase is associated with various absorbing features (HIEI, 1980). Therefore, we consider that the bright flare is only one aspect of the eruptive process. The complete eruptive phenomenon is the comprehensive transitory feature formed by absorbing and emitting structures, evolving in space and time and associated with the same physical origin. In addition, a complete eruptive phenomenon includes a set of elementary eruptions, so the study of an elementary eruptive phenomenon is important to the understanding of a complex phenomenon. Although the entire eruptive phenomenon includes manifestations in other wavelengths, only EUV and "visible" aspects are considered here.

2. Observational data

Studies were made of the subflare of 1973, June 16 at 18:03 observed on the disk (N 14 - E 13). The data used were :

a) the Meudon H_α filtergrams which give line center images every minute as well as the blue and red wings ($\pm$ 3/4 Å) and

b) the EUV spectroheliograms of the Harvard College Observatory in Ne VII (464 Å), Fe XV (417 Å) and Fe XVI (335 Å). These lines have respectively the maximum of abundances at 5.10^5 °K, 2.10^6 °K and 3.10^6 °K.

3. History of the EEP

- t_o : The eruptive instability begins near the region where the flare will start. This instability appears as absorbing arches with radial velocities in both wings of H_α and develops until the end of the flaring phase. It reaches the altitude of $1.5\ 10^4$ km at 18:03 U.T.

- t_o+10 m : Nothing is yet visible in Fe XVI. Note that the H_α flare is not yet initiated, but the H_α mentioned above continues to evolve.

- t_o+18^m : The onset of the bright points (flare) is observed. At this moment great changes occur in the arch : expansion at the top (Tanaka, 1976) and displacement of one of the legs. The direction of the flow of the absorbing material is unchanged.

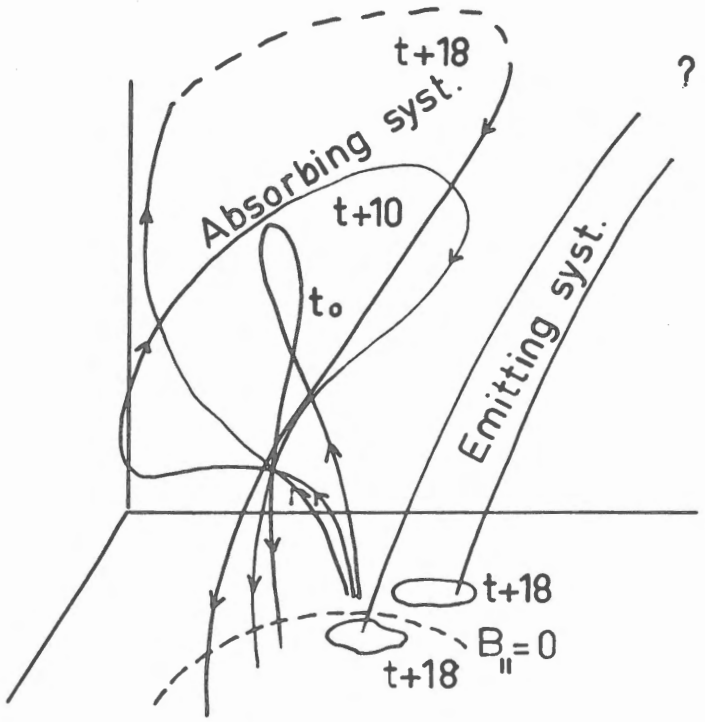

- t_o+37^m : The absorbing and emitting structures in H_α continue to evolve and expand. EUV observations show :

. an emission cospatially with H_α emission, but larger ;

. a dark feature cospatially with H_α absorption, but narrower.

The figure describes the geometrical aspect of the arch system (absorbing and emitting) of this EEP.

An ambiguity remains concerning the "switch off" of the hot arch system.

4. Elements of a model

i) The emission at 10^{6}°K is cospatial with the H_α emission and is not directly connected with the absorption phenomenon which starts first.

ii) At the onset of the H_α bright points, which are the footpoints of the hot arch system, the cool arch expands in altitude and its footpoints are removed.

iii) Consequently, the EEP would be considered by two systems of arches : a cool one visible in H_α on the disk as an absorbing feature and an emitting feature in H_α as well as in EUV lines (Ne VII, Fe XV, Fe XVI).

iv) A flow of matter is observed in the cool system, moving from one foot to the other and always in the same direction.

The hot system probably does not have such motions and if there are any, they must be $\leq$ 5 km.s^{-1}.

REFERENCES

Hiei E., 1980, Proceed. of Japan-France Seminar on Solar Physics, in press.

Tanaka, K., 1976, Solar Phys., 47, 247

AN UNEXPECTED EVENT IN THE STUDY OF REPETITIVE EVENTS

M.J. Martres and I. Soru-Escaut
Observatoire de Paris Meudon

1. Introduction

The most known repetitive events are the homologous flares[*]. These flares occur successively "at the same position and show a strikingly similar pattern of structure and development" (Bruzek and Durrant, 1977).

The flares are not the only repetitive events on the sun. We observed in the wings of H_α ($\Delta\lambda = \pm 3/4$ Å) another kind of homologous events : The Transitory Absorbing Features (TAF). The bright flaring regions (BFR) are very often associated to some TAFs (Martres et al., 1980). When BFRs are homologous, the associated TAFs are also homologous.

Until now, the BFRs were considered as occurring during the magnetic field evolution, the TAFs as short-dated forerunners of local magnetic field changes (Martres et al., 1971, Martres et al., 1977)

Here we show that :

1) The BFRs which are homologous may be also associated with long-dated modifications of the magnetic fields (appearance of new active centers).

2) In one typical case, the homologous flares (BFRs and associated TAFs) may be used to forecast the instabilities of the new active center in the next rotation.

2. Homologous BFRs : statistics

The statistics were established with the data provided by the "Catalogues et Annexes des Cartes Synoptiques" of Meudon Observatory (1974, 1975, 1976, 1977).

We have selected Active Centers lying between the latitudes 8 and 20° (North and South) in order to exclude the possible effects of the differential rotation. In this sample, we kept only the Active Centers which are less than 27 days (1 rotation) old.

---

[*] In this case, the term "flare" corresponds only to the bright component of the flaring region seen on the disk in H_α

We were able to analyse with these criteria the homologous flare productivity of 110 Active Centers related to the new Active Centers which will appear closely, in the same or in the following rotation.

The results are shown in the histogram of the Figure 1.

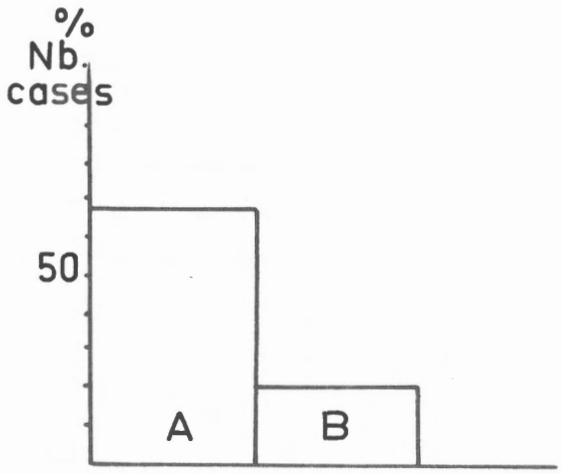

The sample has been divided into two parts : A and B. A represents in percentage the number of Active Centers which provided more than 10 homologous BFRs during the rotation and which are associated to the appearance of a new Active Center. B represents the same, for the Active Centers which provided less than 10 homologous BFRs.

So, we may conclude that when we observe more than 10 homologous BFRs in an active region, we have a good chance to observe the formation of a new Active Center in the surroundings some days later.

3. Homologous flares i.e., BFR and TAF : a typical case

The studied Active Center was in Rotation 1695 (called R in the Figure 2) at S15, 350. It provided a great number of homologous flares (HF) - we were able to analyze 12 of them with the 3 wavelength heliograph of Meudon. These HF occurred in the site S near the western part of the preceeding spots. During the evolution of these flares, some bright points appeared in an apparently quiet region called S', some degrees far from S. The associated TAF joined S and S', underlying the

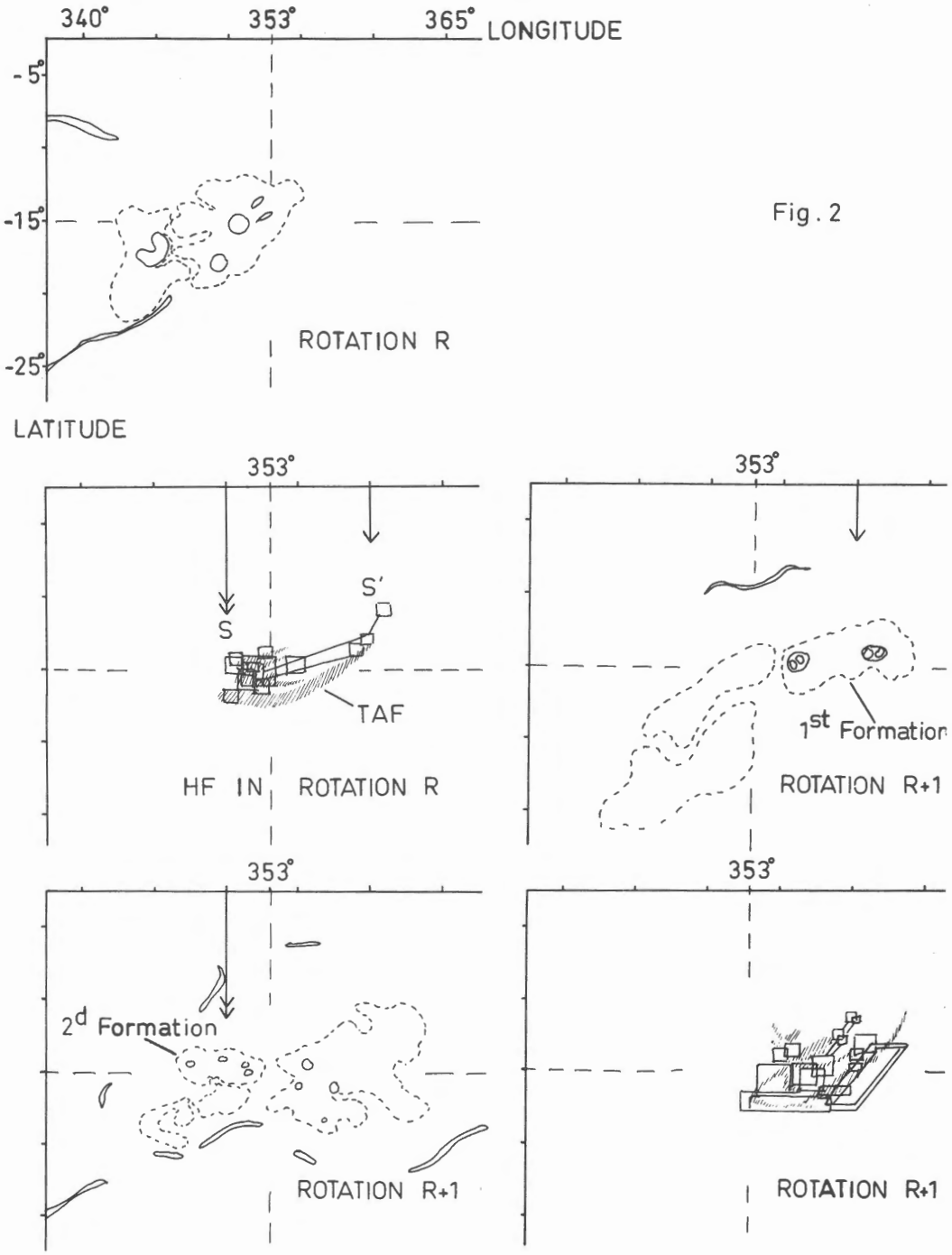
340°
353°
365°
LONGITUDE
-5°
-15°
-25°
LATITUDE
ROTATION R
353°
S'
S
TAF
HF IN
ROTATION R
353°
1st Formation
ROTATION R+1
353°
2d Formation
ROTATION R+1
353°
ROTATION R+1

Fig. 2

continuity of the phenomenon in space. In several cases, the postflaring TAF of one flare may be considered as the preflaring of the next one, showing a continuity in time.

In Rotation 1696 (R+1), a new formation is born near the East limb, as it was described in Part 2. The main magnetic inversion line of the new formation F_1 is situated on S'. During this same rotation R+1, another new formation F_2 appeared in the location of the leading part of the Active Center observed in rotation R. The magnetic inversion line between F_1 and F_2 is situated on S (see Figure 2). During the rotation R+1, many HF occurred , from whom 12 were observed in Meudon in the regions situated from S to S'. We note also that a new Active Region was born at the same location in R+2.

4. Conclusions

The typical case is in agreement with the statistics of the Part 2, but goes further owing to the observations of TAFs. When homologous TAFs are seen in quiet regions, we know that they announce a short-dated appearance of a new Active Center. Here, in an Active Region, the homologous TAF associated to homologous BFR lead to a long-dated forecast of a new activity close to the initial instability.

From the general analysis of the behaviour of the Active Region formed by the four Active Centers described above, we observe that the homologous flares of the first rotation are homologous with those of the second rotation. In spite of the drastic modifications of the magnetic fields : The instabilities are "stable" !

REFERENCES

Bruzek, A., and Durrant, C.J., 1977, Illustrated Glossary for Solar and Solar. Terrestrial Physics, Astrophysics and Space Science Library, 69, 88.

Martres, M.J., Mouradian, Z., Soru-Escaut, I., 1980, Proceed, of Japon-France Seminar on Solar Physics, in press.

Martres, M.J., and Soru-Escaut, I., 1971, Sol. Phys., 21, 137.

Martres, M.J., Soru-Escaut, I., Nakagawa, Y., 1977, Astron., Astrophys., 1977, 59, 255.

IS THE "DISPARITION BRUSQUE" PHENOMENON ALWAYS AN EFFECTIVE DISAPPEARANCE ?

Z. Mouradian, M.J. Martres, I. Soru-Escaut
Observatoire de Paris-Meudon

1. Introduction

A "Disparition brusque" (DB) of a solar filament is announced several hours before its occurence by at least two forerunners events :

a) the optical density of the filament increases and, consequently, it becomes darker (Martres, 1956)

b) Hot arches ($T \sim 10^5$ to 10^{6}°K) span the cool filament (Schmahl et al., 1980).

These events are related and it is possible that the first is the result of the second.

There are two possible explanations for the DB process visible in H_α :

- DB 1 - Expansion of the prominence and, therefore, decrease of the density of the material on the line-of-sight.

- DB 2 - Ionization of prominence material by heating without any expansion.

Possibly the filament expands (DB1) and is heated simultaneously (DB2). In the case DB2 the organization of the photospheric magnetic field is probably not altered and, thus the filament can be reformed. EUV observations should provide a test of the heating hypothesis (DB2).

2. Observational data

Observations of the DB phenomenon and the formation of a filament were made between June 14 and June 18, 1973. The Harvard College Observatory spectroheliograms on Skylab (Reeves et al., 1977) in the first polychromic position and the H_α center and wings filtrograms from Meudon Observatory were used.

3. Results

Figure 1 presents two sets of scans, at left (A), a well-established filament and at right (B), the site where a filament is expected to appear. The H_α filament

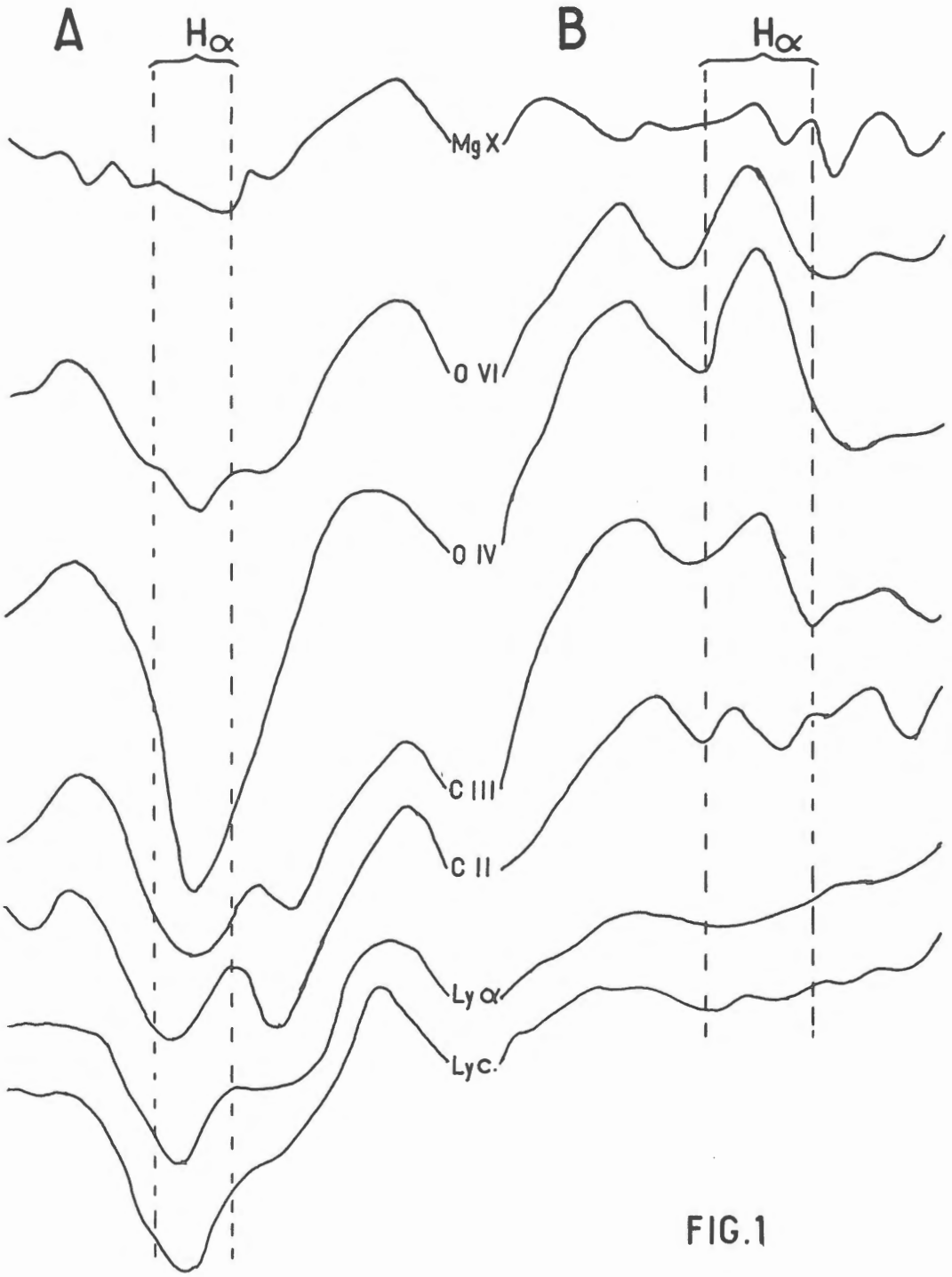

FIG.1

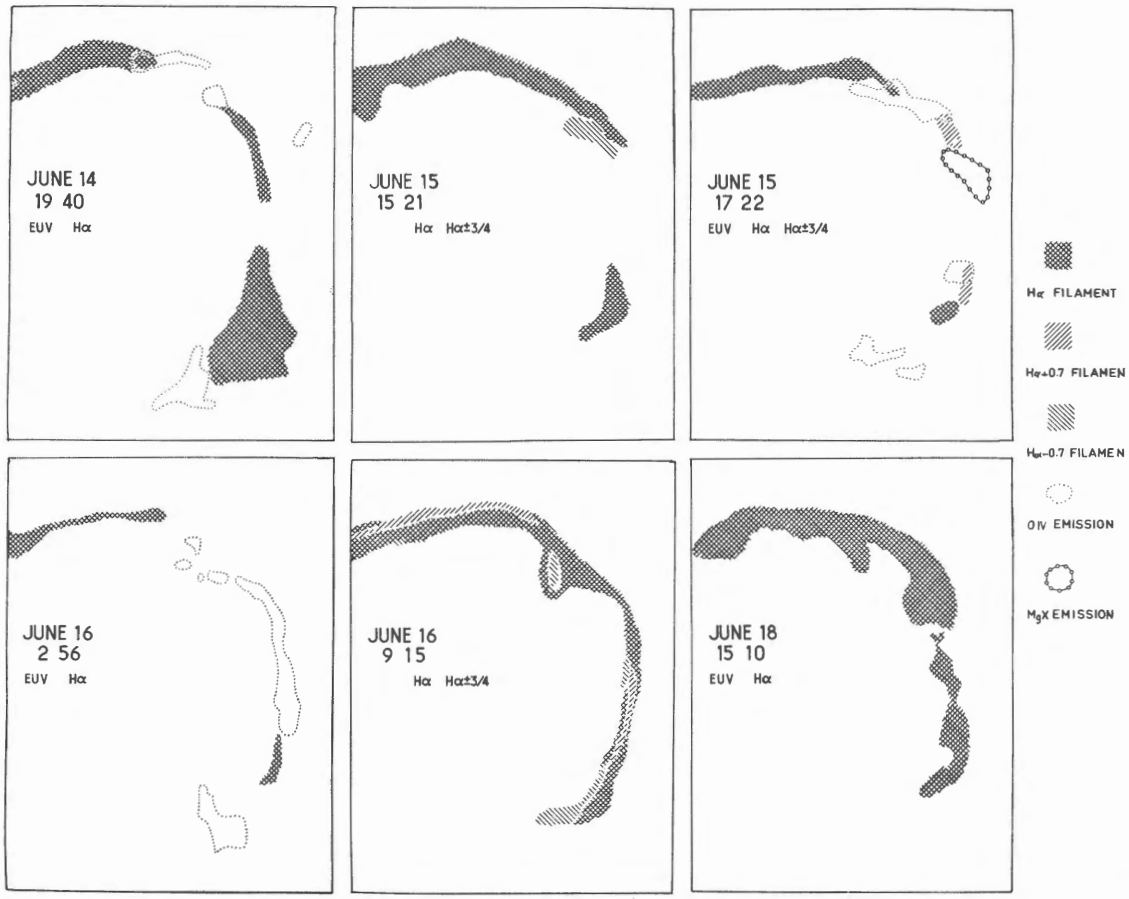
JUNE 14
19 40
EUV Hα
JUNE 15
15 21
Hα Hα±3/4
JUNE 15
17 22
EUV Hα Hα±3/4
JUNE 16
2 56
EUV Hα
JUNE 16
9 15
Hα Hα±3/4
JUNE 18
15 10
EUV Hα
Hα FILAMENT
Hα+0.7 FILAMEN
Hα-0.7 FILAMEN
OIV EMISSION
MgX EMISSION

FIG. 2

position is indicated. The temperature of the maximum abundance of the observed lines are :
Ly cont. : 7.10^3 °K ; Ly_α: 10^4 ; CII : 2.10^4 ; CIII : 6.10^4 ; OIV : 10^5 ; OVI : 3.10^5 and MgX : 10^6.

Note that in case A an absorbing feature is visible in all lines. In B, the cool lines (Ly c.,Ly_α) are not structured ; whereas in hot lines, an emission appears. The greatest contrast can be seen in the OIV line. Consequently hot filaments were identified and their locations were compared with those of the cool filaments which were expected to appear.

Figure 2 presents six composite images of H_α line, OIV and MgX, observed from June 14 at 19:40 to June 18 at 15:10 . During this period the DB phenomenon and the reapparance of a filament was observed. On June 15 at 17:22 the DB is performed but the hot filament is partially visible in the hottest line (MgX). Nine hours later (june 16, 02:56 UT) the hot filament is clearly visible with its OIV emission and MgX disappears. The filament material continues its cooling and is visible in H_α six hours later. Afterwards its stabilizes and no emission in EUV lines is observed .

4. Conclusion

This observation of a DB phenomenon is a good example of the hypothesis DB2 (ionization of the prominence material).

Therefore, at last in some cases the DB phenomenon is more a modification in the ionization temperature rather than a dramatic restructuration of the magnetic field, even if important material movements are observed in H_α.

REFERENCES

Martres M.J., 1956, L'Astronomie, 70, 401.
Reeves E.M., Hubert M.C.E, Timothy J.G., 1977, App. Optics, 16, 837
Schmahl E.J., Mouradian Z., Martres M.J., Soru-Escaut I., 1980, Bull. Amer. Astr. Society. 12, 526.

THE BRIGHTENING OF VERY SHORT DURATION OBSERVED IN THE WING OF H-ALPHA LINE

Ichiro Kawaguchi
Department of Astronomy and Hida Observatory,
Faculty of Science, University of Kyoto

A new domeless solar telescope has been ready to operate at the beginning of 1980 at Hida Observatory. Although the full functions were not yet displayed, some kinds of solar observations were made during the testing period of this spring. The details of the telescope will be published elsewhere.

In the morning of 5 June, a fairly good seeing condition, though not the best in Hida Observatory, continued during almost two hours. The monochromatic image at Hα + 1.2 A which was formed by passing through a Zeiss birefringent filter with a passband of 0.25 A was photographed successively with an exposure time of 1/60 seconds. The time interval between the successive exposures was 4 or 5 seconds on the average. After the observation, Mr. Suêmatsu has made a 16 mm motion picture of 5 minutes long. Special care was paid for the uniform lapse of time. In the original sequence of films, the time interval between the successive exposures was not fixed in order to avoid the poor image due to bad seeing. The inspection of the motion picture revealed at once the progressive brightening of several points in line. The new phenomenon will be discussed in the following.

In the first brightening has occured at $22^h27^m47^s$ UT and the second $22^h32^m32^s$ UT, the second one in two parallel lines. The phenomena are similar to the flare brightening in two parallel ribons. Figure 1 shows the solar radio emission at 9.4 GH_2 observed at Toyokawa. The impulsive enhancement of radio flux was seen approximately at the same time period of the observed optical brightening. Then it seems to be reasonable to suppose that the observed brightening was produced by the bombardment of energetic particles on the chromosphere.

The light curve of each bright point are given in Figure 2 and 3. In the upper part, the vertical bars represent the moment of fine peaks of enhanced radio flux.

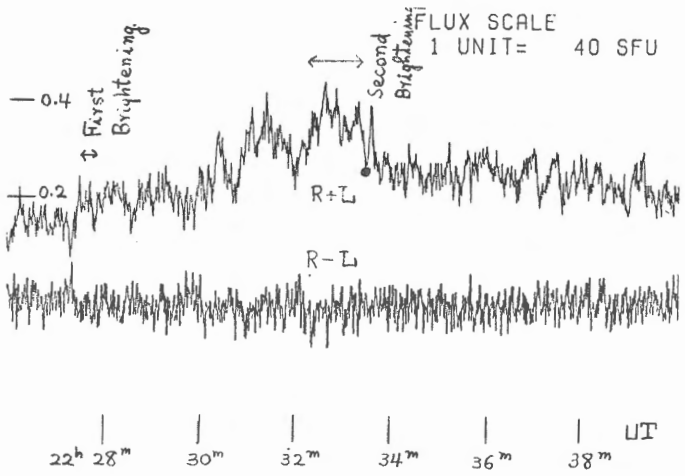

Fig. 1. Radio Flux of 9.4 GHz observed at Toyokawa

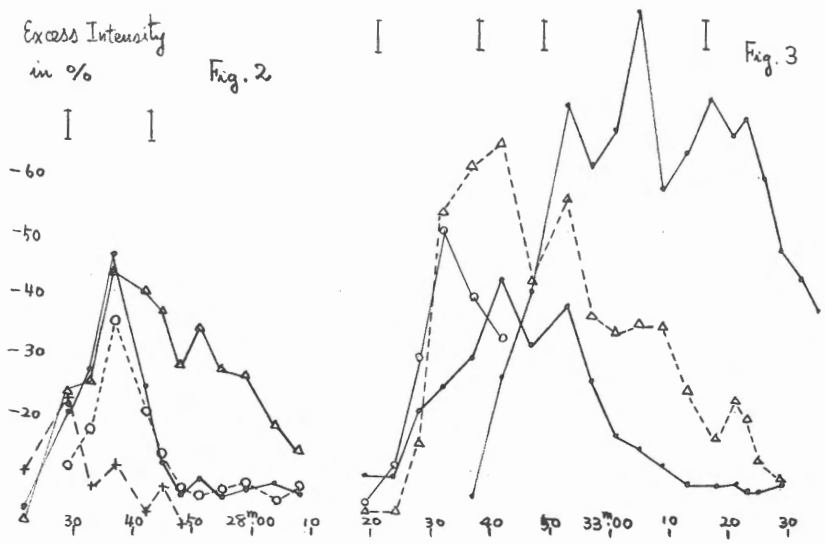

Fig. 2 and 3. The excess intensity versus time. The excess intensity is expressed in units of the undisturbed one. The vertical bars indicate the moment of fine radio peaks.

Recent improved time and space resolution of EUV spectroheliograms of solar flares showed the successive brightening of small magnetic loops. Vorpahl (1976) has interpreted the velocity of propagation as that of magnetoronic wave. He obtained the velocity of 180 - 280 km/sec. On the other hand, Widing and Dere (1977) observed the velocity of only 96 km/sec.

If the flaring small loops form an arcade of magnetic loops, then our bright points can be regarded as the brightening of footpoints of flaring magnetic loops. We obtained 460 ∿ 970 km/sec for the first brightening and 170 km/sec - 440 km/sec for the second. It means that the magnetic field strength required to explain the high propagation velocity - 970 km - is larger than 100 G or more in the flaring region.

The light curves shown in Figures 2 and 3 give a short rise and decay time of about 10 seconds for the first brightening. The light curve only the information about the intensity at Hα + 1.2 A, then we can say nothing about the importance of the flare. However, the effective half-width of Hα emission line increases rapidly at the impulsive and decreases slowly at the decaying phase (Svestka, 1976). Furthermore, the half-widths of Hα emission line of a flare are much larger than 1.2 A, so that we can reasonably suppose that the observed brightening is insignificant as regards to the flare importance.

References

Svestka, Z.; 1976, Solar Flares, D. Reidel p. 3.
Vorpahl, J. A.; 1976, Astrophys. J. 205, 868.
Widing, K. G. and Dere, K. P.; 1977, Solar Phys. 55, 431.

ON THE EMISSION SPECTRA OF MOUSTACHES

Reizaburo Kitai
Department of Astrophysics, Kyoto University

1. Introduction

It is well known that mass mations are frequently observed around moustache points. Severny (1968), from the study of the " Fraunhofer lines kink ", reported the upward velocity field of 1-3 km/s at the upper photospheric levels. Roy and Leparskas (1973) observed a close spatial correlation between the moustaches and the fast moving ($\simeq$ 100 km/s) dark oblong features and suggested that these dark features were ejected matter from the moustache points.

In this work, it is shown that we can deduce the chromospheric velocity fields in moustache points from the emission profiles of moustaches. From our preliminary analysis of some moustache spectra, we have found that matters in moustache moves up- or downwards with velocities of about 10 km/s at the chromospheric levels.

2. Observation

We have analysed an echelle spectrogram and some grating spectrograms of $H\alpha$ and $H\beta$ lines.

FIGURE 1. $H\alpha$ spectra of moustaches

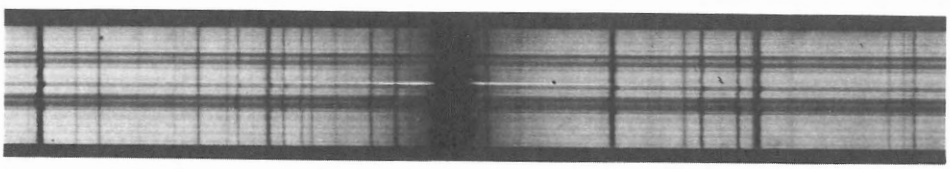

(a)

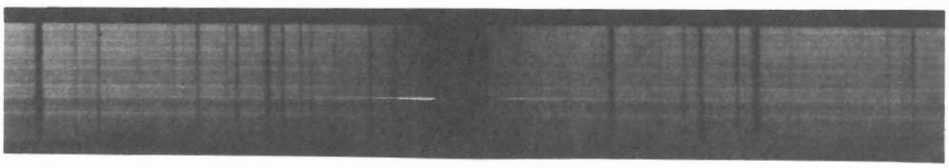

(b)

The echelle spectrogram was taken at Okayama Astrophysical Observatory on August 15,1979. The moustache point was situated near the east limb, r = 0.95. Characteristic emissions were detected in the Balmer lines of Hydrogen and H and K lines of Ca II ion. The spatial resolution of the spectrogram was about 3".

The other grating spectrograms were taken through the Horizontal Spectrograph of the DST at the Hida Observatory on May 23, 1980. Thanks to the good seeing conditions, we have obtained the sharp spectra with spatial resolutions of 1-2". Some examples are shown in Figure 1.

Emission spectra were obtained by subtracting the spectra of neighbouring normal regions from the moustache point spectra.

3. Emission Profiles of H_α and H_β lines

a) Central absorptions due to overlying matters

The emission profiles of moustaches have central absorptions, and the intensities of two peaks are generally different. Blue asymmetry in the intensity peaks is known to be prevailing (Severny ; 1968). Statistical studies by Bruzek (1972) show a strong positive correlation between the blue shift of central absorptions and the red asymmetry of the intensity peaks. In our samples, the correlation is confirmed to exist. A clear example is shown in Figure 1 (b). The central part of the spectrum is absorbed by a red-shifted matter and the emission profile does show a blue asymmetry in the intensity peaks. Thus we can think that the central part of the emission spectra is absorbed by overlying matters and the asymmetry is

FIGURE 2. Plot of a H_α emission profile

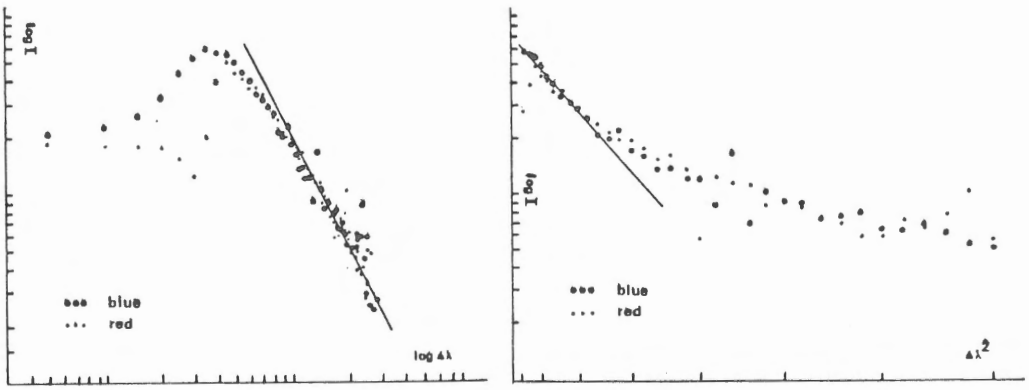

the result of the motion of the overlying matters. However, a sample profile shows blue asymmetry and a blue shift of the central absorption. This points will be considered in the next subsection.

b) Gaussian emission cores and power-law emission wings

As is shown in Figure 2, log $I(\Delta\lambda)$ vs. log$\Delta\lambda$ plot and log $I(\Delta\lambda)$ vs. $(\Delta\lambda)^2$ plot diagrams indicate the decomposition of the emission profile into a core part and a power-law wings, where $\Delta\lambda$ is the wavelength difference from the line center that is determined with reference to some neighbouring weak Fraunhofer lines. A power-law wing is symmetrical referred to the line center and the index of the power is around 2. Core part of the spectrum can be considered to obey a Gaussian profile if the center of the core part is displaced from the line center.

For all the other samples, we can also decompose the emission profiles into two components if we take into accounts some Doppler shifts for the components. The magnitudes of the Doppler shifts for the two components of our samples are summarized in Table I. We can see that the Doppler shifts are generelly bluewards and the core parts show larger shifts ($\simeq$ 6 km/s). We propose here that these blue shifts of the core part,in addition to the motion of the overlying matters, can work to give rise to the blue asymmetry in the intensity peaks.

TABLE I.

Doppler-shifts of the core and wing parts of the H_α emissions for 6 moustaches. (unit : km/s)

	v(core)	v(wing)
1	- 5.8	- 0.3
2	- 0.2	0.0
3	- 5.9	- 2.0
4	?	- 5.6
5	?	+ 0.7
6	- 6.0	- 0.6

TABLE II.

Doppler-shifts and Doppler-widths of the emission cores in the Balmer and K lines. (unit : km/s)

line	v(shift)	v(width)
K	+ 8.2	67.7
H_α	+10.2	98.7
H_β	- 0.4	89.7
H_γ	+ 0.4	87.3
H_δ	- 0.9	73.2

For H_β lines, we have essentially the same results as for H_α lines.

4. The Doppler-shifts of the Emission cores of Balmer lines and K line

In the echelle spectrogram, moustache emissions can be seen in H_α, H_β, H_γ, H_δ and K lines. From the Gaussian fitting to the profiles, we have deduced Doppler-shifts of the emission cores. The results are shown in Table II. Strong H_α and K lines show large red shifts ($\simeq$10 km/s), although other Balmer lines show little motion. So in this case, matters in higher layers were down-falling but in lower layers matters were static.

5. Summary

a) Emission profiles of moustaches are composed of Doppler shifted Gaussian cores and slightly Dopplershifted symmetrical power-law wings with central absorptions due to overlying matters.

b) In upper layers, matters in moustaches move up- or down-wards about 10 km/s. On the other hand, in lower layers matters remain virtually static.

c) Upwards motions are prevailing in upper layers. This may be a factor that give rise to the blue asymmetry in the intensity peaks.

REFERENCES

Bruzek, A. : 1972, Solar Phys. 26, 94.

Roy, J.-R. and Leparskas, H. : 1973, Solar Phys. 30, 449.

Severny, A.B. : 1968, in Y. Öhman (ed.), ' Mass motions in Solar Flares and Related Phenomena ', Nobel Symp. 9, 71.

SOME OBSERVATIONAL RESULTS ON ELLERMAN BOMBS

H. Kurokawa
Kwasan and Hida Observatories,
University of Kyoto

1. Introduction

Ellerman bombs and moustaches are identical phenomena (McMath et al., 1960). They are characterized by the spectrum of very thin and extended emission wings emerging from strong Fraunhofer lines as R. Kitai showed in the last speech. Though some flares, especially flare kernels, show a moustache-type spectrum, the majority of Ellerman bombs are flare independent (McMath et al., 1960; Bruzek, 1972). Bruzek (1972) found a close correlation between Ellerman bombs and continuum facular granules. Roy and Leparskas (1973) pointed out that 86 % of the bombs in an active region near the limb and 56 % in the disk-center region were seen to be accompanied by ejection of dark material. Kitai and Kawaguchi (1975) showed that the Ellerman bombs occur at the locations where the sign of the line of sight velocity changes. This investigation is based on the filtergrams of two active regions just near the solar limb obtained with a $H\alpha$ Lyot filter of Domeless Solar Telescope at Hida Observatory. One active region is McMath region 16224 observed from 221654 UT on 13th to 070506 UT on 14th and from 222156 to 233129 UT on 14th Augast 1979. The central wavelength of the filter passband was changed from $H\alpha$ center to $H\alpha \pm 0.4$, ± 0.8, ± 1.2, ± 1.6, ± 2.0 and ± 5.0 in order. Some frames of these filtergrams are of good quality and enable us to study the shape and size of Ellerman bombs very close to the solar limb (section 2). The other active region is McMath region 16867 observed from 215134 to 232320 UT on 5 June 1980. For this active region we took a photograph every five seconds on the average at the fixed central wavelength of $H\alpha - 1.2$ Å where the bombs show the greatest contrast against the surrounding solar features. This sequential observation of high time resolution enables us to study the life time and the photometric light curve of Ellerman bombs (section 3).

2. Shape and Size

Bruzek (1972) pointed out that moustaches appear as irregular-shaped features (spikes, mounds) at the very limb of the sun. On our filtergrams of two active regions near the solar limb in this study, most Ellerman bombs can be seen as an

elongated shape or a spike. In order to clarify this quantitatively, we measured the widths and lengths of 214 bombs in 11 filtergrams which are listed in Table 1.

TABLE 1

Ellerman bombs measured

Date	8/13 1979	8/13 1979	8/13 1979	8/13 1979	8/13 1979	8/14 1979	8/14 1979	8/14 1979	6/5 1980	6/5 1980	6/5 1980
Time of observation (UT)	2222	2225	2232	2321	2333	0004	0009	2224	2225	2248	2255
Wavelength shift from Hα ceneter	-2.0	-2.0	-2.0	+1.6	+0.8	-1.6	-5.0	-1.2	-1.2	-1.2	-1.2
Position of active region	S 28 E 80	S 28 E 80	S 28 E 80	S 28 E 79	S 28 E 79	S 28 E 79	S 28 E 79	S 28 E 66	S 10 W 78	S 10 W 78	S 10 W 78
Number of bombs measured	12	16	13	18	8	27	16	22	21	30	31

We used nearly the same methods as Bruzek (1972) : (a) the widths and lengths were measured directly on the negatives (1" = 156μ) with a Nikon measure scope, (b) they were measured on the projected negatives providing a scale 1" = 3 mm, and (c) photometric intensity profiles were determined for 30 typical bombs and the full half width of the profile was considered the width or length of the bombs. the results derived from the methods (a) and (b) agreed well each other. Systematic differences were found, however, between (a) and (c). Then we derived a simple empirical formula to reduce the results by the method (a) to the full half widths of the photometric profile. The results are presented in the form of histograms in Figure 1. Since the lengths of the bombs in Hα - 5 Å are distinctively shorter than those in other wavelengths, we excluded the lengths in Hα - 5 Å from Figure 1. The bombs of 2224 UT Aug. 14 were also excluded from the histogram of lengths because of their smaller heliographic longitude. According to Figure 1, 37 % of bombs have the width less than 0.4 second of arc. Moreover, it appears that even larger bombs are often consisted of two or more smaller spikes, on which we will discuss further in section 3. After all a typical width of a bomb spike is probably less than 0.4 second of arc. The result we have obtained is less than those found by Bruzek (1972) (0".5 - 1".0); this is probably due to the better resolution of our observations. The distribution of apparent lengths is nearly symmetrical around the peak number and most of these lengths clearly exceed the resolution of our photographs. We can therefore obtain 1".1 as a significant mean apparent length of a bomb spike. Due to the foreshortening effect, these apparent values give only a minimum of the real length.

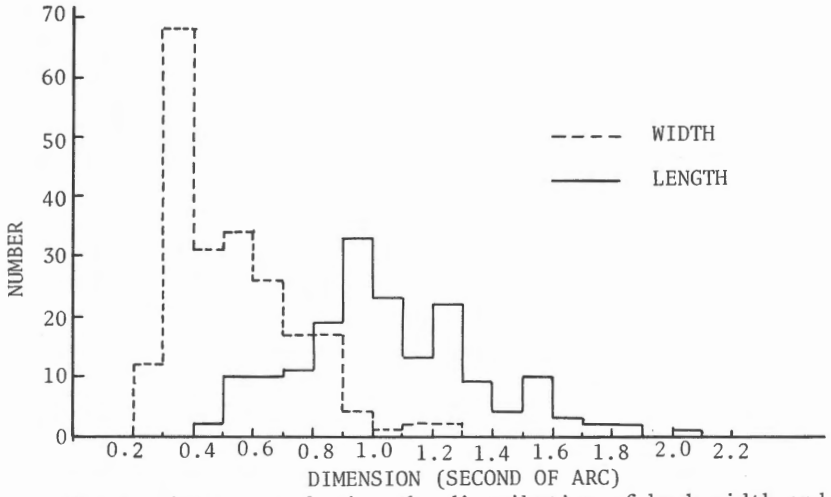

Fig.1 Histograms showing the distribution of bomb width and length.

3. Lifetime and Light Curve

From 2151 to 2323 UT on 5 June 1980, 921 frames of filtergrams in Hα -1.2 Å were obtained at nearly constant time rate for McMath region 16867 (S 10, W 78). We selected 101 bombs in this active region and estimated their lifetimes by tracing them on successive frames of negatives. The lifetime of a bomb was defined as the duration between the start of brightening and complete dimming into surrounding brightness. The results are presented in the form of a block diagram in Figure 2.

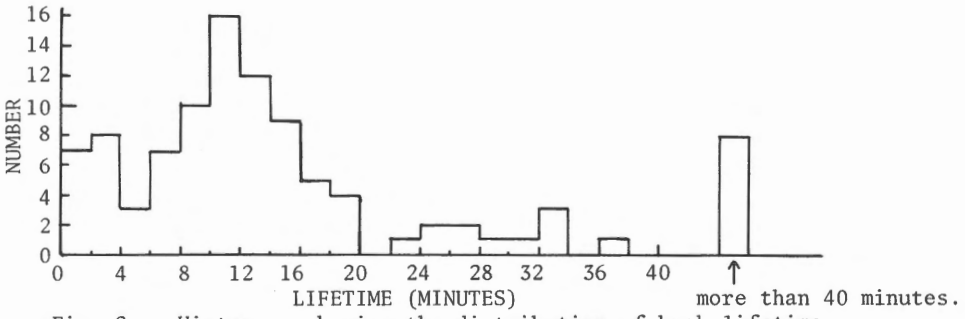

Fig. 2 Histogram showing the distribution of bomb lifetime.

In this figure, 7 bombs of (0-2)-minutes' lifetime and 3 of (2-4)-minutes' are corresponding to the foot points of impulsive surge activities at the same location. These 10 bombs were excluded from the calculation of the mean lifetime because of their flare-like feature. The all bombs with lifetime longer than 28 minutes in Figure 2 were found to pulsate from one to sevral times before disappearing. Excluding also these bombs from the calculation, We obtained 12 minutes as a mean

lifetime of typical Ellerman bombs. This result is in a good agreement with that found by Roy and Leparskas (1973) (11 min), but much smaller than found by Bruzek (1972) (15 - 38 min). In order to study a life of a typical Ellerman bomb in more detail, we derived the photometric light curves for 9 typical bombs. Five of them are shown in Figure 3.

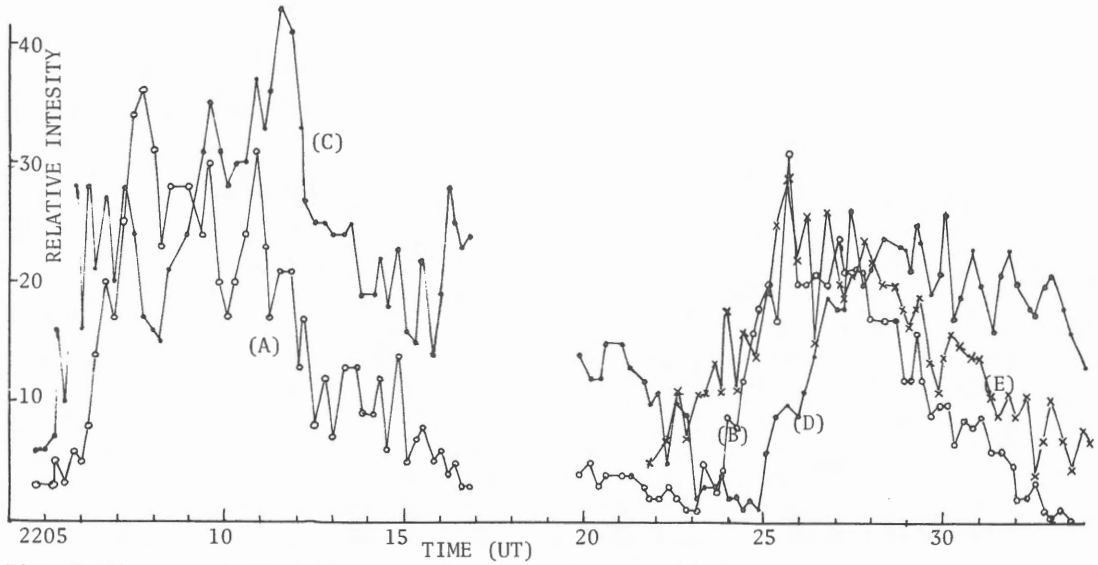

Fig. 3 Photometric light curves of typical Ellerman bombs.

From these light curves of 9 bombs we can obtain the average time scales for brightening and decaying: the first maximum brightness is attained in about 2.2 ± 0.4 minutes, then nearly the same brightness is kept for about 4.7 ± 1.0 minutes, and the decaying is completed in about 4.9 ± 1.3 minutes on the average. In Figure 3, the bombs (A) and (B) brightened in the same location and the bomb (D) occured at the same point as (C). Such a recurrence seems to be a rather common characteristic of Ellerman bombs as pointed out by McMath et al. (1960). We confirmed that 45 % of bombs recurred during our observation on 5 June 1980. The bomb (C) pulsates two or three times before dimming at 2223 UT. The pulsation of brightness also seems to be distinctive feature for large and bright bombs. This pulsation may be due to the fine structures inside a large bomb which brightens and dims one after another.

References

Bruzek, A.: 1972, Solar Phys. 26, 94.

Kitai,R. and Kawaguchi, I.: 1975, Solar Phys. 44, 403.

McMath,R.R., Mohler,O.C., and Dodson,H.W.: 1960, Proc. Nat. Acad. Sci. U.S. 46, 165.

Roy, J.R. and Leparskas, H.: 1973, Solar Phys.30, 449.

ENERGY RELEASE AND ENERGY TRANSFER IN FLARES

Jean Claude HENOUX
Observatoire de Paris

It is of primary importance to understand the preflare stage which leads to the triggering of the flare instabilities. However, despite of the fact that the increase of entropy associated with an explosive phenomenon reduces the useful information, we might expect to improve our understanding of the solar flares mechanisms by studying also the characteristics of the energy released in flares.

I.- Distinction between p.e.r. (primary energy release) and secondary phenomena.

All the observations give some information on the flare energy output. However, they do not discriminate between p.e.r. and secondary phenomena. The p.e.r. is the in situ liberation of energy associated with a local conversion of magnetic field free energy in other forms of energy. On the other hand, in secondary phenomena there is no in situ dissipation of magnetic energy. The energy comes from the vicinity of the observed site via different modes of energy transport.

Theorical arguments give some information on the p.e.r. Therefore in order to check the theory with the observations it is necessary.

1°) To discrimate between p.e.r. and secondary phenomena in the observed flares.

2°) To determine the p.e.r. characteristics i.e. nature duration and location.

These two points will be considered in this paper using existing observations The emphasis will be put on the location and on the amount of the nergy released. Then, as a conclusion, an attempt will be made to discriminate between flare models using existing observations.

I.A.- Model of p.e.r.

To determine the location and the nature of the p.e.r. process we need a model

giving a first approximation of these parameters. Then the secondary phenomena will be estimated and compared to the observations. The major difficulty of such an approach is that the unicity of any proposed solution cannot be proved.

The proposed model must include the location the nature and the duration of the p.e.r. The relevant mode of energy transport to be considered must include particle beams, convection, conduction, radiation. The transport coefficients could be modified from their classical values by waves-particles interactions. The geometry of the magnetic field has to be included and transfer technics have to be used. The building of a model is therefore so complex that there is not yet any fully satisfactory approach of the problem. The existing works deal with limited aspects of it in order to reduce the number of terms to consider.

I.B.- Nature of the p.e.r.

All the products of the p.e.r. phenomenon will not be considered here in detail. Despite of the fact that, in some events, mass motions and shock waves could carry more energy than radiation or particles they will not be considered here. From the conclusions of the Standford SERF workshop (1980) and of the Skylab flare workshop there is a lack in our knowledge of the precise timing of the initiation of transients vis a vis other flare effects. Then it is impossible now to distinguish between effects and causes.

Ion and proton acceleration also will not be considered in detail. A still valid review on this topic is given in the Skylab flare workshop. Proton beams will be invoked only to explain some characteristics of the radiative output from the low atmosphere.

The main effects of the p.e.r. to be considered here are electron heating and electron acceleration. Our knowledge of the high energy electrons comes predominantly from X-ray and γ continuum emission. These high energy electrons appear to be produced during the impulsive phase of the hard X-ray emission. They are sometime present in the preflare phase too, which will not be considered here.

I.C.- Duration of the p.e.r. phase

I.C.1. Impulsive phase

Most of the flares show an impulsive phase in X-ray emission. However from the study of more than 100 X-ray bursts. Datlowe et al., (1974) concluded that 1/3 of the events they observed did not show any detectable impulsive emission. The processes which take place in the decay phase of flares with impulsive phase are probably not too different from the ones taking place in flare without impulsive

phase. Therefore we will restrain ourself to the study of flares with an impulsive phase.

1.a- Site of the p.e.r. models of X-ray sources during the impulsive phase.

The p.e.r. site is most probably located inside the observed X-ray source. Very little is known about the vertical structure of the impulsive X-ray source. Observations with two spacecraft separated in heliographic longitude (Kane et al., 1979) indicate that the X-ray source (E > 50 KeV) extends from low altitude up to well above 25 000 Kms.

SMM observations (Hoyng et al., 1980) have shown that 20-30 KeV X-rays originated from the feet of flare loops. On the other hand radio-observations at centimetric wavelengths (Marsh et al., 1979) using the VLA showed that the microwave source was located between the Hα kernels at the time of peak emission. Contrary to the X-ray source the cm radio source appears to be located at the top of loops.

Some information on the velocity distribution fonction of energetic electrons could be derived from the measurement either of the directivity or of the linear polarization of hard X-ray emission. No significant observation has been obtained yet.

No quantitative information on the total energy carried by the high energy electrons and on their total number can be derived from the hard X-ray spectrum without taking into account the interaction between the p.e.r. site and the surrounding atmosphere.

There is no unique and satisfactory model of hard X-ray sources. Two extreme situations have been considered which are the thick-target and thin-target models. In the thin-target model electrons escape from a low density target. In the thick target model electrons lose all there energy by colliding with a dense atmosphere. A somehow more realistic model is the trap model where the electrons are partially trapped in magnetic arches. If the target inside the arch is made of cold electrons and protons the emission is thick target emission. If all the trapped particle have the same mean energy we obtain the quasi thermal model corresponding to smaller energy requirements. The only common feature of all these models is that the p.e.r. site is located in the corona in any of them.

In the thick-target emission energetic electrons lose their energy in Coulomb collisions. The hard X-ray energy yield is small (10^{-5} to 10^{-6}). Therefore the total energy E and the total number of electrons N_e required to explain the observed X-ray flux are very high. For events associated with 3B flares $N_e \simeq 10^{39} - 10^{40}$ and $E = 2\ 10^{31} - 10^{32}$ ergs. If we assume that the electrons come from the low corona and that the energy is taken from a 100 gauss magnetic field huge volumes up to 10^{29} cm^3 are required. Thin target models use the energetic electrons rather

inefficiently, and hence they are putting more stringent requirements on the acceleration process.

To overcome the efficiency problem different authors (Brown et al., Smith and Lilliequist 1979, Smith and Auer 1980) discussed a quasithermal model. Before discussing further this model and before discussing the need of confining the energetic electrons the observed interaction between the p.e.r. site and the surrounding medium will be presented.

1.b.- Interaction between the energic electrons and the low atmosphere.

The most convincing evidence of interaction between the energetic electrons and the lower atmosphere comes from the comparison of the temporal variation of the hard X-ray and EUV emission (10-1030 Å). The studies by Donnely and Kane 1978 have shown that the maxima of X-ray and EUV emission are coincident within ± 1 s. Because more than 50 % of the 10-1030 Å flux comes from chromosphere or transition zone these observations are supporting a model of thick-target emission where the electrons are bombarding the low atmosphere. This model has been checked in two different ways :

1) by computing the Φ (EUV) / E_B ratio where Φ (EUV) and E_B are respectively the total energy radiated in the EUV and the total energy deposited by electron bombardment in a tick-target model. This ratio is always much lower than one leading to the assumption that only a fraction of the energetic electrons are bombarding the atmosphere.

2) the second approach is the one used by Brown et al., (1978) who compared Hα profils observed in flare kernels with computed profiles for electrons heated models. These models were calculated assuming thick-target X-ray emission and neglecting the effects of the return current. The computed Hα profiles are much stronger than the observed one and the energy input has to be reduced by more than one order of magnitude to minimize the disagreement. Including the return current effects would not change the conclusion (Emslie 1979).

Then it appears that :

- There is no need of in situ energy release in the chromosphere during the impulsive phase
- The high energy electrons must be partially confined in the X-ray source.

1.c.- Confinement of the energetic electrons in the p.e.r. site.

There is some addition evidence of the need of confining the X-ray source. Mäzler et al., (1978) observed in small flares a variation of the emission measure

$Em \sim T^{3/2}$ in agreement with what can be expected from an adiabatic compression of the plasma. X-ray observation from TANSEI IV of small flares suggest a compression of energetic electrons (Tanaka et al., 1980). These models require some confinement mechanism to keep the electrons trapped during the compression.

There is no satisfactory model of electron confinement. The most promising approach uses collective interactions of the beam with the plasma target. In a recently proposed model of quasithermal source (see references in 1a) the plasma is confined between two ion acoustic turbulents fronts which are created by an ion acoustic instability driven by the return current associated with the beam.

In this model electrons of high energy ($E > 2.6\ KT_e$) are no scattered by the turbulence and escape freely. The main interest of the model is to be more efficient than the thick target model. The gain being of the order of $V_e/C_s = 40$. The rate of energy deposition in the low atmosphere is reduced by this factor, leading to a better agreement with the observations quoted in 1b, and the energy requirement are relaxed. On the other hand this model fails to reproduce two observational facts i.e. first HXIS observations (Hoyng et al., 1980) show simultaneous impulsive brightenings at the feet of loops indicating velocity higher than sound speed and no X-ray emission (20-30 KeV) between the feet contrary to model predictions. Secondly VLA observations seems to indicate that energetics electrons are at the top of loops contrary to model predictions.

I.C.2.-Decay phase

The decay phase is the phase following the impulsive phase. There is no hard X-ray emission during this phase and soft X-ray and Hα emission reach their maximum intensity. The study of the decay phase rises two questions :

- Does the p.e.r. terminate with the impulsive phase or not ?
- Is there enough energy transferred from the hot plasma towards the lower atmosphere to explain the observed energy release from these layers as a secondary phenomenon ?

2.a. - Morphology and origin of the thermal X-ray plasma.

Soft X-ray filtergrams and EUV spectroheliograms from Skylab have established than the basic structural form of the thermal X-ray plasma in the decay phase of flares is that of closed loops or arches.

It is very uncertain just how the thermal X-ray plasma is generated. Among the proposed mechanisms are direct heating of the plasma either in the upper portion of the magnetic arches by current dissipation or heating at the feet of arches by the high energy electrons impinging on the chromosphere. There is no obvious reasons why the first process would stop at the end of the impulsive phase.

2.b.- Is there some p.e.r. during the decay phase ?

From the analysis of Skylab data, Moore et al., (1980) made a distinction between large two ribbon flares and compact flares. In large two ribbon flares heating of the thermal X-ray plasma continues far into the decay phase. The required heating seems to be associated with the continued growth of the loop system. This growth seems to support the hypothesis of continuous heating by reconnection, and not the heating by anomalous dissipation. However we do not clearly know what would be the driver of the reconnection.

In small compact flares which occur in small bipolar regions far away from the main neutral line there is no clear indication of continued heating.

2.c.-Atmospheric response to the energy input from the thermal source. The low temperature flare as a secondary phenomenon.

In the T.Z. (transition zone) and low corona the studies of Underwood et al., (1978) and Machado and Emslie (1979) show that there is more material above 10^6 K than predicted by assuming that energy is deposited from above by conduction. Such excess of 10^7 K material could result from the heating of the chromospheric material to coronal temperature during the impulsive phase. Chromospheric emission is observed in flares even in the absence of hard X-ray emission. Some other mechanism of energy input than electron bombardment has to be invoked in order to explain the chromospheric emission as a secondary phenomenon.

In the high chromosphere above 10^{4° K, Ly α flux is the most efficient radiator Comparison of the Ly α flux with the conductive flux in the middle of the T.Z., made by Machado and Emslie (1978), indicates that the radiative output from the high chromosphere can be explained by thermal conduction from above.

Machado et al. (1980) have build empirical models of faint and bright flares. One interesting result of their radiative losses computations is the backwarming of the high chromosphere by Ly α radiation. However the Hα cooling exceeds the heating and an extra heating is needed. Heat conduction, the effect of which is negligible in the low chromosphere, cannot produce the required extra heating. This extra heating can be provided by XUV radiation.

Indeed a subtantial amount of energy is radiated at soft X-ray wavelengths. Half of this energy is radiated downwards and heats the chromosphere. The height dependance of the X-ray energy deposit was computed by Somov (1975) and Henoux and Nakagawa (1977). The flare model computed by these last authors for a given XUV irradiation does not greatly differ from the Machado et al. model F1. Moreover taking into account the actual shape of the X-ray source during a specific event, Henoux and Rust (1980) showed that X-ray illumination can produce a two ribbon structure in the horizontal variation of the energy deposit very close to the

observed Hα two ribbon flare.

With a 50 % accuracy there is no need of in situ energy release in the low atmosphere. The observed energy deposit in these layers is provided by the hot plasma above via conduction and radiation. The chromospheric flare in the decay and in the impulsive phase of flares is a secondary phenomenon.

On the other hand the energy balance of the lowest part of the solar atmosphere is not understood in any of the flare phases. Therefore the heating of the temperature minimum region (TMR) and upper photosphere (UP) will be traited separatly.

I.D. - Location of the p.e.r. site and in situ heating of the upper photos-phere and TMR.

Using Ca II lines and UV SiI ^3P and ^1D continua Machado et al extended their models down to the U.P. These models show a subtantial temperature enhancement at the TMR. Electron beams, protons beams and soft X-ray can penetrate down to the U.P. However the flux required to explain the observed heating is more than one order of magnitude higher than the one inferred for large events.

Analyzing the effect of EUV radiation Machado and Henoux (1980) and Chambe (1980) concluded that EUV radiation strongly modify the ionization balance of Si and C atoms. The first authors have shown that non L.T.E. effect are induced in the SiI continuum. Hence SiI continuum observations alone cannot be used to measure temperature enhancement. Anyhow previous studies of CaII spectra are not affected and in situ heating of the upper photosphere is not yet ruled out.

Observations of white light flares can be interpreted also as a heating of the upper photosphere. The two independant observations of two differents events by Machado and Rust (1974) and Hiei (1980) lead to two radically different interpretations. The first authors concluded that white light emission was due to free bound transition of hydrogen at 8500 °K. On the other hand Hiei found a flat continuum above 3646 °K which he interpreted as H^- emission from the upper photosphere. Proton flux of the order of magnitude of the one observed in other large flare events could provide the required energy deposit. Unfortunatly there was no γ-ray observations for this event. Therefore the origin of white light flares and their association with proton beams is still on open question.

The origin of the heating, if any, of the temperature minimum region and upper photosphere is not understood yet. The present interpretation of existing observations implies some in situ energy release. Ohmic dissipation due to a large electric current in layers where the resistivity is maximum was suggested by Spicer (1980) and Sturrock (1980). The required current is unreasonably high. However multiply reversed currents over the flare area could explain the observations.

Such interpretation is supporting the hypothesis of a participation of the whole atmosphere to the flare energy release via the effects of electric currents.

I.E.- Conclusion of chapter I

A good deal of progress has been made in the modelling of the energy distribution in the flaring atmosphere. Nevertheless there are still some open questions: on the nature, the amount, and the location of the primary energy release. More work has to be done on :

1°) The confinement of energetic particles,

2°) the heating of the upper photosphere and temperature minimum région,

3°) the dynamics of the atmospheric response.

II.- Observations and flares models

There is not enough satisfactory tests to discriminate between flare models like reconnection in neutral sheet, reconnection in sheared magnetic field or current interruption. These tests could deal with :

The location of the p.e.r. site. Models of reconnection in sheared field or current interruption could be in agreement with a wide extension of the flare site from corona to upper photosphere. Unfortunatly the required spatial resolution to localize the instabilities greatly exceeds the capability of existing or planned solar telescopes.

The identification od the driver for the neutral sheet models like new magnetic field emergence.

The current characteristics and current evolution associated with current interruption or reconnection in sheared magnetic fields.

The investigation of turbulence which is required in some models (reconnection in neutral sheets, quasithermal model of X-ray source, current interruption).

SMM and the international coordination of the Solar Maximum year will help to understand the flare problem. However there will still be some questions left open for the next solar maximum.

REFERENCES

Brown, J.C., Canfield, R.C. and Robertson M.N. : 1978, Solar Phys. 57,399

Brown, J.C., Melrose,D.B. and Spicer, D.S. : 1979, Astrophys. J 228,592

Chambe , G. 1980, Submitted to Astron. Astrophys.

Datlawe, D.W. , Hudson, H.S. and Peterson, L.E. : 1974, Solar Phys. 35, 193

Donnely, R.F. and Kane, S.R. : 1978 Astrophys. J. 222,1043

Emslie, A.G. : 1980, Astrophys. J. 235,1055

Henoux, J.C. and Nakagawa, Y. : 1977, Astron. Astrophys. 57,105

Henoux, J.C. and Rust, D. : 1980, Astron. Astrophys. in press

Hiei, E. : 1980, to be submitted

Hoyng, P. et al : 1980, Communication SERF Workshop Standford

Kane, S.R., Anderson, K.A., Evans, W.D., Klebesadel, R.W., Laras, J. : 1979, Ap J Letters 233,L151

Machado, M.E., Avrett, E.H., Vernazza, J.E. and Noyes, R.W. : 1980, Astrophys. J in press

Machado, M.E. and Henoux, J.C. : 1980 submitted to Astron. Astrophys.

Machado, M.E. and Emslie, A.G. : 1979, Astrophys. J. 232,903

Machado, M.E. and Rust, D. : 1974, Solar Phys. 38, 499

Marsh, K.A., Hurford, G.J., Zirin, H. and Hjelliming, R.M. : 1980, submitted to Astrophys. J.

Mätzler,C., Bai, T., Crannell, C.J. and Frost, K.J. : 1978, Astrophys. 223,1058

Moore, R., Mac Kenzie, D.L., Svestka,Z., Widing, K.G., Antiochos, S.K., Dere, K.P., Dodson-Prince, H.W., Hiei, E., Krall,K.R., Krieger, A.S., Mason, H.E., Petraso, R.D. Pneuman, G.W., Sick, J.K., Vorpahl, J.A., Withbroe, G.L. : 1980 Solar flares a monograph from Skylab Solar Workshop II

Smith, D.F. and Lilliequist, C.G. : 1979, Astrophys. J. 232,582

Somov, B.V. : 1975, Solar Phys. 42,235

Spicer, D.S. : 1977, Discussion at II Skylab Workshop on Solar Flares

Sturrock, P.A. : 1980, Solar Flares a monograph from Skylab Solar Workshop II

Tanaka, K et al : 1980 this seminar

Underwood, J.H., Antiochos , S.K., Feldman, U and Dere, K.P. : 1978 Astrophys. J. 224,1017

SOFT X-RAY LINE EMISSION FROM SOLAR FLARES

Katsuo Tanaka
Tokyo Astronomical Observatory
University of Tokyo

I. Introduction

Soft X-ray line spectrum in the wavelength region of 1.85-1.94A provides a powerful tool for the diagnostics of the 10-20 million degree plasmas produced in the solar flare (Gabriel 1972 : Mewe and Schrijver 1980). Many observations of this spectral region have been performed and currently in progress improving spectral and temporal resolutions (Newpert et al., 1967 ; Doschek et al., 1971 ; Grineva et al., 1973 ; Doschek et al., 1980 ; Gabriel et al., 1980). Observations of the spectrum at the early stages of flare are particularly important to study the heating phase of flares as theoretical studies of transient flare plasma (Mewe and Schrijver, 1980) indicate. To study this phase, however, both high sensitivity and high time resolution are required to the spectrometer since the rapid variations of the spectrum is expected to occur at low flux level. A crystal spetrometer designed on a new conception (Tanaka and Nishi 1978) which satisfies this condition has been flown on the Tansei-IV satellite launched on 17 February 1980 by the Institute of Space and Aeronautical Science, University of Tokyo. It measures spectra in the two wavelength bands of 1.8-2.0A and 3.1-3.25A with variable time resolution of 6-30 seconds. The sensitivity of the specrometer is such that an incident flux of I photons $cm^{-2}s^{-1}$ at 1.85A at the earth orbit produces a count of 0.14-0.7I corresponding to the above time resolution. Spectral resolution of the crystal (LiF) is 0.005A at 1.85A. This spectrometer differs form ordinary ones in that incident angle of X-ray photons to the crystal is varied for a fixed crystal and detector system by the spin of the satellite. For this purpose the satellite's spin axis is pointed always to a fixed direction slightly (0.7-1.7 degrees) away from the sun. The wavelength scan is made automatically twice in one spin period, at different rates depending on the spin period (n=1-5 resolutions per minutes). This allows for variable time resolution, spectral dispersion and sensitivity. During net observation time of 240 hours in the eight months operation of the satellite, the spectrometer recorded 300 flares. Most of these are small flares

with X-ray class less than M1. In this letter we report possible detections of two kinds of variation in the spectrum in the heating phase of flare. A slow spectral variation is generally seen in the rising phase of the flare, while rapid spectral changes have been detected only for a short interval at the initial phase of the flare which shows impulsive rise of flux.

II. Observations

The data are sampled in two kinds of rates : 32ms and 250ms which correspond to a scan step of the spectrometer, respectively, of 0.00026nA and 0.0021nA (n:spin rate in r.p.m.). Fig.1 shows a time series of the spectrum 1.8-2.0A obtained with a scan step of 0.0008A for the May 28 flare (X-class M2.8). The time resolution is 10 seconds. Seven peaks recognizable in the spectra are identified with blended lines from FeXXI to FeXXV(cf. Doschek et al., 1980), FeXXV resonance line at 1.850A and Kα emissions at 1.935A. A gradual variation of the spectrum can definetely be seen. In the initial phase the FeXXV resonance line at 1.85A is apparently weaker than the 1.865A peak. Toward the maximum the resonance line becomes most pronounced among the all. Intensity time profiles in seven wavelength bands in Fig.2 shows that the rate of increase and decrease in the intensity is largest for the resonance line, and for the other wavelength regions the rate is nearly the same but slowly decreases to the longer wavelengths. Intensity curve of Kα emission is similar to the total Fe line emission, I(Fe), or the sum of the intensities from 1.84A to 1.95A. This variability may be characterized by a time profile of a single index : R which is defined as the flux ratio of the combined emissions $\lambda<\lambda o$ to those $\lambda>\lambda o$. For the dividing wavelength λo we chose λo =1.88A as this wavelength position can be determined precisely, even in lower dispersion spectra, with the reference to the emission line obtained in the other band (3.2A) of the spectrometer. In the condition of ionization equlibrium R may be converted to an equilibrium temperature as will be discussed later. Time profiles of R for two deifferent flares are plotted in the lower parts of Fig.3. Compared to the total emission I(Fe) shown in the upper part of Fig.3 R is found to attain maximum at the same time as I(Fe). The coincidence of the times of both maxima has been found generally for all the flares with the X-ray class than M3. In contrast the intensity maximum is delayed to the maximum of R by one to two minutes in those flares with the X-ray class greater than M7, although we have observed only four such large flares. For small flares steady increase of R with the ascent of the flux appears to be quite universal. The duration of this phase ranges from one to three minutes depending on the type of flare.

Large instrumental width of our spectrometer may prevent measurement of the line profile. However line profiles definitely broader than the instrumental width

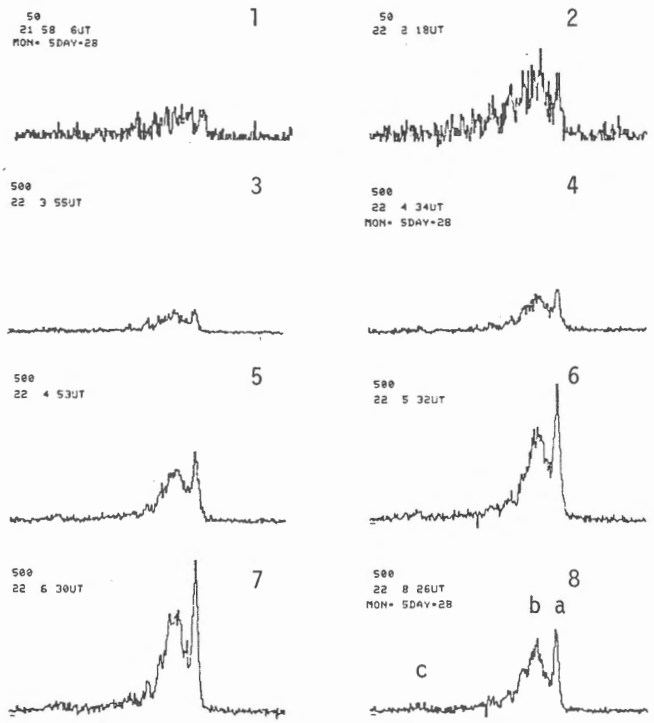

Fig.1
Time sequence of the iron line spectrum:1.80-2.00A.
(Ordinate scale for the top two is 1/10 that for the lowers.)
a.1.85A(FeXXV),b.1.865A,
c.1.94A(Kα)--frame 8
1.21 58 06 UT
2.22 02 18
3.22 03 55
4.22 04 34
5.22 04 53
6.22 05 32
7.22 06 30
8.22 08 26
(1980 May 28 flare)

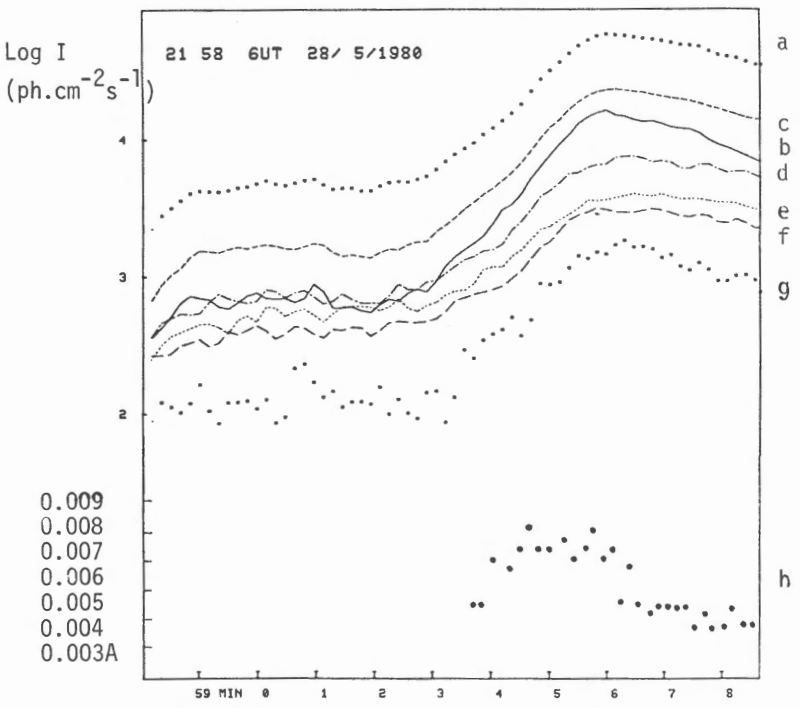

Fig.2
Time variations of the flux in seven bands and of the FeXXV resonance line width(FWHM).
a.1.84-1.96A(total)
b.1.845-1.86A(FeXXV)
c.1.865-1.879A
d.1.879-1.887A
e.1.887-1.896A
f.1.896-1.909A
g.1.92-1.95A(Kα)
h.line width

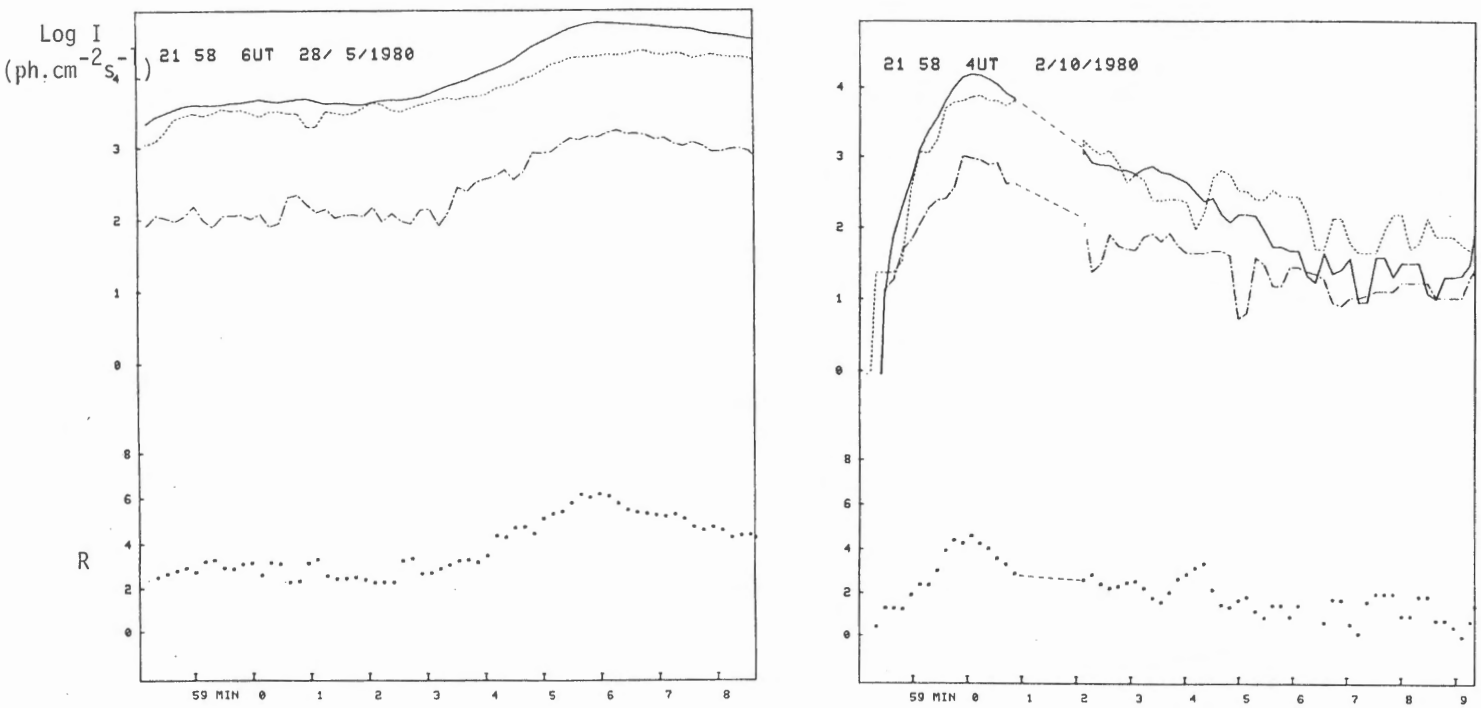

Fig.3 (Top) Time profiles ofthe total fluxof the iron complex(thick line),calcium lines(3.16-3.22A)(dotted line) and K_{α} line at 1.94A.
(Bottom) Time profile of the flux ratio(R) of combined emission 1.88A to 1.88A.
(Left) 1980 May 28,21 58 06 UT Flare
(Right) 1980 October 2,21 58 04UT Flare

of 0.005A have been recorded in the rising phase of the May 28 flare (Fig.1). The FWHM of the resonance line as plotted at the bottom of Fig.2 shows rapid increase at the time of rapid flux increase, and sudden decrease after the maximum. The intrinsic line width (FWHM) at the peak is estimated to be 0.0056A by deconvoluting the rocking curve width. This value corresponds to the turbulent velocities of about 200kms^{-1}, if the broadenning is due to non-thermal motions.

Rapid spectral variations we present here have been observed only in the fast rise flares.. The rise time of these flares are less than 2 min., and the increase rate of the total flux (ΔlogI(Fe)/Δt) is in the range of 1-2 min^{-1}. The rapid changes occur only for a short interval (10-40 sec.) at the initial phase. Time sequences of the spectra in the two flares are shown in Fig.4. The light curves for these flares are shown in Fig.3. Since the spectra were obtained in low dispersion mode with a sampling interval of about 0.005A, fine structure of the spectrum cannot be seen. However it is clear that the increase of the counting rates started around 1.935A and 1.89A. In the March 31 event (Fig.4a) the double peak structure in the spectrum is replaced in six seconds by a pronounced single peak at 1.885A(0050 01UT). The next profile taken at 00 50 07 UT this peak is shifted to 1.865A. The total iron line flux I(Fe) shows significant increase of a factor of ten in only 12 seconds. No detectable change in the position of the maximum intensity is apparent in the subsequent scans. Spectral variation in the October 2 event is more complex. The spectrum taken at 21 58 51UT shows four peaks at 1.94A, 1.895A, 1.865A and 1.850A with the intensity reducing in this order. In subsequent frames the peaks at 1.865A and 1.85 A grow most rapidly with other peaks appearing at 1.920A, 1.90A and 1.885A. The peak of Kα emission is pronounced for 30 seconds during this phase, and then dissappear. After 21 59 29UT the spectral shape remains constant showing double peaks at 1.865A and 1.850. Clear evidence for the rapid shift of the intensity maxima from 1.885A to 1.865A such as have been seen in the May 31 event has been given in other two flares. The shift was accompanied by rapid increase of the flux with the exception of the February 29 event, in which the intensity maxima shifted from 1.885A to 1.86A in 6 seconds without changing the peak intensity. In slow rise flares, too, there can be seen fluctuative changes in the initial sequences of the spectrum, but they are not significant from the count statistics.

In the events shown in Fig.4 microwave bursts at 17GHz have been obtained at the Nobeyama Station. The bursts (Fig.4) show a sharpspike with a short duration coincident with the phase of rapid variation in the X-ray spectrum. Detailed comparisons have revealed that the initial enhancement at Kα and 1.89A occurs at the start of the radio burst, when the flux of the burst is only 3% of the peak flux. The sharp spike of the burst, on the other hands, coincides with the rapid shift of the intensity maximum in the spectrum. In the October 2 event an increase

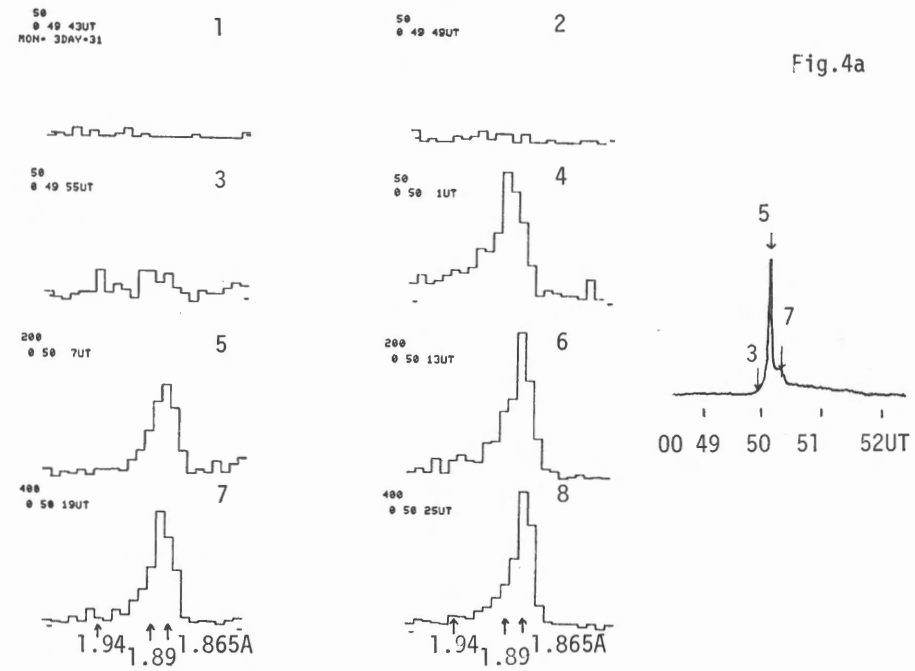

Fig.4a

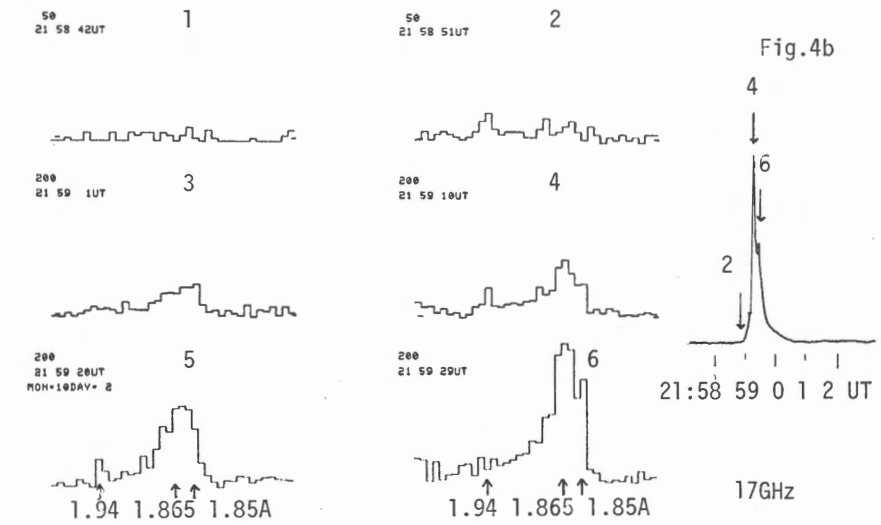

Fig.4b

Fig.4 Rapid spectral changes

Fig.4a March 31, 00 49 43UT-00 50 25UT(time resolution 6s)

Fig.4b October 2, 21 58 42UT-21 59 29UT(time resolution 9s)

Time profiles of 17 GHz radio burst obtained at Nobeyama Station (courtesy of Dr.K.Kai) are shown in the right. Numbers indicate the time at which corresponding spectrum was taken

of the Kα intensity occurred simultaneously with the sharp rise of the burst. But during a flux increase of the burst by a factor of twenty the Kα emission increased only a factor of four. For the other event no microwave data are avaiable. Preliminary comparison with the hard X-ray burst obtained by SMM indicates coincidence of the sharp spike of the hard X-ray burst with the rapid shift of the intensity maximum in the spectrum (May 31 event).

III. Analysis and Discussions

Rapid spectral changes simultaneous with the microwave burst may be identified with the initial heating of flare plasma. The fact that the changes are seen only at the low intensity level ($I(Fe) \sim 10^{2.5}$ ph·cm^{-2}s^{-1}) makes it difficult to observe this phase in the high resolution spectra. To obtain high resolution spectra by means of Ge or SiO_2 crystals to the same intensity level and time resolution as the present observations a large crystal area over 500cm^2 would be required. Even in the low resolution spectra like present cases, however, sudden enhancement of emissions at Kα and around 1.89A and subsequent shift of the peak to 1.865A can be safely recognized. Comparing with the theoretical simulations of the iron line spectrum in the transient flare plasma by Mewe and Schrijver (1980), sudden appearance of Kα emission and emissions at longer wavelength region fit the case in which the electron temperature steeply jumps from an initial value of 5×10^6K to a constant higher value of $Te > 14 \times 10^6$K. On the other hand, the shift of the intensity maximum from 1.885A to 1.865A can be reproduced when the temperature rises linearly with time. The speed of this shift determines the electron density if the temperature time profile is known. Among various model calculations by Mewe and Shrijver the observed short time scale (>10 sec.) of the shift appears to be consistent with the case of high density ($ne = 10^{11}$cm^{-3}) in which linear temperature rise to 20×10^6K occurs in one minute. In our observations, however, temperature profile is unknwon and there remains a possibility of non-thermal ionization due to high energy electrons producing the microwave or hard X-ray bursts. The emission peaks at 1.885A and 1.865A are dominantly contributed from FeXXII, and FeXXIV and FeXXV, respectivly. The time required for collisional ionization from FeXXII to FeXXV is equal to $3.3 \times 10^{15} T\, ne^{-1} \exp(7.7 \times 10^7/T)$s. Therefore even with high temperature limit of 10^8K, which may be equivalent to the non-thermal ionization, high density of the order of 10" is expected. The strong Kα emission observed at the initial phase is a dominant component of the spectrum. The origin of the Kα emission at the phase may be either due to impact collision of the high energy electrons or due to sudden jump of the electron temperature. The former possibility, however, meets a difficulty by the fact that the Kα emission increase without being proportional to the burst flux. Impact ionization

origin of the Kα emission simultaneous with hard x-ray burst is reported in the SMM observation (Gabriel et al., 1980) In contrast the Kα emission visible in later phases is proportional to the total iron line flux. The fluolesence origin is suggested for this case since ionizing of K-shell electron at 7 Kev will vary, more or less, similarly to the toatl iron line flux.

The spectral variation which is observed during the rise of small flares in commom proceeds gradually with a time scale of 1-3 minutes. The high dispersion spectra taken before the rise of the flux and at the maximum in the May 28 flare (Fig.1) show close similarities to the spectra calculated in the ionization equilibrium for 15×10^6K and 20×10^6K, respectively (Mewe and Schrijver, 1980). In a relatively, high electron density close to 10^{11}cm^{-3}, the ionization equilibrium will immediately follow the slow temprature rise if this rise occurs in the above time scale. The quasi-stationary ionization equilibrium has been suggested from the studies of the high resolution spectra (Doschek et al. 1980). We, therfore, assumed ionization equilibrium and calculated theoretical intensities of the 208 lines of FeXIV-FeXXV which are found in the region 1.85-1.94A of the line list of Mewe et al. (1980) to derive the equilibrium emission rates for the total flux I(Fe), combined emissions for $\lambda<1.88$A and for $\lambda>1.88$A as a function of temperature. If the flare region is assumed to be iso-thermal, the ratio R, which is also found to be smooth and monotonic function of temperature, gives an equilibrium temperature, and then the emission measure is determined from the total flux. Time profiles of the temperature and emission measure thus derived are shown in Fig.5. A typical small (<M1) but impulsive flare shows a temperature rise from 13×10^6K to 18×10^6K.
In the line ratio analysis using high resolution spectra by Doshek et al.(1980) no increase of the electron temperature has been found in the rise phase of X-class and most of M-class flares. Only for a M3 class flare they have found an increase of temperature from 18 to 20×10^6K. The M2.8 flare in our data shows a rise in the equilibrium temperature from 16 to 20×10^6K, consistent with their result for the electron temperature. Present analysis, combined with their result, suggests that the increase of temperature is found only when the flux is lower than certain level. The critical flux for the FeXXV resonance line appears to be 10^4 ph$\cdot$ cm^{-2}s^{-1}.
An interesting aspect commonly observed in small flares is the similarity of time profiles of R and I(Fe). As found from Fig.5 this is converted to the similarities of the temperature and emission measure time profiles. The result appears to contradict with earlier results derived from the continuum analysis (e.g.Horan 1971) However, the large flares (>M7) in the present cases show a time delay of the emission measure maximum behind the temperature maximum as have been found previously. Rather, the effect seems to depend on the size of flares. Presumably basic behavior may be observed in small flares, in which the structure of X-ray emitting loops

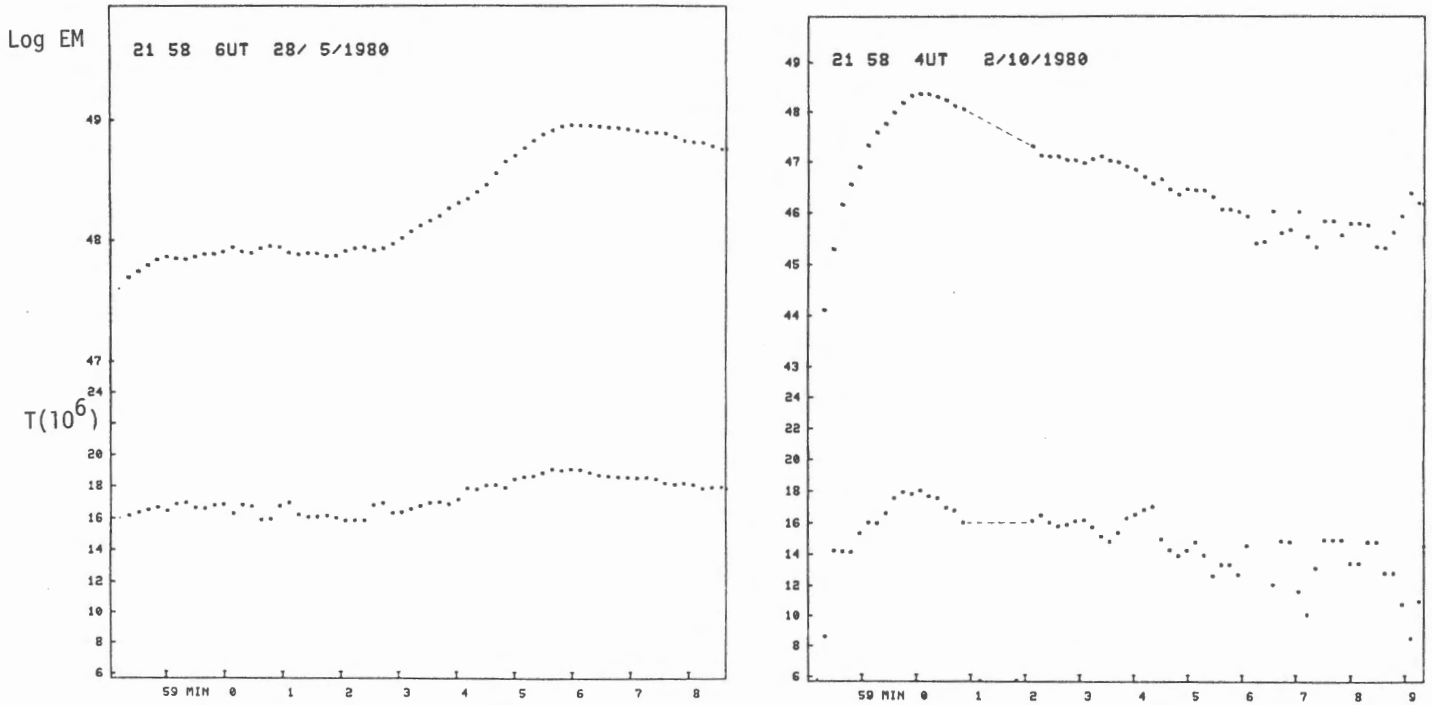

Fig.5 Time profiles of emission measure(upper) and equilibrium temperature(lower)
(Left) 1980 May 28 Flare (cf. Fig.1,2,3)
(Right) 1980 October 2 Flare(cf. Fig.3,4b)

is conidered as simple (Sturrock 1979). Then, an apparent time lag between the two maxima observed in large flares may be caused by complex evolutions which involve many loops. If many X-ray loops develop successively in the large flare and the peak temperature of each loop is lower for the loop developed later, such effect will result. Although finer analysis are needed to the definite answer, we may tentatively, conclude that the temperature and emission measure increase simultaneously in individual loops. With the assumption of constant mass this indicates simultaneous increases of the temperature and density suggesting a plasma compression.

References

Doschek, G.A., Meekins, J.F., Kreplin, R.W., Chubb, T.A. and Friedman, H.
1971 Ap. J. 170, 573.
Doschek, et al. : 1980 Ap.J. in press.
Feldman, U., Doschek, G.A., Kreplin, R.W. 1980, Ap.J. 238, 365.
Gabriel, A.H. 1972, Mon.Not.Roy, Astron.Soc. 160, 99.
Gabriel et al. : 1980, Ap.J. Letter in press.
Grineva, V.I., Karev, V.I., Korneev, V.V., Krutov, V.V., Mandelstam, S.L.,
Vainstein, L.A., Vasiliev, B.H. and Zhitnik, I.A. 1973, Solar Phys. 29, 441.
Horan, D.M. 1971 Solar Phys. 21, 188.
Mewe, R. and Schrijver, J. : 1980, Astron. Astropys. 87, 261.
Mewe, R., Schrijver, J., Sylwester, J. :
1980, Astron.Astrophys. Suppl. Ser. 40, 323.
Neupert, W.M., Gates, W., Swartz, M., Young, R. 1967, Ap.J., 149, L79.
Sturrock : 1979, Proc. Skylab Workshop (Solar Flare), Reidel.
Tanaka, K. and Nishi, K. : 1978, Jap.J.Appl.Phys. 17, Suppl.17-2, 461

35 GHz OBSERVATIONS OF SOLAR FLARES

Kin-aki Kawabata and Hideo Ogawa
Department of Physics and Astrophysics
Nagoya University, Chikusa-ku, Nagoya 464

1. Introduction

Observations of the sun at 35 GHz have been carried out by using the sixteen element east-west fanbeam interferometer since May 1976 and 189 distinctive bursts have been observed until July 1980. 88 of these bursts were great or impulsive bursts and 99 were GRF. Some observational results on these bursts and the quiet sun brightness have been already published elsewhere(Kawabata et al 1978,1980a,1980b). In this paper we describe some recent results of observations.

The longest baseline of the interferometer is 5849.1 wavelengths (50.1m). The east-west HPBW and the beam intervals in the meridian are 29" and 8'49" respectively. HPBW of the primary beam is 69'. The whole solar disk are scanned by drift scanning for example in each 35 sec in the meridian observations and in each 70 sec in off-meridian observations at the hour angle of 4 hours. Under ideal conditions, the accuracy of positional determination of radio sources is $\pm$10" in absolute measurements and $\pm$3" in relative measurements.

2. Motion of Radio Sources

On 3 April 1979, an Hα flare occurred at 0105 in the preceding part of McMath Region 15918 at S25 W14. The flare produced GRF at 35 GHz started at 0110(Fig.1). Apparent motion of the radio source seen in Fig. 1 from 0110 through 0300 is due to the solar rotation. The radio source is composed of a core with angular size less than 30" and an extended source with angular size 100". McMath Region 15918 produced also Hα flares at 0246 and 0417 respectively and these flare were accompanied by impulsive bursts started at 0306 and 0417 respectively. The position of the brightest point at the beginning of these bursts were in the following part of the active region and moved toward the preceding part. The velocity of the motion is 30 Km/sec.

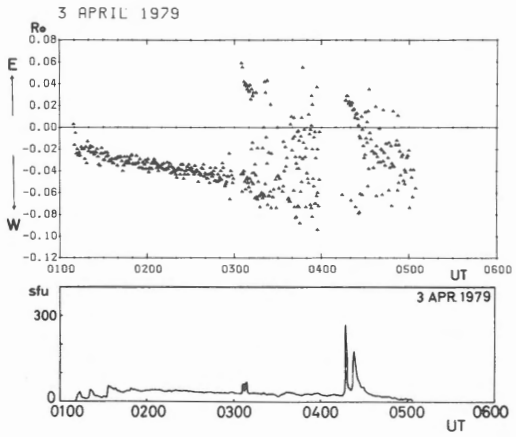

Fig. 1. The fanbeam distance of the source from the disk center(upper) and the time history of flux densities (lower) on the 3 April 1979 flare.

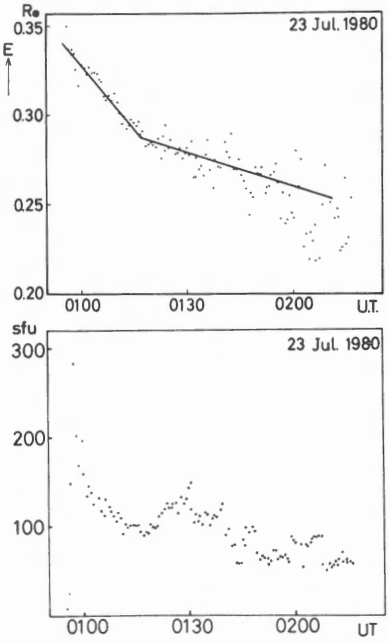

Fig. 2. The same as Fig. 1 but on the 23 July 1980 flare.

The similar motion of a radio source can be seen more clearly in Fig. 2. In this example, the change of the fanbeam distance after 0145 is mainly due to the rotation of the fanbeams relative to the sun by the earth rotation. The change of the fanbeam distances before 0120 indicates the motion of the source. The velocity of the motion is also 30 Km/sec.

When a solar flare occurs near the limb, rising motion of the source is also observed. An example of observations has been published in Kawabata et al(1980b). The velocity of the rising motion is 20-70 Km/sec. The horizontal and rising motion occurs in a declining phase of impulsive or great burst and in an early phase of post-burst increase. Radio sources appear to be stationary in GRF and in the late phase of post-burst increases.

3. X-ray Fe Lines and 35 GHz Emission

X-ray lines of highly ionized iron of 28 May 1980 flare have been

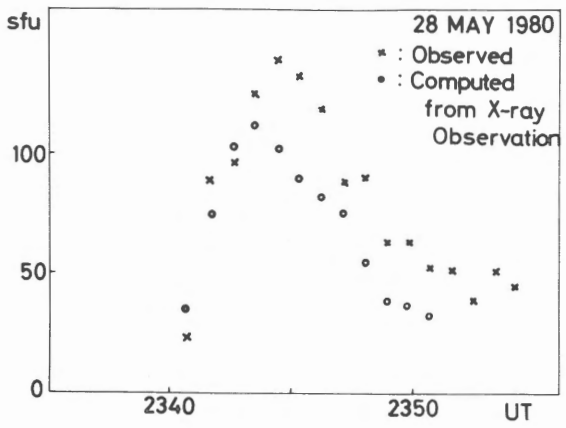

Fig. 3. Flux densities at 35 GHz of the flare on 28 May 1980.

measured by Brag spectrometer on board Tansei-4 by Tanaka, Watanabe, and Nishi. The time history of the flux densities at 35 GHz is compared with the f-f-emission computed from emission measure and temperature deduced from Fe XXV and XXVI lines by Tanaka et al. The general characteristics of the time variation of the observed flux densities is in good agreement with computed ones, though the observed ones are a little bit higher than the computed ones.

The position of the brightest point of the source has been determined two dimensionally from the change of the fanbeam distance from the disk center as a function of position angle under the assumption that the source is stationary. The determination gives the results that the brightest point locates inside the rectangle of the off-band Hα photograph(Fig. 4(b)). If we assume that the radio source is composed of 3 or 4 sources with Gaussian brightness distribution, 70% of 35 GHz emissions is emitted from a small

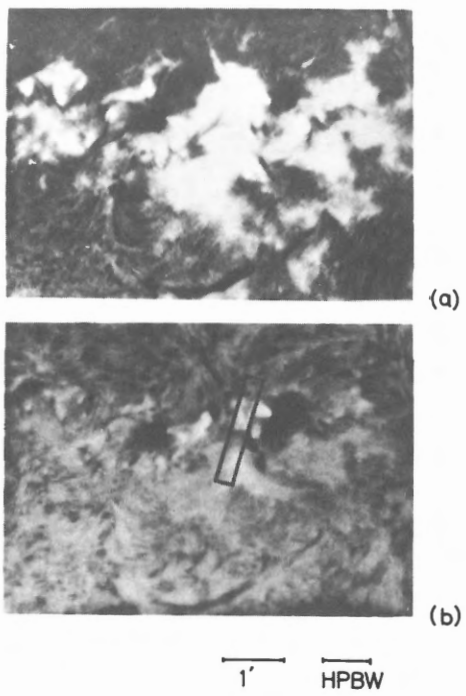

Fig. 4. (a): Hα phtograph of the flare on 28 May 1980 exposed at 2341.49. (b): 0.5 A off-band Hα photograph of the flare exposed at 2359.21. The brightest point of the radio source located inside the rectangle. Photographs are taken at Mt. Norikura by Prof. Moriyama.

source with a size less than 25"(0.5 x HPBW) and the remainings are emitted from extended sources with a size of 70-80" at the two big sunspots. The time variation of the total flux densities is mainly due to the time variation of the small source. These observations indicate that the X-ray line emissions are emitted from the small main source.

If we assume that the source size is 25", X-ray observations yield the electron temperature of 1.3×10^7K, the electron density of 1.5×10^{11}cm^{-3}, the optical depth at 35 GHz due to ff-absorption of 0.05 and the brightness temperature at 35 GHz of 6×10^5K at the time of maximum. In this case, the optical depth due to the thermal gyro-resonance absorption is smaller than the ff-absorption, in so far as the magnetic field strength in the source is less than 2500 Gauss. the radio burst on 28 May 1980 is a typical example of frequent radio bursts at 35 GHz. The observation suggests that some of radio bursts at mm wave have a thermal origin.

Acknowledgements

Authors wish to acknowledge to Dr. M. Fujishita and Mr. K. Akita for their cooperation of observations.

The 35 GHz solar interferometer in Nagoya was constructed under the support by the Grant-In-Aid for Scientific Research 942026 of the Ministry of Education, Science and Culture. This work was supported by the Grant-In-Aid for Scientific Research 342003 and the Grant-In-Aid for Special Project Research 511403 of the Ministry of Education, Science and Culture.

References

Kawabata,K.,Ogawa,H.,Omodaka,T.,Fujishita,M., and Kato,T.,1978,Solar Terr. Environ. Res. Japan,2,68.

Kawabata,K.,Fujishita,M.,Kato,T.,Ogawa,H., and OmodakaT.,1980a,Solar Physics,65,221.

Kawabata,K.,Ogawa,H.,Fujishita,M.,Kato,T.,Ishiguro,M., and Omodaka,T., 1980b,Radio Physics of the Sun,eds.M.R.Kundu and T.E.Gergely, p.127,Reidel Publishing Co.

PULSATING TYPE IV BURSTS AT METRIC WAVELENGTHS AND CORRESPONDING OPTICAL AND MICROWAVE FEATURES

Takeo Kosugi
Tokyo Astronomical Observatory, Mitaka, Tokyo 181, Japan

EXTENDED ABSTRACT

Pulsating type IV solar radio bursts or radio pulsations are characterized by quasi-periodic modulation of meter-wave continuum emission. The main properties of them are summarized by Wild (1973). The aims of this paper are (i) to re-examine the spectral characteristics of the radio pulsations in some more detail using the unified data set of 21 events obtained with the Nobeyama 70 - 600 MHz radiospectrograph (Kai et al., 1980) since September 1977, and (ii) to discuss their association with other flare phenomena such as Hα flares, microwave bursts and so on.

From the spectral study I have found out that, in the cases of about two thirds of the 21 events, the pulsation is confined in a clear frequency band and separated from other type IV or continuum emissions, if any, on the dynamic spectrum. Almost all such events show a type II-like frequency-drift, the drift rate of which is typically - 0.2 MHz/sec at a frequency of about 200 MHz, a little bit smaller than that of the type II burst. I suggest, from the morphological study of the dynamic spectra such as mentioned above, that the radio pulsations can be divided into three subclasses : (i) subclass (A) — Frequency-drift Type, (ii) subclass (B) — Complex or Well-developed Type, and (iii) subclass (C) — Amorphous or Decimetric Type.

The optical associates of the radio pulsations are relatively brilliant flares : among the 21 events, 8 are associated with B-flares, 9 with N-flares, and none with F-flares (2 — no flares reported, 2 — flare patrol report not so far available, in the Solar-Geophysical Data). On the other hand, though 20 out of the 21 radio pulsations are associated with microwave bursts, the intensity of associated microwave bursts are generally very weak : less than 50 s.f.u. at 17 GHz in 16 cases out of the 20.

I have investigated several individual pulsation-associated microwave bursts in detail using the interferometric observations made at 17 GHz at Nobeyama (Nakajima et al., 1980). I suggest that the pulsation at metric wavelengths always has a corresponding component in the associated microwave burst, and also

that the component shows a nature of weak, nonthermal source. One of typical events has been discussed in a separate paper (Kosugi, 1980). I lay stress upon the fact that the interconnection exists between nonthermal microwave source and the pulsation. This observational fact may afford a clue to explain the physical processes involved in the radio pulsation.

References

Kai, K., Sawa, M., Shiomi, Y., Aiba, S., Sekiguchi, H., Shibuya, N., Kosugi, T., and Nakajima, H. : 1980, Publ. Astron. Soc. Japan 32, 371.

Kosugi, T. : 1980, submitted to Solar Phys.

Nakajima, H., Sekiguchi, H., Aiba, S., Shiomi, Y., Kuwabara, T., Sawa, M., Hirabayashi, H., Kosugi, T., and Kai, K. : 1980, Publ. Astron. Soc. Japan (in press).

Wild, J. P. : 1973, in R. Ramaty and R. G. Stone (eds.), 'High Energy Phenomena on the Sun', NASA SP-342, pp589-593.

STELLAR ACTIVITY

A. MANGENEY
Observatoire de Paris

1) INTRODUCTION

Stellar flares were first discovered by Hertzsprung in 1924 as a two magnitude increase, in an unusually short time, of the brightness of the star DHCar

This initial discovery was soon forgotten and one has to wait 1947 to see the subject of stellar flares attract again the attention of the astrophysicists. At that time it was observed that the brightness of the star UV Cet changed by an order of magnitude in three minutes.

Since then, a large observational material has been accumulated, both on the properties of the stars which are the sites of the flaring process, and on the stellar flares themselves.

The general conclusion which comes out when studying this material is that although the energy involved in the stellar flaring process is much larger than in the solar case, solar and stellar flares as well as the associated magnetic activity are of a basically similar character although stellar flare appear to be 2-4 order of magnitude more energetic, and on the average much faster (see Gershberg 1978, for a good review of eruptive stellar phenomena).

2) FLARE STARS

Flare stars, or "UV Ceti type stars" are far from being rare exotic stars. Of the 33 stars which lie within 4 pc of the sun, at least 13 are known to be UV Ceti type flare stars.

They are found in the lower end of the main sequence in the Hertzsprung-Russell diagram, being dwarves of late type (dM), with masses ranging from 0.06 $M_\odot$ to 0.6 $M_\odot$, surface temperatures 2700°K - 4000°K and radius 0.2 to 0.6 $R_\odot$ and which exhibit strong permanent hydrogen line emission (dMe).

Joy and Abt, 1974, have shown that the proportion of flare stars among a particular spectral type increases from a few percent for dM0 stars up to nearly 100 % for dM 5.5 and later type stars.

Statistical studies, reviewed by Gershberg, 1978, indicate that flare activity is inherent for stars, the age of which are within 3 10^5 to 10^{10} years, the older ones having a lower flare activity than younger ones.

As most of the stars with spectral type later than mid F, they present evidence of having stellar chromosphere by showing H and K Calcium emission line. But as pointed out by Giampapa, 1980, the radiative losses due to this emission, estimated by the excess flux in these lines over the expected H and K line flux for a stellar atmosphere in radiative equilibrium, seem to be systematically larger for dMe stars than for non flaring (dM) stars of the same effective temperature.

Similarly, the characteristic presence of the hydrogen Balmer line emission indicates the presence of a hot and dense chromosphere (Gershberg, 1975, Cram and Mullan, 1979) with electron densities of 10^{12} cm^{-3} at the height where the temperature is of the order of 10 000° K.

Based on solar experience it is not unreasonable to expect the Balmer and Ca II H and K emission to predominantly originate in localized active regions.

This is supported by the fact that at times , Balmer emission in excess to the continuum is absent. Moreover the equivalent width of the emission lines show variations of up to a factor of three at times when no flares can be detected photometrically ; with time scales of a day or less, a time too short to allow a uniform chromosphere to respond to a change of its boundary conditions. (Bopp, 1974)

The U.V. spectrum of dwarf stars appear to be generally similar to that of the sun in that they exhibit the typical lines of the transition zone and lower corona. However while quiet dwarves have line ratio and surface fluxes roughly similar to that of the sun, for flare stars, the surface fluxes can be up to 20 times larger and are more reminiscent of a solar active region plage. (see the review by Dupree and Hartmann, 1979).

Let us now end this brief description of the atmosphere of flare stars, by noting that there are now direct evidence of the presence of Coronae in these cool active dwarf stars, thanks to the X-ray observations made on board of the Einstein Satellite (see the review by Vaiana, 1980). Their X-luminosity ranges from 10^{27} to 10^{30} erg/sec with a ratio $L_X/L_{opt} \simeq 10^{-4}$ to 10^{-1}.

Thus these flare stars appear to possess extremely active atmospheres, compa-

red to those of quiet stars of the same spectral class. When looking at many of their properties, it is tempting to interpret this activity as a sign of the presence of active regions, just like on the sun, the various level of atmospheric activity of a particular star being related to percentage of the stellar disk covered by these active regions for that particular star (see Giampapa 1980) .

We are then immediately led to the question: do stellar spots exist also on these stars? The answer is yes. Indeed, among dMe Stars, a number exhibit quasi sinusoïdal variations in their V light, with periods of the order of a few days, and varying phases and amplitudes. This is the so called BY Draconis Syndrome. (see for example Bopp and Espenak 1977).

This is interpreted as a non uniform brightness distribution accross the stellar disk, which combined with the rotation of the star, produces the variation of the light received at the earth. An example taken from Petterson, 1980, is shown in figure 1.

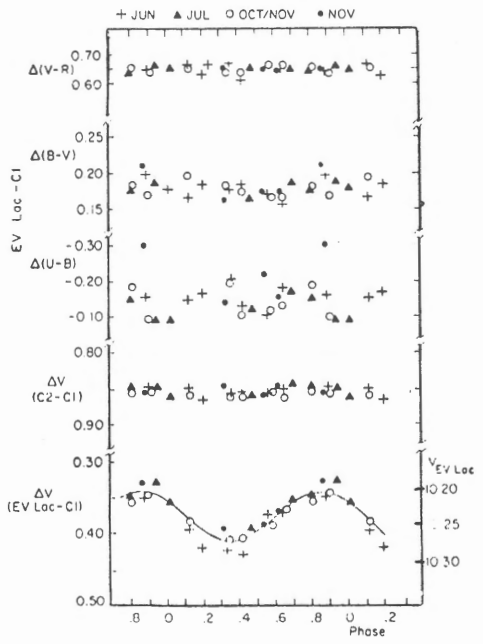

Figure 1. Magnitude and color or EV Lac relative to a nearby comparison star. The right hand scale gives the magnitude of EV Lac itself. The solid curve in the lowest panel result from a fit with a rotation period of 4.378 days (equatorial velocity : 4.2 ± 0.5 km/s ; Pettersen 1980).

A little more than ten stars are known to posses this type of variability but there are good reasons to believe that all dMe stars are affected by it.

All present models rely on the hypothesis of the existence of giant dark spots covering up to 20 % of the visible stellar hemisphere, and temperatures lower by 200 - 1500°K than the surrounding photosphere. The changes in amplitude or phase are then interpreted as the growth or decay of the star spot.

By analogy with the sun, these spots were though to be produced by the emergence of strong magnetic fields.

However, although searches for fields on late type dwarves have be made for quite a long time, it was not until very recently that the direct confirmation by Robinson (1980) of the existence of such fields was obtained. He used a method based on the deconvolution of a field perturbed line profile by that of a very similar field insensitive line. This method, in principle, is not sensitive to the averaging effects which affect the conventionnal stellar field measurements of unresolved bipolar fields regions.

He was able to determine the magnetic field strength for two dMe stars, ξ Boo and 70 Oph A with respective amplitude of 2500-3000 gauss and 1800 gauss, covering respectively 40-45 % and 7-10 % of the star's surface.

3) STELLAR FLARES

Before entering the discussion of stellar flares let us give a very brief overview of what we know of solar flares, as the result of the numerous investigations in the whole spectral range of electromagnetic radiation (see the report from the Skylab Solar Workshop II, Sturrock, 1980).

As far as comparison with stellar flares goes, let us stress that it is now commonly accepted that solar flare regions contain both a hot and a cool plasma.

The latter is responsible for the optical emission which constitutes the much studied " chromospheric flare " as seen for example in Hα . Spectral observations of the optical line emission indicate that they are formed in a thin layer a few ten of kilometers wide, of dense ($n_e \simeq 10^{12} - 10^{13}$ cm^{-3}) chromospheric plasma situated within the lower 5000 km of the solar atmosphere.

The hot, X ray emitting plasma ($\simeq 10^7$°K, $n_e \simeq 10^{10}$ cm^{-3}, emission measure $10^{48} - 10^{50}$ cm^{-3}) is observed at the top of closed magnetic field lines bridging the magnetic neutral line which separates opposite polarity regions of the chromospheric flare. Estimate of the energy content of the thermal X-ray plasma, at

flare maximum, indicate that a major part of the total energy released in the flare goes into that plasma. Thus it can be taken as a good witness of the flare energetics.

The flash phase of duration 10 - 100 seconds is clearly the phase, when the primary energy release takes place ; during that period, magnetic energy is probably transferred to the coronal flare plasma, the temperature of which is sufficiently high to drive, through conduction, chromospheric evaporation, which increases rapidly the density of the X ray plasma as it cools.

The cool plasma, during the process, is heated through various processes : non thermal electrons, thermal conduction, X rays, motions according to its magnetic connection with the corona.

Figure 2, show the result of an extensive statistical study by Drake, 1971, showing the distribution of rise times and total X ray radiated by a large sample of X ray bursts (within the frequency range 2-12 Å).

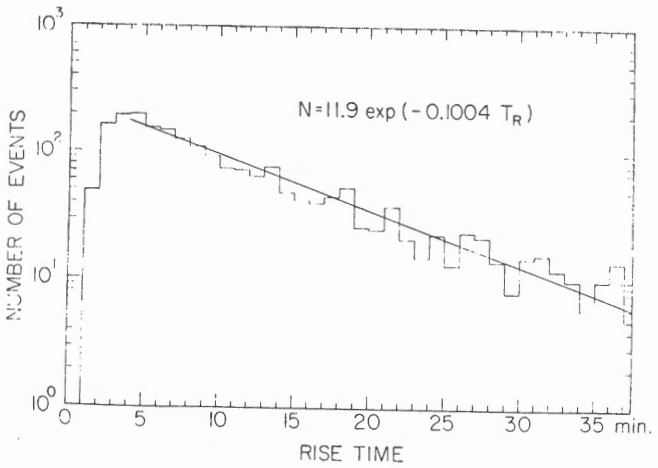

Figure 2a (see legend on next page)

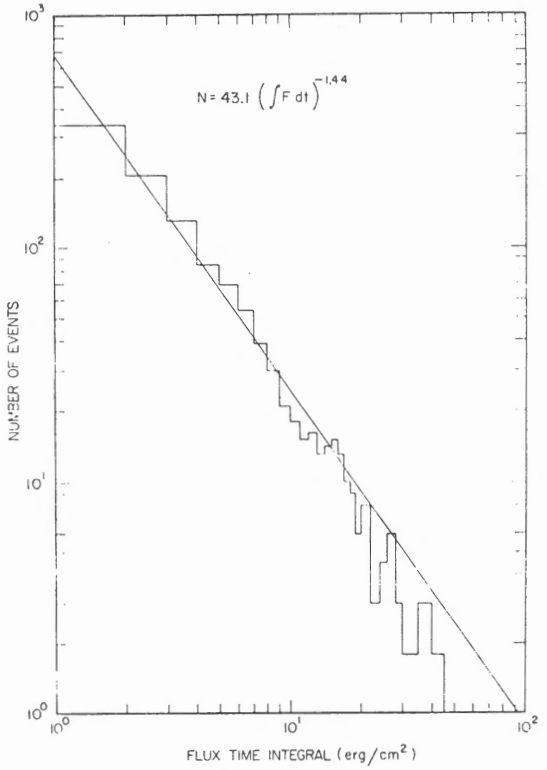

Figure 2b

Figure 2 : a) Differential distribution of 2-12 Å-ray bursts with respect to the value of the time integral of the burst flux for the duration of the burst. The straight line is a least-squares fit over the region indicated.

b) Differential distribution of 2-12 Å-ray bursts with respect to rise time. The straight line is a least-squares fit over the region indicated. (Drake, 1971).

On the other hand, Kahler, 1978, by comparing X-ray images and X-ray flux profiles was able to show a number of correlations between rise time, energy and the flare loop morphology. For example :

rise time t_r (minutes) = 0.63 $V^{0.34}$

energy E (ergs) = 0.11 $V^{0.60}$ (V : flaring volume)

Let us now come to stellar flares.

Most of the stellar flares observations have been made in the optical domain, and it is only very recently that a much wider frequency coverage has been obtained.

In the optical domain, a light curve for a typical flare is characterised by a sharp spike of enhanced brightness (rise time of the order of a few seconds to a few minutes, i.e. much shorter than for a typical solar flare) followed by a much slower phase of return towards "quiet" brightness level (this phase may last from a few minutes to several hours). In figure 3, is shown the light curve for a flare on the prototype star UV Ceti (Bopp and Moffet, 1973) which exhibits these characteristics, together with the timing of the various radiative processes which characterise the optical flare : enhancement of the hydrogen emission lines, of Ca II, He I, occasionally He II, just as in solar flares.

Note however that not all flares have this spiky structure ; some have a much more gradual rise and fall ("slow flares"). Only in spike flares, is the continuum also enhanced during the fastest phase of the flare process.

The flares certainly originate from localised region of the stellar disks since 1) cold atmosphere characteristics (such as the TiO absorption band) persist in the stellar spectra during a flare, 2) the smallest flare time scales have proven to be smaller than the time needed for ligth to travel accross the stellar disk.

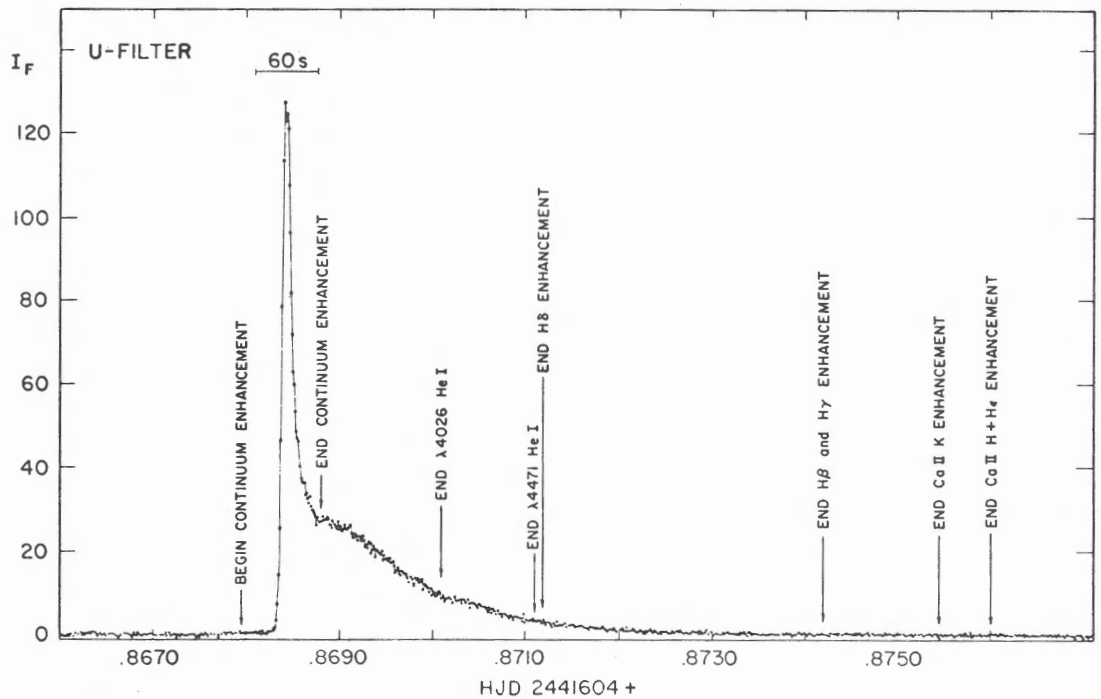

Figure 3. Light curve of a flare on UV Ceti in U-bandpass with integration time of 1 s. Vertical arrows indicate the times at which the various spectral features were noted ($I_f = \frac{I(t) + I_o}{I_o}$; I_o "quiet"intensity, I(t) total intensity) (Bopp, Moffet, 1973).

A number of empirical relations have been shown to relate some characteristics of the flares with the absolute visual magnitude M_V or effective temperature of the star. For example the duration T of the flash phase has a relatively well definite value for a given star and varies like

$$\log T = 2.862 - 0.119\, M_V \qquad (T \text{ in seconds})$$

from star to star, while a flare of ultraviolet magnitude U occur at a mean rate R(U).

$$R(U) = e^{\alpha (U - U_o)} \text{ per day}$$

where α is roughly independant of the star, $\alpha \simeq 0.9 - 1$, whereas the "typical" ultraviolet flare magnitude U_o varies from star to star (Kunkel, 1975). Another piece of information concerns the total visible energy emitted during the duration of the flare was obtained by Lacy et al, 1976. In figure 4 the frequency of flare occurence versus the energy of flares is shown for UV Ceti, and exhibits a remarquable saturation at low energy.

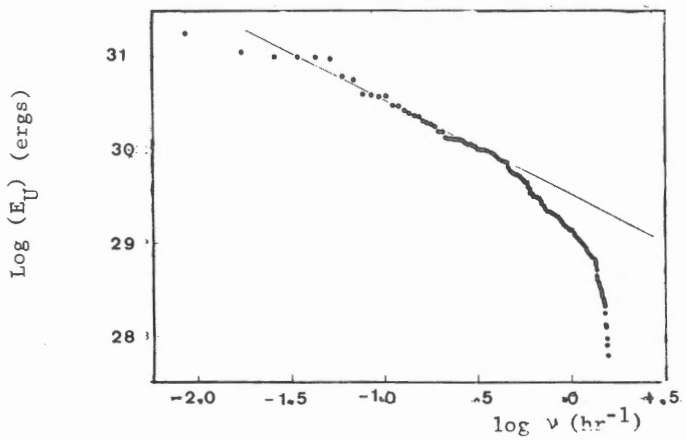

Figure 4. UV Cet cumulative distribution of flare energy as derived from U data.

As pointed out by Rosner and Vaiana, 1978, this is hardly interpretable by selection effects due to the difficulty of detecting low energy flares, since then one would expect the frequency of flares to decrease below a certain energy threshold. Furthermore all dMe stars studied by Lacy et al, covering a wide bande of quiescent luminosity, exhibit the same behaviour.

Thus this reflects most probably a intrinsic behaviour of the stellar flare mechanism. When comparing to the figure (2a), one notices that no such behaviour appears in the solar case.

Finally let us mention that

a) It appears that (Lacy et al, 1976) intrinsically brighter stars have more energetic but much less frequent flares than fainter ones. This law must clearly break for luminosity smaller than the solar one, since it would predict much more energetic flares than actually observed.

b) The flare activity of a particular star measured for example by the excess intensity emitted by flares in a given spectral band, during a certain time, divided by that time, correlates well with the indices of chromospheric activity as defined above. See figure 5, Gershberg et al, 1971)

3b) The radio flare

The first positive detection of radioemission from the flare star UV Ceti was reported in 1968 by Lovell et all (1968).

In figure 6 B shown a radioburst observed at 196 and 3/8 MHz and associated with a flare on Wolf 424 (Spangler and Moffett, 1976). These radiobursts are several Jy in amplitude and may have durations from several seconds up to several hours.

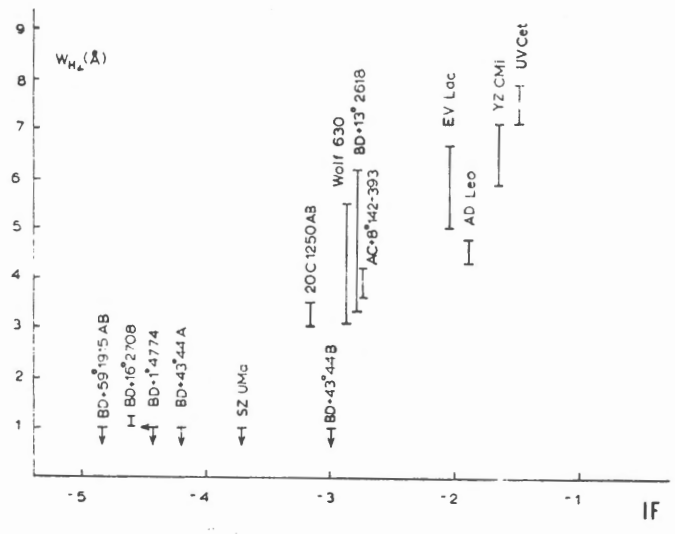

Figure 5 a) Correlation between flare activity levels of stars and H_α emission equivalent width in their quiet state spectra.

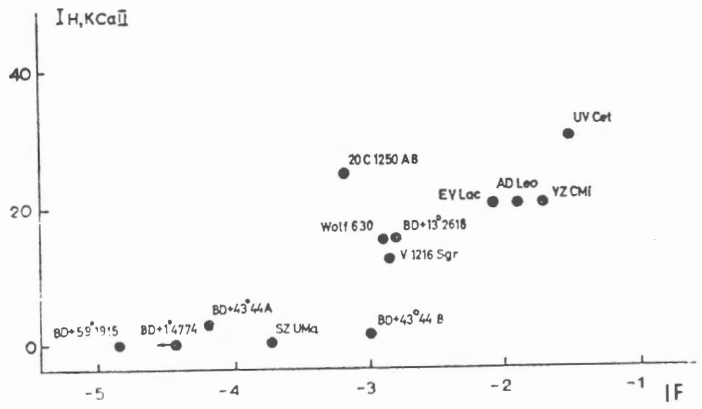

Figure 5 b) Correlation between flare activity levels of stars and Ca emission intensities in their quiet state spectra.
(The flare activity index IF is a measure of the energy emitted by the flaring process by unit time, Gersherg et al, 1971).

Recently, Nelson et al (1979) have undertaken a correlative study of optical and radio emission of flares on 14 flares stars.

They observed, with the Culzoora Radioheliograph (80 and 160 Mhz) meter wave emission of variable intensity originating from the close vicinity of 11 of the examined stars.

A typical radio burst duration was $\sim$ 2 hours ; some were highly circularly polarized ; the intensity ratio between the two observing frequencies indicate a non thermal spectrum.

Evidence from the positions of the flare sources at 160 Mhz suggest that the burst sources are, at least in some cases, displaced from the star. Their brightness temperature at 80 Mhz is $\sim 10^{14} - 10^{15}$ °K if they are assumed to cover $\sim$ 1 % of the stellar disk ; this rules out any explanation in terms of incoherent emission.

The relationship between optical and radioflares is a very complex one ; one does not observe any correlation between the respective amplitudes of the optical

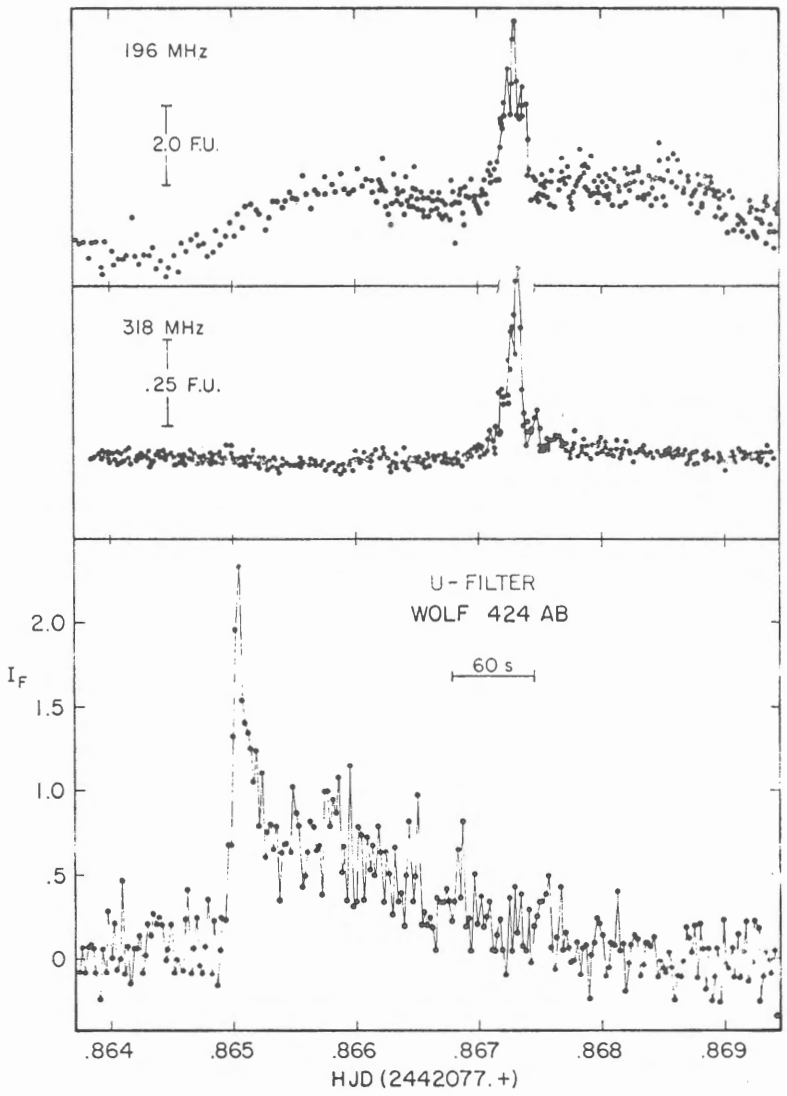

Figure 6 . Optical and radio observations of flare from Wolf 424, 1974 January 30 (Spangler and Moffet, 1976).

and radio emissions. The time delay between these two emissions is extremely variable ; the radio burst can occur before the radio event, or up to 5 minutes later, as one would expect from a perturbation travelling from the flare site to the outer layers of the star (Kahn, 1974).

3c) The EUVX flare

Detection of transient X-ray emission from YZ CHi and UV Ceti (Heise et al, 1975), and transient EUV emission from Proxima Centauri (Heish et al, 1977) widened considerably the wavelength range over which stellar flares could be observed.

Recently Hahn et al, 1979, obtained with the A.2 experiment on board HEAO 1, the first X-ray spectrum of s stellar flare on AT MIC ; they concluded that this spectrum is consistent with the thermal emission of a 4 Kev plasma, with its 6.7 kev iron Kα line.

The total X-ray luminosity L_X during this particular flare was $\simeq 10^{31}$ergs/s, and the emission measure EM $\simeq 10^{54}$ cm^{-3} (compare with typical values for a solar flare $L_X \simeq 10^{27}$ ergs/s, EM $\simeq 6\ 10^{49}$ for a very large solar flare).

Combining their own observations and previous ones, Kahn et al, assuming that all soft X-ray or EUV emission was of a thermal nature, and estimating the optical luminosity of the corresponding flares when they were no directly available by using the empirical laws mentionned above, were able to derive the ratio L_X/L_{opt} for eigth stellar flares. Although there is a large scatter in the values of L_X/L_{opt} they are systematically larger than those predicted by a model by Mullan, 1976, based on conductive cooling of the soft X-ray flare plasma.

CONCLUSION

In view of the recent developments of the diagnostic of chromosphere-coronae-stellar wind complexes, the phenomenon of flare stars poses an intriguing problem.

One of the outstanding results of these last years in the physics of stellar atmosphere has been to show that among late type stars, which all show sign of chromospheres some had very active ones (Linsky, 1980), which presumably are related to the presence of extended solar plage-like regions, i.e. to strong magnetic field eruption at the stellar surface.

Flare stars certainly belong to the class of stars with active chromospheres. Now why do the signs of flare activity disappear with increasing stellar mass, the earliest stellar type for which flaring has been detected being dK 7 ?

Most probably the answer must be related to the interaction between the convection and rotation in stars. Indeed, there are some indications for stars with active chromospheres being also fast rotators ; in that respect, flare stars for which the rotation has been measured using the BY Draconis syndrome, show faster rotation that quiet stars of the same stellar type.

They are also in the range of masses where the convection zone covers a significant portion of the stellar radius and eventually for masses $\sim 0.2\ M_{\odot}$ the whole stellar radius.

In that case, it is reasonable to expect that these stars will have different patterns of differential rotation than stars with shallow convection like the sun (Gilman, 1980). In particular the scales of the dominant modes, and the influence of rotation or convection will be larger than for stars of the same type but with slow rotation.

Thus one expects, if dynamo theories of the $\alpha\omega$ - type are at work in these stars (Mullan, 1974), that the generated fields have large values, and exhibit clearly large scale coherence, an occurrence which could modify the process of emergence of fields at the stellar surface.

That subject is still a matter of controversy in the case of the sun ; flare stars may help to progress in the understanding of this basic mecanism of stellar activity by providing example of stars with different regime of rotation and convection. This touches the question of comparability of solar and stellar activity.

Indeed, the sun is a slowly rotating star, with a " quiescent " chromosphere, compared to other stars of the same spectral type (see Smith, 1980).

This most probably explains, why the physics of the fine details of stellar flare activity is so similar between the sun and flare stars, there are nevertheless strong differences between the two kind of objects.

A number of related questions are : are there spot cycles in flare stars, possibly masked by the intense sporadic activity ? What becomes of the convective flux blocked in the giant star spots ? (Hartmann and Rosner, 1979) What is the effect of magnetic braking due to flaring on the distribution of angular momentum ? etc... (Carasco et al, 1980).

Finally let us mention that magnetic activity related to fast rotation is increasingly invoked to explain phenomena like those occuring in T. Tauri stars, RSCVn binaries etc... (Gershberg 1978, Hall, 1980).

REFERENCES

Bopp, B.W., 1974, Mon. Not. R. Astr. Soc, 166, 79

Bopp, B.W., Espenak, F., 1977, Astron. J. 82, 916

Bopp, B.W., Moffett, T.J., Ap.J. 185, 239

Carasco, L., Franco, J., Roth, M., 1980, Astron. Astrophys. 86, 217.

Cram, L.E., Mullan, D.J., 1979, Ap.J. 234, 579.

Drake, J.F., 1971, Solar Phys. 16, 152

Dupree, A.K., Hartmann, L., 1979, in "IAU Colloquium n° 51, edited by Gray and Linsky, Springer Verlag, Berlin, p. 279.

Gershberg, R.E., 1975, in "Variable stars and Stellar evolution" edited by Sherwood and Plaut, Reidel, Dordrecht, p. 47

Gershberg, R.E., 1978, Mem. S.A. It., 49, 781

Gershberg, R.E., Shakhoskaya, N.T., 1971, IAU Colloquium n° 15 (Bamberg), p. 126.

Giampapa, M.S., 1980, paper presented at the high energy astrophysics division Meeting

Gilman, P.A., 1980, in "Stellar Turbulence", IAU Colloquium n° 51, edited by Gray and Linsky, Springer Verlag, Berlin, p. 279

Haish, B.M., Linsky, J.L., Lampton, J.L., Paresce, F., Margon, B., Stern, R., 1977, Ap.J., 213, L 119

Hall, D.S., 1980, Highlights in Astronomy 5, 84

Hartmann, L., Davis, R., Dupree, A.K., Raymond, J., Schmidtje, P.C., Wing, R.F., 1979, Ap.J., 233, L69

Hartmann, L., Rosner, R., 1979, Ap.J., 230, 802

Heise, J., Bruckman, A.C., Schrivjer, J., Mewe, R., Gronenshild, E., Den Boggard, A., Grindlay, J., 197 J, Ap.J. 202, L73

Joy, A.H., Abt, H.A., 1974, Ap.J. Suppl. 28, 1

Kahler, S., 1978, Solar Phys. 59, 87

Kahn, F.D., 1974, Nature 250, 125

Kahn, S.M., Linsky, J.L., Mason, K.O., Haisch, B.M., Bower, C.S., White N.E., Pravdo, S.H., 1979, Ap.J. 234, L 107

Kunkel, W.E., 1975, in "Variable stars and Stellar evolution", IAU Symposium n° 67, Reidel, Dordrecht, p. 15

Lacy H.L., Moffett, T.J., Evans, D.S., Ap.J. Suppl. 30, 85.

Linsky, J.L., 1980, paper presented at the high energy astrophysics division Meeting.

Linsky, J.L., 1980, in "Stellar turbulence", IAU Colloquium n° 51, edited by Gray and Linsky, Springer Verlag , Berlin, p. 248

Mullan, D.J., 1974, Ap.J. 192, 149

Mullan, D.J., 1976, Ap.J. 204, 530

Nelson, G.J., Robison, R.D., Slee, O.B., Fielding, G., Page A-A, Walker, W.S.G., 1979, Mon. Not. R. Astr. Soc. 187, 405

Pettersen, B.R., 1980, Astron. J., 85, 871

Robinson, R.D., Worden S.P., Harvey J.W., 1980, Ap.J. 236, L 155

Rosner, R., Vaiana, G.S., 1978, Ap.J. 222, 1104.

Smith, M.A., 1980, Highlights in Astronomy 5, 827

Spangler, S.R., Moffett, T.J., 1976, Ap.J., 203, 497

Sturrock, P.A., 1980, editor, "Solar Flares", Skylab Solar Worshop II, Colorado Associated University Press, Boulder.

SOME COMMENTS ON THE PROPAGATION OF ALFVEN WAVES IN AN ATMOSPHERE.

B. LEROY
Observatoire de Paris, Département d'Astrophysique Fondamentale, 92190 Meudon,France.

The transverse character of Alfvén waves makes them virtually undetectable. This, however, is no reason why they should not contribute to the energy balance of the solar chromosphere and corona. Now, when astronomers refer to Alfvén waves in the solar atmosphere, they very often (if not always) fail to take into account the density stratification of the atmosphere. The reason for this is of technical order: under the assumption of a uniform medium the propagation of Alfvén waves is in many respects comparable with that of sound waves. In this short communication we wish to point out the effects of the density stratification on the propagation of Alfvén waves.

In the case of a uniform magnetic field being at an arbitrary angle to the (vertical) uniform gravity field, the equations of motion are coupled to each other; thus thus describing complicated interactions between the different types of waves susceptible of existence in an atmosphere in hydrostatic equilibrium permeated by a magnetic field (Leroy and Bel,1979). Under certain conditions Alfvén waves decouple from the magneto-acoustic-gravity waves (Leroy, 1980a). One case is when the magnetic field is aligned with the gravity field and that only vertical propagation is considered; in teh following, we limit our study to this particular situation.

For the sake of mathematical simplicity the solar atmosphere is assumed to be plan-parallel. The photosphere and low chromosphere are represented by an isothermal layer comprised within the altitudes z=0 (top of the convection zone) and z=2000 km. At this altitude lies the transition region, which is represented by a density discontinuity. Above the transition zone there is another isothermal layer, representing the corona. The parameters necessary for the description of the photosphere and low chromosphere on the one hand, and of the corona of the other, are determined from the HSRA model and the "average" corona as given by Athay (1976),respectively.

In a real atmosphere the magnetic field is not constant and the density does

not decrease exponentially with height. As a result, for a fixed value of the wave period, there exists a height above which the stratified medium behaves as if non-stratified. Roughly speaking, the effect of stratification is to induce reflection of the waves. This is easily understood if one regards the stratified medium as a pile of slabs of constant density, with a density discontinuity between two neighbouring slabs. In the case of the solar atmosphere, it can be shown that the waves whose period is less than, say, 10^5s "see" the part of the corona located above z=3 $R_\odot$ as a non-stratified medium (Leroy, 1980b); in other words, once arrived in this part of the corona, the waves suffer no further reflection.

The question we wish to answer is the following: under the assumption of the Alfvén waves being generated by the motions in the convection zone, how much energy flux will be recorded in the form of Alfvén waves at heights $z \geq 3R_\odot$?

The equation governing the propagation of Alfvén waves in the solar atmosphere is (assuming a time dependence $\exp(i\omega t)$):

$$d^2a/dz^2+(4\pi\rho(z)\omega^2/B^2)a = 0, \qquad (1)$$

where a is the wave amplitude. If convection is thought of as some driving mechanism shaking the field lines, and thereby generating Alfvén waves, a reasonable boundary condition to be imposed on Eq.(1) is that the velocity amplitude be given at the base of the photosphere. A second boundary condition is that no Alfvén wave (in the range of period of interest) shall come into the corona from above z= $3R_\odot$.

Having solved Eq.(1) with these boundary conditions one can determine the transmissivity of the solar atmosphere with respect to Alfvén waves as a function of the wave period. The result is plotted on Fig.1. For extremely short periods (not shown on the figure) the media lying on either side of the transition zone are "seen" by the waves as non-stratified media; as a consequence, the transmissivity is constant and assumes its eikonal value, which is here of about 25%. For extremely long periods, the transmissivity turns out to be also constant, assuming a rather low value of about 10^{-7}. Between these two limits the most striking feature of the transmissivity is its resonant behaviour at certain discrete values of the wave period. We have been able to show that these values correspond to resonances in the layer representing the corona. They are not due, as claimed by Hollweg (1972,1978), to the discontinuity in scale height at the transition zone.

It is worth mentioning that, except for the resonant peaks, the actual values

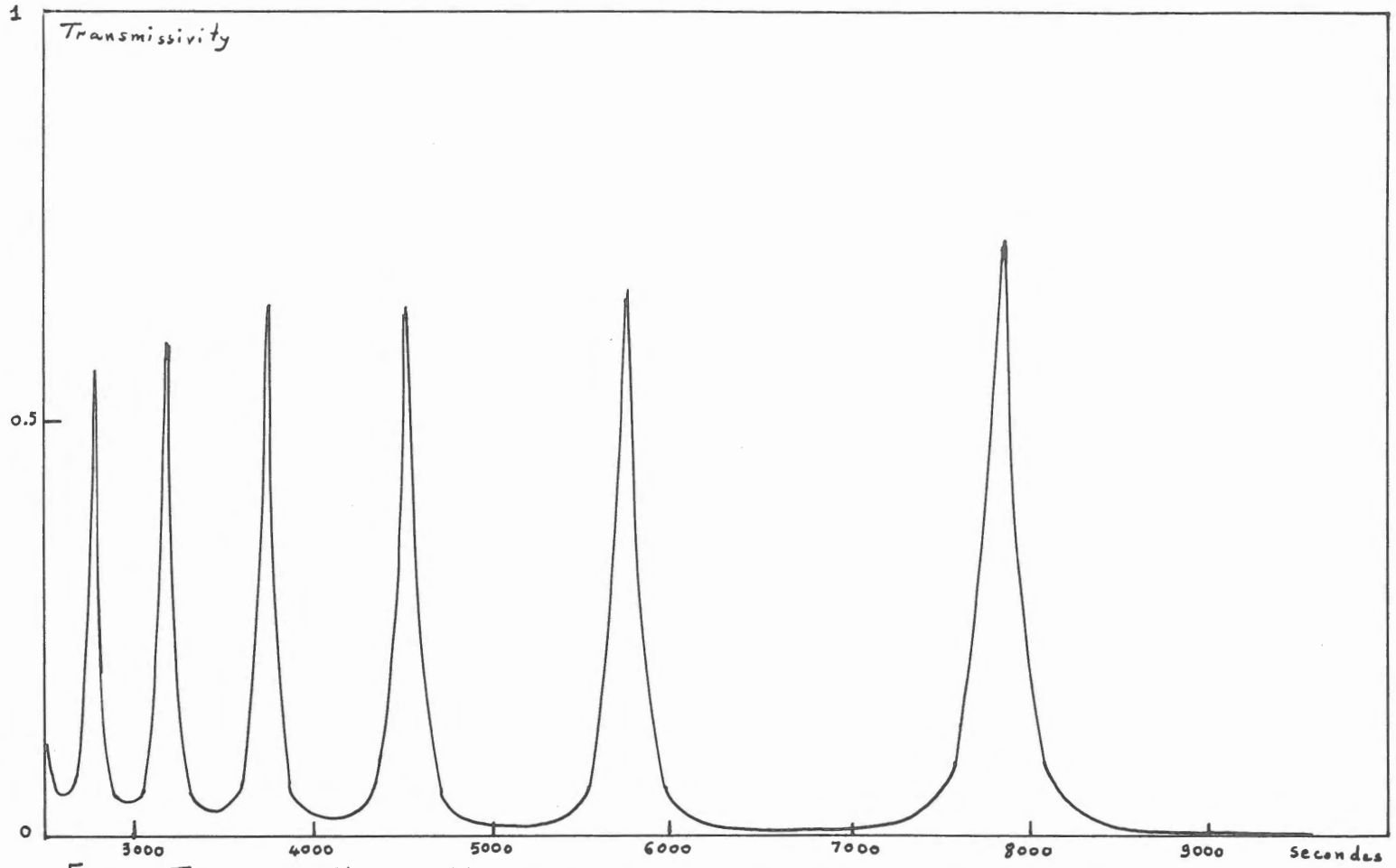

Fig.1 : Transmissivity vs. Wave period.

of the transmissivity always lie below the eikonal value. This implies that the energy flux recorded at $z \gtrsim 3R_\odot$ will generally be less than its eikonal value. As a consequence, one can say that the solar atmosphere is rather opaque to Alfvén waves, except at certain discrete frequencies.

Expressions for the relative velocity amplitude and the relative magnetic fluctuations as a function of the wave period can be derived. A numerical anlysis of these expressions reveals that both are oscillating functions and that both display a resonant behaviour. However, whereas the relative velocity amplitude all in all assumes rather low values in the photosphere and low chromosphere, less than 10^{-2}, it increases more rapidly than $\rho^{-1/4}$ (as the eikonal approximation would require) to values of the order of 10 at $z= 3R_\odot$. As a consequence, non linearities (e.g., shocks) are likely to develop at lower altitudes than is usually believed on the basis of the eikonal approximation. The magnetic fluctuations as a function of period are much alike the velocity amplitude. However, their dependence on height is rather insignificant, and they assume extremely small values, typically less than 10^{-5}. Finally, let us mention that an increase in the magnetic field just shifts the curve on Fig.1 as a whole towards the short periods. As a result, the solar atmosphere is still more opaque to Alfvén waves. Heating of the upper chromosphere and corona by Alfvén waves therefore appears to be very difficult.

Without going into details, let us mention another consequence of this study. When one computes the energy flux recorded at $z= 3R_\odot$, and not only the transmissivity, one finds a function which display still much more resonant peaks (at any rate, far more than in Hollweg's work); this implies, following the same line of reasoning as Hollweg's, that Alfvén waves detected in the solar wind are not generated in the convection zone.

References:

Athay, R. G.:1976,The Solar Chromosphere and Corona: Quiet Sun,Reidel, p.330.

Hollweg,J.V.:1972, Cosmic Electrodyn.2, 423.

1978, Solar Physics 56, 305.

Leroy,B.: 1980a, Astron. Astrophys. (in preparation).

1980b, Astron. Astrophys. (in press).

Leroy,B. and Bel,N.: 1979, Astron. Astrophys. 78, 129.

ON THE EXISTENCE OF HOT CORONAE IN HOT STAR WINDS

Jean-Pierre J. LAFON
Observatoire de Meudon
Département Recherches Spatiales
92190 - Meudon (France)

It is now well known that early type stars, like O and B stars, loose mass at a very high rate (10^{-6}-10^{-5} M_o/yr). Besides, observed P-Cygni line profiles in ultrviolet radiation indicate that the outer layers of their extended atmospheres are moving with large expansion velocities (600-3000 Km/s). Both phenomena seem to occur under the form of rather steady state regimes, at least for O and B type stars. This communication is concerned with the mechanism which produces the motion of the matter.

This mechanism is far from being cleared up. It is established that Parker's (1958) mechanism, i.e. The thermal expansion of a gravitating gas in a vacuum in the case where the force due to the thermal pressure can exceed gravity is not sufficient in this case: even if the total thermal energy was converted into kinetic energy, expansion velocities could be of the observed order of magnitude only for coronal temperatures like 10^7°K, for which the observed ions (CIV, NV, SiIV) would be destroyed by collisional ionisation. Now, since the stars under consideration are very luminous, one can think that the radiative pressure is active and drives the wind. Of course, this is the basic assumption of papers dealing with models of dynamically consistent winds for hot stars (Lucy and Solomon, 1970; Castor, Abbot and Klein, 1975). In such an approach of the problem the equations describing the radiative transfer and the statistical equilibrium must be solved together with equations describing dynamics: this is a formidable numerical problem which, for time being, cannot be solved without rather crude approximations.

The models are based on the usual assumptions concerning no time dependance (steady state) and spherical symmetry (rotation and magnetic field are assumed negligible so far as the dynamics of the wind is concerned). Radiative equilibrium is also assumed throughout the extended atmosphere. The equations solved are those describing mass conservation and momentum transport, assuming that the whole momentum supplied to the highly ionised atoms (carbon, oxygen ...) is transmitted by strong collisions to the protons which, with electrons, are the major components of the extended atmosphere.

The differences come mainly from the computation of the radiative force appearing in the equation describing the momentum transport. The main drawback of the most sophisticated model (Castor, Abbot and Klein, 1975) is that the radiative force is estimated as a purely local function of the velocity gradient ($\sim (dv/dr)^{\alpha}$) based on Sobolev's approximation (large velocity gradients) throughout the extended atmosphere.

First, concerning physics, this assumption is not reliable for all radial distances for which it should be. Indeed, the condition that the solution is required to satisfy in the outer part of the wind expresses the existence of non negligible thermal effects in the wind at large radial distances of the order of 10^4 stellar radii. Thus, the mathematical expression of the radiative force should be a good approximation up to such radial distances at least. However, because of the decrease of the velocity gradient (the velocity tends to the

terminal velocity) Sobolev's approximation breaks for radial distances much smaller than 10^3 stellar radii (Leroy and Lafon, 1980a). Moreover, for radial distances of the order of 10^4 stellar radii the wind is very tenuous and its interaction with the surrounding medium should be taken into account, so that a condition derived from the only physics of a spherically symmetric expanding atmosphere is probably irrelevant (for instance the spherical symmetry may be upset, the ionisation may be changed ...).

On the other hand, the assumption could be allowable only if the processes governing the wind structure were active mainly in the supersonic part of the wind (out of which Sobolev's approximation breaks) and if those active in the subsonic part of the wind were much less important and could be described very crudely. Now, using a new model based on a full solution of a simplified transfer equation (continuum + lines modelized with a picket-fence model), Leroy and Lafon (1980b) solved the coupled radiative and hydrodynamical equations simultaneously. They did not get rid of the strongly non local nature of the radiative transfer and did not neglect the inner boundary conditions concerning radiation (thermalization): the results show that these two phenomena are very important and, through the way in which the radiative force increases at the base of the wind, govern the mass loss and the terminal velocity. Besides it was noted that thermal effects at large distances produce weak effects and cannot be crucial for the topology of the density and velocity profiles.

Then, from a mathematical point of view, the expression of the radiative force as a function of the radial distance, the local velocity gradient, the whole velocity profile throughout the extended atmosphere is crucial for the existence, thenature, the location of a critical point for the velocity profile. For instance, if one expresses the radiative force as a function of the only local velocity gradient, one finds a critical point different in nature from that of Parker's type solutions and distinct from the sonic point at which the velocity reaches the thermal velocity (Castor Abbot and Klein, 1975). This can alter in a non negligible way the structure of the solution and so the derived terminal velocity and mass loss rates (Leroy and Lafon, 1980a,b).

Finally, Leroy and Lafon (1980b) found that, for realistic star parameters like those of Zeta Puppis, driving forces taking into account the inner radiative boundary conditions and the non local properties of radiative transfer do not allow winds with both realistic terminal velocities and realistic mass loss rates. Roughly, the reason why this happens is that the radiative force increases with radial distance too slowly to become efficient as soon as the force due to the thermal pressure becomes small.

Thus, under the assumption of no additionnal heating, in the case where radiative equilibrium holds throughout the extended atmosphere, the radiative force seems not to be sufficient to drive the observed winds. One is lead to think that, in fact, the radiative equilibrium can be disrupted somewhere so that the temperature no longer decreases smoothly from the photosphere to infinity: in other words a hot corona may exist. Upon these grounds we can propose the following scheme illustrated by the figure:

The curve represents the temperature T as a function of the radial distance r. Close to the photosphere T is of the order of T_{eff}, the effective temperature. Farther, there is a thin region of width H where some energy is dissipated, leading to a high temperature like a coronal temperature. At larger r the

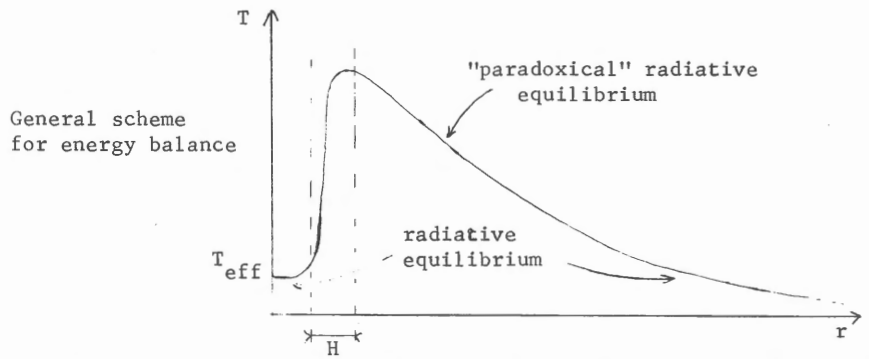

radiative equilibrium holds; thus there is a region in which the radiative equilibrium can be called "paradoxical" in the sense that the temperature can be large compared to the usual radiative equilibrium temperatures ($\lesssim T_{eff}$) because it has to fit in with that in the thin corona.

Assuming that the corona is heated by dissipation of acoustic waves, one can estimate thet H is of the order of 10^{-5} stellar radii, which is much smaller than the scale height of density ($\approx 10^{-3}$ stellar radii). Although this region is very thin it is large enough to account for the presence of highly ionized atoms such as OVI if produced by X-rays according to Cassinelli's and Olson's (1979) mechanism. Of course the corona may be heated by another (magnetic?) source of energy.

In any case, a localized dissipation of energy (the cause of which is to be found) in a very thin region may give rise to a thick hot region that can change strongly the dynamics and finally explain the observed winds.

REFERENCES

- Cassinelli J.P. and Olson G., Astrophys. J., 229, 1979, 304
- Castor J.I., Abbot D.C. and Klein R.I., Astrophys. J., 195, 1975, 157
- Leroy M. and Lafon J.-P.J., On the importance of boundary conditions and non local properties of radiative transfer coupled with hydrodynamics in hot star winds, 1980a
  Can hot star winds be driven by radiation pressure? I and II, 1980b
  Rpt DESPA 202 Observatoire de Meudon; 92190 Meudon (France). To appear.
- Parker E.N., Astrophys. J., 128, 1958, 664

MAGNETIC FIELD OBSERVATIONS IN MEUDON OBSERVATORY

Jean Rayrole
Observatoire de Paris-Meudon

I am going to discuss the problems which are raised in magnetic field observations by describing the French project "THEMIS[1]" and the new photoelectric magnetograph operating in Meudon Observatory since April 1980.

Before that, I would like to discuss two important points for the future in Solar Physics :

1) Why optical Solar Research must be pursued in the future ?
2) Why do we have a need of new ground-based instruments ?

These two points have been discussed recently by C. Zwaan in an European JOSO report :

The sun is the only star that can be observed with sufficient spatial, temporal and spectral resolution to investigate structures and process occurring in parts of its atmosphere which are much smaller than the visible hemisphere. Consequently there is a large class of astrophysical problems which can be studied best or exclusively in the sun.

The advantages of the optical solar research are due to the facts that the deepest part of the solar atmosphere, which is the top of the convection zone, can only be studied in the optical window where the atmosphere is most transparent to continuum radiation.

Structures and process which connect the convection zone with the outer layer can be followed through all the atmosphere by using continuum windows and spectral line profiles.

Many of the problems occur in structures of a very small horizontal extent and many of them are magnetic. The evolution times of the various structures range from seconds to days.

---

(1) T.H.E.M.I.S. Telescope Heliographique pour l'Etude du Magnétisme et des Instabilités Solaires.

These considerations lead to the following requirements :

1) High spatial resolution in the horizontal direction

2) Sufficient resolution in height, which requires observations in several spectral lines simultaneously

3) Adequate time coverage to follow the evolution of individual structures

4) Sufficient spectral resolution

5) Accurate polarization measurements.

Observations with a high spatial resolution may be obtained in space. Ultraviolet and Infra-red observations can be only made in plane, balloons, rockets or satellites. However, space instruments are limited in volume, weight and time operation.

Space observations can never replace ground-based observatories ; on the contrary they are complementary but ground-based instruments must be put in the best sites.

Magnetic field is one of the most important physical parameters in star atmosphere. The dimension of individual force tubes is of the order of the scale height of the atmosphere, so as good as the resolution we could hope, in ground-base or in space, the geometrical structures of such features could not be observed directly. The only way to solve the problems is to progress in theoretical model computation in order to be able to obtain good coherence between several simultaneous determinations of the same observed physical parameters with different lines.

The knowledge of such features distribution with solar latitude and the phase of the solar cycle will be of the greatest interest for dynamo theory.

The study of MHD waves in fine magnetic structures is necessary to understand heating mechanism.

The determination of current density (i.e. determination of the vector $\vec{B}$) is essential to study the dynamics of active regions and instability process.

For the future, new solar instruments should be designed in this way. The French project "THEMIS" is a solution.

A perfect magnetograph should allow :

1) Observations of the magnetic vector $\vec{B}$.

2) Simultaneous observations of a great number of lines the profiles of

which depend differently on the physical parameters (temperature, pressure, density...) defining the solar atmosphere at each point.

3) To be used simultaneously with different observational techniques in order to control coherence between several independant determinations of the same parameter.

The first condition requires the instrument to be free of effects due to instrumental polarization. The structure of the instrument and the place of the polarization analyser have been designed so that the instrumental polarization does not interfere with the shape of line profiles.

The second condition is satisfied by a spectrograph predisperser followed by an echelle spectrograph having a useful field corresponding to the free spectral range of the grating. Selective slits situated in the first spectrum allow simultaneous isolation of a great number of lines in a wide spectral range.

The third condition is satisfied by designing the polarization analyser to obtain the whole profiles of the different lines. These profiles will be recorded either on a photographic receiver or on a photoelectric one by using integrated diode arrays. The computer treatment of recorded profiles allows one to define and to change at will and a posteriori the reduction process.

Principle of THEMIS (Figure 1)

A vacuum Cassegrain Telescope pointed to the sun focuses a solar image on the spectrograph slit. Behind it, we put achromatic crystalline plates, a quarter of wavelength for the linear polarization or a modulated electro-optic crystal. The axis of these plates are both parallel and perpendicular to the spectrograph slit. Then we put two quartz crystal the sides of which are cut at 45° of the crystallography axe. In relation one to the other, they are crossed and directed so that the two crosses linear beams they transmit have the same optical length and are polarized at 45° of the entrance slit.

At this stage the polarimetric analysis of the light is finished so that the polarization state has the least interference with the instrument. Then nothing can change the shape of the line profiles if one can separate completely the two beams given by the analyser at the spectrograph exit. The predisperser characteristics and the echelle spectrograph allow this separation without any pollution. The dispersions of the two spectrograph being correctly choosen by changing the distance between P2 and P3, we are able to do that for any lines and simultaneously for a great number of lines.

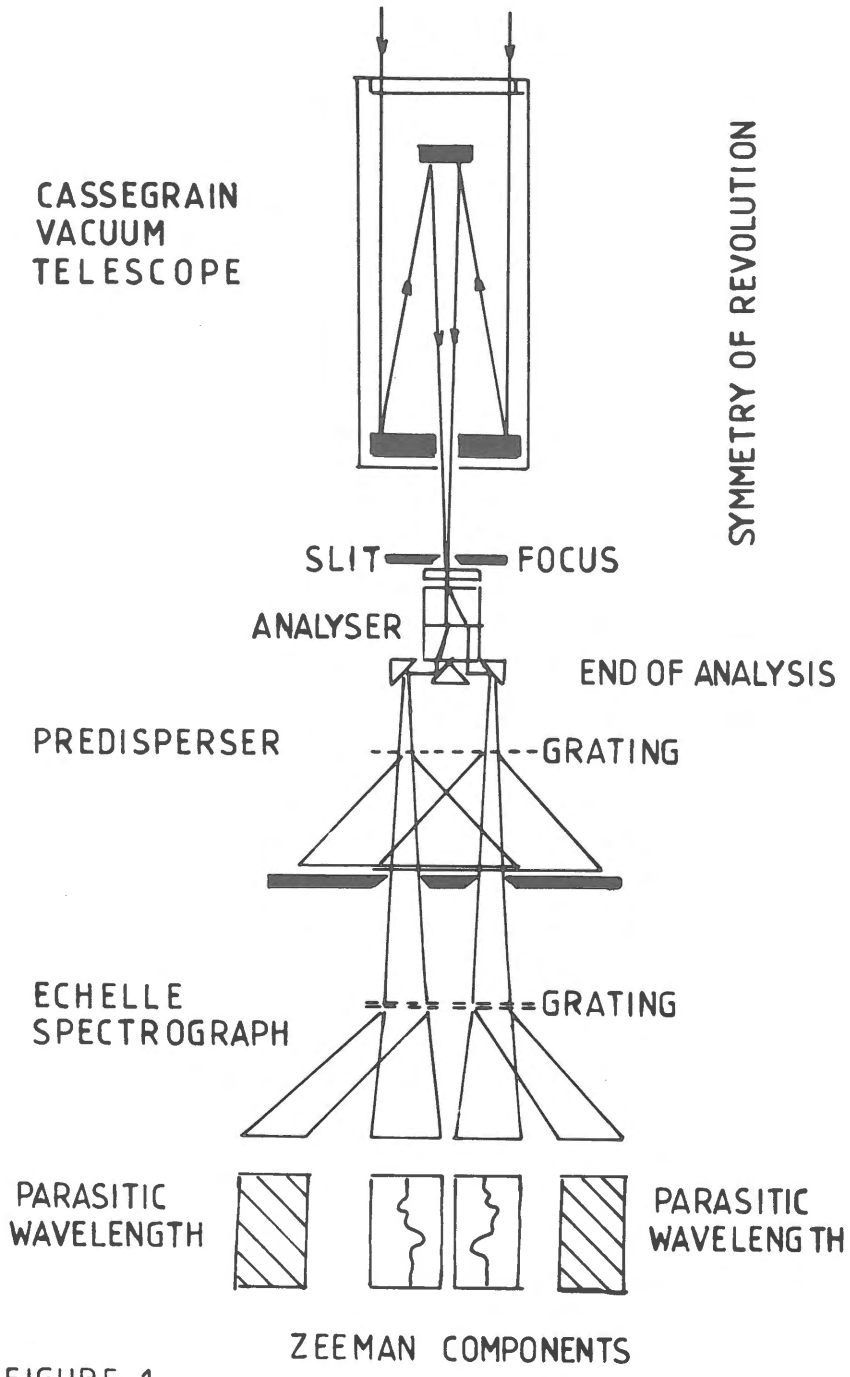
CASSEGRAIN
VACUUM
TELESCOPE
SYMMETRY OF REVOLUTION
SLIT
FOCUS
ANALYSER
END OF ANALYSIS
PREDISPERSER
GRATING
ECHELLE
SPECTROGRAPH
GRATING
PARASITIC
WAVELENGTH
PARASITIC
WAVELENGTH
ZEEMAN COMPONENTS

FIGURE 1

Structure of the instrument

For the framework, several solutions were considered. We adopt an entirely metallic structure both for the instrument and the tower. The vertical spectrographs are stiffly tied to an azimutal mounting which bears the telescope. The aperture of the telescope is 90 cm. It is certainly the largest aperture allowing us to deal with the problems of the entrance window.

Entrance window problems

For a vacuum telescope the entrance window is subject to :

1) Mechanical stresses, beacuse of the difference in pressure between its two sides and the reactions of its supports and the air-tight joint.

2) Thermal stresses, because of the local difference of temperature due to radiation (sun, sky, structure),conduction and convection (ambient air).

These local stresses, according to Brewter's Law introduce variations of glass index and hence optical phase retardation which are proportional to them. Only the mechanical reaction of the joint and the radial gradient of temperature introduce polarization. The main results are the following (Figure 2) :

1) The local mechanical or thermal polarization is equal to zero in the center and maximal on the rim.

2) The total mechanical or thermal polarization is equal to zero for a revolution symetry distribution of the local stresses.

High resolution scanning of the sun surface

For many astrophysical problems we need good maps of the space or time derivatives of the observed parameters. The inertia of telescope introduces a loss of efficiency of the drive mechanism to scan the solar image with high accuracy and low time constant.

Optical scheme of "THEMIS" has been designed so that such effects would be as less as possible. High accuracy scaning is obtained by moving the spectrograph slit in the focal plan of the telescope. A servo controlled flat mirror holds the beam on the predisperser optical axe.

R = 30 cm

FIGURE 2

R = 30 cm

LOCAL POLARIZATION

MECHANICAL

$$\phi' = \frac{360}{2\pi} \cdot \frac{C \cdot p}{\lambda} \cdot \frac{R}{1 + \left(\frac{R-r}{e}\right)^2}$$

C = Brewster's constant = $2{,}78.10^{-7}$ cm²/kg

p = atmospheric pressure = 1kg/cm²

λ = wavelength = 6.10^{-5} cm

e = thickness of the disc

R = radius of the disc

r = any radius

THERMAL

$$\phi' = \frac{720 \cdot E \cdot \alpha \cdot T_R \cdot C \cdot e}{\lambda} \cdot \frac{\sum_{n=1}^{\infty} \frac{n}{2n-1} \cdot \frac{1}{(n!)^2} \cdot \left(\frac{R^2 K}{4 e \Lambda}\right)^n \cdot \rho^{2n}}{\sum_{n=1}^{\infty} \frac{1}{(n!)^2} \cdot \left(\frac{R^2 K}{4 e \Lambda}\right)^n \cdot \rho^{2n}}$$

E = Young's modulus = $8{,}5.10^5$ kg/cm²

α = coeff. of thermal expansion = $7{,}1.10^{-6}$

T_R = differ. of temperatures rim-center = 0.1 °K

K = coeff. of linear exchange = $1{,}8.10^{-3}$ W/cm².°K

Λ = coeff. of conduction = $11{,}1.10^{-3}$ W/cm.°K

$\rho = \frac{r}{R}$

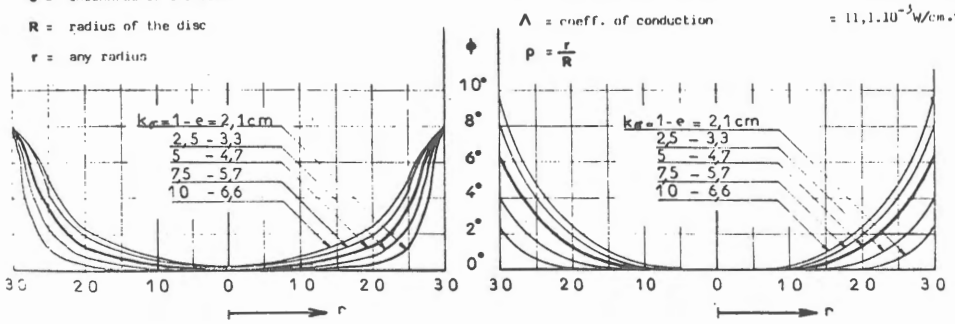

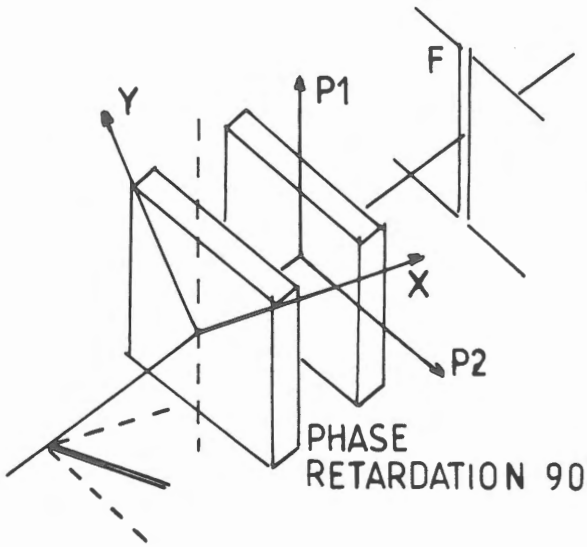

IP1 = 1/2 (I + V)

IP2 = 1/2 (I - V)

FIGURE 3

How take out magnetic field from observed profiles ?

With a circular analyser of polarization (Figure 3) we obtain the stokes parameters I and V.

1. Unsaturated line and weak field

In this case we can use the linear approximation

$$I \overset{\sim}{\sim} P(\lambda)$$
$$V \overset{\sim}{\sim} G\Delta\lambda\, H \cos\psi \frac{dP}{d\lambda}$$

where $P(\lambda)$ is the profile of the undisturbed line ($H = 0$) ; ψ the angle between $\vec{H}$ and the line of sight ; G the landé factor of the line and $\Delta\lambda H$ the displacement of the Zeeman component for the magnetic field H with $G = 1$.

Babcock magnetograph :

This instrument measures the variations of the V Stokes parameters at :

$$\lambda = \lambda o + \Delta\lambda VR + \Delta\lambda$$

where λ_o is the wavelength of the line, $\Delta\lambda VR$ the Doppler shift for the radial velocity VR and $\Delta\lambda$ the half Doppler width of the line.

Leighton magnetograph

With this technique we measure the variations of V at $\lambda = \lambda o + \Delta\lambda$ (no correction for VR)

With these two techniques some difficulties occur :

- the profile $P(\lambda)$ of the undisturbed line is unknown at any point where a magnetic field is present. (Problems of calibration)

- saturation effect if $\Delta\lambda H > \Delta\lambda$

Center of gravity method (Semel)

$$CG = \frac{\int_{-\infty}^{+\infty} \lambda P(\lambda)\, d\lambda}{\int_{-\infty}^{+\infty} P(\lambda)\, d\lambda}$$

Observed through a circular analyser of polarization the displacement of the center of gravity of the blend of the Zeeman components equals $G\Delta\lambda H\cos\Psi$, and this result is independent of the line profile $P(\lambda)$. It is a consequence of the Zeeman effect.

Lambdameter technique : DZA Sacramento Peak
Meudon magnetograph

Gives the same results as the center of gravity method for an adequate choice of the slit.

2. Strong magnetic field and saturated line

It is necessary to solve the transfer equations to calibrate the observations. We can used :

- Either the analytical solutions given by Unno
- or numerical integrations of the transfer equations if we want to take into account the variations with depth of the physical parameters.

3. Unresolved fine structures

It is necessary to observe simultaneously a great number of lines the profiles of which depend differently of the physical parameters (temperature, pressure, density...) inside and outside the magnetic regions. The center of gravity method gives the true average field (Rees-Semel).

The Meudon Solar Magnetograph

Sice April 1980, a new type photoelectric solar magnetograph using two 256G Reticon integrated diode arrays (Figure 4), is operating at Meudon Observatory. The Newton-Gregory telescope (equivalent focal length 23 m) receives the solar beam from a Foucault Siderostat. In front of the entrance window, a flat mirror deflects a part of the beam to a photoelectric guiding. The analyser of polarization is of the "THEMIS" type. The controlled temperature quarter wave plate

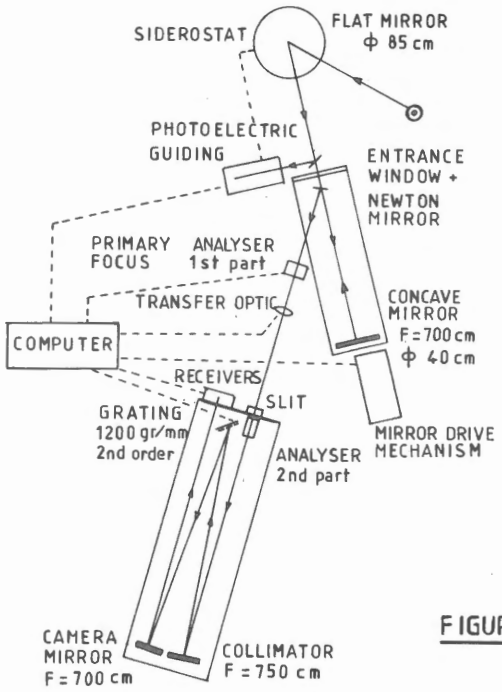

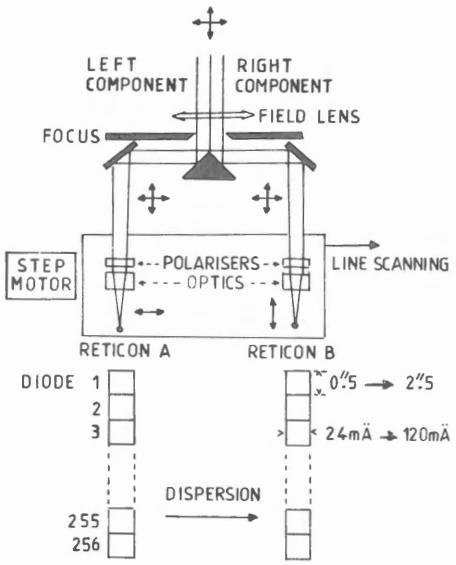

FIGURE 4 EXIT PART OF THE SPECTROGRAPH

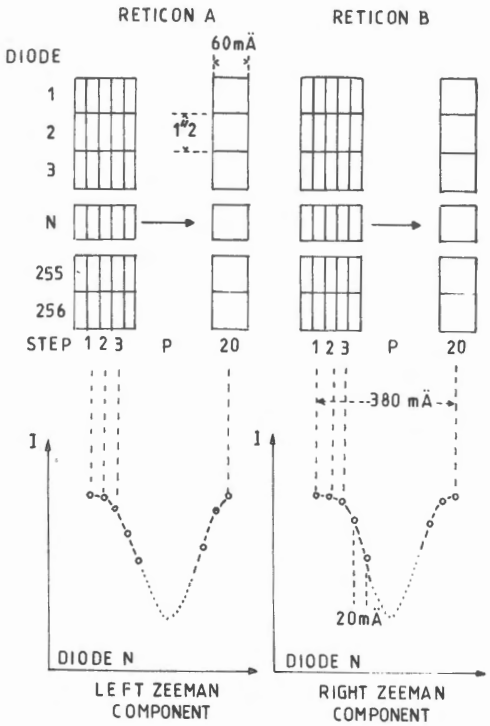

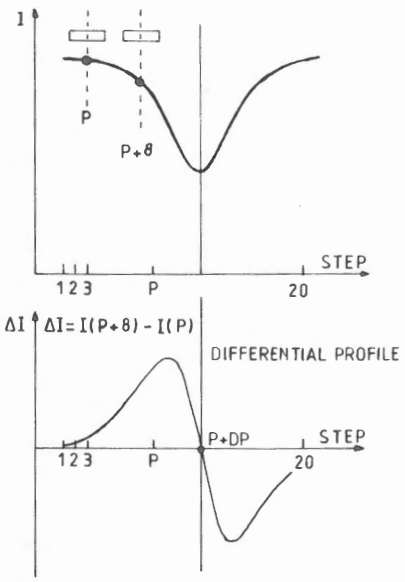

CONTINUUM INTENSITY ----------► A1

RIGHT COMPONENT P+DP=C+VR+GΔλH - - - - - ► A2

LEFT COMPONENT P+DP=C'+VR-GΔλH - - - - - ► A3

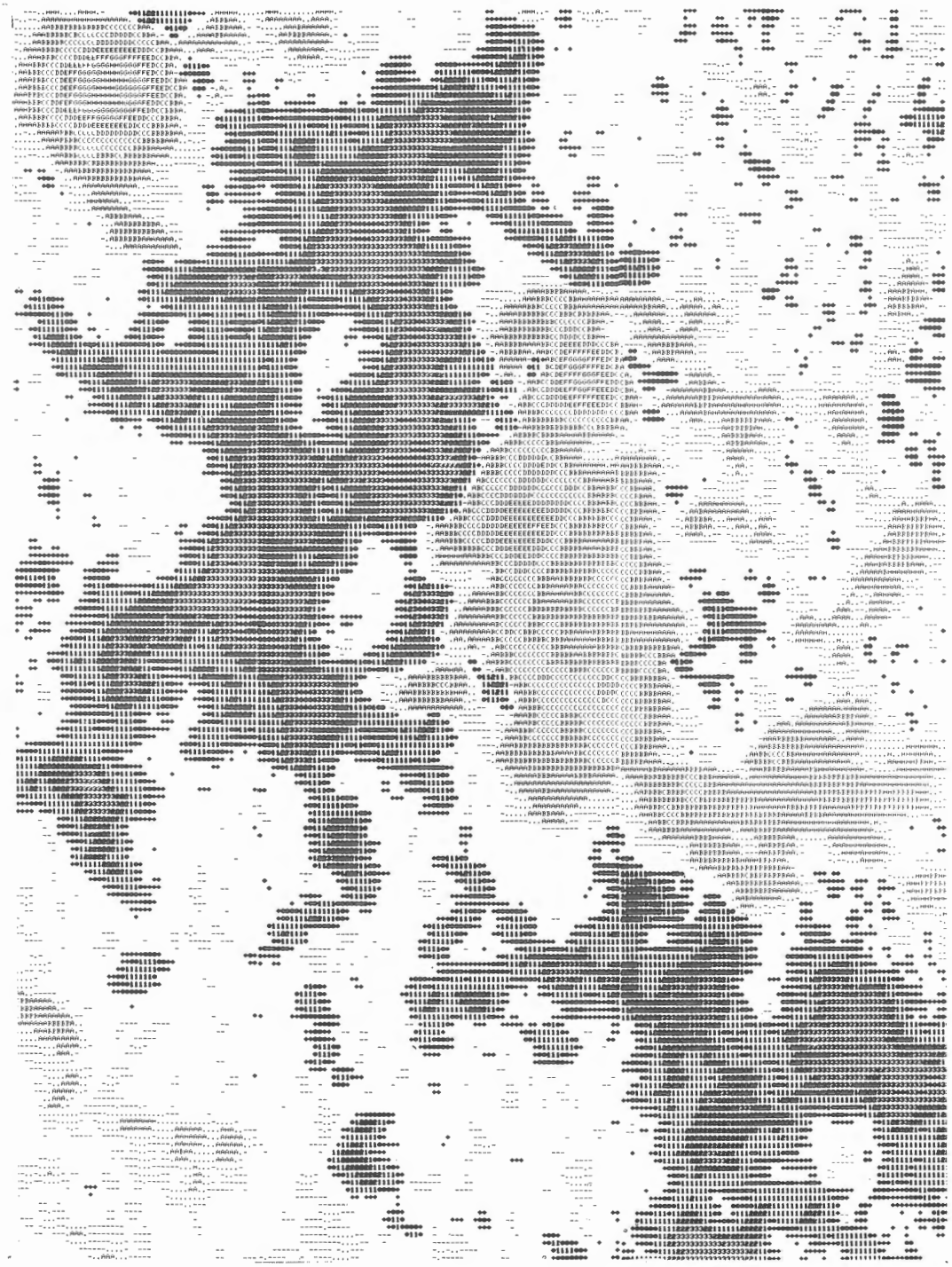

FIGURE 5 : MAGNETIC FIELD

(Analyser 1st part) is put in the telescope primary focus. Behind the entrance slit of the spectrograph, a calcite plate (Analyser 2nd part) transmits simultaneously the right and left Zeeman components which are separated in the exit part of the spectrograph. A microcomputer TEXAS 990/4 controls all the active parts of the instrument and data acquisition. The two Reticon diode arrays, perpendicular to the spectrograph dispersion are shifted to scan the Zeeman components. For each diode the differential profile I(P+8)-I(P) and the line position P+DP are computed in real time (Figure 4). The three parameters A1, A2 and A3 are stored on standard IBM 3740 "floppy disk". About six minutes are sufficient to scan an active region with a resolution of 1.2" x 2". From the A1, A2 and A3 values we are able to obtain maps of the longitudinal magnetic field, the radial velocity and isophote continuum.

Figure 5 shows an example of magnetic map. (Black numbers for North polarity and grey letters for South polarity). The intensity of the longitudinal component is given by the following symbols :

0	10	20	40	100	200	400	600	800	1000	1500	2000	2500	3000
white	-	x	1	2	3	4	5	6	7	8	9	0	#
	+	.	A	B	C	D	E	F	G	H	I	J	$

THE SOLAR INSTRUMENTS OF THE PIC-DU-MIDI OBSERVATORY

Jean RÖSCH
Observatoires du Pic du Midi et de Toulouse

Apart from sunspot records in the last decades of the last century, solar work began at Pic-du Midi just fifty years ago, when Bernard Lyot first observed the corona, thanks to his coronagraph, without a total eclipse of the Sun. This instrument with its wooden tube built on the spot, although very primitive (apart from the optics!) yielded outstandingly new results and was succeeded in 1936 by a more elaborated one which was then operated continuous for nearly forty years, covering, from 1943 on, three cycles of photometric measurements of the green and red lines.

By now, the status of the solar instruments at Pic-du-Midi is as follows :

1.- Four instruments are the successors of the above mentioned coronagraph or other instruments invented by Bernard Lyot:

a/ A new coronagraph for emission lines has been built (but still with the excellent original 20 cm objective), aiming at photoelectric measurements of intensities of three Fe XIII lines (3388, 10747 and 10798 Å) which can yield good values of the electron density in the coronal features.Monochromatic images of the 5303 line are used as a referenceframe for the location of the points observed.

b/ A 10 cm polarimeter for the electron corona provides data on the electron density along the line of sight, using the same reference system to the green line as the coronagraph; it is installed on a different but nearby mounting, so that independant but simultaneous observations are feasible.

c/ Another polarimeter (26 cm) has been built by J.L. LEROY and G. RATIER to measure the polarization of prominences and relate it to the magnetic field through the Hanle-effect.

d/ The Lyot coronameter has been developed by P. CHARVIN and is now currently used by J. ARNAUD to extract magnetic maps from the polarization of the green line.

2.- The 23 cm refractor which Lyot used to try some pictures of the granulation has been succeded by the 38 cm objective which he had applied to the Moon and planets. This objective has been installed under the so-called "Turret Dome", and, later on, replaced on the same mounting by a very good 50 cm objective (f = 6.50 m) now used by R. MULLER and other observers.

3.- On the occasion of the IGY in 1957-58, R. MICHARD and his group had built two large spectrographs fed by a cœlostat and a 40 cm mirror. One of them (high dispersion) is still on the place. But, considering the good resolution provided by the 50 cm refractor, and the progress in the spectroscopic techniques, the DASOP has recently built and associated to this refractor a modern spectrograph which is very likely to replace the old one.

THE NEW SOLAR SPECTROGRAPH AT PIC DU MIDI OBSERVATORY

Z. Mouradian[*], F. Chauveau[+], F. Colson[*], G. Darré[**], P. Kerlirzlin[*], G. Olivieri[*].

[*] Observatoire de Paris-Meudon

[+] Observatoire du Pic du Midi et Toulouse

The solar department of the Paris Observatory has built a modern spectrograph for the study of the fine structure of the photosphere and the chromosphere. The site selected is within reasonable distance of Paris and affords very fine seeing. Both selection criteria were satisfied by the telescope of the "Coupole Tourelle" of Pic du Midi Observatory. The spectrograph resulting from our studies was mounted in September 1980 and the first spectra have been made. Indications are that we may expect high-quality observations in the future.

1. The Instrument

The telescope is a refractor with a focal length of 6.45 meters and an aperture of 500 mm (F/12.5). One fifth of the solar image is enlarged 5 times (ϕ_0 = 300 mm or 1" = 150 μ) and refocussed on the slit of the spectrograph.

A fine guiding system is provided on the preliminary image given by the telescope.

On the fork of the telescope was mounted a Littrow-type spectrograph with a 8 m collimator mirror (Fig.1). It is equipped with three interchangeable gratings :

grating	grooves/mm	Θ_{blaze}	λ_{blaze} I ord.	lin.dispersion
BLD	600	36°52'	2,0 μ	0.60 K mm/Å
BL2	600	48°36'	2.5 μ	0.73 K mm/Å
BLS	300	63°26'	6.0 μ	0.54 K mm/Å

At present the spectra are taken with 35 or 70 mm film or 9 x 24 cm plates. In the future, diode arrays will also be available.

In addition the spectrograph is equipped with a MSDP system (Mein, 1977), see also P. Mein's contribution in these Proceedings. A simple tilt of the grating changes from single to double pass, and at the same time the slit is replaced by a window of 1' x 6'.

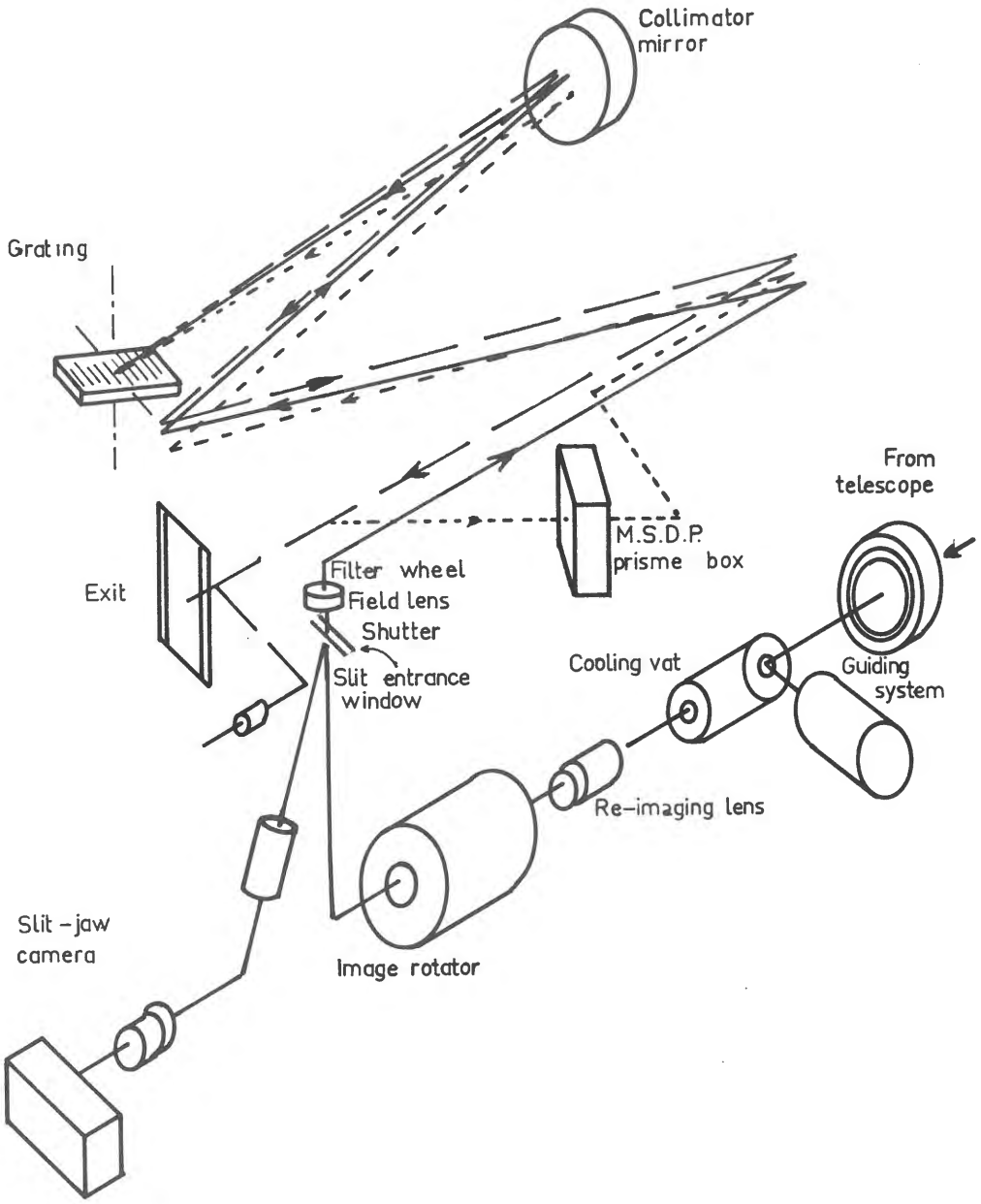
Collimator mirror
Grating
From telescope
M.S.D.P. prisme box
Exit
Filter wheel
Field lens
Shutter
Slit entrance window
Cooling vat
Guiding system
Re-imaging lens
Slit-jaw camera
Image rotator

Fig. 1

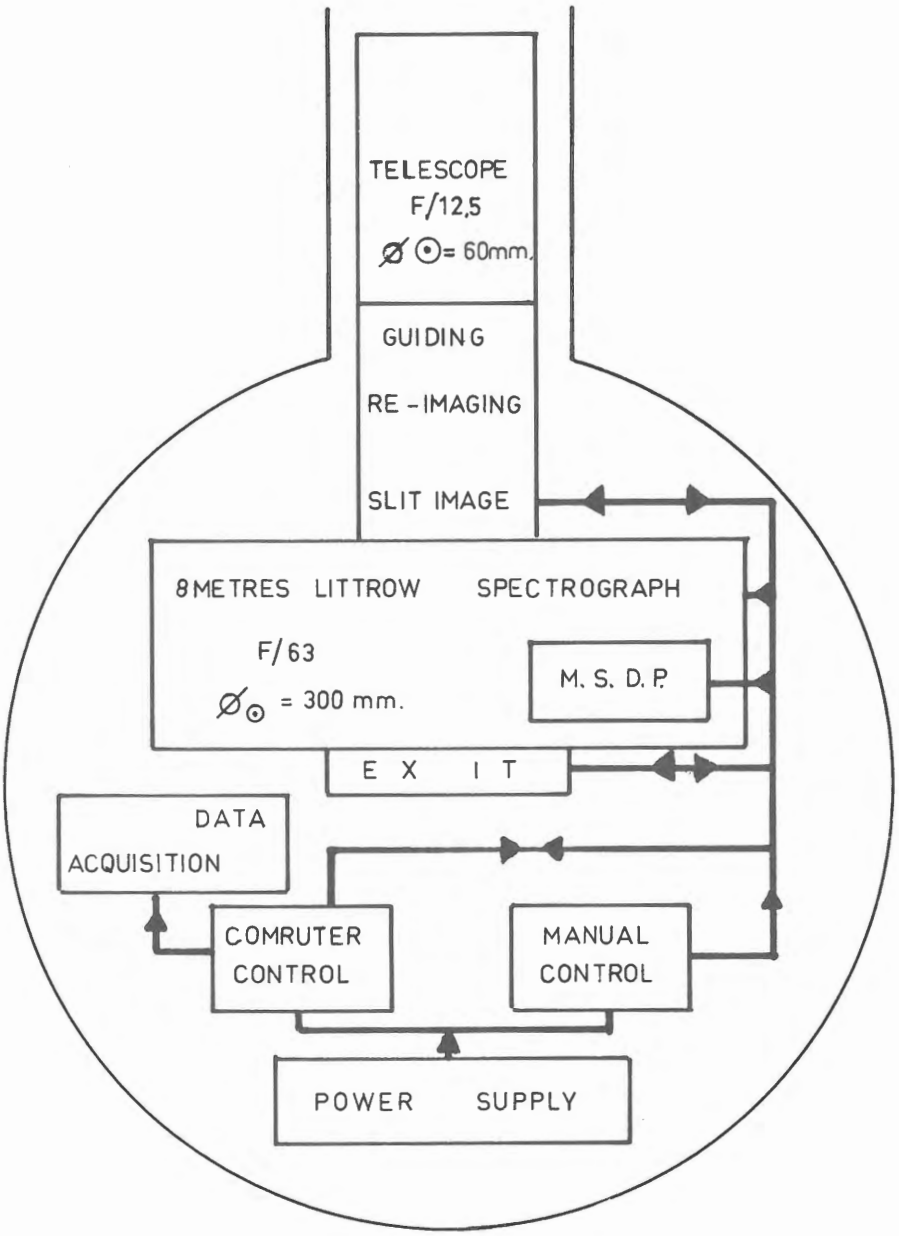
TELESCOPE
F/12,5
Ø ⊙= 60mm.
GUIDING
RE - IMAGING
SLIT IMAGE
8METRES LITTROW SPECTROGRAPH
F/63
Ø⊙ = 300 mm.
M. S. D. P.
E X I T
DATA
ACQUISITION
COMRUTER
CONTROL
MANUAL
CONTROL
POWER SUPPLY

Fig. 2

As the telescope is a refractor, instrumental polarization is very low, thus permitting good polarization measurements. Therefore, a polarization analyser (Semel, 1980) will be set in the primary focus of the telescope.

2. Organization

The general organization of the telescope-spectrograph is given in Figure 2. At present (October 1980), only the manual control is operating, in the near future a micro-computer will direct the observations and command data acquisition on film or with diodes.

REFERENCES

Mein, P. : 1977, Solar Phys. 54, 45.

Semel, M. : 1980, Astron. and Astrophys. (in press).

NEW DOMELESS SOLAR TOWER TELESCOPE IN HIDA OBSERVATORY

Yoshihiro Nakai
Kwasan and Hida Observatories,
Kyoto University

1. Introduction

After many years' experiences of solar observation with the solar telescope at Kwasan observatory (Nakai and Kubota, 1963), the recognition that the instruments for modern solar observations should produce a high resolution image of 0".5 first and then be accompanied by a high dispersion spectrograph of 0.1 Å/mm, became common. We were planning a new solar telescope accordingly. During the time, from 1962 to 1974, some solar telescopes were built at Sydney (Loughhead, et al., 1968), Sacramento Peak (Dunn, R.B.,1969), Kitt Peak (Pierce, A.K.,1969), Big Bear (Zirin, H.,1970), and etc., and produced high resolution photographs, which were resulted from the comprehensive studies of seeing.

In our case, we wanted to minimize the image defects due to local seeing caused by solar radiation and wind. In our design, the dome, the origin of turbulences, was eliminated. We put the telescope up to about 23 meters high on the tower in order to put the entrance-window into laminar air flow. The concrete tower in the sunshine is the source of convection. Then its surface was covered with stainless panels, whose surface-temperatures are controlled to keep nearly the same temperature as that of the surrounding air, in order to reduce convection from its surface. There is another problem of stability. Vibrations and twist-motions of the concrete tower, on which 24 tons telescope was supported, was analyzed and the results showed that 50 cm thickness of the reinforced concrete wall was stiff enough to be stable with an accuracy of 0.2 sec. of arc against the wind of 10 meters per sec..
We wanted high dispersion spectrograph and medium dispersion spectrograph with a wide spectral range. For the former, 14 meters vacuum vertical spectrograph was planned. For the latter, 10 meters horizontal spectrograph was adopted instead of Echelle system. Because, we had much necessity in the spacial wide field than in wide and continuous spectral range. Fig. 1 shows a schematic drawing of the system.

2. Local Seeing

On the solar observation, image qualities are affected by refractive inhomo-

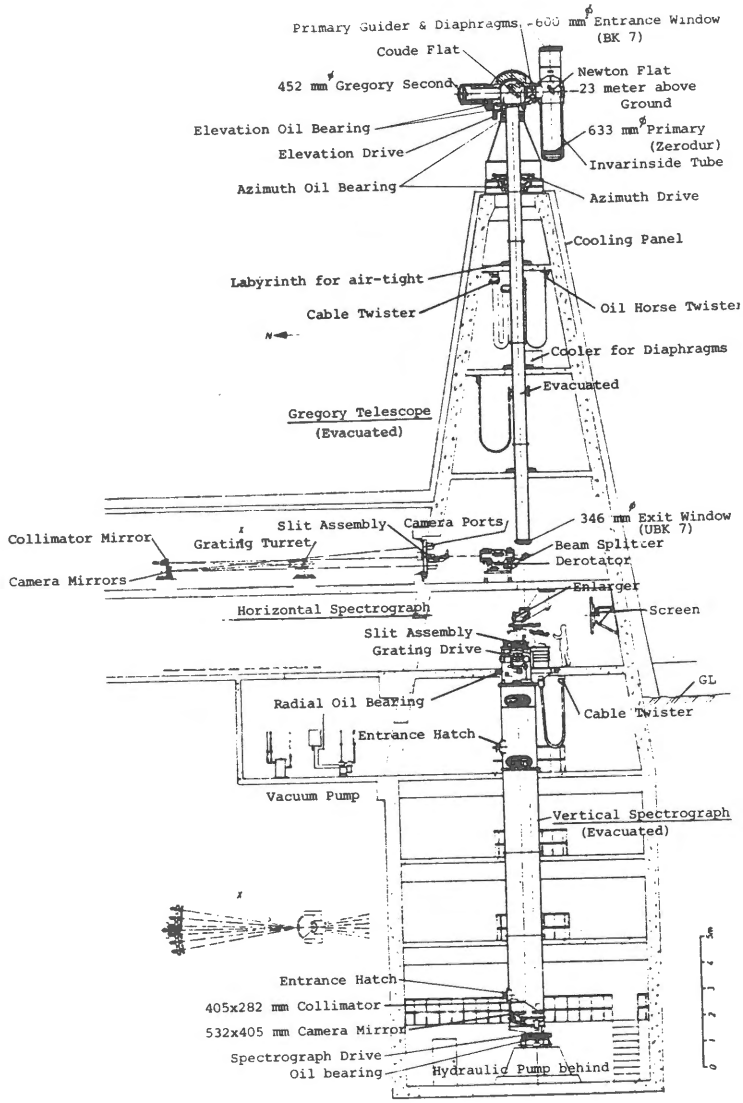

Fig. 1. Schematic drawing of the Domeless Solar Tower Telescope. System consists of Gregory telescope, Vertical vacuum spectrograph and Horizontal spectrograph.

geneties of the lower atmosphere caused by the convection from the heated ground, as well as the upper atmosphere. Especially, fluctuations in the refractive index of the air --- proportional to the thermal fluctuations of the air --- are dominant in the plume arisen from the heated ground due to the solar radiation. On the other hand, fluctuations are rather quiet outside of the plume. This difference becomes dominant in proportion as the height increases, because turbulence is mainly due to mechanical turbulence caused when the wind shears off the heat-bubble from the ground.

Our approach to decide the optimized height of the telescope was to observe the thermal fluctuations at several heights and then select the better site where the duration of quiet time are reasonablly long at the height accessible to us. We made similar experiments (Lynds, 1962) in the precinct of the Hida observatory (Mitsuda, 1977). Before that time, we had made some experiments to see the flows of air over the site with smoke-screen stacked up to 20 meters high. According to the results, two points had been proposed already. Temperatures at 8, 13, 18, 23 and 28 meters high were measured with high speed thermal sensors. At 23 meters high, the humidity and wind-velocity were being measured simultaneously. Figure 2 shows a portion of thermal records played back to a pen recorder. Quiet regions can be separated easily from turbulent regions. Figure 3 shows typical figure of a plume occurred at the site 2. At the upper left, the existing position of the telescope is shown.

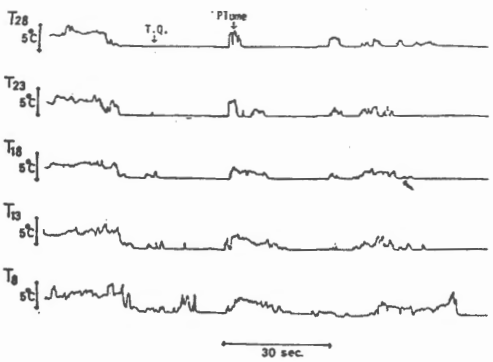

Fig. 2. 5 traces from bottom to top give the temperatures at 8, 13, 18, 23, and 28 meters elevation respectively. Time increase from left to right.

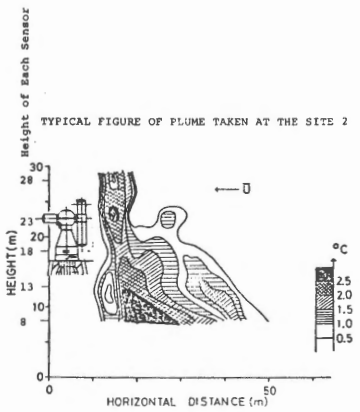

Fig. 3. Typical figure of a PLUME occurred at the site 2. An abscissa , horizontal distance is converted from wind velocity U and duration time. Existing position of the telescope also shown.

Probabilities that after a given time, how long the quiet period can be expected at each height are calculated. In our case, a quiet region is defined as the region where the temperature fluctuation is less than 0.05 °C. Figure 4 shows the results.

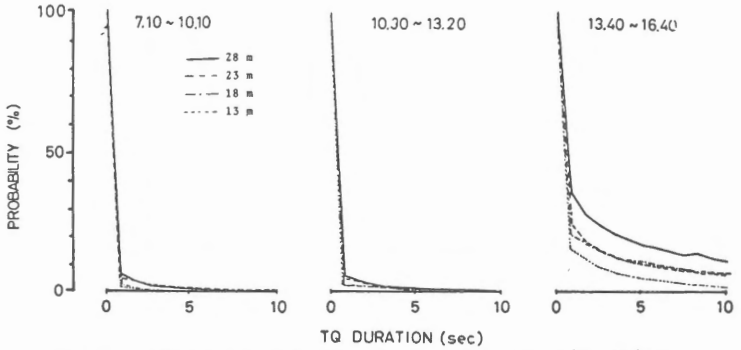

Fig. 4. Probability that after given time, how long quiet period can be expected is calculated for each height. From the left to right, graphs of morning, noon and afternoon are shown. Here, as a quiet region, we adopted that temperature variation is less than 0.05°C. (Fig. 2,3, and 4: after Mitsuda).

It is clear that the higher is the better. But, besides evening, no significant improvement can be seen between the two curves of 28 and 23 meters high. So, we decided to put the elevation axis at 23 meters high above the ground in order to let the entrance-window higher than 23 meters at all time.

Another turbulence arises from the tower itself. Concrete surfaces in the sunshine absorb heats and get warm up to more than 50 °C. These make new turbulences nearer to the entrance-window. If we leave them as they were, our purposes for building the tower to reduce turbulences from the ground could not be accomplished. So, we planned to reduce turbulences that 1) passively concrete surface was covered with high reflective stainless-steel-plates or painted with titantium-dioxide paint, 2) positively temperatures of the surfaces were controlled to keep the air temperature surrounding the tower. As a matter of course, the tower is fully covered with cooling panels. Figure 5 is a typical record of the temperature of each panel-section around the tower. Figure 6 is a portion of records of tracking error test. Signals are taken from two Reticons put radially on the solar limb of the primary image. Upper trace is of the elevation component and lower one is of the azimuthal. Left half was recorded without cooling and right hand was with cooling. Improvements in reducing the amplitude and in eliminating sharp spike-pulse can be seen.

3. Gregory Telescope

Many considerations led us to the following. The telescope is of alt-azimuth

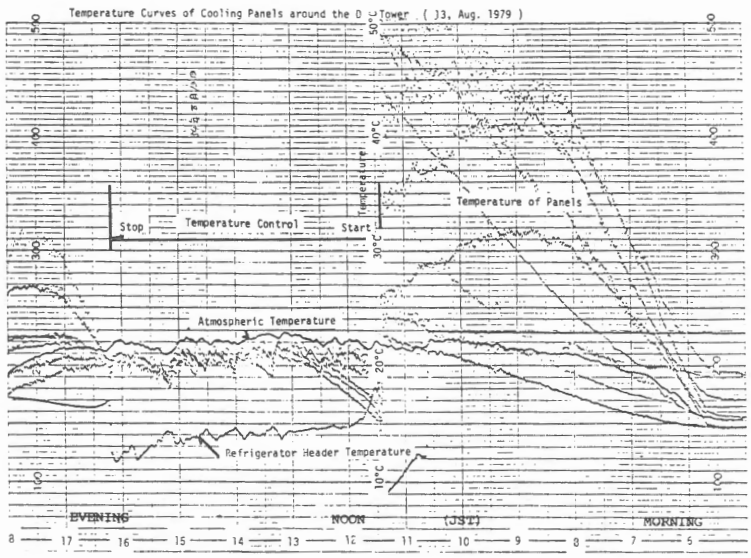

Fig. 5. This record shows temperature variation of each section of cooling panels around the concrete tower and atmospheric temperature. 5:00; after Sunrise, temperatures went up, 11:30; circulation of cooled water into the water-jackets behind the panels started , some of them were over cooled, but soon settled within $^{+0}_{-3}$°C.

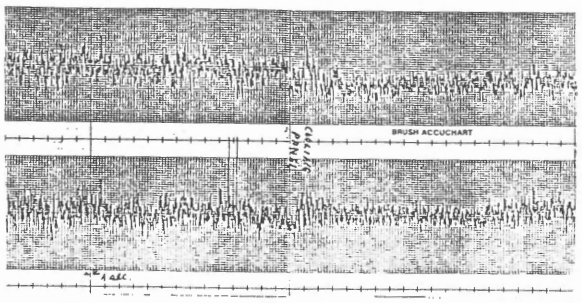

Fig. 6. Two traces are taken during the test of the telescope tracking. Signals were come from Reticons put on the limb of the primary Solar image. Pen deflections are proportionally corresponding to the shift of the limb. Upper trace is of altitude component, lower is of azimuth component. Left half was without cooling the panels.

mounted Newton-Gregory configurations. As shown in Figure 7, solar ray enters the BK 7 entrance-window with a free aperture of 605 mm and thickness of 40 mm.

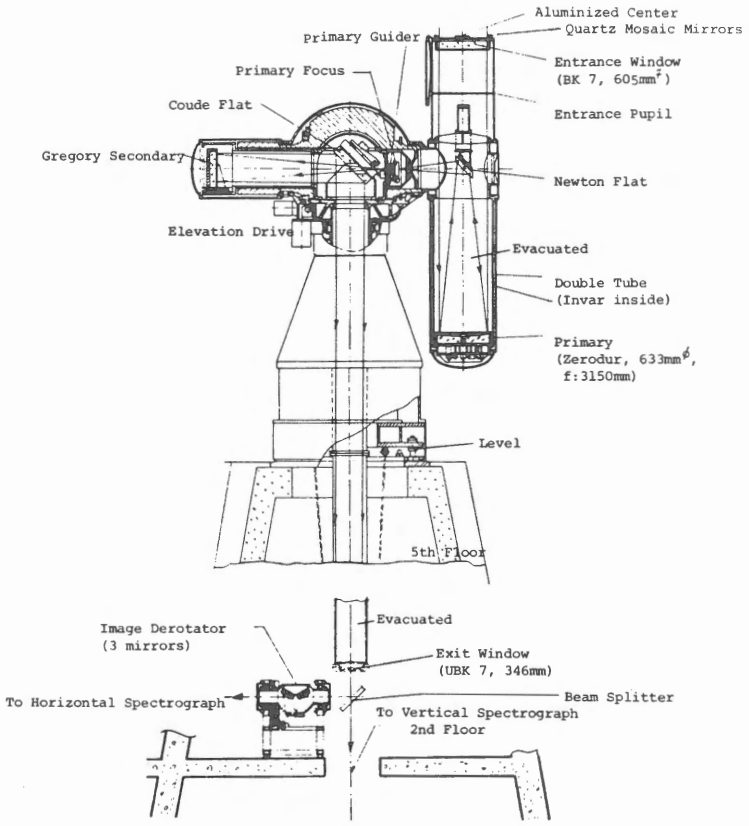

Fig.7. Schematic drawings of Domeless Solar Tower Telescope. Residual wave front error is 60 nm (RMS) and 335 nm (p-p). Mirrors are made of Zerodur.

Around free aperture, the edge of the window is covered with aluminized mosaic quartz mirrors, in order to avoid the heat concentration on the cell. Then ray goes through the entrance pupil with an aperture of 600 mm until it strikes the primary mirror of 633 mm in diameter. Primary is made of Zerodur and its cell is supported by inside Invar tube in order to fix the primary image on the focal plane defined mechanically by occulting cones and diaphragms. All other mirrors also made of Zerodur and there are no problems with thermal distortion of the optics. The primary has a focal length of 3150 mm long and forms about 30 mm image of the sun on one end of elevation axis near to the tube, where a primary guider and a turret of

occulting cones and diaphragms are located. Unnecessary light could be reflected and eliminated with insertion of suitable one. All of them are cooled with refrigerated water. Light goes further through a central hole of Coudé mirror until it strikes the Gregory secondary mirror of 452 mm in diameter.

The system focal length is 32,190 mm long and the f-ratio is 53.7. The Gregory mirror forms a solar image of about 30 cm in diameter on the observing table on the first floor. About 88 % of total light path, 28 meters, from the entrance-window to the exit-window is evacuated up to 2 mmHg. A deformation of both windows due to pressure difference amounts to 90 μm at the center, which results in defocussing of 0.07 mm and the corresponding additional wave-front error of 1/100 λ. Total wave-front errors at the secondary image is 1/10 λ (RMS). A linear obscuration with a Newton flat mirror and its mountings is 0.39. Effective image field is 36 min. of arc wide.

4. Vertical Vacuum Spectrograph

For high dispersion spectrography, we planned 14 meters vertical vacuum spectrograph. The focal length was decided according to the circumstances that several kinds of grating with ruled area of 306×408 mm is easily obtained. Czerny-Turnar type optics are enclosed in 12 m^3 vacuum tank and its optical configurations are shown in Figure 8. Light passes through UBK 7 mirror slit, whose rear surface is figured to be a field lens, and through filters -- order sorter --, and through UBK 7 entrance-window shaped as weak negative cylindrical lens at upper surface, then goes down until it strikes the collimator mirror of 405×282 mm in area.

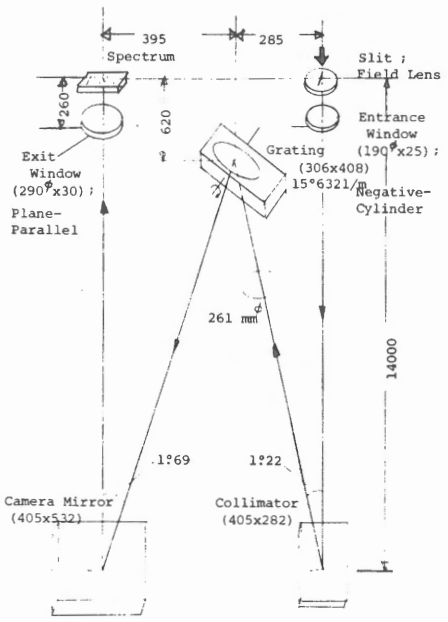

Fig. 8. Schematic drawing of the vertical spectrograph. Plate factor is 0.3 to 0.1 Å/mm (3 to 7 th order), with the grating of Blaze angle;56° and 632 grooves/mm.

The collimator sends the parallel light beam of 261 mm in diameter to the grating and illuminates uniformly.

The camera mirror of 532×405 mm in area images a solar spectrum on the focal plane through UBK 7 plane parallel exit-window. Maximum format size of spectrum is 60×240 mm in area. Improvement in the introduction of cylindrical lens to the entrance-window is some amount of compensation of astigmatism. Spot-diagrams made on the utmost edge of the format show the reduction of

diameter of minimum circle in which all spots calculated is included. Improvement is from 63 μm to 22 μm in diameter. The maximum slit height is 50 mm. This spectrograph can be applied to the heliograph used with 150 mm height curved slit.

4. Horizontal Spectrograph

We planned a horizontal spectrograph, whose functions are complimentary to the vertical spectrograph. 10 meters spectrograph is of Czerny-Turnar configurations of off-plane where gratings are put at 0.45×focal length. Figure 9 shows its configurations clearly. Light limited to less than 60 mm with diaphragm at primary focus is reflected by a beam splitter (cf. Fig. 7) to the slit through the image-derotator, and goes through slit and filters, then goes until it strikes a collimator mirror of 215 mm in diameter, whose focal length is 10 meters. The collimator sends parallel beam to one of the three gratings selected.

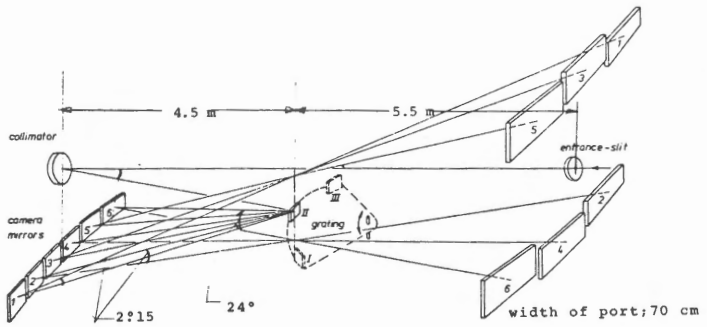

Fig. 9. Optical configurations of the horizontal spectrograph. One of three gratings can be selected. 6 camera mirrors correspond with 6 camera ports each other. Plate factor is 0.82 to 0.75 Å/mm in first order.

The size of ruled area is 154×206 mm in area. Diffracted light spreads over six camera mirrors, and each camera mirror forms solar spectrum on each corresponding camera port, whose width is 70 cm wide. For example of wide spectral range use, selecting #1 grating (Blaze angle; 17°27', Space; 1200 l/mm), solar spectrum from 3300 Å to 6900 Å is formed on six ports continuously with exception of small five gaps between camera mirrors. But, because of limited width of camera format of only 240 mm long, practically we can get discrete spectra with camera gaps. However, in order to take pictures of several interesting spectral ranges, selections of dispersion, grating, its order, grating angle and positions of camera are easier to obtain than expected, and a spacially wide field with 50 mm height slit (equivalent to 5 min. of arc) and a wide spectral range are more powerful than the spectra obtained by Echelle spectrograph.

5. Control

Systems are controlled by DEC 11/45 computer, which has a 32 KW main core-memory and two drives of 1.2 million words disk. The control program is written in

FORTRAN in about 5500 lines and still being improved. Data are transferred in DMA mode at 20 Hz for control operations and 4 Hz for computations and displays. Calculations of R.A., Dec., solar diameter, alt-azimuth coordinates, atmospheric refraction and etc. are made at 4 Hz. The computer combines existing positional data of every axis and calculated ones, then transfers it to every axis with appropriate speed. Three sensors are equipped with the telescope. A primary guider near the primary focus, and secondary guiders on top of the vertical spectrograph and in front of the horizontal spectrograph respectively. Error signals from the former correct the positions of the telescope itself, and from the latter correct the image positions by moving the Coudé mirror. On the other hand, the solar image can be shifted in polar coordinates according to the motions of both guiders. So, we can select image positions in polar coordinates as well as Cartesian coordinates and read off the position (p,r) referred heliocentrically. Figure 10 shows relation between the motion of the guiders and the image position.

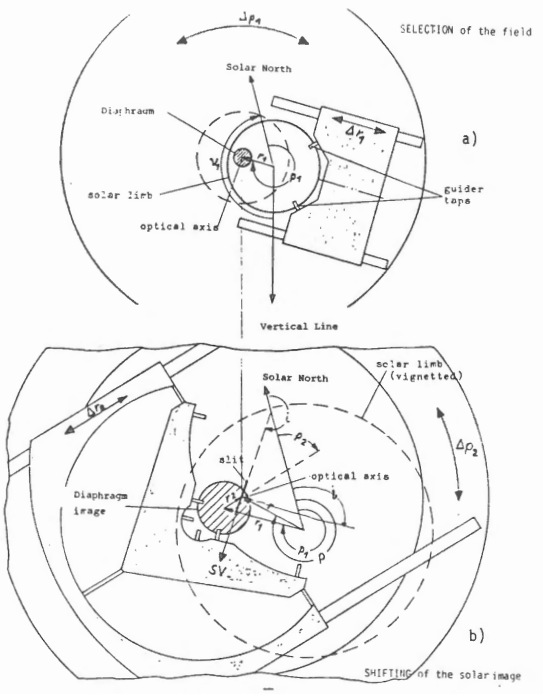

Fig. 10. Taps of PG and SG are to be moved axially and radially around the main optical axis. a); shifting the PG, limb of the solar image follows to the taps and coordinates changes to p_1 and r_1. In this case , a diaphragm is used. b); corresponding taps catch the limb of the diaphragm instead of the solar limb. Shifting SG, its coordinates changes to p_2 and r_2. Polar sum is p and r.

According to the shift of one pair of taps of the PG, which are to be moved axially and radially around the main optical axis, the solar image follows it and coordinates at the center are changed from (0,0) to (p_1,r_1). As is shown in a), a diaphragm can be inserted into the center. b) shows similar functions of SG. In this case, corresponding pair of taps catches the limb of the diaphragm instead of the solar limb. Shifting SG, the diaphragm follows it and coordinates of the center is changed from (0,0) to (p_2,r_2). Then, coordinates of the solar disk at the center of slit are of polar sum of them, p and r.

The observational mode such as with sequential shifts of image can be done automatically. After starting computer, interfaces between solar astronomers and

the telescope are only push-buttons and digital rotary-switches.

The most important for astronomers is not the system configurations but the simplicities in handling.

5. Schedule

At 1975, we started to manufacture the telescope at Carl Zeiss, Oberkochen, and at the beginning of 1978, delivered it to Hida observatory. On August of the same year, we started to assemble. After nine monthes' efforts, the telescope systems, buildings and their auxiliary equipments are roughly assembled and adjusted. At the same time, the control sotware was being developed. Systems are big and we were suffered from many problems such as defects of connectors of MIL standard used in open air, defects of unreliable encoders, noises in the data-bus, bugs in the program, vibrations of the telescope resulted from the hydraulic oil bearings and the resonance of the telescope with the frequency of intermittent refreshment of digital drive-speeds and etc..

On April 1979, test observations, combined with debugging the software and examining the hardware, proceeded to take fine details of the solar atmospheric structures through the H-α filter. Pictures of 14, Aug. 1979, shows fine details of moustaches, which are solved up to 0".5 and the smallest separation measured is about 0".3 of arc. In June of this year, average seeing of about 1" of arc continued during two hours, and pictures of active regions were analyzed with cinematographic techniques. (Kawaguchi et al.). As an electronic data acquisition system, SIT-TV was tested at the focus of the vertical spectrograph to see the feasibilities in the feature. We are now planning to introduce a cinecamera, a high-speed densitometer, TV and its image analyzer. Combined with these modern techniques, the Domeless Solar Tower Telescope will be a more powerful instrument in the field of solar observation.

References

Dunn, R.B. ; 1969, Sky and Telescope, Dec., p368.

Loewen, E.G. ; 1972, ESO/CERN Conference May 1972, p193.

Loughhead, R.E. ; 1968, Solar Physics, 4, p185.

Lynds, C.R. ; 1962, IAU Symposium No.19, p126.

Mitsuda, Y. ; 1977, 飛騨天文台ドームに太陽望遠鏡新設計画に伴う気象調査報告書
京都大学 防災研究所

Nakai, Y. & Kubota, J. ; 1964, Memoires, Sci. Dept. Kyoto Univ., 30 p323.

Pierce, A.K. ; 1969, Solar Physics, 6, p498.

Zirin, H. ; 1970, Sky and Telescope, Apr., p215.

MULTI-CHANNEL SUBTRACTIVE DOUBLE PASS SPECTROGRAPH

P. Mein
Observatoire de Paris-Meudon

1. Principle

In the MSDP spectrograph, the slit is replaced by a two-dimensional window (Fig.1). At the focus where the spectrum is usually formed, a multiple slit selects N wavelengths (N = 9). Then N prisms translate the beams in order to isolate N different pictures of the field, after a second pass on the grating which compensates the previous dispersion (subtractive double pass). These N pictures are recorded simultaneously on a 70 mm film. The useful wavelength λ depends on the channel number n ($1 \leq n \leq 9$), and also on the location inside the channel (x and y coordinates). Fig. 2 shows the relationship between x, y and λ for each channel. Using a full scanning by a microdensitometer, we can restore the intensities in N points of the spectrum for the whole observed field. If the spectral range includes a solar line, we can derive dopplergrams, intensity maps and any function of the line profile. The spectral resolution is limited by the multiple slit, but this limitation is not cumbersome in case of broad chromospheric lines.

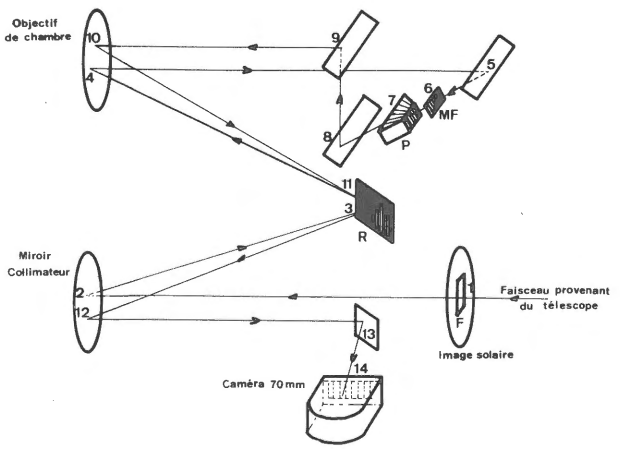

Fig.1 - Schematic MSDP spectrograph

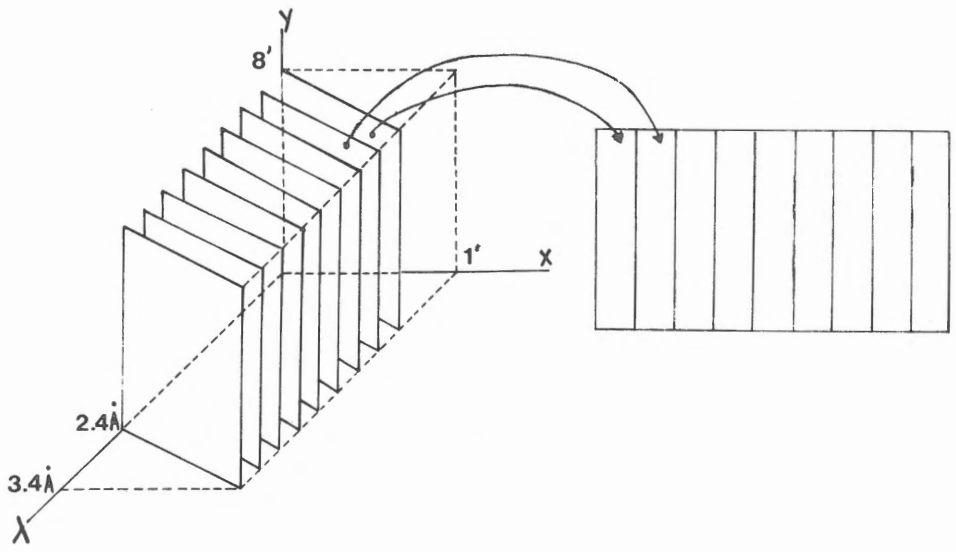

Fig. 2 - Wavelength as a function of the location inside the N channels of the MSDP

2. Comparison with other techniques

It is interesting to compare the capabilities of MSDP with capabilities of classical techniques. In each case, we list below the coordinates which are recorded simultaneously:

Single pass spectrograph:	λ, x	
Filter, interferometer:	x, y	
Multiple slit spectrograph:	λ, x, y	(y degraded)
MSDP spectrograph :	λ, x, y	(λ degraded, sufficient for broad lines)

The MSDP spectrograph appears to provide in many cases the largest rate of useful data. As a consequence, it is very well appropriate for fast phenomena observations (instabilities) and also in case of events the locations of which are difficult to predict accurately (flares). Let us note that the spatial resolution of MSDP is highest both in the x and y coordinates, so that it is very efficient for spectrography of small fine structures.

3. Existing or planned MSDP

We summarize some characteristics of three MSDP : Meudon Solar Tower

(operating), Pic du Midi (turret dome, early 81), Canary Islands (attached to the Freiburg telescope, 1982-83) :

	Meudon	Pic du Midi	Canary Islands
ϕ telescope (cm)	60	50	60
F telescope (m)	45	33 (equivalent)	45
F' spectrograph (m)	14	8	15
Typical H_α exposure time	1/3 s		
Spatial resolution	∿1"(limited by seeing)	.3" ?	.3" ?
field	4' x 35"	5' x 45"	4'30 x 35"
field with enlarger	8' x 1'		
field with automatic scanning	8' x 5' (with enlarger)		4'30" x 4'30"
shortest cycle	∿ 2 s	∿ 2 s	∿ 2 s
channel number	9	9	9 (x2 simultaneous lines)
possible successive lines	2	2 or 3	4 or 6
wavelength resolution	∿ .15A	∿.25A	∿.15A

4. Coordinated observations in 1980 with the MSDP of the Meudon Solar Tower

The Meudon MSDP has already been used many times in connection with other instruments. We list the programs for which observations have been obtained in 1980 :

- Prominences : coordinated with Pic du Midi
- Flare Build up Study : actions 1, 2, 4, 5, 6, 7, coordinated with SMM (spacecraft), Grand Siderostat Meudon, 3 λ-heliograph Meudon, Radioheliograph Nançay,....
- Guest Investigator Program on SMM (Moreton wave study)

We hope that this list will be extended in the future, especially with Japan for simultaneous as well as complementary observations.

REFERENCES

Mein, P. : 1977, Solar Phys. 54, 45.

THREE INTERESTING PROPERTIES OF BIREFRINGENT FILTERS

Jean-Louis LEROY
Observatoires du Pic du Midi et de Toulouse
65200 Bagnères-de-Bigorre - France.

It is the purpose of this note to describe three interesting properties of birefringent filters which do not seem to have been quoted previously although they could be used with some benefit for solar observations.

1 - Solc elements in Lyot filters.

It is well known (Evans, 1958) that the Solc filter has one main advantage (high transmission) and some drawbacks (large number of plates; strong secondary maxima) with respect to the Lyot-Öhman filter. Further work (Solc, 1965) has shown that one could build apodized Solc filters which improves the value of this device; I have recently considered the design of Solc filters whose passband would be identical to that of Lyot filter : the main interest of such an apparatus would be obviously to improve the transmission of Lyot filters already in use without modifying their spectral characteristics.

It is easily shown that the equivalent of a N elements Lyot filter must be a n plates Solc filter with $n = 2^N - 1$; it is also possible to derive the set of plate orientationswhich makes the two filters equivalent. A most interesting combination is the 3 plates Solc filter equivalent to a 2 elements Lyot filter, that I call the SL 3 filter. This device reminds of course the Evans compound elements (1949) but it has the important advantage to avoid $\lambda/2$ and $\lambda/4$ plates which means that it is perfectly achromatic. Therefore a complete Lyot filter could be replaced by SL 3 elements with only half as many polarizers. Field properties of the SL 3 have also been investigated and appear to have about the same limitations as classical Lyot elements.

A detailed study of SL filters is given in a recent paper (Leroy, 1980).

2 - Birefringent filters with multiple useful pass-band.

Zirin (1966) has shown first that modern interference filters allowed to reduce drastically the number of plates in birefringent filters. As a matter of

fact birefringent elements must be kept only for the high resolution filter section because they have a wider angular field and a much more stable pass-band than multilayer devices.

With a rather large thickness for the thinnest plate of a Lyot filter it is possible to search for interesting combinations which would allow to isolate several lines of astrophysical interest at the same temperature (a problem which had been considered very early by Lyot (1944). Using SL elements which are achromatic allows to consider widely spaced spectral lines.

As an example I have shown that with a basic thickness of 8605 microns of quartz one can build a filter which selects at the same temperature four interesting solar lines : Hα; D3 (He I); b 2 (Mg I); Hβ. The bandwidth is about 2.5 Å wide, making this filter (now in progress at the Nice Observatory) a useful tool for studying solar prominences. More detailed data are reported in the previously quoted paper (Leroy, 1980) where a detailed bibliography on birefringent filters has also been gathered.

3 - Fourier transform spectrography with birefringent plates.

Mertz (1958) has shown how a birefringent wedge could be used as a polarizing interferometer for Fourier transform spectrometry. As it is fruitful to build the interferogram by a step-by-step scanning (Connes, 1966) one can also use a set of birefringent plates : figure 1 shows that the plates of a Lyot filter can be oriented in a simple way to provide a regular increase of the path difference which gives a convenient wide-field interferometer. Possible applications are likely in conjunction with the development of modern two dimensional detectors and preliminary estimates show that the birefringent device of figure 1 would have roughly the same performances than a wide field Michelson interferometer. Further, even with a noise-free detector, spectral analysis performed by Fourier transform method with the apparatus of figure 1 would be more efficient than spectral scanning with a tunable Lyot filter using the same plates because the transmission of birefringent plates alone is much higher than that of a complete filter including polaroïds.

Eventually, a very promizing application of figure 1 scheme would be spectropolarimetry : if the plates with variable orientation are set after the analyzer of a photoelectric polarimeter, one can perform a spectral analysis in polarized light without any loss of light !

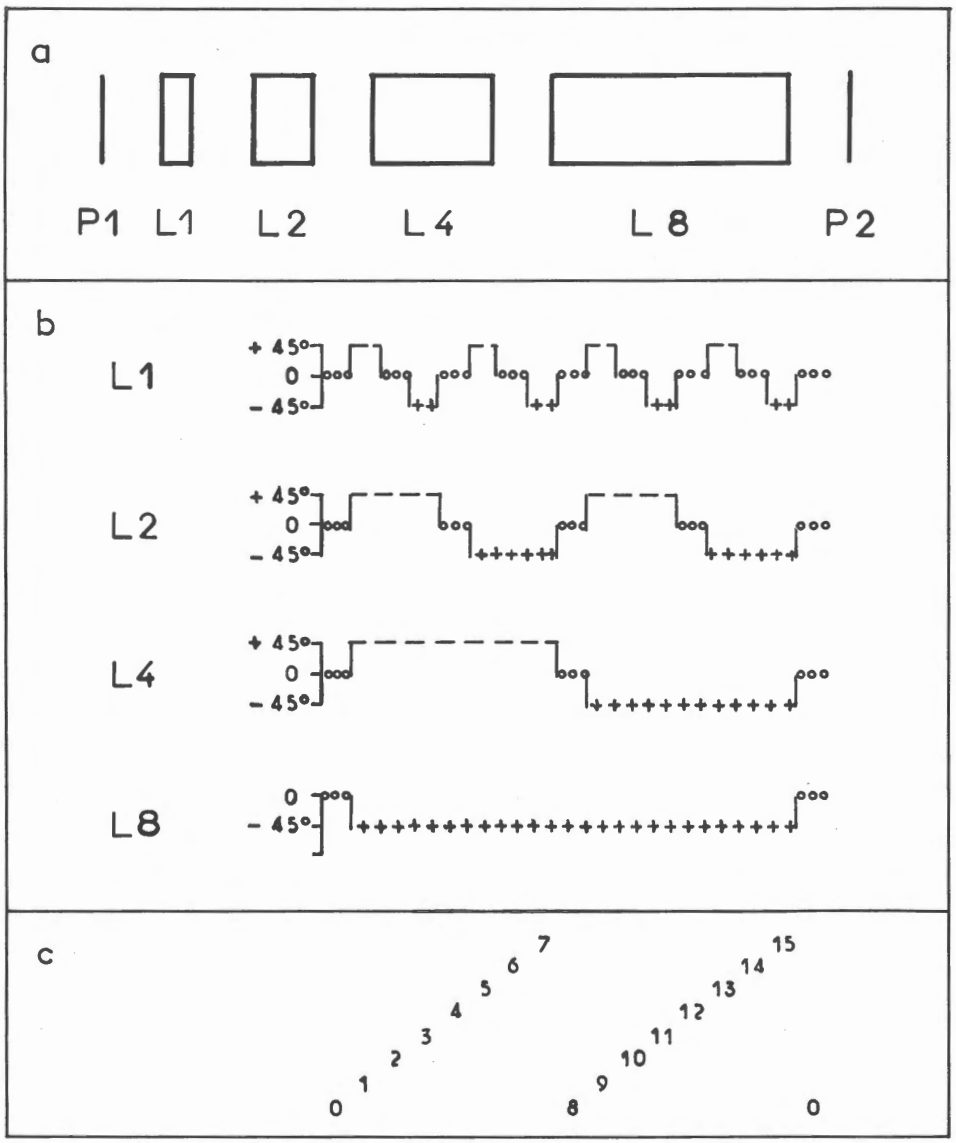

Figure 1

a/ Overall view of the birefringent device

b/ Time variation of plate orientations

c/ Resultant time variation of the path difference, in unit of plate L 1.

References

Connes, J., Connes, P., 1966, J.O.S.A., 56, 896

Evans, J.W., 1949, J.O.S.A., 39, 229

Evans, J.W., 1958, J.O.S.A., 48, 142

Leroy, J.L., 1980, Journal of Optics, 11, 293

Lyot, B., 1944, Ann. Astrophys., 7, 31

Mertz, L., 1958, J. Physique, 19, 233

Solc, I., 1965, J.O.S.A., 55, 621

Zirin, H., 1966, Applied Optics, 5, 474.

SOLAR DIAMETER MEASUREMENTS, A NEW APPROACH

J. RÖSCH and R. YERLE
Pic du Midi and Toulouse Observatories.

The experiment we would like to present was originally intended, in the early seventies, to confirm - or not - by a completely different observing method, the solar oblateness announced by DICKE (1967) - a 0.1" difference between equatorial and polar diameters. This result has raised well known arguments, both experimental and astrophysical, the latter mostly related to the problem of a fast rotating core inside the sun. It appeared, afterwards, that various relativistic tests at least did not confirm the Brans-Dicke cosmology. Therefore, if an oblateness does exist, what about the secular advance of the perihelion of Mercury, etc..? Thus, it seemed worth to pursue our program.

Then, H.A. HILL and co-workers (1975) announced that they had found, in a different way, the solar oblateness to be consistent with the 27-day rotation of the outer layers, but the solar diameter to oscillate at a number of discrete frequencies; later on, HILL (1976) suggested that they could mean, rather oscillations in temperature, and developed with his associates, (HILL et al., 1979), the interpretation by fluctuations in the brightness distribution around the limb.

On another hand, it seems that more and more interest is taken, now, in the solar diameter in itself, leading to its possible secular changes. Therefore, a physical definition of what does "solar diameter" mean is needed, and the results below show the way to a measure of such a diameter, which could provide, in a second step, an absolute value.

Moreover, we shall see that an unexpected result already emerges from our preliminary observations, possibly bringing a new point into the problem of solar oscillations.

The main drawback of Dicke's as well as Hill's method is that they measure integrals of the flux around or across the limb (with a weighting in the second one)

and do not, therefore, discriminate directly between temperature and diameter changes. The approach we had in mind from the beginning was to have a differential definition of the limb, and then to detect, separately, through an integral, possible temperature changes.

The most obvious differential definition of the limb is as the point where the brightness gradient along a solar radius is maximum. But, then, two questions need to be answered : first, to which extent is the limb defined in that way independent from a temperature change ? And second, how to manage with the classical effect of the atmospheric spreading function upon the position of the inflexion point of the profile ?

For the first question, the simplest idea is to take a model of the solar atmosphere and compute the position of the maximum gradient on the resulting limb profile; then introduce various changes in the distribution of temperature versus altitude and compare the positions of the maximum gradient. HILL et al. (1975), in their first treatment of the problem of the solar diameter, used a model, based on the Stratoscope observations (ROGERSON, 1959), where they assumed a "vertical" drop of brightness down to zero at a position which, of course, they take as the very limb. In a more recent paper (HILL et al, 1978) they compute, through a theoretical model, the effect of non-adiabatic oscillations on the appearance of the limb, which, again, shows an onset of brightness from zero to a finite value at the very origin of the radial coordinate. We prefered to start with the classical HSRA model (Fig. 1) established upon a bulk of data collected in various spectral ranges, leading to a steep (but not vertical) drop of the limb brightness to a non-zero minimum, which one cannot forget when dealing with observational problems (X).

Thanks to a program kindly provided by S. DUMONT, and dividing the solar atmosphere into 95 layers, 20 km thick in average, we could compute the position of the maximum gradient of the limb, first for the initial temperature vs height

(X) Refinements to HSRA suggested by VERNAZZA et al. (1980) introduce only moderate shifts in the position and value of the temperature minimum, but do not change appreciably the shape of the temperature vs altitude distribution, and would not modify our conclusions.

distribution (Fig. 2), and then with various modifications as follows (the layers are numbered 1 to 95 inward, see Fig. 1) :

- a : constant ΔT for all layers;
- b_1, b_2, b_3 : constant ΔT in the outer (1-30), middle (31-65), or inner (65-95) slices;
- c_1, c_2 : 0 to $\pm \Delta T$, proportional to the altitude, from layer 95 to layer 1.

The results (Table 1) show that :

1) The drift is proportional to ΔT, the temperature difference, and does not exceed a few milliseconds of arc for temperature changes of the order of magnitude which is likely to occur; it will anyhow be possible to apply a small correction in position if, by measurements of another type, temperature differences are detected.
2) Only changes in the "middle" slice do result in a drift; this is not surprising, since only that one is effective in producing the limb profile;
3) A significant change in the value of the maximum logarithmic gradient appears as a function of temperature differences; this is a very important fact which will be taken into account later on in this paper.

Thus, we can conclude thatthe definition of the solar diameter by the distance between the inflexion points of opposite limb profiles has a definite geometrical value, since it does not depend upon possible temperature variations in the layers involved. Moreover, measuring directly the distance has the advantage of separating the variables diameter and temperature.

Now, about the observational problems. The main concern is the fact that the convolution of a uniformly bright half plane by a spreading function having a center of symetry gives a profile with its inflexion point exactly on the geometrical edge of the object. If the object has a limb-darkening, the inflexion point is shifted inward by an amount δ increasing with the width of the spreading function. HILL et al (1975) computing this effect for a simplified model of the solar limb and for gaussian spreading functions of increasing widths, concluded, also from unsuccessful observations, thatthe method was hopeless.

Taking into account the angular resolution we are used to experience at Pic-du-Midi with our 50 cm refractor, we thought, from our part, that it was worth to be developed, and we tried to demonstrate it by a preliminary series of observations on one limb only.

Fig. 3 shows CRO tracings of the signal and of its first derivative during a scan across the limb. The scan, produced by a rotating glass cube, is very fast

(≃ 3000" per sec.) and this is fundamental to freeze the image; the scanning aperture is quite small (0"1 x 0"1); the signal is sampled and stored for further computation of three quantities : the maximum slope m, the abscissa x of the point where the slope is maximum, taking as origin the edge of the window which limits the scan (on Fig. 3 the window is purposedly out of focus to provide a slope calibration) and the integral A of the flux throughout the scan.

It can be shown that A depends only of the abscissa x_o of the true limb and practically not of the width of the spreading function. As, during a daily observational run, x_o varies because of guiding errors, variation of the refraction with zenith distance, and random image motion, a plot of x against A is theoretically equivalent to a plot of x against x_o . Fig. 4 is an example of such a plot. The non-symetrical dispersion is conspicuous : it simply demonstrates the existence of the shift $\delta = x_o - x$. The aim is to establish a calibration curve of δ against the maximum slope m which is known for each point.

The first step is to draw a curve assumed to represent x_o against A, through the points known to have the highest values of m. Then, the distance in ordinate of each point to the curve is a first approximation to the value of δ, refered to an arbitrary origin. Such values when plotted against the corresponding values of m would lead to the correlation we are looking for. But now, to find the origin for x_o, and therefore the position of the true limb and the correct value of δ, one must extrapolate to large values of m. Of course, this should be done on a inverse scale; we have chosen to number it conventionaly in Full Width at Half Maximum, ε, of the gaussian spreading function which, applied to the HSRA limb, produces the slope m. Where to extrapolate ? The theoretical FWHM of our objective is 0"25, so that the maximum theoretical slope of the limb would correspond to about 0"30. Fig. 5 shows the result for one day of observation under conditions we call "good", but not outstanding. For clarity each dot is the average of five points. A "very good day" shows a nice clustering of the points between 0"50 and 0"35.

The probable error on one scan can be estimated, at the moment, to ± 0"1. But there are at least two reasons which substantially contribute to it and are to disappear soon. One is that, as said before, the curve x_o against A is a first approximation and should be improved by an iteration process which has not yet been applied here. The second and most obvious reason is that the sampling interval of the signal is, by now, as large as 0"8, thus badly affecting the accuracy of the determination of x; this interval will be reduced, soon, to 0"2. Therefore, we can expect that, in the final stage, the dispersion will fall well below, say, the pole-equator difference found by DICKE.

For the future of this experiment, an instrument which could logically be

called a heliometer is approaching completion, to be associated with the 50 cm refractor under our "turret-dome". The principle is to project the focal image (diameter about 60 mm) onto a Cer-Vit rod cut with sharp edges at both ends, slightly shorter than the solar diameter, and to scan both limbs simultaneously (Fig. 6). The diameter is the sum of the ($x + \delta$) quantities, as defined above for each limb, plus the length of the rod. The whole system rotates around the optical axis to explore all the solardiameters in succession. It is planned to have, in a next step, a permanent measurement of the focal length, in order to obtain at any time the angular diameter of the sun.

Now, we must mention an important by-product of these preliminary experiments, namely the oscillations of the value of the maximum gradient (YERLE, 1980). When plotting the values of m for up to six hours of continuous observation, and computing the $\Delta I/I\Delta X$ values (in order to eliminate the variations of atmospheric transmission) residuals of the order of ± 2% appear around a mean value which decreases from morning to afternoon. This trend is very likely due to the deterioration of the image quality while day-time is advancing. The difference between the values measured and an average curve gives the final residuals (Fig. 7), which could have two completely different origins, or both at once : either the time fluctuations of image quality, or solar effects.

The power-spectrum of these residuals (Fig. 8) shows an evident similarity with those obtained from high-sensitivity Doppler measurements of solar oscillations (ISAAK et al. 1979). It is not easy to imagine that local turbulence in the terrestrial atmosphere could present so definite frequencies in its fluctuations; but, as, unfortunately, it does exist, it should at least produce noise in the power spectrum.

As for the emergence of already known solar frequencies, an attractive explanation may be put forward, pending confirmation. It has been shown, above, that a change in temperature in the layers contributing to the formation of the limb changes the value of the maximum gradient; therefore, if spatial solar oscillations (e.g. at 3.3.m Hz) imply also temperature oscillations, they could appear in the gradient measurement.

Comparing the face value of ± 2 % for the fluctuation of the maximum gradient with the change produced by a temperature modification in region b_2 as it appears in Table I, one would conclude that it corresponds to a ΔT of about ± 70°. But in fact, the trueamplitude of the gradient fluctuation must be corrected by a deconvolution using the spreading function at the moment of the scan, which can only increase the above value of the temperature change.

References

1. R.H. DICKE and H.M. GOLDENBERG, Phys. Rev. Letters. 18, 313 (1967)
2. H.A. HILL, R.T. STEBBINS and J.L. OLESON, Astrophys. J. 200, p. 472 and p.484 (1975)
3. H.A. HILL, private communication (1976)
4. H.A. HILL and T.P. CAUDELL, M.N.R.A.S., 186, 327 (1979)
5. J.B. ROGERSON, Ap. J., 130, 985 (1959)
6. H.A. HILL, R.D. ROSENWALD andT.P. CAUDELL, Ap. J. 225, 304 (1978)
7. J.E. VERNAZZA, E.H. AVRETT and R. LOESER, Center for Astrophysics, Cambridge Mass., Preprint Series n° 1308 (1980)
8. R. YERLE, 1980, Letter to the Editor submitted to A. and A.
9. G.R. ISAAK, A. CLAVERIE, C.P. Mc LEOD, H.B. van der RAAY, 1979, Nature, 282,591.

+++

TABLE I

Layers n°	ΔT	x arc sec.	Δx	ΔI/IΔX (°)
(a) 1 to 95	- 300	- 0.444	+ 0.018	6.77
	000	- 0.426	0.000	7.94
	+ 100	- 0.418	- 0.006	8.27
	+ 300	- 0.410	- 0.016	9.00
(b_1) 1 to 30	+ 300	- 0.426	0.000	8.09
(b_2)31 to 65	+ 300	- 0.413	- 0.013	8.66
(b_3)66 to 95	+ 300	- 0.426	0.000	7.94
(c_1)95 to 1	0 to - 285	- 0.435	+ 0.009	7.51
(c_2)95 to 1	0 to + 285	- 0.420	- 0.006	8.36

(°) ΔI/IΔX expresses formally the relative change in brightness ΔI/I over a radial interval ΔX taken equal to 1"0, although the gradient is roughly constant over 0"2 only.

CAPTIONS

Figure 1.- The HSRA model temperature vs height, and modifications introduced. In abscissae, height in kilometers from the level $\tau_{5000} = 1$ at the center of the disk (positive for the inner photosphere, negative for the chromosphere). In ordinates, temperature in degrees K.
Full line : normal HSRA model;-•--•--•-- model a for constant ΔT from layers 1 to 95; models b_1, b_2, b_3 are shown for constant ΔT between layers 1 - 31. 31 - 66 and 66 - 95 respectively and zero elsewhere; -------- model c_2 with ΔT linear function of height, with zero at layer 95 (for the clarity, the ΔT on the figure are three times larger than those mentioned on Table I).

Figure 2.- The solar limb computed from HSRA model; the origin in abscissae is $\mu = 0$ for $\tau_{5000} = 1$; $\lambda = 5000$ Å; the intensity at the center of the disk is 32.8. Lower and left scales for the full line curve a; upper and right scales for the dashed curve b (where the location of portion a is indicated).

Figure 3.- Oscilloscope tracings of the signal (top) and of its first derivative (bottom), showing the definitions of the abscissae of point of maximum gradient on the true limb L (x_o) and on the blurred limb (x)(δ is the shift), of the maximum gradient itself m, and of the integral flux Λ. For this preliminary experiment, the edges of the window limiting the scan are purposely blurred to provide a calibration of the gradient.

Figure 4.- Observed correlation between the area (integral flux) measured and the abscissa of the point of maximum gradient. The slightly curved parabola shows the best fit among points corresponding to high values of m.

Figure 5.- The correlation shift (arbitrary origin) vs FWHM (both in seconds of arc). The true origin for the shift should be determined by extrapolation to small values of FWHM (see text).

Figure 6.- Left : the solar image, as seen looking to the sky. S_p and S_a are the solar images at perihelion and aphelion; R is the CERVIT rod; Rh_1 and Rh_2 are two rhombohedra; S_ℓ and S_r are the portions of the limb as seen through the rhombohedra.
Right : the profile of a complete scan, on left limb ℓ, calibration beam b, (drawn from the center of the disk) and right limb r, with scales in arc and time seconds.

Figure 7.- Residuals of $\Delta I/I\Delta X$ on Sept. 11, 1979, in percent of the average value. A periodicity of about two and half hours is visible but has to be confirmed.

Figure 8.- Power spectra : top,of the maximum gradient on the limb, on Sept. 11, 1979, expressed in (arc $sec^{-1})^2 mHz^{-1}$ (YERLE, 1980); middle and bottom, of integrated radial velocity, measured simultaneously at Izaña and Pic du Midi on Aug. 8. 1978, expressed in $(ms^{-1})^2 m\ Hz^{-1}$ (ISAAK et al., 1979).

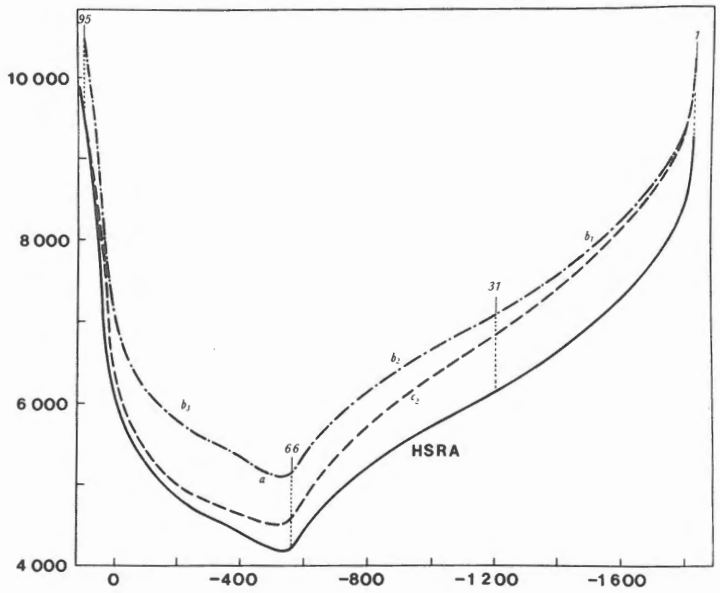

Figure 1.

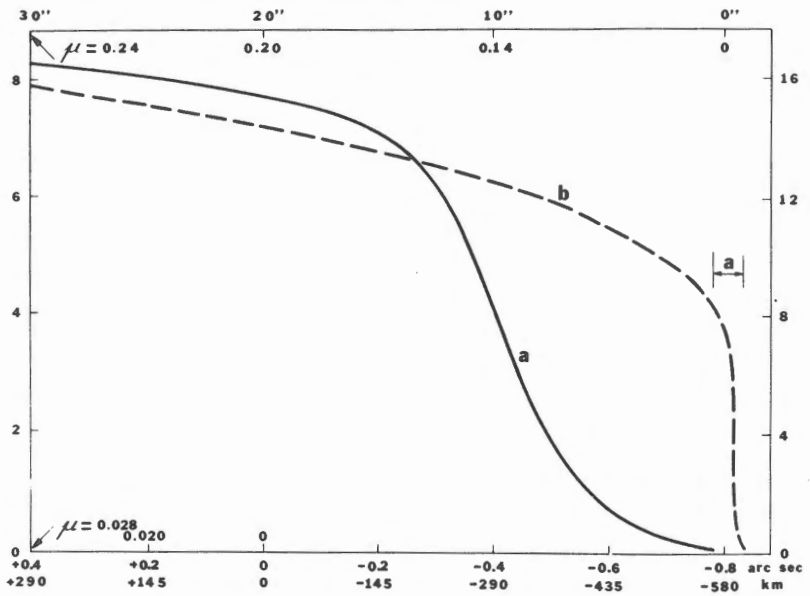

Figure 2.

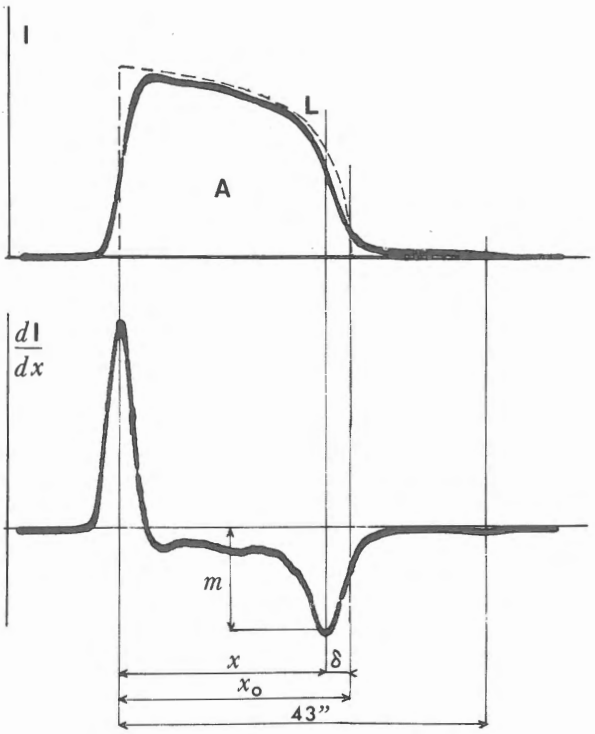

Figure 3.

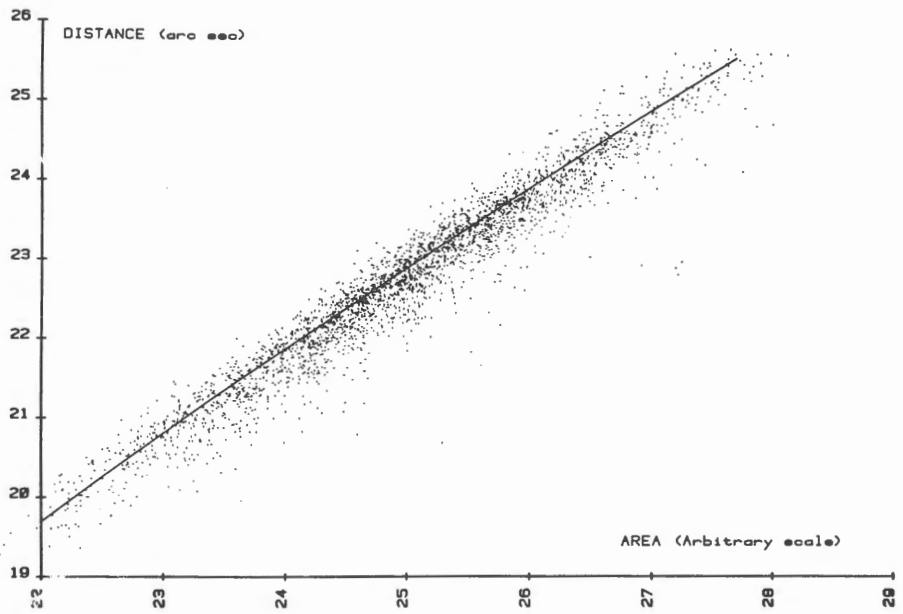

Figure 4.

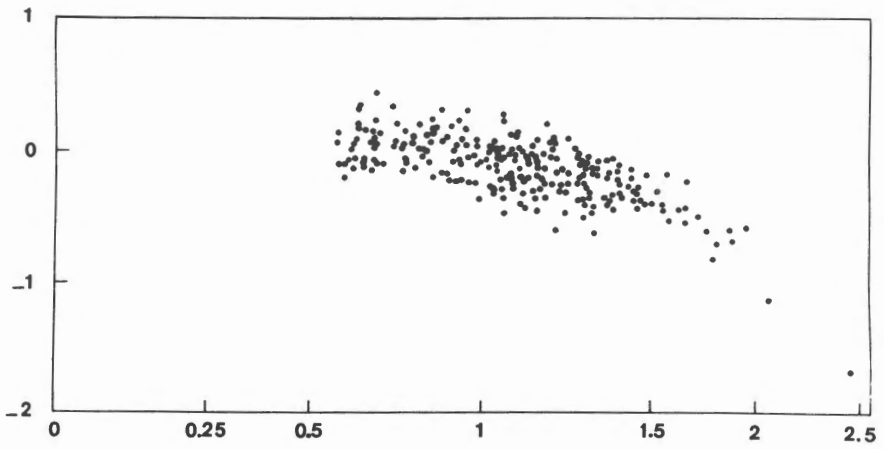

Figure 5.

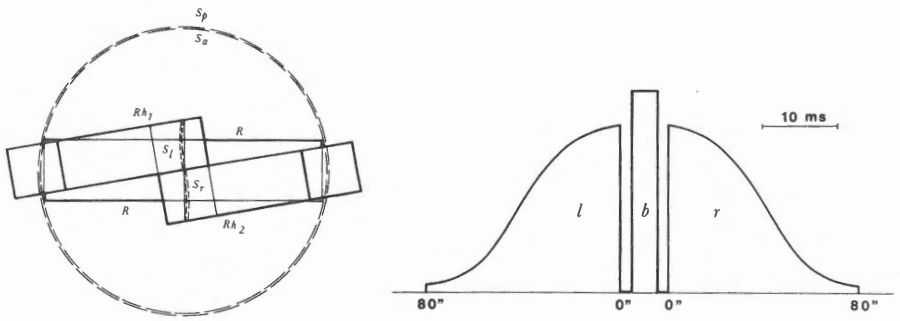

Figure 6.

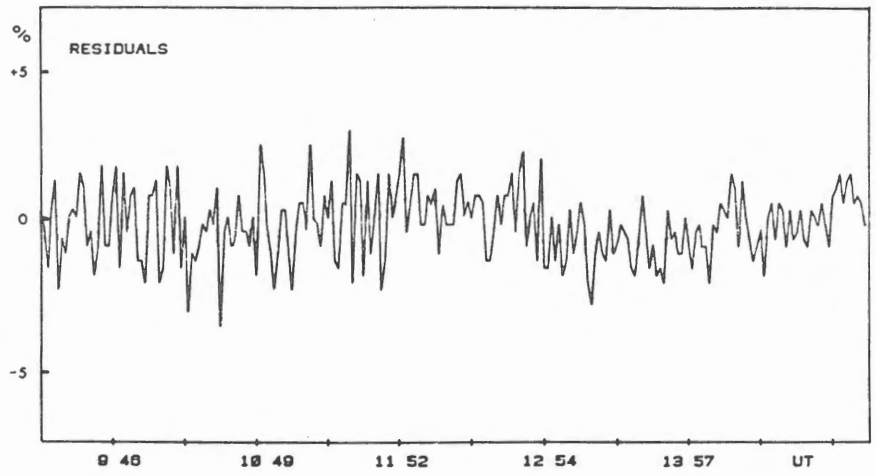

Figure 7.

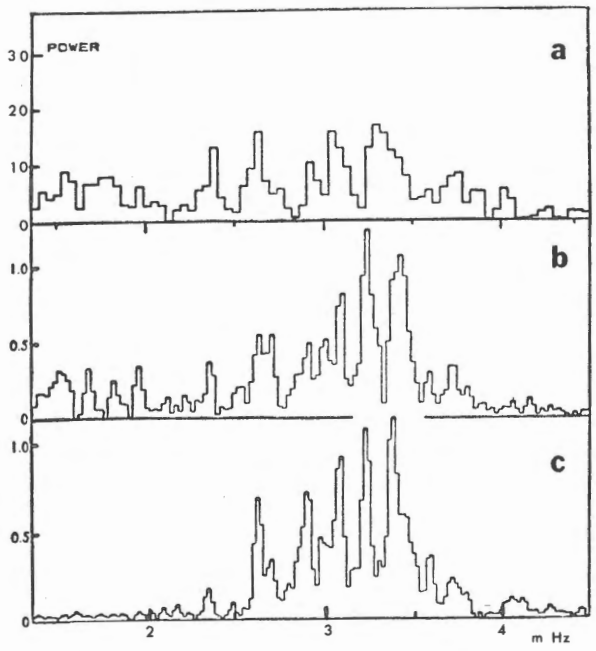

Figure 8.

ATTEMPTS TO DETECT EMERGING TWISTED FLUXTUBE

Katsuo Tanaka
Tokyo Astronomical Observatory

1. A Proposal for Future Ground-Based Solar Observations

We have been discussing over years about our future plans of ground-based solar observations. I report some points of the discussions and my own proposal of telescope system and observations. Since observations in very high spatial resolution can only be performed in the space, future ground-based observations should emphasize very high precision, long-term observations and systematic determinations of physical quantities which require large instruments. The scientific objectives we consider would be, firstly to study the sun as a star, and secondly to study detailed dynamics of the magnetic fields which causes sun's activities. More specifically, for the first objective, we should start and continue for long period over a 100 year the full-disk measurements of magnetic field vector, velocity field and brightness distribution and monitor large scale magnetic patterns, velocity fields-global convection and circulation and non-uniform rotation, torsional oscillation and their short and long term variations. This kind of observations should be combined with diagnostics of internal structure(particularly convection zone) and its 11 years or any other variations by means of measurements of non-radial and radial pulsations. Long term observations will clarify solar dynamo mechanism and natures of long period activity cycles and their effect on the earth climate and solar system environment. Short term full-disk measurements are also important to examine e.g. energy inbalance due to sunspots, faculae, and coronal hole. Required precisions for these rather routine type observations would be 0.1G for $B_{\parallel}(10^4)$, at least 10G for $B_{\perp}(3\times10^4)$, 0.1-1 m-s for $v_{\parallel}(5\times10^3\text{-}5\times10^4)$ and 0.01% for $I(10^4)$. Number in the parenthesis indicate signal to noise ratio required. It is necessary to acomplish measurements of $B_{\parallel}$,($B_{\perp}$),$v_{\parallel}$,I simultaneously in a short time to increase data coverage at cloud-rich site.

For ultimate understanding of physics of surface magnetic structures

or for the second objective, we will need simultaneous determinations with high spatial and time resolutions of three dimentional distributions of velocity, magnetic vector field, density and temperature in each strucrure. Although this should be performed in the space ultimately, perfect determinations even with restriction to visible bands have not been achieved in the ground-based observations. We should obtain two-dimentional maps of v, $\underset{\sim}{B}$, I at least at two photospheric levels and chromosphere simultaneously for each active region or quiet region with time resolutions depending on the purpose (1s-1hr) and good spatial resolution of the order of 1". Requirement of the S/N would be 10^3.

For simultaneous and quick measurements at different lines it is essential to use diode-array type detectors and place them at foci of various lines. Diode-array may be two-dimentional; one for the spatial points along the slit the other for the wavelength points of a line profile. The photon count rate (E) in each pixel of the array reads $E=eD^2/I^2 xy\,\eta\Delta\lambda$(e: input photon per $cm^2$and A), D: telescope diameter, I: image size of the sun, x: slit width, y: slit length in each pixel=x, η: efficiency of telescope, spectrograph and detector=0.05 typically, $\Delta\lambda$: wavelength bandpass at the detector=25mA). Taking into account that the measurement is shot-noise limited we obtain $S/N=90D(cm)x(\text{″})\sqrt{t(s)}$. To scan a region of L'xL' using slit length equivalent to L' it takes $\Delta t \simeq 9.3x\ 10^{-4}L(S/N)^2/(D^2x^3n)$ seconds, where n is number of slits.

To achieve above mentioned observations we propose a system shown in Fig.1. Two telescopes feed two kinds of images on the top of a common vertical spectrograph. One telescope should have an aperture as large as possible and aims measurements of linear polarization and very small $v_{\perp}$and $B_{\perp}$. As an analyzer a rotaing quarter wave plate and KDPs are adopted. Lense system is favored for the primary to avoid instrumental noise produced by the obstacles in the light path. Total noise level including uncancelled instrumental polarization would be less than a few times 10^{-5}. Adopting D=65cm a measurement of a region 8'x8' with $N/S=10^{-4}$ and 2" resolution is fulfilled in 40s. Because of difficulty of quick motion in large telescope and requirement of simultaneous measurement in many lines, a second small and achromatic telescope($D\geq 30cm$) is placed horizontally after coelostat and produces 9cm solar image on the 9cm long slit. The full disk measurement at 12 different lines can be performed in 1700/n seconds with the accuracy of 1 ms^{-1} and $0.2G(B_{\parallel})$ and 1" resolution. These lines may be B-sensitive, v-sensitive and T-sensitive lines formed at deep, middle and upper photosphere, respectively

Fig.1 A proposed telescope system

a. telescope 1(refractor)
   D ≥ 65cm F/15
b. primary image(10cmΦ),guider,slot
c. analyzer(a rotary λ/4 plate, KDPs)
d. telescope 2(reflector)
e. image(9cmΦ), slit(9cm l)
f. analyzer(KDP or calcite)

spectrograph

g. collimator
   f=10m, F/30
h. grating(effective aperture=30cm)
i. camera mirrors

detectors

j. two-dim.arrays
   (2000x200)
   for telescope 1
k. two-dim. arrays
   for telescope 2
   (12 arrays for
   $B_{\parallel}$, $v_{\parallel}$, T measurement
   at 4 layers)

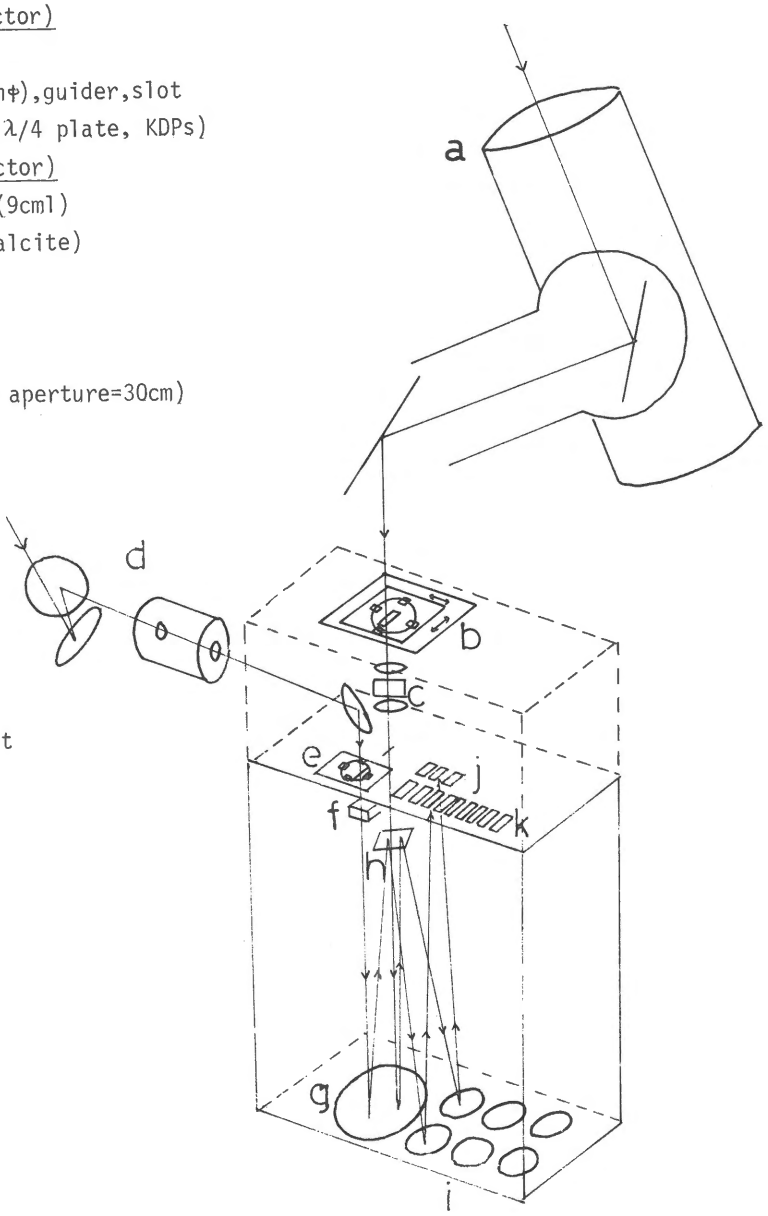

and at chromosphere.

A test model of the latter system is under construction at Mitaka. Here a mirror telescope of D=20cm and F/15 makes 2.8cm solar image at the entrance of a horizontal vacuum spectrograph, and line profiles of two circular polarizations are measured for four lines simultaneouly by stepping linear CCDs across line profiles with the smallest step of 1 micron (1.6mA). Calcite block is used as a beam splitter and $\lambda/4$ wave plate. Selection of lines can be achieved by displacing the detectors. Test performances using this system and also the vector magnetograph at Okayama would be the basis to realize proposed observatory in the future.

2. Detection of Emerging Twisted Fluxtubes

One of the specific key problems that belongs to the second objective mentioned in §1 would be the study of magnetic flux emergences. Generally sun's surface activities are initiated by the emergence of bipolar fluxloops. There is a smaller scale version of the flux emergence outside active region known as an ephemeral active region. A third kind of flux emergence which would occur in much shorter and smaller scales may be expected in the quiet region. Eruption of small loops in the quiet region is suggested by recent UV observations by Brueckner. Physical consequence of the flux emergence would be that some extra energy of the magnetic fields which is injected in the convection zone is convected out directly into the corona. Then, it may be conjectured that these extra energies in three different regions are responsible for flares, x-ray bright points and coronal heating in the quiet region, respectively. Although this is still umproved hypothesis, for the special family of spot goups called δ-group in which intense flares occur frequently, there are some observational materials which suggest that the fluxtube constituting δ-group emerges out as it is twisted and that flare occurs in the individual fluxtube which have emerged out as described below.

(1) Configurations of δ-group

Any complex configuration of δ-group can be decomposed into sets of compact bipoar spots in which two poles are closely located, large horizontal fields exist in between the two poles, and spiralled penumbral structure surrounds the two spots. This photospheric configurations (Fig.2a) suggest a compactly twisted magnetic knot as shown in Fig.2b.

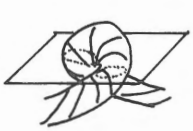

Fig.2a Fig.2b

Fig.2a Typical bipolar configuration element in δ-group

Fig.2b A twisted magnetic knot and its photospheric cross section as sunspots

(2) Characteristic evolution patterns

A bipolar part of the complex δ-group or a single bipolar δ-group develope in the pattern of mode A (Fig 3a) : two spots grow rapidly with penumbral filaments connecting straightly, then there occurrs a relative motion between the two spots (shear motion) together with the filaments showing curls, finally well-developed spirall appears. In the decay phase of a complex group a mode B evolution (Fig.3b) is seen : one growing spot approaches one of the bipolar pair which showed modeA evolution, the neutral line between the two spots is dominated by a part of the curled filaments which developed in mode A. As the new spot (f) approaches, these filaments become less curled and connected to the two spots at the ends. Finally filaments connect straightly the two spots similar to the initial stage of mode A and one of the spot shrinks rapidly. Since photospheric fields would represent the field configuration of high beta region, these peculiar evolution can be explained by the continuous emergence of a twisted knot like the one shown in Fig.3c considering that photospheric spot configuration is an intersection of the fluxtube with a horizontal plane.

Fig.3a
Mode A

Fig.3b
Mode B

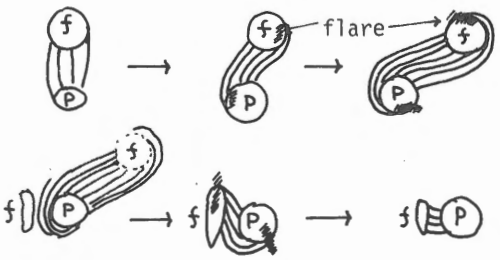

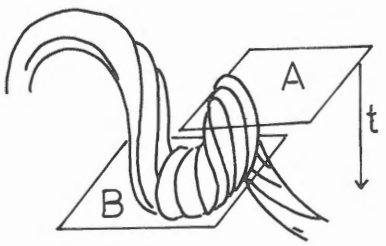

Fig.3c A magnetic knot whose continuous emergence explains mode A and mode B evolutions of sunspots.

(3) A general law of configuration and motion

All the cases after 1969 show a rule shown below concerning direction of the magnetic axis, helicity of the penumbral spiralls and direction of the shear motion, for the mode A evolution. This is easily explained by an emergence of the twisted knot.

magnetic axis	helicity	shear motion
p/f(p-spot north of f-spot)	left-hand twist	f-spot-- east
f/p(f-spot north of p-spot)	right-hand twist	p-spot--west

(4) Anomalous velocity field

There have been observed in the last stage of mode B evolution a large blue shift (>1kms) at the neutral line consisting of strong horizontal fields. The two spots on the sides of the neutral line showed continuous shear motion and disappeared gradually (Fig.4) since this group is close to the disk center, this motion probably manifest the last stage of the flux emergence in which a tube concave to the surface emerges out (Fig.3 c).

Fig.4 Velocity contours superimposed on spot configuration(1974 July 4). Thick line for blue shift.

(5) Evolution of the flare site

In course of Mode A and B evolution Hα flare sites successively shift to the new positions which correspond to the feet of the newly developed penumbral filaments. This suggests that flare occurs in the individual twisted tube which has emerged out.

(6) Energetics of flares

Energy input evaluated under the assumption that flare energy is directly supplied to corona by emergence of the twisted part of the flux tube agrees quite well with the energy output of flares evaluated from soft x-ray flux and interplanetary shock wave flux (Tanaka, Smith, and Dryer 1978 IAU Symp.91)

Whether this model applies to other flares than occur in δ-group may be tested by measuring magnetic field vector structure in the flare region outside sunspots. The measurement of the velocity field at

several levels would be important to distinguish vertical flow associated with the flux emergence of the knot from usually dominant horizontal flow. Transient loop eruption in the quiet region occurs in a short time (20s), thus high time resolution measurement with high sensitivity magnetograph is essential to detect it. These observations may, hopefully, be enabled by the proposed instrument.

ON-AXIS STELLAR MAGNETOGRAPH

Kyoji Nariai
Tokyo Astronomical Observatory, the University of Tokyo

The double-circular analyzers of Babcock-type for stellar measurements are used at Hale, Lick, and Mauna Kea observatories. With this type of instruments, we obtain partial information of polarized light, namely I and V. In order to obtain all the Stokes parameters, we have to modify the Babcock's instrument in the following way;

1. rotate the analyzer at the diurnal rate,
2. move the retarder with respect to the analyzer,
3. use a plane-parallel plate so that the instrumental polarization due to the difference in the reflectivity of two linear polarization is compensated,
4. use an image rotator so that the two images corresponding to two linearly polarized light at the end of the analyzer be put into the slit of the coudé spectrograph at the same time.

Another way to make the same measurements is to put the retarder and the analyzer in the telescope tube so that the oblique reflections by coudé flat mirrors take place after the light passes the analyzer. Then, we can avoid the light losses and the errors due to the compensator, but we need a special secondary mirror and a relay lens system. 2 and 4 in the preceding paragraph are used with this type of instrument, too. For a horizontal coudé system for which the reflection angle at the fifth mirror changes with time, the use of "on-axis analyzer" is almost indispensable. I hope that the future project of the large telescope of Japan include it as one of the main auxiliary equipments. My colleagues and I also plan to have a proto-type on-axis magnetograph with the 188cm reflector of Okayama Astrophysical Station of the Tokyo Astronomical Observatory.

SOLAR RESEARCH FROM SPACE

Roger M. Bonnet
Laboratoire de Physique Stellaire & Planétaire
Centre National de la Recherche Scientifique
P.O. Box 10, 91370 Verrières-le-Buisson, France

1. Introduction

The programme of solar observations from space was initiated in the early 1960's under the original ideas of Professor J.C. Pecker. I had the privilege of carrying out the first elements of this programme at the Service d'Aéronomie du C.N.R.S. as early as 1961, and I have had the opportunity to continue working in this field since then. At that time, the American programme was already well underway. It included a large number of rocket launches per year and the first satellites of the OSO series ware ready to be launched. For a small country like France to undertake research in the same area, was of course very ambitious, and as J.C. Pecker said at that time : "The American have or will very soon do everything which is possible, so we are left with the impossible." So we did it ...!

This paper intends to describe briefly

i. what are the most important results obtained in the not too distant past ;
ii. the programme which is presently underway and finally
iii. the proposed programme for the near future.

The accent will be given to results and programmes which involve the production of hardware and we do not include herein presentations of the numerous results obtained in the framework of Guest-Investigator Programmes. References to the most important publications will be given extensively throughout the text so that the interested reader may find out more details than is possible to give herein, due to obvious editorial limitations. For the same reson, this presentation does not include either the remarkable results obtained in solar radio astronomy by J.L. Steinberg using the very elegant stereoscopic observations from the ground and a spacecraft.

2. An overview of the most important results of the past programme.

As mentioned in the introduction, solar instrumentation designed to carry out observations with the means of space techniques started to be developed in France in 1961. I was in charge of the ultra-violet part of the spectrum and P. Léna was in charge of the infra-red part. Very soon after, P. Lemaire joined our group and increased our task force. The "Impossible" covered mostly the need to reach spatial as well as spectral resolution, since most of the pioneering work had already been done. Our directions of work were therefore twofold and have developed from thereon.

a. Center-to-Limb measurements.

P. Léna and myself have been conducting these measurements in our "respective spectral region. The first measurements in the ultra-violet between 200 nm and 300 nm and the far infra-red (around 10-25 μm) were obtained and are still used now as references (Bonnet, 1968, Léna, 1969). Absolute intensity measurements were also obtained which could fix upper limit to the surface temperature of the sun and served as inputs to the Bilderberg Continuum Reference Atmosphere (B.C.A.), (Léna, 1968, Bonnet and Blamont, 1968). This work has been continued since then by J.P. Baluteau (1970) and D. Samain. Because of its importance, we describe here Samain's work in more detail now.

The technique used by Samain(Samain et al., 1975) was an extrapolation of that used by, and described in, Bonnet et al., 1967 : an image of the sun is formed on the slit of a stimatic spectrography, with the center of the disk positioned on the slit. The spectrum consists in a series of monochromatic and stigmatic images of the slit recorded on photographic film. The photometry of these images allows the measurement of the center-to-limb variation of the ultra-violet solar intensity. Samain's instrument operated between 120 and 210 nm. It was launched successfully on April 17, 1973 on board a Veronique rocket, and provided excellent absolute intensity and center-to-limb measurements. Samain's central intensities (Samain, 1979) are reported on Figure 1 and can be compared to Nishi's similar results. The agreement can be seen to be very good. Samain's data have been analyzed in terms of solar models andwere able to give the first empirical determination of the ultra-violet opacity and of the departures from Local Thermodynamic Equilibrium of Si I in the U.V. They are published in an extensive form in Samain (1980). They also allowed obtaining values of the solar U.V. irradiance which are currently used widely by aeronomists (Samain and Simon, 1976).

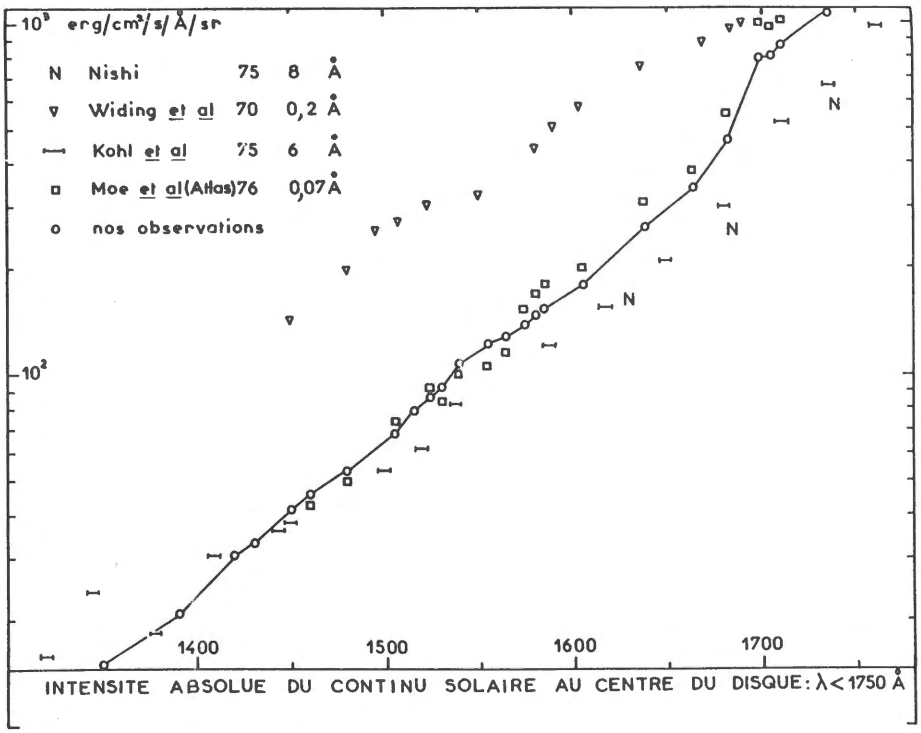

Figure 1 : The absolute spectral radiance of the sun as measured by Samain (1979) between 120 and 210 nm, and compared with other measurements.

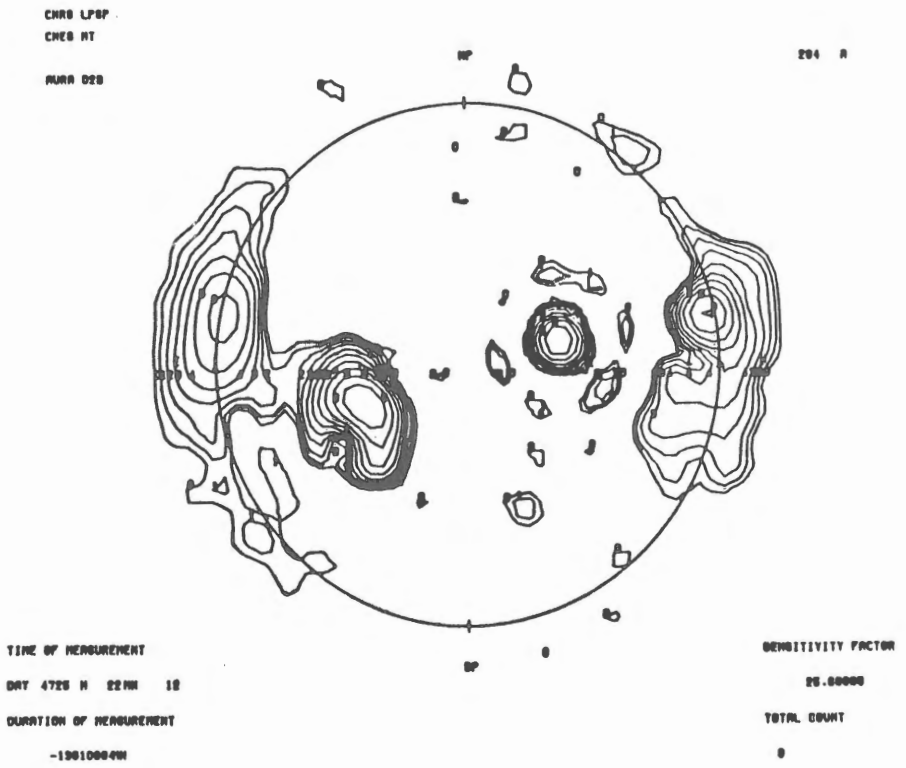

Figure 2 : Spectroheliogram of the Fe XV 28.4 nm EUV line obtained with the LPSP instrument onboard the French D2B Aura Satellite. The angular resolution of that instrument was one arc-min., good enough to show active regions on the disk and the corona at the limb.

Later on M. Hersé (1979) obtained high resolution images in the vicinity of 200 nm with a resolution below one arc-sec using a high resolution balloon borne telescope.

The French D2-B AURA satellite launched on September 21, 1975 had a solar pointing capability and carried a moderate resolution instrument (Delaboudinière, 1973) which could make solar spectra (0.2 to .3 nm)and full sun spectroheliograms (1 arc min resolution) in the region 20 to 125 nm. During the 16 months of operation of the satellite, excellent images of the sun and spectra were obtained (Figure 2), (Delaboudinière and Millier, 1977). The E.U.V. images have been published in Solar Geophysical Data for the period September 1975, December 1976. The main aim of this instrument however was to study the chemical composition of the earth atmosphere by means of extinction measurements at sunsets and sunrises using the active regions on the disk as point sources.

b. High spectral resolution observations.

Using more economic and more easy to work techniques, P. Lemaire was particularly successful in obtaining the first high resolution profiles of the Mg II h and k resonance doublet at 279.5 and 280.3 nm (Lemaire and Skumanich, 1973). Delaboudinière and Crifo (1976) obtained excellent high resolution spectra of the 58.4 nm He I line using a helium resonance cell.

Lemaire's work was a key element in our decision to propose a multichannel high resolution U.V. and visible instrument on board OSO-8. This proposal was accepted in 1970 and the French instrument received its first photons from the sun on 21 June 1975. It operated successfully for more than 3 years and was turned off by NASA in October 1978. The instrument is described in Artzner et al. (1977) and Bonnet et al. (1978). The data obtained consist in high resolution profiles of the Ca II H and K, the Mg II h and k, the H I Lα and Lβ lines, observed simultaneously with a spatial resolution as good as two arc seconds. We are still now in the process of data analysis but some important results have already been published from a set which represents no more than ≃ 20 % of the whole quantity of data.

To summarize, three areas have been exploited in more depth :

i. Modelling of active regions.

Figure 3 shows an empirical model of active region obtained by P. Lemaire (1980) through the best fit of computed Lα, H and K and h and k profiles with corresponding observed profiles. The typical observed profiles are shown on Figure 4 together with the computed ones.

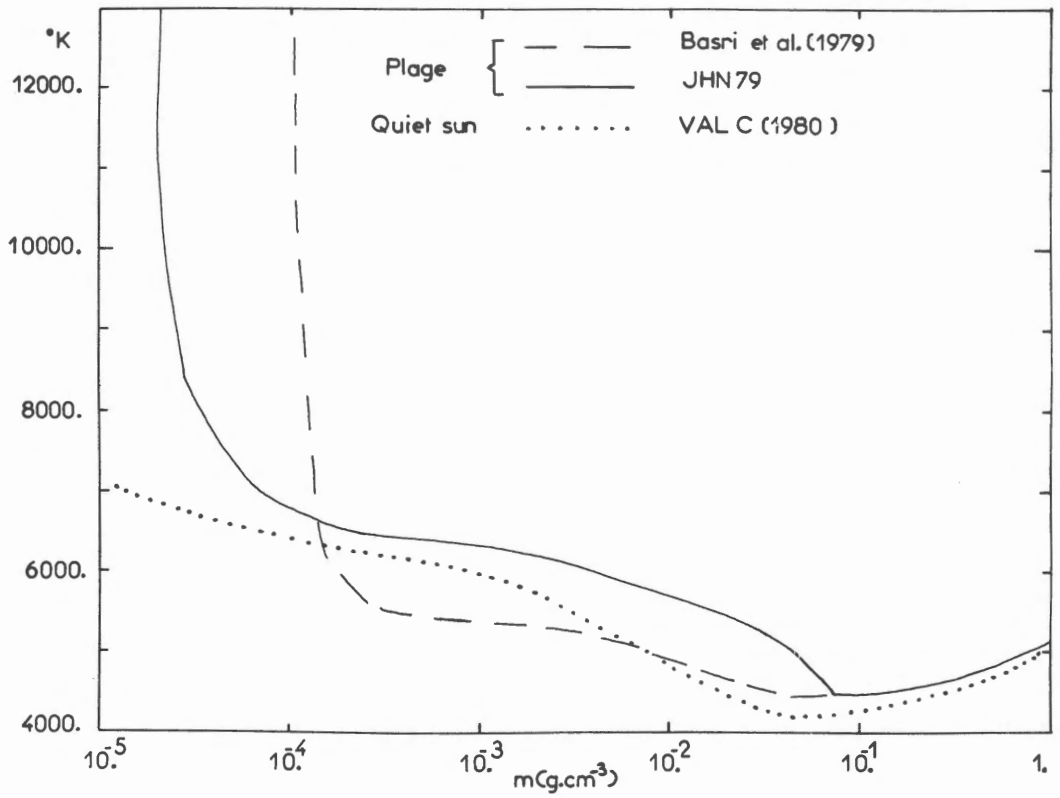

Figure 3 : Active region model JHN 79 derived by P. LEMAIRE (1980) from OSO-8 observations of the Ca II HK , Mg II h and k , L α and L β lines. The model is compared with Basri's plage model and the Quiet sun model of Vernazza Avrettand Loeser.

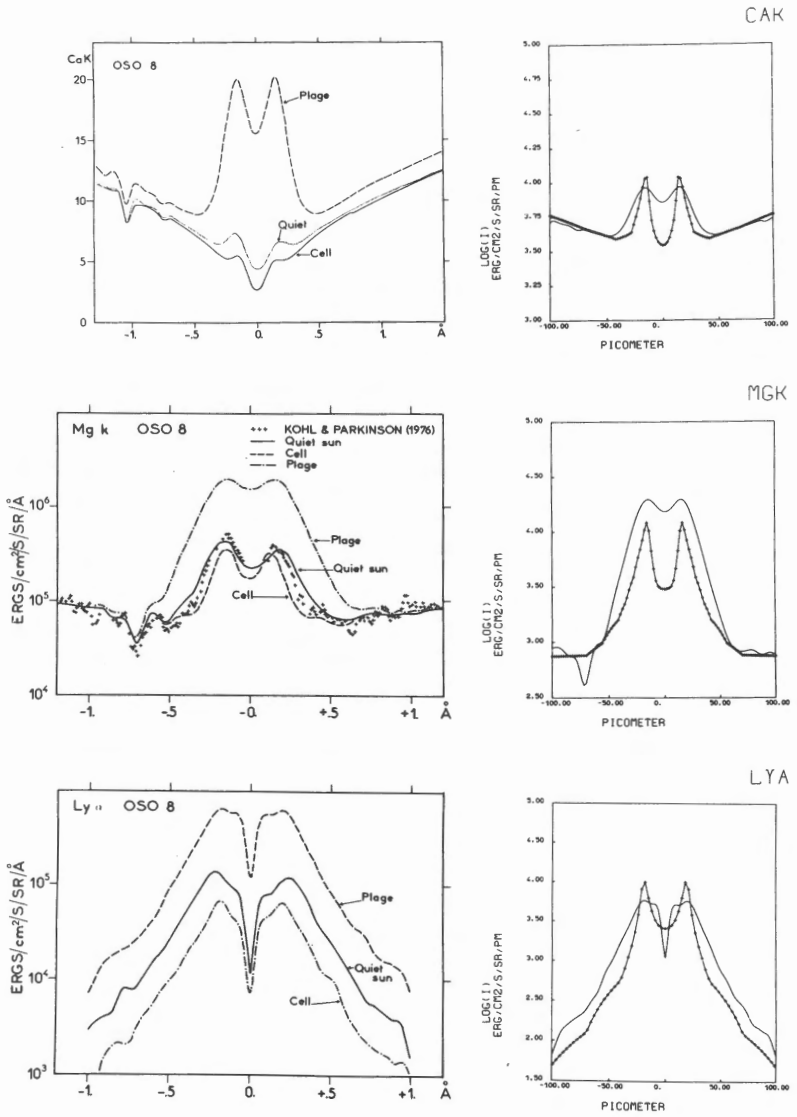

Figure 4 : Comparison between OSO-8 observed and computed Ca II, Mg II and Lα line profiles, using the model of Figure 3. Observations are on the left side, and computed profiles are represented by the dotted line on the right.

ii. Study of chromospheric oscillations.

With its high spectral resolution of 2 pm our instrument was well suited for velocity measurements. Artzner et al. (1978) were able to observe the 200 s chromospheric oscillations in the periodic deformations of the core of the Lα profile. These results compare reasonably well with the computations of Gouttebroze (1980). Any attempt to detect oscillations in the transition region lines (O VI 103.2 nm) have failed within the present limitation of 3 km/s imposed by the spectral resolution of the instrument. Figure 5 is a summary of observations of the 200 s oscillations.

iii. Observations of prominences.

Excellent data on quiet and active prominences have been obtained by Vial et al. (1979, 1980). In Lα the prominences are optically thick with an optical depth at line center of 10^5. In general, as could be expected all six line profiles show complicated time and spatial dependent structures evidencing the existence of strong movements in the prominence (Figure 6). A curious observation is that the ratio $\frac{K}{H}$ is different from $\frac{k}{h}$ in active prominences. Vial is working presently on this problem.

Numerous observations of sunspots, active regions, flares, coronal holes and the chromospheric network have been undertaken but the data analysis is not yet completed.

3. The presently approved space programme.

The decision by the Centre National d'Etudes Spatiales, the French Space Agency to terminate the national sounding rocket programme in 1974 and the national scientific programme in 1975 has had two consequences. First, the number of flight opportunities offered to French scientists has crecreased substantially, and today the national programme is limited stricto sensu to the use of balloons. Balloons however have limited capabilities and do not permit access to the far end of the ultra-violet spectrum. Subsequently we are more and more involved in bi- or multilateral cooperative ventures with American institutes or laboratories and also with Soviet and European groups.

a. The Transition Region Camera (T.R.C.).

One of the best illustrations of a cooperative programme is the joint rocket venture between L.P.S.P. and the Lockheed Palo Alto Research Laboratory (L.P.A.R.L.). L.P.A.R.L. kindly offered L.P.S.P. some space on their rockets. They developed a high resolution X-ray spectrometer and spectrograph. L.P.S.P. developed the T.R.C.

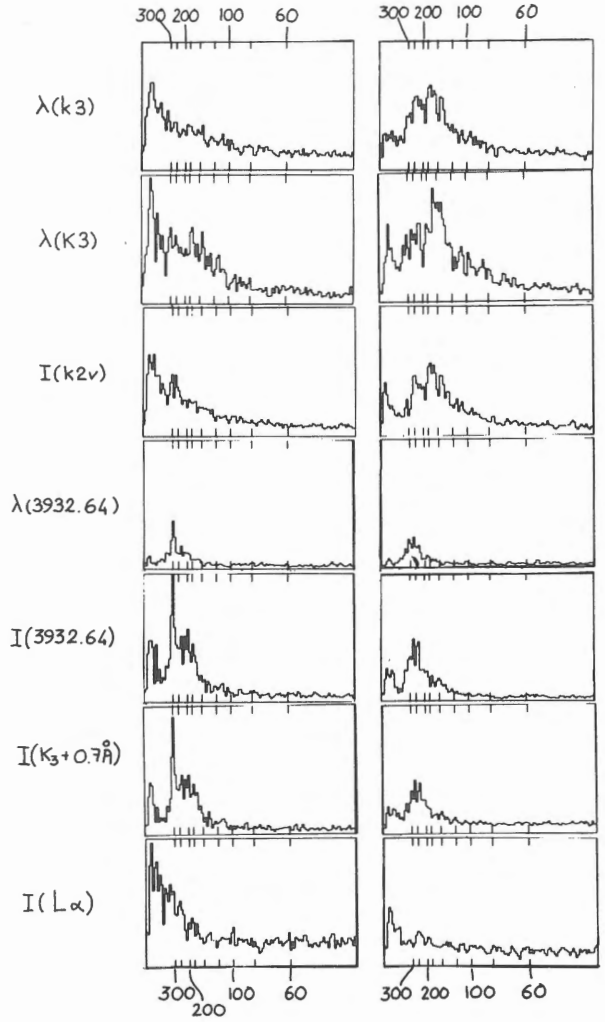

Figure 5 : Power spectra of velocity and Intensity fluctuations in the photosphere and the chromosphere as observed with the LPSP instrument onboard OSO-8 (Artzner et al. 1978). The left row corresponds to observations made in the chromospheric network ; the right row corresponds to dark cell centers. OSO-8 was the first to detect the 200 s line profile oscillation in Lα (line center). However intensity fluctuations in Lα do not evidence any specific well identified period.

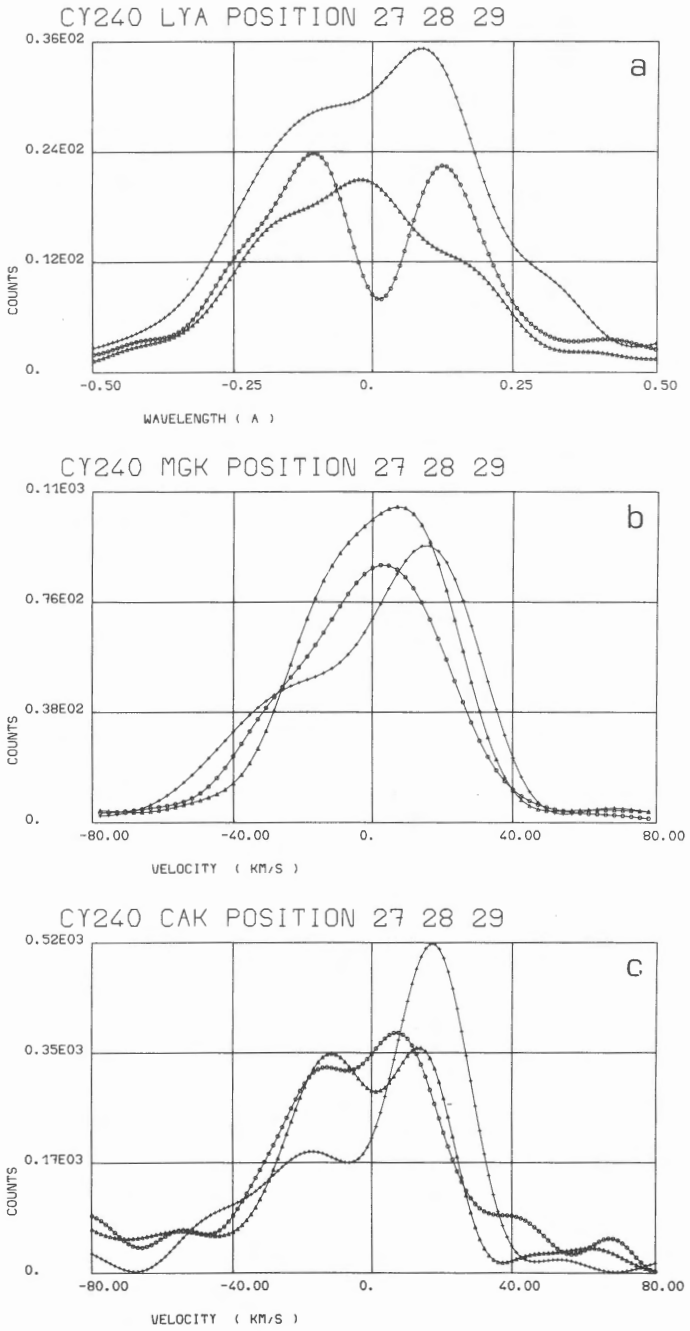

Figure 6 :

Ca II, Mg II, and L α profiles as observed with the LPSP instrument onboard OSO-8 by Vial et al (1979) at various positions across an active prominence.

which consists in a 10 cm Cassegrain telescope, a series of filters and a film camera. This instrument has been launched twice on July 3, 1979 and September 23, 1980. These two flights provided excellent high resolution images in Lyman alpha and at 160 nm. The results of the first launch have been published in Bonnet et al. (1980). They strongly evidence the presence of small scale loops in the chromosphere and the corona. Bonnet and Tsiropoula (1980) have shown that some of these loops are cold (50 000 to 150 000°K), through the absorption of the disk Lα emission by neutral hydrogen. The results obtained during the second launch concern the temperature minimum. As shown on Figure 7 they reveal the fine structure of the network and the numerous bright points already seen in CN and K_2v but with a substantially higher contrast (at 160 nm a 10 % increase in intensity corresponds to $\Delta T = 20°K$).

This programme is intended to continue and another launch of the T.R.C. is scheduled for the summer of 1981.

b. The balloon RASOLBA project.

Following a very successful first generation of balloon spectroscopy by Lemaire and Samain (Lemaire, 1970, Samain, 1971), the L.P.S.P. has defined a second generation instrument aimed at the spectroscopy of the sun between 190 and 300 nm with sub-arc second angular resolution. The characteristics of the instrument are described in Table I.

TABLE I : Main characteristics of the RASOLBA project

Telescope	Cassegrainian, 40 cm diameter Spatial resolution, 0,5 arc sec Inflight focusing.
Slit jaw camera	Hα images displayed in real time for target acquisition.
Spectrograph	λλ : 190-300 nm Spectral resolution, 1.5 pm Detector, photographic film.
Inflight calibration	

The instrument is in its final stage of fabrication and integration proceeds on the telescope and at the sub-assembly level. The first launch is scheduled for October 1981 from the French launching range in South-Western France. Figure 8

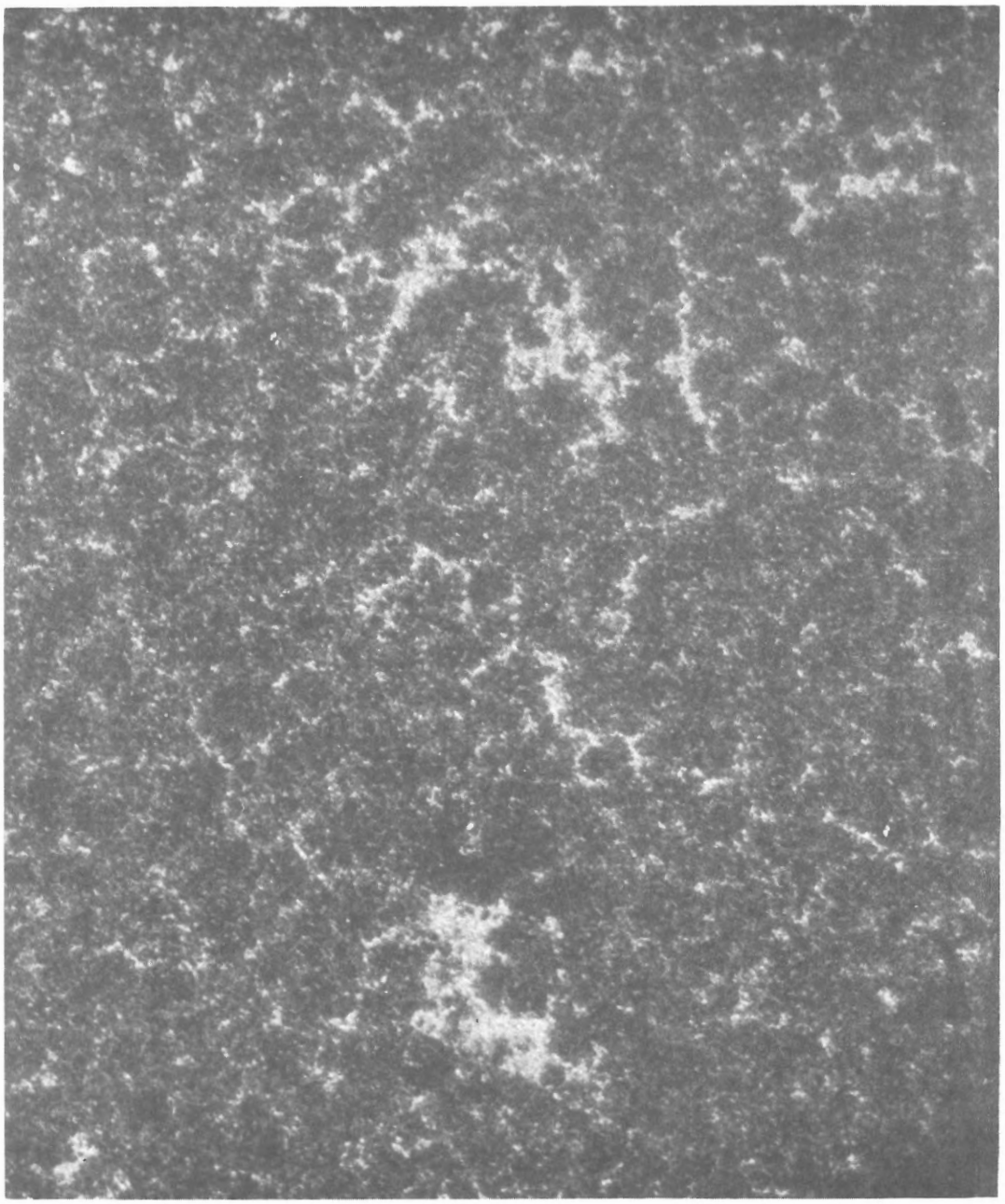

Figure 7 : Detail of a high resolution solar image obtained during the second flight on 23 Sept. 80 of the Transition Region Camera (TRC), (Bonnet et al, 1980) at 160 ± 10 nm. The 160 nm photons originate at the temperature minimum level. On this picture one easily recognizes the highly contrasted chromosphere network and numerous bright dots inside the chromospheric cells.

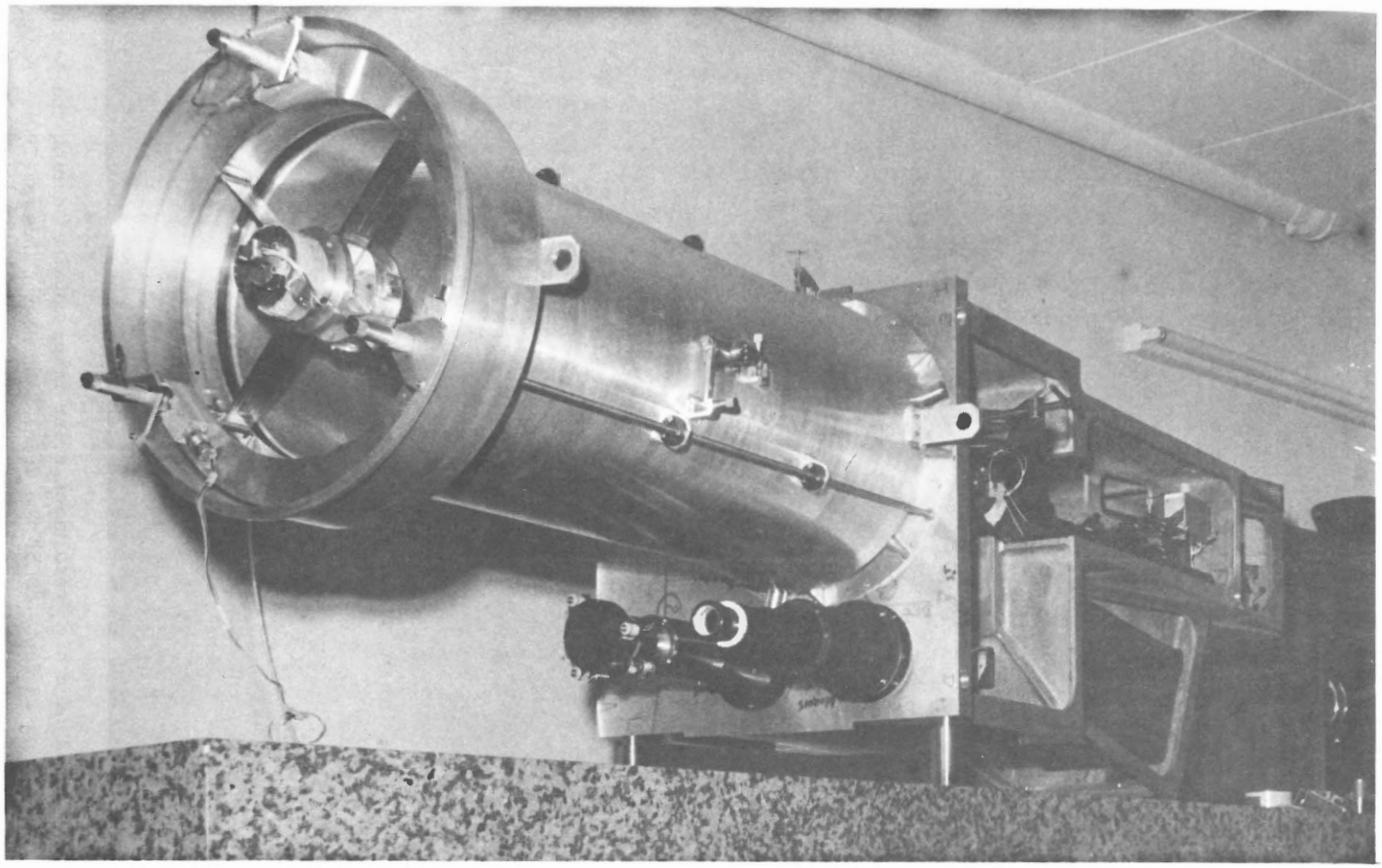

Figure 8 : The main structure and telescope of the balloon RASOLBA project, on the optical bench during mechanical integration. One also the sun sensors and the automatic inflight focussing system on the front face of the main structure. The diameter of the telescope is 40 cm.

represents the telescope and the main position of the spectrometer in the process of mechanical integration.

c. The SCALP project

The Solar Calibration Package (SCALP) is intended to make full sun spectra between 18 and 180 nm, mostly for aeronomy purposes, but it is also well suited to variability studies.

The principle of the instrument is shown in Figure 9. Two identical grazing incidence holographic grating mono chromators cover the ranges from 15 to 62.5 nm and 30 to 180 nm respectively (only one is represented in the figure). The spectrum is analyzed through rotation of the gratings, by a channeltron detector.

The field of view of the instrument is 3° by 1°. Successive diffraction orders are separated by means of broad band thin film filters.

Table II indicates the main characteristics of the two channels :

Channel	Wavelength range (nm)	Grating constant (grooves per nm)	Band pass (FWHM in nm)	Elementary grating step (nm)
A	15-62.5	1100	0.15	0.1
B	30-180	550	0.3	0.2

A rare gas ionization chamber is used in flight for the detection of possible drifts in the sensitivity of the monochromators. The same filters which serve to separate orders in the monochromators are used to define, in conjunction with the appropriate rare gas, narrow sensitivity bands.

In flight calibration will insure that the best photometric accuracy is achieved. We aim at 5 to 1 %. More descriptive details are given in Delaboudinière et al (1976).

SCALP has been proposed to the European Space Agency (ESA) to fly on one of their Spacelab flights. Unfortunately European Spacelab payloads have not been approved yet and have not consequently been assigned a Spacelab flight number. This is the reason why the SCALP instrument is also under negociation between CNES and InterKosmos (the Soviet International Space Organization) to fly on one of their satellites. If approved, the project will be a cooperative venture between LPSP and the Crimea Astrophysical Observatory, and will be rebaptized "OGIS".

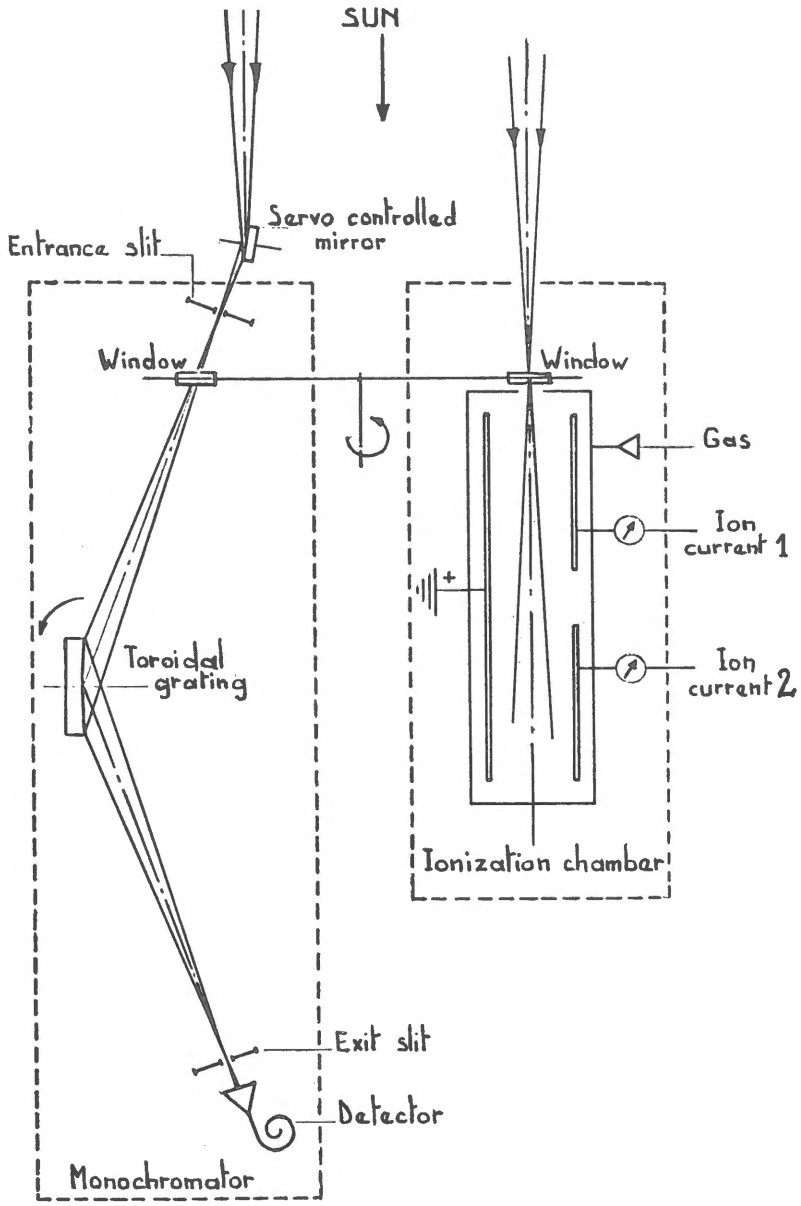

Figure 9 : Schematic diagram of the SCALP instrument (Delaboudinière et al 1976) showing one of the two grazing incidence monochromator and the absolute calibration detector on the right. Each absorbed photon in the ionization chamber produces an electron-ion pair which is collected by two electrodes. Departures from the one to one correspondance between the number of absorbed photons and collected ions are small. The second electrode allows to evaluate which proportion of the incoming flux is absorbed in the first portion of the chamber.

d. The International Solar Polar Mission (ISPM) :

Several French institutes are involved in major investigations of the interplanetary medium on the ISPM, a joint mission between ESA and NASA. The observatoire de Meudon is in charge of fabricating the external occulting disk of the coronagraph on ISPM, an instrument which is built under the responsibility of the High Altitude Observatory.

3. The future programme

The future programme will focus on the availability of the Solar Optical Telescope (SOT) already under development by NASA in the United States. The SOT is a 1.25 m solar telescope, supposed to be diffraction limited at 5000 A, ensuring a resolution of 0.1 arc second (70 km equivalent at the surface of the sun). Various baseline focal plane instruments have been identified such as a visible spectrograph, a magnetograph, a universal filter and an ultra-violet spectrograph. Under the initiative and responsibility of LPSP, two proposals have been submitted to NASA in July 1980, in cooperation with various French, European and American institutes. The selection of these investigations is likely to be announced in mid 1981. We briefly describe here these two proposals.

a. The Ultra-violet spectrograph (UVS).

The UVS provides simultaneously high spatial, spectral and temporal resolution It is made of three main parts :

i. a first spectrograph (1) using a planowadsworth mount and a film camera
ii. a high resolution spectrograph (2A) with an electronographic camera as detector ;
iii. a high resolution spectrograph (2B) with a detector combining the use of a microchannel plate and a CCD for detector.

The characteristics of the three parts are detailed in Table III.

Table III

Spectrograph	1	2A	2B
Spatial resolution (arc-sec)	0.1	0.1	0.3
Spectral resolution (pm)	4.5	1.8	4
Spectral range (nm)	117.5-200	117.5-200	117.5-300
Simultaneous Spectral Coverage (nm).	82.5	3	1

Besides LPSP, the Naval Research Laboratory and the Goddard Space Flight Center in the USA will take important responsibilities in hard ware fabrication and data analysis, together w ith numerous other US institutes or individuals. In France the Observatoire de Meudon have had major involvement in the proposal.

b. The Ultra-violet Imaging System (UVIS).

The excellent results obtained with the TRC (see paragraph II above) have been at the origin of this proposal. The UVIS intends to take high resolution pictures of the largest field of view available at the SOT focus (i.e. 3 x 3 arcmin^2), at 6 wavelengths from the near to the far UV, in order to explore the sun from the top of the convective zone (400 nm), up to the middle of the transition region (CIV 154.8 nm) through the temperature minimum and the chromosphere (Mg II 279.5 nm, L α 121.6 nm).

UVIS is a simple instrument which includes a capability for changing the focal ratio from f/12.5 to f/150. In the latter mode, UVIS should achieve the diffraction limit of the telescope (i.e. 16 km at L α) using interferometry techniques to overcome the degraded resolution inherent to UV observations. The detection will make use of both a CCD and photographic film .

The Lockheed Palo Alto Research Laboratory and the Center for Astrophysics in the US are the main co-investigators on this proposal. In France, the Institut d'Astrophysique de Paris, the Observatoire du Pic du Midi and the Faculté des Sciences and the Observatoire de Nice have taken part in the proposal.

c. The Grazing Incedence Solar Telescope (GRIST).

The GRIST is not yet an approved project. It is under phase A study at ESA and is supposed to fly together with SOT in one common spacelab flight. The LPSP and the Observatoire de Meudon might be involved in the fabrication of focal plane instrumentation. A decision to include GRIST in ESA's scientific programme will be taken in mid 1982.

d. The South Pole Balloon

The extraordinarily excellent results by Fossat (1980) which be obtained from the South Pole during the austral summer 1979-1980 are still strongly affected by the presence of atmospheric perturbations.
This is why CNES is presently studying the possibility of making this experiment again, from a tethered balloon anchored at the south pole. The result of this study will probably be known in 1981 or 1982 and a decision to go ahead with or to abandon the idea will be taken soon after.

4. Conclusion

As it can be seen from the above description, Solar Physics from space is still a lively activity in France. It is encouraging to observe that more and more institutes and individuals do participate in this programme either as hardware manufacturers or a guest investigators at the level of operations and data analysis.

We wish that the excellent relationships that we entertain with our japanese Colleagues meterialize some day in the future and that several projects will be undertaken in cooperation between France and Japan. The high level of the experiments which are under developement in both countries provides, in addition, the assurance that the highest scientific quality could be reached.

We hope that the present state will not last for ever.

REFERENCES

ARTZNER G., BONNET RM., LEMAIRE P., VIAL JC., JOUCHOUX A., LEIBACHER JW., VIDAL-MADJAR A., and VITE M., 1977, Space Sci. Instrum., 3,2, 131.

ARTZNER G., LEIBACHER JW., VIAL JC., LEMAIRE P. and COUTTEBROZE P., 1978, Astrophys. J., 224, L 83.

BALUTEAU JP., 1970, Thèse de 3ème cycle "Mesure de la température de brillance du soleil entre 12 et 24 microns", Paris 1970.

BONNET RM., 1968, Comm. Astrophys., 31, N° 6, 597.

BONNET RM., BLAMONT JE., and GILDWARG P., 1967, Astrophys. J., 148, L 115.

BONNET RM., and BLAMONT JE., 1968, Solar Phys., 3, N°1, 64.

BONNET RM., LEMAIRE P., VIAL JC., ARTZNER G., GOUTTEBROZE P., JOUCHOUX A., LEIBACHER JW., SKUMANICH A., and VIDAL-MADJAR A., 1978, Astrophys. J., 221, 1032.

BONNET RM., BRUNER EC., ACTON LW., BROWN WA., and DECAUDIN M., 1980, Astrophys. J., 237, L 47.

BONNET RM., and TSIROPOULA G., 1980, Submitted to **Solar Phys.**

DELABOUDINIERE JP. 1973, La Recherche Spatiale.

DELABOUDINIERE JP. and CRIFO JF., 1976, Space Res XVI, Akademie Verlag Ed., 803

DELABOUDINIERE JP. FIEFFE-PREVOST, P., SCHMIDTKE G., and SIMON PC., 1976, LPSP S-76 Internal Report : "Solar calibration package for Spacelab".

DELABOUDINIERE JP. and MILLIER F., 1977, Space Res. XVII, Akademie Verlag Ed., 519.

FOSSAT E., 1980, In Proceedings of the NATO-ASI Solar Phenomena in Stars and Stellar Systems". Bonas 25 August - 5 September 1980, RM. BONNET and A. DUPREE Ed.

GOUTTEBROZE P., 1980, Paris Thèse d'Etat.

GOUTTEBROZE P., and LEIBACHER JW., 1980 Astrophys. J., 238, 1134.

HERSE M., 1979, Solar Phys. 63, 35.

LEMAIRE P., 1970, in Proceeding of "Ultra-violet Stellar Spectra and Ground based Observations".L. HOUZIAUX and HE. BUTLER, Eds., 332.

LEMAIRE P., 1970, In "New Techniques in Space Astronomy", Labhum and Lüst, Eds., 263.

LEMAIRE P., 1980, to be published

LEMAIRE P., and SKUMANICH A., 1973, Astron. Astrophys., 22, 61.

LEMAIRE P., CHARRA J., JOUCHOUX A., VIDAL-MADJAR A., ARTZNER G., VIAL JC., BONNET RM; and SKUMANICH A., 1978, Astrophys. J., L 55.

LENA PJ., 1968, Solar Phys. 3, N°1, 28.

LENA PJ., 1970, Astron., Astrophys., 4, 202.

SAMAIN D., 1971, CR Acad. Sci. B, 273 , 1133

SAMAIN D., 1979, Astron. Astrophys. 74, 225

SAMAIN D., 1980, Astrophys.J. Suppl. In Press

SAMAIN D., BONNET RM., GAYET R., and LIZAMBERT C., 1975, Astron. Astrophys., 39, 71.

SAMAIN D., and SIMON PC., 1976, Solar Phys., 49, 33.

VIAL JC. , GOUTTEBROZE P., ARTZNER G., and LEMAIRE P., 1979, Solar Phys. 61, 39.

VIAL JC., MARTRES JM., and SALM PLATZER J., 1980, Solar Phys. , In Press

VIAL JC., LEMAIRE P., ARTZNER G., and GOUTTEBROZE P., 1980, Solar Phys. 68, 187.

SPACE OBSERVATIONS OF THE SUN AT TAO

Keizo Nishi
Tokyo Astronomical Observatory (TAO),
University of Tokyo

1. Introduction

Many of the recent progress in Solar Physics have been the result of extensive observations from outside the terrestrial atmosphere. More than twenty years have passed since the solar observation from outside the terrestrial atomosphere was started by TAO staff in close collaboration with the Institute of Space and Aeronautical Science(ISAS) of the University of Tokyo.

Balloon projects so far conducted since 1967 contain spectroscopy of the Sun in Infrared(IR) and Ultraviolet(UV) regions, the study of the fine structure of the solar atmosphere in visible region, and the measurement of the solar X-ray bursts. The last two programs will be continued by using a larger 30 cm aperture telescope from Balloon and X-ray modulation collimator with better spatial resolution (15") and high time resolution from the Astro-A satellite to be launched next year respectively.

Rocket observation by TAO staff was started in 1958 as one of the IGY programs. The measurements of the absolute intensity and the center to limb variations of the Sun in the vacuum ultraviolet region have been successfully performed from 1971 to 1975, and further experiments will be hopefully expected.

The astronomical observation from Japanese satellite was started in 1971, and the solar radio emissions were measured by the first satellite for the scientific study -Shinsei-. The study of solar flares, particularly in the soft X-ray region, was successfully performed by a Bragg type spectrometer on the Tansei-4 satellite which was launched in this February as a test flight for the Astro-A satellite. The Astro-A is the seventh scientific satellite of ISAS to make detailed study of solar flares mainly in the X-ray region during periods of enhanced solar activity, and will be launched coming February.

Table 1 contains a list of all successful experiments from Balloon, Rocket, and Satellite with general view of each experiment, a list of planned experiments in the near future, and a long range plan.

Table 1

List of successful Observations of the Sun from Space performed by TAO

Balloons

Infrared region

Date of launch	Instrumentaion	Pointing accuracy	Spectral resolutin	Spectral range	Maximum height	References
1968 Sept. 5	Czerny-Turner type scanning monochrometer Detector PbS	1°	10A	0.98μm～ 2.19μm	24 km	1
1970 Sept.14	Imaging tele-scope and the monochromator	0.1°	0.5A	0.73μm～ 1.36μm	27 km	2
1972 Sept.20	nearly same system	1'	0.5A 1.0A	1.15μm～ 2.47μm	27 km	3

Visible region

Date of launch	Instrumentation	Pointing accuracy	spatial resolution	Spectral band	Maximum height	References
1971 Sept.14	Imaging tele-scope (ϕ=5cm), camera and TV system	Test for pointing and focusing by TV technique, thermal effects		about 400A centered at 5300A	26 Km	4, 5, 6
1973 Sept.15	Imaging tele-scope(ϕ=10cm) and same system	1"	1"	same as before	28 km	
1976 Sept. 2	nearly same system	"	"	"	"	
1977 Sept. 2	nearly same system	"	"	"	"	

Ultraviolet region

Date of launch	Instrumentation	Pointing accuracy	Spectral resolution	Spectral range	Maximum height	References
1971 Sept.16	Imaging tele-scope(ϕ=5cm) scanning mono-chromator	10"	7A	2750A～ 2850A	34 km	7, 8, 9
1975 Sept.11	Piezoelectric scanning Fabry-Perot Interference spectrometer	1"	0.14A	2780A～ 2820A	38 km	

X-ray region

Date of launch	Instrumentation	Spatial resolution	Spectral (energy) range	Maximum height	References
1969 Sept.27	Modulation collimator Detector; NaI scintillation counter	1.32' (FWHM)	20 keV∼ 60 KeV	35 km	10
1970 July 26	nearly same system			36 km	

Rockets

Date of launch	Instrumentation	Spatial resolution	Spectral resolution	Spectral range	Result	References
1971 Sept.1	Double-dispersive trichromator	1.3'	8.3A	1629A 1684A 1739A	Abs. I and CLV	11
1973 Feb.19	Single dispersive, Ion Chamber	Whole disk	78A	1550A∼ 1950A 1216A	Abs. I Abs. I	12
1975 Sept.24	Grating-spectrometer	50"	3.3A	1630A∼ 2000A	CLV	13

Satellites

Date of launch	Instrumentation	Spectral range	Spectral resolution	Name	References
1971 Sept.28	Superheterodyne receving set	8 MHz 5 MHz	180kHz(3dB) 150kHz(3dB)	Shinsei	14
1980 Feb.17	Bragg type spectrometer LiF crystal	1.8A∼1.98A 3.12A∼3.24A Time resolution 6 sec.	0.007A	Tansei-4	15

List of planned experiments in the near future

(1) A 30 cm aperture Balloon-borne telescope will be launched in 1981.

(2) A X-ray modulation collimator with high spatial resolution (15") and A set of Bragg type spectrometers with spectral resolutions of 0.00068A and 0.000042A will be launched by the Astro-A in 1981.

Long range plan

UVSAT project

A satellite for observing stars and the Sun in the vacuum ultraviolet region and extreme ultraviolet region is under consideration to be launched in 198?.

2. Experiments and related results

The spectroscopic observation in IR region from Balloon was started in 1968. A very simple Czerny-Turner type scanning monochromator with a PbS detector was used. Two other successful flights were performed in 1970 and 1972 by the improved monochromator with a 0.5A spectral resolution combined with small imaging telescope. By these experiments more than 1500 absorption lines were recorded. Paschen series, Brackett series of Hydrogen and many metal lines were identified. From these experiments we have studied a pointing technique of the observation from Balloon. The balloon gondra itsself is directed by means of a servo-controlled wire-twisting system with a geomagnetic sensor, which was developed by the staff of balloon engineering section of ISAS. The pointing accuracy is about 1°, and this system was used for almost of all experiments as a coase pointing.

Direct photography for Solar surface by balloon-borne telescope was started in 1971 to study the fine structures in the Solar atmosphere. The first step of the project was to test for a fine pointing and focusing by the TV technique which was developed by ISAS staff and temperature measurement of the instrumentation with a 5 cm aperture telescope. After the first successful flight, several flights of 10 cm aperture telescope were performed almost once a year from 1972 to 1977. More than 1000 photographs were obtained by these flights.

The results obtained from the data are as follows;

(1) The life time of facular granules with the average size of 2" is about 4 hours and they fluctuate in intensity with a time scale of approximately 20 min.

(2) Center to limb variation of the excess brightness of facular granules was obtained.(Fig.1) This result shows that facular is 600K~1000K hotter than the photosphere, if the diameter of facular granules is assumed to be 600~150km respectively.

(3) It is found that the soft X-ray bright points as observed with the Skylab do not correspond spatially to the facular granules near the polar region.

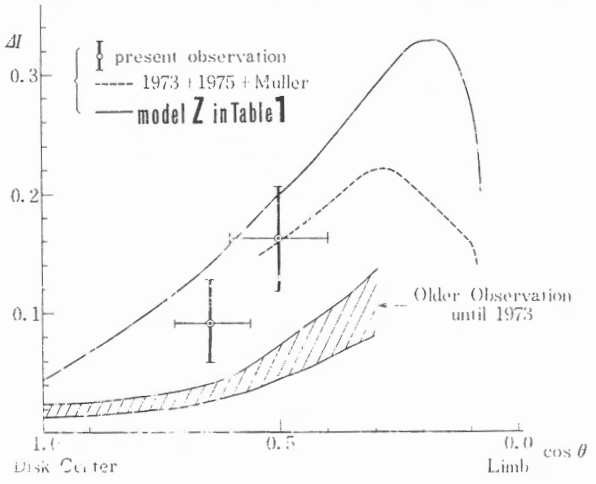

Fig.1. The excess brightness against cosθ, θ being an angle between the sun's normal and the line of sight.

The resonance lines of MgII of 2802.7A and 2795.5A have been used for the study of the Solar chromosphere, and many observations of these lines were done by using balloons, rockets, and satellites worldwidely. The first preliminary experiment with a small grating monochromator was successfully performed in 1971 in collaboration with the staff of Mechanical Engineering Laboratory. The spectral resolution was 7A and the pointing accuracy was 10". In order to obtain better spectral resolution a Farby-Perot interference spectrometer was launched in 1975. The spectrometer consisted of a Piezoelectric scanning Farby-Perot interferometer and a grating as predisperser. The measured resolution was 0.14A. The spectrometer was calibrated absolutely, and the pointing accuracy was about 1". The result is shown in figure 2.

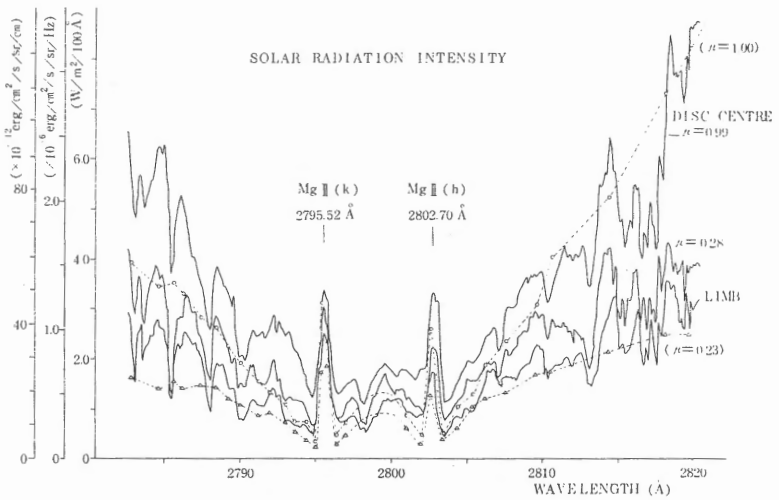

Fig.2. Solar UV spectrum observed by a balloon-borne FP-grating spectrometer. Brief level plots from Kohl and Parkinson(1976) are shown for comparison.

The measuments of size and location of the Solar X-ray burst (20-60 keV) were performed by the balloon-borne modulation collimator in 1969 and 1970. The device has been developed for the measuments of the celestial X-ray sources by the staff of ISAS. The collimator consisted of three grids made of parallel wires, and the angular resolution was 1.32'(FWHM). The X-ray detector was a scintillation counter with NaI(Tl) equipped with a veto-counter of a plastic scintillator. The observable energy range of the detector was from 20 keV to 60 keV. From these experiments it became clear that the size of the X-ray sources was remarkably small (less than 1'), much smaller than the H_α flare size. The finer experiments of the same kind is on schedule for the Astro-A satellite which will be launched next February.

The observation of the solar spectrum from rocket was begun in 1958 as one of the IGY programs. The rocket technique was still on a progressing stage at that time, and the upper limit of launch height was about 50 km, and the pointing technique was not performed yet. Since the rockets could be flown higher than 200 km, the observation of the solar spectrum in the vacuum ultraviolet region (1216A～2000A) became feasible together with the construction of laboratory for the basic experiments of spectroscopy in VUV region. In order to study the physical situation of the solar surface between upper photosphere and lower chromosphere the measurements of the absolute intensity and the center to limb variation were planned. Three flights were successfully performed in 1971, 1973, and 1975. The results are shown in figure 3.

Our result of the absolute intensity of solar spectrum in this wavelength region seems to nicely coincide with others shown by Samain and Simon (16). Those of the center to limb variation seem to be in good coincidence with the Samain's (17) from 1730A to 2000A but not down to 1630A. It may not be fair to compare ours with others simply, because the spectral and spatial resolutions are different. One thing which we can notice is that the HSRA model can not fit these results. Should we continue to do the extensive calculation taking into account of the effects of many lines like Bonnet, Samain, and many others have tried? Or should we see the fine structures in the spectrem shown by the HRTS performed by Brueckner? And we should also think of the results of flux variations in accordance with the solar activity obtained by recent long-term observation from satellites. The continuous observations with high resolutions and accuracy in the future are quite hopeful.

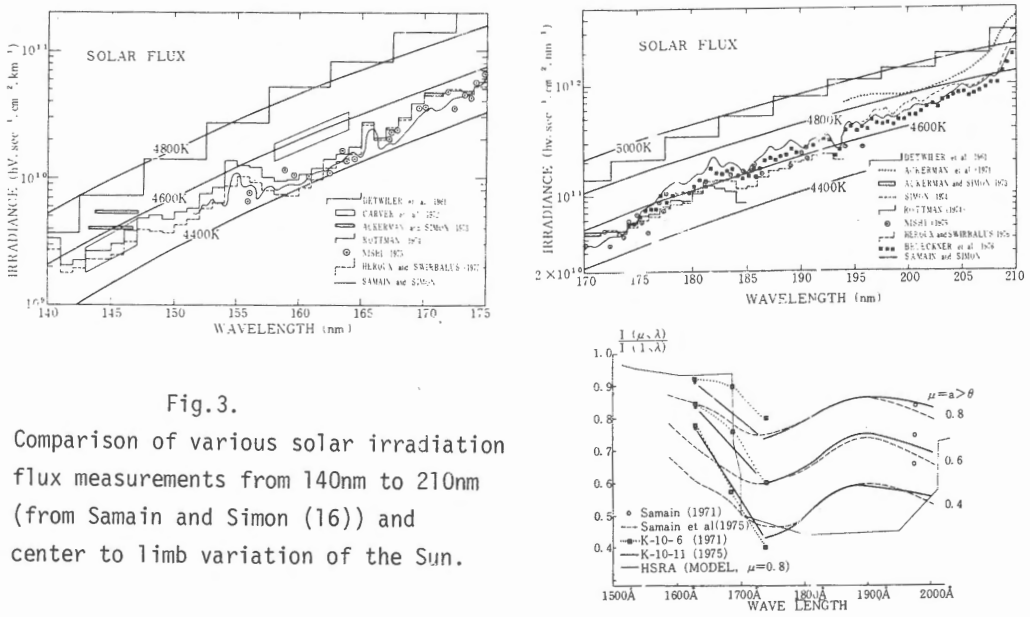

Fig.3.
Comparison of various solar irradiation flux measurements from 140nm to 210nm (from Samain and Simon (16)) and center to limb variation of the Sun.

Solar radio emission in 5 MHz and 8 MHz was measured by the first Japanese scientific satellite Shinsei-, and about ten type III bursts were observed during four months in 1971. The data were compared with those obtained by the IMP-6 USA satellite, and a normalized time profile of type III burst was obtained. On the hypothesis that the time profile corresponds to the one of electron flux, it is shown that the similarity of time profile is maintained even if the electron velocity decreases with the travel distance, provided that the time is normalized at the time of maximum flux.

A test satellite Tansei-4- for the Astro-A satellite, which is on schedule to launch next February, was successfully performed this year. The instrumentation and some results are reported by K.Tanaka in detail. Since the sensitivity of the Solar Bragg Spectrometer is very high, we have big hope and large expectation for the data analysis and for the further observations with the Astro-A which has high spectral resolutions.

3. Planned experiments in the near future

A Balloon-borne telescope for the observation of the fine structure on the Solar surface will be launched next year. The telescope system consists of a 35 cm aperture plane mirror which is used for the fine pointing, a 30 cm aperture main mirror for imaging, a diagonal small mirror which locates at the focus of main mirror to take out a part of solar image, and an enlarging lens system for fine focusing and making the solar image of 44 cm in diameter, two cameras one for white light (5300A, $\Delta\lambda$~400A) and another for UV light (3835A or 3933A $\Delta\lambda$~20A), and the TV system to be used for pointing and focusing.

A satellite named Astro-A is on schedule under various tests to be launched next February. The satellite body is an octagonal pillar with a cirumscribed diameter of 106 cm and a height of 85 cm. Four solar paddles are deployed after the satellite achieves orbit. The satellite will spin at a rate of 5rpm, and the spin axis will be controlled to point 1.2° ± 0.5° from the center of the Sun. The prime object of the satellite is to make detailed study of solar flares mainly in X-ray bands by observing various aspects with good spatial, spectral and temporal resolutions. The physical instruments aboard the satellite are as follows:

(A) Solar X-ray imaging telescope (SXT)
(B) Solar hard X-ray monitor detector (HXM)
(C) Solar γ-ray detector (SGR)
(D) Soft X-ray crystal spectrometer (SOX)
(E) Solar soft X-ray monitor detector (FLM)
(F) Particle and X-ray monitor detector (PXM)
(G) Plasma impedence probe (IMP)

(H) Plasma electron temperature probe (TEL)

TAO has three instruments responsible for the Astro-A, and they are SXT, HXM, and SOX. Here the discription of the SOX is reported.

The SOX will obtain high resolution spectra from highly ionized iron emitted by the hot thermal plasmas produced in flares. The following types of features can be obtained with a time resolution of 6 seconds.

(1) line intensities in the range 1.72-1.99A
(line of Fe XX-Fe XXVI and Fe K_α)

(2) line profiles in the range 1.83-1.89A

(3) continuum intensities around the lines

(4) degree of polarization

These may be reduced in order to determine the electron temperature, ion temperature, ionization temperatures, and emission measures. These quantities combined with radio, hard X-ray, and soft X-ray continuum data will hopefully explain the heating mechanisms producing flares. A spectral scan is made automatically by the crystals fixed to the satellite utilizing the satellite spin (5 rpm). This method has been successfully tested by the satellite -Tansei-4-. Two crystal spectrometers independently measure overlapping spectral ranges. Characteristics of the two spectrometers are shown in Table 2.

Table 2 : Characteristics of the crystal spectrometer (SOX)

	SOX-1	SOX-2
crystal	SiO^2(1011)	SiO^2(1340)
2d	6.69A	2.36A
integrated reflectivity	79 x 10^{-6}rad	23 x 10^{-6}rad
rocking curve FWHM	22"	6"
angle (α) fixed to the satellite	16.111°	52.01°
crystal size	44 x 133mm	40 x 53mm
effective area (A)	6.4cm^2	8.2cm^2
sensitivity	4.9 x $10^{-2}cm^2s$	1.8 x $10^{-2}cm^2s$
ARc η/ω		
wavelength range	1.72 - 1.99A	1.83 - 1.89A
scan step	min max	min max
	0.0001-0.0011A	0.00002-0.0023A
spectral resolution	0.00068A	0.000042A

The detectors are NaI(Tl) scintillation counters with 5cm apperture. The signals are handled in two modes : in PC-mode those pulses within the lower and upper discrimination levels are simply counted and read out every 15.6ms. The

wavelength resolution is determined by the sampling time which corresponds to $\Delta\phi$=0.47° in the satellite spin angle (ϕ). The measured wavelength (λ) is related to the satellite spin angle (ϕ) by :

$$\lambda = 2d\ (\sin\alpha\cos\delta + \sin\delta\cos\alpha\cos\phi)$$

Where α is the fixed angle of the crystal (Table 2) with respect to the spin axis and δ is the off-set angle of the spin axis to the flare position (δ ranges from 0.7 to 1.7 degrees). In PH-mode, 16 channel pulse-height analysis is performed for each signal with a time resolution of 250ms. This mode is mainly used for detector calibration. A ^{109}Cd source emitting 22 KeV X-ray is used for the calibration. The amplifier gain, discrimination levels, and high voltage values are selectable by commands. The instrument performance is effectively limited to the maximum count rate of 200 KHz due to plus pile-up.

4. Long range plan

There is a long range plan -UVSAT- project, but this is not definite yet as far as the budget situation is concerned. The plan consists of two parts; the one is a VUV telescope for the observation of stars and the other is a EUV telescope for the Sun. The explanation of the second one is reported. The main aim of this plan is to understand the energy transport on the solar surface, where the physical state is the boundary condition in space and time from which the analysis of the solar interior and its evolution must start. What is the ordinary process to convert energy from the nuclear source at the core of the Sun to the photosphere, layer by layer, and uphill beyond the temperature minimum into the chromosphere and corona? By what extraordinary process can some of this energy be converted into various phenomena like sunspots, flares, flare-related nonthermal process, loop and surge prominences, and less active features like plages etc.. To study above mentioned questions the observation with simultanious heliograms of photosphere, chromosphere, transition region, and corona with high spatial resolution (2") and high temporal resolution (1 sec.) from a satellite is greatly hoped. The design of the satellite is not clear yet, but an Aplanatic Gregorian telescope (ϕ=12cm, f=1.5m, F/12.5) is combined with a 50cm stigmatic spectrograph of 11A/mm spectral resolution. Multi-Anode Microchannel Array (MAMA) and CCD are used for detectors. The selected lines for the observation are 624.9A (MgX), 770.4A(NeVIII), 997.0A(CIII), 1031.9A(OVI), 1215.7A(HI), 1335.7A(CII), 1600A, and 5000A. For the long range plan the fundamental experiment devices should be prepared, and several rocket flights should be also planned.

References

(1) W.Tanaka and Z.Suemoto : Bulletin of the ISAS, 6, 316 (1970)
(2) W.Tanaka and Z.Suemoto : Bulletin of the ISAS, 9, 231 (1973)
(3) W.Tanaka and Z.Suemoto : Bulletin of the ISAS, 10, 201 (1974)

(4) T.Hirayama, I.Shimizu, S.Hamana, A.Tokuya, H.Imai. and F.Moriyama : Bulletin of the ISAS, 10. 183 (1974)
(5) T.Hirayama : Publ. Astron. Soc. Japan, 30, 337 (1978)
(6) T.Hirayama and F.Moriyama, Solar Physics, 63, 251 (1979)

(7) T.Kohno, N.Yajima, and Z.Suemoto : Bulletin of the ISAS, 10, 166,174 (1974)
(8) T.Kohno and N.Yajima : Optics Commum., 17, 297 (1976)
(9) T.Kohno : Optica Acta, 26, 1057 (1979)

(10) T.Takakura, K.Ohki, N.Shibuya, M.Fujii, M.Matsuoka, S.Miyamoto, J.Nishimura, M.Oda, Y,Ogawara, and S.Ota : Solar Physics, 16, 454 (1971)

(11) K.Nishi : Solar Physics, 33, 23 (1973)
(12) K.Nishi : Solar Physics, 42, 37 (1975)
(13) K.Nishi, K.Higashi, A.Yamaguchi, and Z.Suemoto : Bulletin of the ISAS, 12, 959 (1976)

(14) T.Takakura, Y.Naito, and K.Ohki : Solar Physics, 41, 153 (1975)
(15) K.Tanaka and K.Nishi : Japanese Journal of Applied Physics, 17, Supplement 17-2, 461 (1978)
(16) D.Samain and P.Simon : Solar Physics, 49, 33 (1976)
(17) D.Samain, R.M.Bonnet, R.Gayet, and C.Lizambert : Astron. & Astrophys, 39, 71 (1975)

Bulletin of the ISAS is written in Japanese.